



---

# TRIS(8-QUINOLINYL)PHOSPHITE: SYNTHESIS, COORDINATION CHEMISTRY AND CATALYTIC APPLICATIONS

---

Dissertation zur erlangung des  
Doktorgrades der Naturwissenschaften  
**DOCTOR RERUM NATURALIUM**  
am Institut für Anorganische Chemie  
der Fakultät für Chemie und  
Pharmazie der Universität Regensburg

Vorgelegt von:

**MIGUEL ÁNGEL CHACÓN TERÁN**

aus Maracaibo-Venezuela

Regensburg 2020



**UNIVERSIDAD SIMÓN BOLÍVAR**

DECANATO DE ESTUDIOS DE POSTGRADO

COORDINACION DE POSTGRADO EN QUIMICA

DOCTORADO EN QUIMICA

DOCTORAL THESIS

**TRIS(8-QUINOLINYL)PHOSPHITE: SYNTHESIS, COORDINATION CHEMISTRY  
AND CATALYTIC APPLICATIONS**

by:

**Lic. Miguel Ángel Chacón Terán**

Licenciado en Educación Química, Universidad del Zulia

Born October 12<sup>th</sup>, 1991

Sartenejas, September 2020



**UNIVERSIDAD SIMÓN BOLÍVAR**

DECANATO DE ESTUDIOS DE POSTGRADO

COORDINACION DE POSTGRADO EN QUIMICA

DOCTORADO EN QUIMICA

**TRIS(8-QUINOLINYL)PHOSPHITE: SYNTHESIS, COORDINATION CHEMISTRY  
AND CATALYTIC APPLICATIONS**

by:

**Lic. Miguel Ángel Chacón Terán**

Licenciado en Educación Química, Universidad del Zulia

Born October 12<sup>th</sup>, 1991

**Supervisor:** Dr. Rafael Emilio Rodriguez Lugo

**Co-supervisor:** Prof. Dr. Robert Wolf

DOCTORAL DISSERTATION

Submitted to the Universidad Simon Bolivar  
in partial fulfilment of the requirements for the degree of

DOCTOR OF PHILOSOPHY IN CHEMISTRY

(PhD. in Chemistry)

Sartenejas, September 2020



**UNIVERSITÄT REGENSBURG**

**FAKULTÄT FÜR CHEMIE UND PHARMAZIE**

**INSTITUT FÜR ANORGANISCHE CHEMIE**

**TRIS(8-QUINOLINYL)PHOSPHITE: SYNTHESIS, COORDINATION CHEMISTRY  
AND CATALYTIC APPLICATIONS**

Vorgelegt von:

**Lic. Miguel Ángel Chacón Terán**

Licenciado en Educación Química, Universidad del Zulia

Geboren Oktober 12<sup>th</sup>, 1991

**DISSERTATION ZUR ERLANGUNG DES DOKTORGRADES DER  
NATURWISSENSCHAFTEN (DR. RER. NAT) DER FAKULTÄT FÜR CHEMIE UND  
PHARMAZIE DER UNIVERSITÄT REGENSBURG**

aus

Sartenejas-Venezuela

in Jahr 2020



**Das Promotionsgesuch wurde eingereicht am: 21.09.20**

**Die Arbeit wurde angeleitet von:**

Dr. Rafael Rodriguez Lugo, **Instituto Venezolano de Investigaciones Científicas**, Venezuela.

Prof. Dr. Robert Wolf, **Universität Regensburg**, Deutschland.

**Unterschrift:**



The present work entitled

**TRIS(8-QUINOLINYL)PHOSPHITE: SYNTHESIS, COORDINATION CHEMISTRY  
AND CATALYTIC APPLICATIONS**

by Miguel Angel Chacon Teran

was performed under the joint supervision of

**Universität Regensburg**

and

**Universidad Simón Bolívar**

as part of the international doctoral program of the University of Regensburg (*iPUR*)

as a double degree doctorate



Die vorliegende Arbeit mit dem Titel

**TRIS(8-QUINOLINYL)PHOSPHITE: SYNTHESIS, COORDINATION CHEMISTRY  
AND CATALYTIC APPLICATIONS**

vorgelegt von Miguel Angel Chacon Teran

entstand unter der gemeinsamen Betreuung

**der Universität Regensburg**

und

**der Universidad Simón Bolívar**

im Rahmen des internationalen Promotionsprogramms der Universität Regensburg (*iPUR*)

als Doppelpromotion

## DEDICATION

*A mis padres, amigos y en especial a mi  
negrita Melanie, mi gran pilar para la  
materialización de este logro.*

## ACKNOWLEDGEMENTS

## ABSTRACT

The ability of many transition metal complexes to catalyze organic reactions (in the homogeneous phase) is one of the most powerful strategies to address the issue of the "ideal" synthesis. The choice of the transition metal and the possibility of rationally designing a particular ligand, provides the opportunity to adjust the steric and electronic properties of the complex, having a significant relevance on the selectivity and efficiency of a particular reaction. In the last 60 years, the increase in work related to the chemistry of transition metals has resulted in the great progress of homogeneous catalysis, this being a fundamental tool both in academia and industry. Part of these achievements has been due to the fundamental role that phosphorus ligand chemistry has occupied in an infinite number of catalytic processes. These have contributed strongly to the broad development of the field of homogeneous catalysis which is an important piece in the organic synthesis and industrial production of a wide variety of chemical products.

This work focuses on studying the synthesis of the novel tris(8-quinoliny)phosphite,  $\text{P}(\text{OQuin})_3$ , **1** and its reactivity with metal complex precursors of groups 8, 9 and 10. Both  $\text{P}(\text{OQuin})_3$  and its coordination compounds were evaluated in catalytic bond formation reactions.  $\text{P}(\text{OQuin})_3$  has a phosphorus atom that can strongly coordinate to a metal atom, and three quinoline groups, in which nitrogen atoms are present, which can be weakly coordinated. It is expected that in  $\text{P}(\text{OQuin})_3$ , the hemilabile character is greatly influenced by competition between the three quinoline groups with the same coordination probabilities.

Phosphites are widely used in catalytically active metal complexes, but they have very rarely exploited as catalyst themselves. Transfer hydrogenation reactions are commonly catalyzed by precious-metal compounds for which crustal abundance, expense, and toxicity are significant issues. Therefore, the development of metal transfer hydrogenations is an attractive objective. In CHAPTER II, the synthesis and characterization  $\text{P}(\text{OQuin})_3$  is applied as a precatalyst in a metal-free transfer hydrogenation.  $\text{P}(\text{OQuin})_3$  promotes the dehydrogenation of  $\text{H}_3\text{N}\cdot\text{BH}_3$  (**AB**) and reduction of symmetric/asymmetric azoarenes using **AB** as an  $\text{H}_2$  source in good yields (up to 95%). Mechanistic studies suggest that  $\text{P}(\text{OQuin})_3$  is a precatalyst for an unknown catalytically active species. Kinetic studies and deuteration experiments reveal that the transfer of protic and hydride hydrogen from **AB** occurs at the same time with a large negative activation entropy of  $\Delta S^\ddagger = -31$  e.u. In the frame of sustainable chemistry, systems like this fulfills at least six of the twelve principles of the green chemistry.

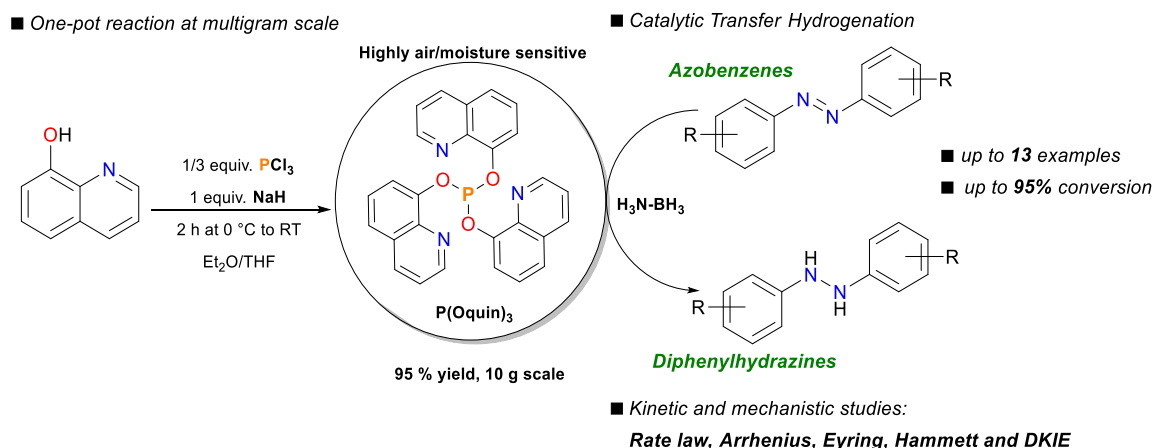


Figure A1. Synthesis of  $P(OQuin)_3$  and its application at the organocatalytic reduction of azoarenes using ammonia borane as  $H_2$  source.

In CHAPTER III, a novel  $Pd(II)$  metal complex bearing  $P(OQuin)_3$  has been isolated and fully characterized. X-ray diffraction analysis shows that the ligand  $P(OQuin)_3$  binds the metal center as a bidentate P-N chelate. The complexes  $[Pd\{P(OQuin)_3\}Cl_2]$  is an efficient catalysts for the oxidative coupling of benzylamine to N-benzylidenebenzylamine using air as terminal oxidant. This methodology avoids the use of dangerous oxidants, additives, high temperatures or organic solvents. Other primary amines can be converted to their corresponding imines with moderate yields. The cross-coupling of benzylamine with substituted anilines to yield aldimines was achieved. The catalyst can be recovered from the reaction mixture and was reused in a next run without significant loss of its activity.

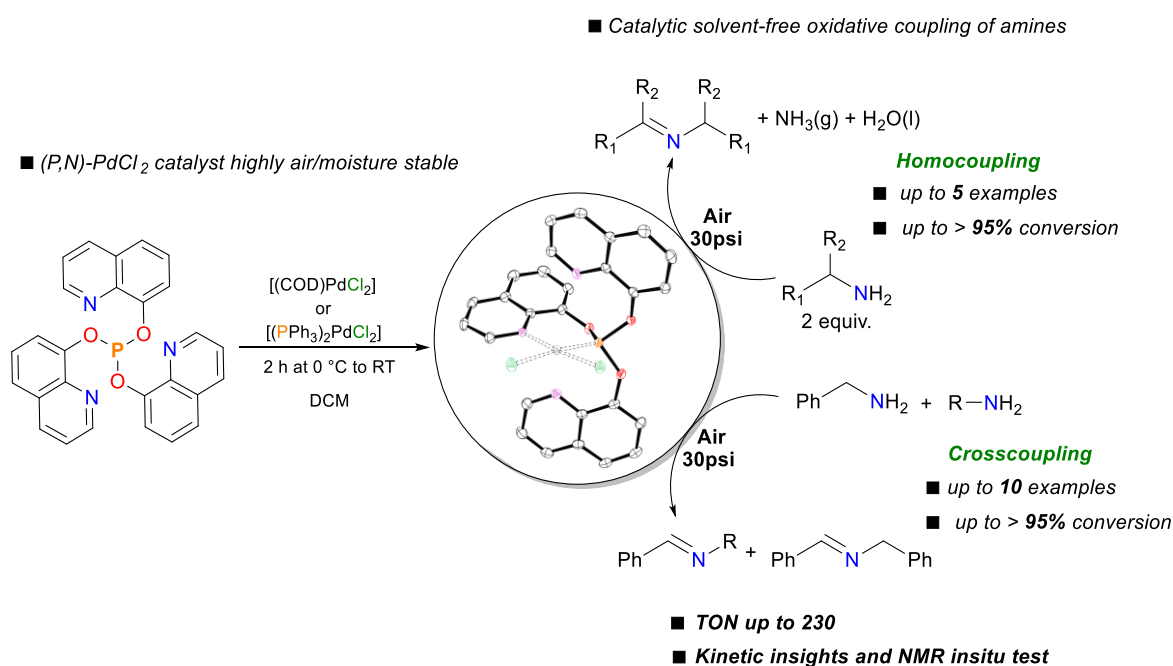


Figure A2. Synthesis of novel  $Pd(II)$  complex bearing  $P(OQuin)_3$  and its catalytic application in oxidative coupling of primary amines to imines.

In CHARTER IV, two novel Rh(I) metal complexes bearing  $P(O\text{Quin})_3$  have been isolated and fully characterized.  $[(\kappa^2\text{-}P,N)\{P(O\text{Quin})_3\}\text{Rh}\{P(R)_3\}\text{Cl}]$  ( $R = \text{Ph}, \text{Cy}$ ) (PN-RhPh and PN-RhCy) can be obtained from different Rh(I) precursors as starting material. PN-RhPh has a dynamic behavior at variable temperature and  $\text{PPh}_3$  dissociate from coordination sphere. One uncoordinated quinoline of  $P(O\text{Quin})_3$  can take up the empty coordination site, yielding a tricoordinate mode of  $P(O\text{Quin})_3$ ,  $[(\kappa^3\text{-}N,P,N)\text{RhCl}]$ . PN-RhCy is obtained by a ligand exchange  $\text{PPh}_3/\text{PCy}_3$  using PN-RhPh as a starting material. PN-RhPh is a very efficient catalyst for the 1,2-chemoselective hydroboration of pyridines. This reaction is carried out under mild conditions using 0.5 mol%  $[\text{Rh}]$ , ratio  $\text{Py}/\text{BH}$  1:1.1 at 50 °C, yielding the *N*-boryl-1,2-dihydropyridines with 100% of conversion and 95% of regioselectivity. This methodology represents the best system reported for late transition metal catalyzed hydroboration of pyridines.

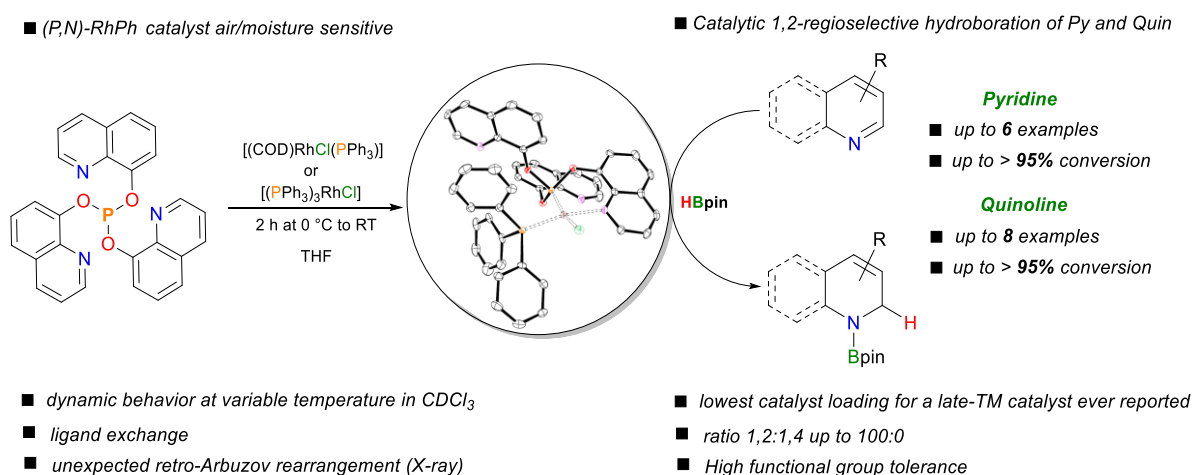


Figure A3. Synthesis of novel Rh(I) complex bearing  $P(O\text{Quin})_3$  and its application in regioselective 1,2-hydroboration of substituted pyridines and quinolines.

Finally in CHAPTER V, two novel Ru(II) metal complexes bearing  $P(O\text{Quin})_3$  have been isolated and fully characterized.  $[(\kappa^3\text{-}N,P,N)\{P(O\text{Quin})_3\}\text{Ru}\{P\text{Ph}_3\}\text{Cl}_2]$  had the same dynamic behavior as the Rh(I) complexes discussed in CHAPTER IV. A new complex with a tetracoordinate mode of  $P(O\text{Quin})_3$ ,  $[(\kappa^4\text{-}N,N,P,N)\text{RuCl}_2]$  ( $\text{PN}_3\text{-Ru}$ ) is obtained.  $\text{PN}_3\text{-Ru}$  resulted is an efficient as catalysts for the dehydrogenative coupling of silanes w or w/o alcohols to yield polysilanes and polysiloxanes respectively, forming high MW polymers with >95% yield.  $\text{PN}_3\text{-Ru}$  presents an alternative to early transition metal catalysts which frequently require the use of additives such as  $n\text{BuLi}$ .



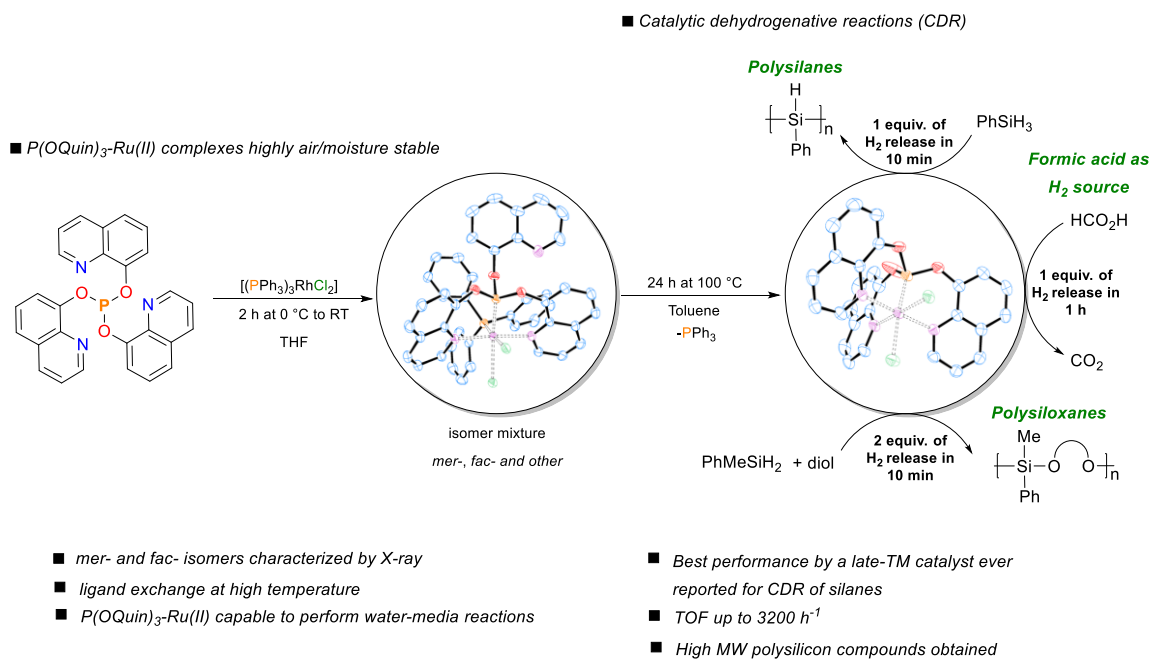


Figure A4. Synthesis of novel Ru(II) complexes bearing P(OQuin)<sub>3</sub> and its applications in dehydrogenative reactions.

## RESUMEN

La capacidad de muchos complejos de metales de transición para catalizar reacciones orgánicas (en la fase homogénea) es una de las estrategias más poderosas para abordar el tema de la síntesis "ideal". La elección del metal de transición y la posibilidad de diseñar racionalmente un ligando en particular, brinda la oportunidad de ajustar las propiedades estéricas y electrónicas del complejo, teniendo una relevancia significativa en la selectividad y eficiencia de una reacción particular. En los últimos 60 años, el aumento de trabajos relacionados con la química de los metales de transición ha resultado en un gran progreso de catálisis homogénea, siendo esta una herramienta fundamental tanto en la academia como en la industria. Parte de estos logros se debe al papel fundamental que la química del ligando de fósforo ha ocupado en un extenso número de procesos catalíticos. Estos han contribuido en gran medida al amplio desarrollo del campo de la catálisis homogénea, que es una pieza importante en la síntesis orgánica y la producción industrial de una amplia variedad de productos químicos.

Este trabajo se centró en el estudio de la síntesis del nuevo tris(8-quinolinil)fosfito,  $P(OQuin)_3$ , y su reactividad con ciertos precursores metálicos de los grupos 8, 9 y 10. Tanto  $P(OQuin)_3$  como sus compuestos de coordinación fueron evaluados en reacciones para la formación de compuestos orgánicos de interés.  $P(OQuin)_3$  tiene un átomo de fósforo que puede coordinarse fuertemente con el centro metálico y 3 grupos quinolina, en los que están presentes átomos de nitrógeno, que pueden coordinarse débilmente a este. Se espera que en  $P(OQuin)_3$ , el carácter hemilabil esté muy influenciado debido a la competencia entre las 3 quinolina con las mismas probabilidades de coordinación.

En la literatura se encuentra que los fosfitos se usan ampliamente en complejos metálicos catalíticamente activos, pero muy raramente se han explotado como catalizadores cumpliendo un rol protagonista. Por otro lado, las reacciones de hidrogenación por transferencia son comúnmente catalizadas por metales preciosos para los cuales la abundancia, el valor y la toxicidad son problemas importantes. En este sentido, en el CAPÍTULO II se describe la síntesis y caracterización del nuevo y voluminoso  $P(OQuin)_3$  y se estudia su aplicación como precatalizador en una reacción de hidrogenación por transferencia libre de metales.  $P(OQuin)_3$  es capaz de promover la deshidrogenación de  $H_3N \cdot BH_3$  (**AB**) y la reducción de azoarenos simétricos / asimétricos utilizando **AB** como fuente de  $H_2$ , obteniendo rendimientos realmente buenos (hasta 95%). El estudio mecanístico sugiere que  $P(OQuin)_3$  actúa como precatalizador, así como los estudios cinéticos (DKIE) revelan que la transferencia de los hidrógenos prótico e hidruro desde **AB** ocurre al mismo tiempo en el estado de transición

del paso determinante con un  $\Delta S^\ddagger = -31$  eu, siendo este más factible (energéticamente hablando) que sistemas anteriormente reportados. En el marco de la química sostenible, sistemas como este cumplen al menos 6 de los 12 principios de la química verde.

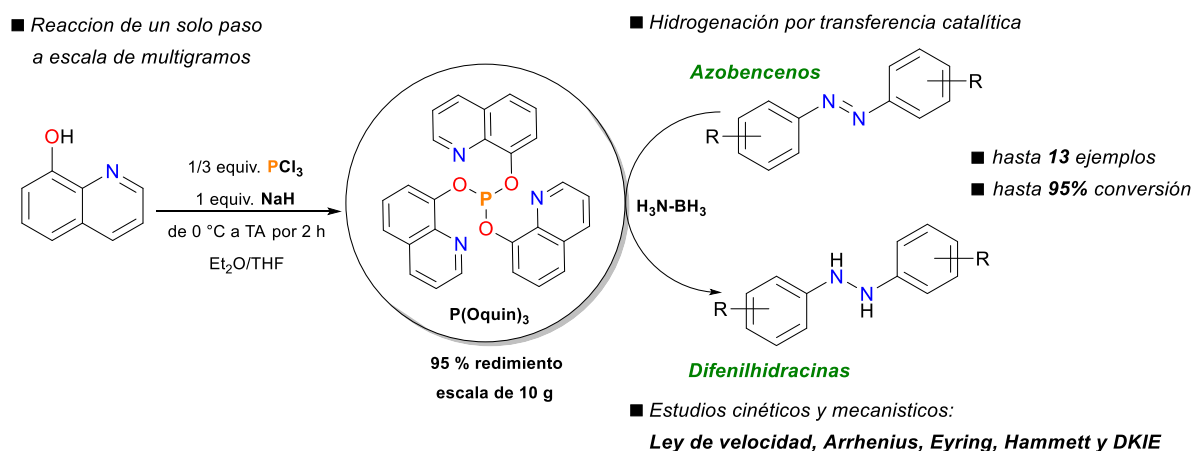


Figura R1. Síntesis de  $\text{P}(\text{OQuin})_3$  y su aplicación en la reducción organocatalítica de azoareños utilizando amoniacoborano como fuente de  $\text{H}_2$ .

En el CAPÍTULO III, un nuevo complejo de Pd (II) que tiene  $\text{P}(\text{OQuin})_3$  como ligando principal ha sido aislado y completamente caracterizado. El análisis de difracción de rayos X muestra que el ligando  $\text{P}(\text{OQuin})_3$  se coordina al centro metálico mencionado como un quelato P-N bidentado. El complejo  $[\kappa^2(P,N)\{\text{P}(\text{OQuin})_3\}\text{PdCl}_2]$  resulta ser un catalizador eficiente para el acoplamiento oxidativo de la bencilamina para formar N-bencilidenbencilamina utilizando aire como oxidante terminal.

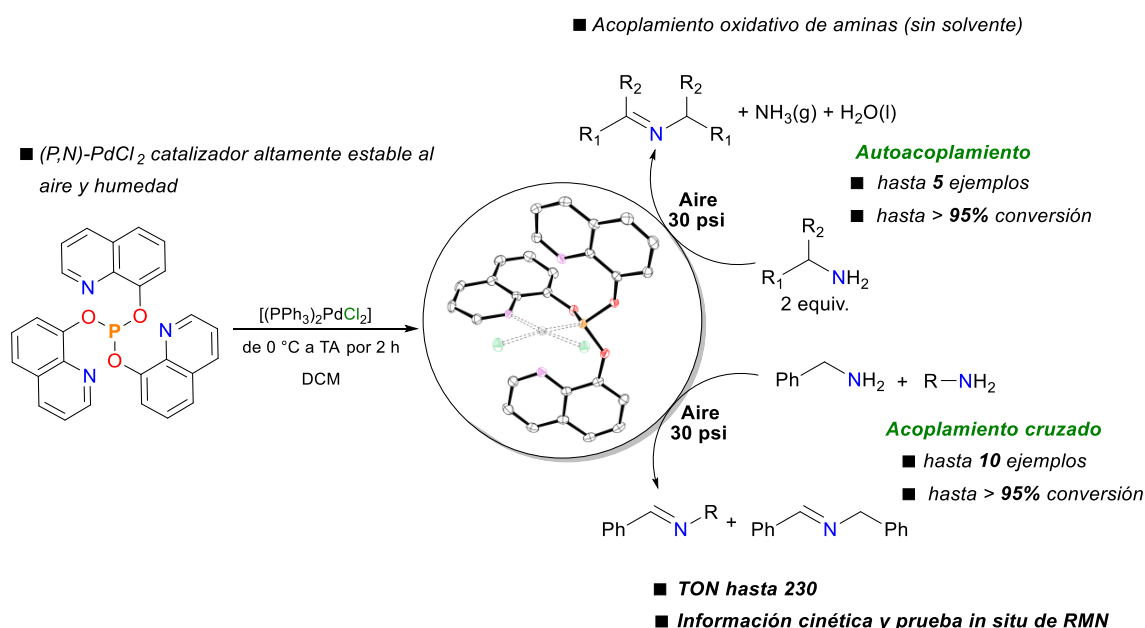


Figura R2. Síntesis de un nuevo complejo de Pd (II) que lleva  $\text{P}(\text{OQuin})_3$  y su aplicación catalítica en el acoplamiento oxidativo de aminas primarias.

Esta metodología evita el uso de oxidantes peligrosos, aditivos, altas temperaturas o solventes orgánicos. Otras aminas primarias son transformadas en sus iminas correspondientes con rendimientos moderados. Se logró el acoplamiento cruzado de bencilamina con anilinas sustituidas para producir aldiminas. El catalizador se puede recuperar de la mezcla de reacción y ser reutilizado en una próxima ronda sin pérdida significativa de su actividad.

Mientras que en el CAPITULO IV, dos nuevos complejos metálicos de Rh (I) con  $P(OQuin)_3$  han sido aislados y completamente caracterizados.  $[\kappa^2(P,N)\{P(OQuin)_3\}Rh\{P(R)_3\}Cl]$  (R= Ph, Cy) (PN-RhPh y PN-RhCy) se pueden obtener de diferentes precursores de Rh (I) como material de partida. PN-RhPh tiene un comportamiento dinámico a temperatura variable y  $PPh_3$  disocia, saliendo de la esfera de coordinación. Una quinolina no coordinada de  $P(OQuin)_3$  puede ocupar el puesto de coordinación vacío y así generar un modo tridentado de  $P(OQuin)_3$ ,  $[\kappa^3(N,P,N)RhCl]$ . PN-RhCy se obtiene mediante un intercambio de ligando  $PPh_3/PCy_3$  utilizando PN-RhPh como material de partida. PN-RhPh es un catalizador muy eficiente para la hidroborcación quimioselectiva-1,2 de piridinas. Esta reacción se lleva a cabo en condiciones suaves, 0,5 mol% [PN-RhPh], relación Py/BH 1:1.1 a 50 °C, produciendo las N-boryl-1,2-dihidropiridinas con hasta un >95% de conversión y 95% de regioselectividad. Bajo esta metodología, una serie de quinolinas son reducidas con los mismos porcentajes de rendimiento y selectividad. Esta metodología representa el mejor sistema reportado para la hidroborcación de piridinas catalizadas por un complejo de metal de transición tardío.

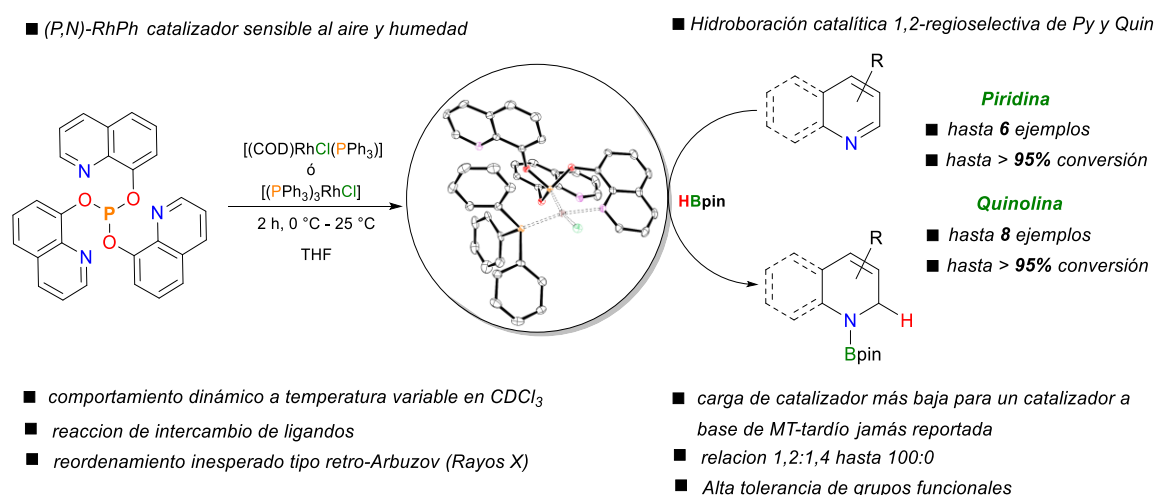


Figura R3. Síntesis de un nuevo complejo de Rh (I) y su aplicación en la hidroborcación 1,2-regioselectiva de piridinas y quinolinas sustituidas.

Finalmente, en el CAPÍTULO V, dos nuevos complejos metálicos de Ru (II) que llevan  $P(OQuin)_3$  como ligando principal han sido aislados y completamente caracterizados.

$[\kappa^3(\text{N,P,N})\{\text{P}(\text{OQuin})_3\}\text{Ru}\{\text{PPh}_3\}\text{Cl}_2]$  puede formar isómeros en solución y estos han sido determinados por difracción de rayos X con una configuración meridional (*mer*) y facial (*fac*).  $[\kappa^3(\text{N,P,N})\{\text{P}(\text{OQuin})_3\}\text{Ru}\{\text{PPh}_3\}\text{Cl}_2]$  tiene el mismo comportamiento dinámico del complejo de Rh (I)  $[\kappa^2(\text{P,N})\{\text{P}(\text{OQuin})_3\}\text{Rh}\{\text{P}(\text{R})_3\}\text{Cl}]$  a temperatura variable y un nuevo complejo con un modo tetradentado de  $\text{P}(\text{OQuin})_3$  es obtenido  $[(\kappa^4\text{-P,N}_3)\text{RuCl}_2]$  ( $\text{PN}_3\text{-Ru}$ ). Dado que los polímeros a base de silicio con alto peso molecular son importantes en el desarrollo de nuevos materiales y derivatización de superficies,  $\text{PN}_3\text{-Ru}$  resultó ser un catalizador eficiente para el acoplamiento deshidrogenativo de silanos con o sin alcoholes para producir polisilanos y polisiloxanos, respectivamente, obteniendo polímeros de alto peso molecular con rendimientos mayores al 95%. Catalizadores a base de metales de transición tempranos los cuales han sido hasta ahora los más eficientes para dicha reactividad, con frecuencia requieren el uso de aditivos como  $n\text{BuLi}$ , esta metodología basada en  $\text{PN}_3\text{-Ru}$ , evita su uso o de cualquier otro aditivo.

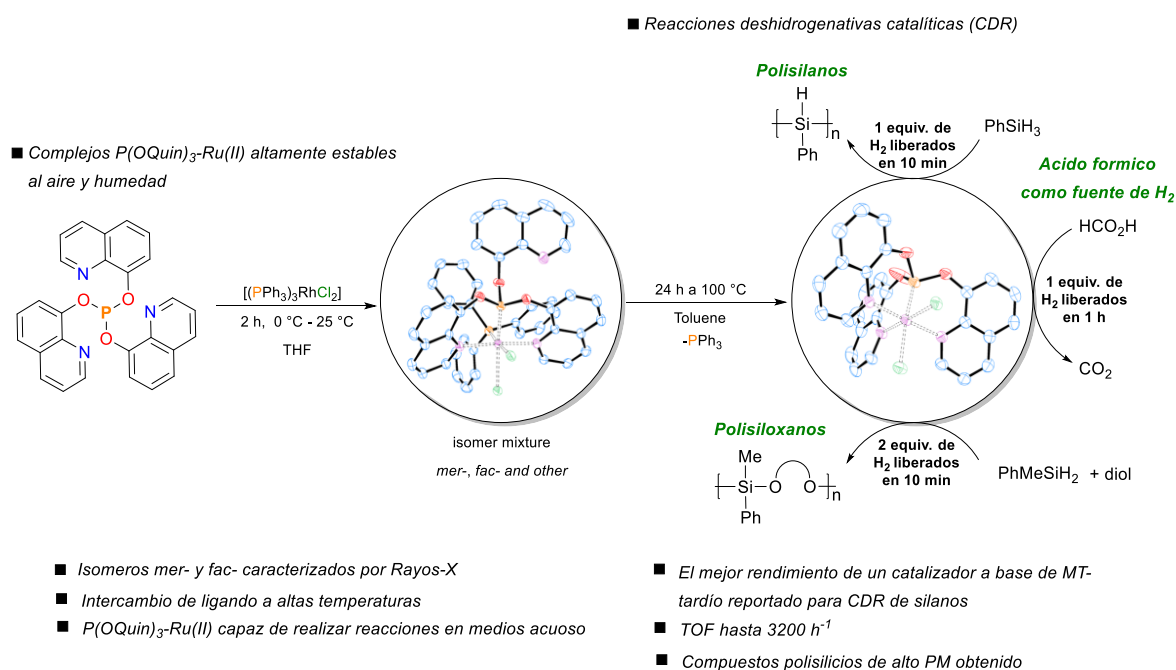


Figura R4. Síntesis de nuevos complejos de Ru (II) y sus aplicaciones en reacciones deshidrogenativas.

## ZUSAMMENFASSUNG

Die Fähigkeit vieler Übergangsmetallkomplexe, organische Reaktionen (in der homogenen Phase) zu katalysieren, ist eine der wirksamsten Strategien, um das Problem der "idealen" Synthese anzugehen. Durch die Wahl des Übergangsmetalls und die Möglichkeit, einen bestimmten Liganden rational zu entwerfen, können die sterischen und elektronischen Eigenschaften von Metallkomplexen so eingestellt werden, dass eine optimale Selektivität und Effizienz einer bestimmten Reaktion erreicht wird. In den letzten 60 Jahren hat die Zunahme der Arbeiten im Zusammenhang mit der Chemie der Übergangsmetalle zu großen Fortschritten bei der homogenen Katalyse geführt. Ein Teil dieser Erfolge ist auf die grundlegende Rolle zurückzuführen, die die Phosphorligandenchemie bei einer unzähligen katalytischen Prozessen gespielt hat. Diese hat stark zur breiten Entwicklung des Gebiets der homogenen Katalyse beigetragen, welche eines der wichtigsten Werkzeuge in der organischen Synthese und der industriellen Herstellung einer Vielzahl chemischer Produkte darstellt.

Diese Arbeit befasst sich mit der Synthese des neuen Tris(8-quinoliny)phosphits ( $\text{P(OQuin)}_3$ , **1**) und seiner Reaktivität gegenüber Metallprecursoren der Gruppen 8, 9 und 10. Sowohl  $\text{P(OQuin)}_3$  als auch seine Koordinationsverbindungen werden in Reaktionen zur Bildung von interessierenden organischen Verbindungen bewertet.  $\text{P(OQuin)}_3$  hat ein Phosphoratom, das stark an ein Metall koordiniert werden kann, und drei Chinolingruppen, in denen Stickstoffatome vorhanden sind, die schwach koordiniert werden können. Es wird erwartet, dass  $\text{P(OQuin)}_3$  hemilabile Koordinationseigenschaften aufweist. Der hemilabile Charakter wird durch die Konkurrenz zwischen drei Chinolingruppen beeinflusst.

Das Literaturstudium zeigt, dass Phosphite in katalytisch aktiven Metallkomplexen weit verbreitet sind, aber sie wurden sehr selten selbst als Katalysator genutzt. Andererseits werden Transferhydrierungsreaktionen üblicherweise durch Edelmetalle katalysiert, für die Krustenhäufigkeit, Kosten und Toxizität bedeutende Probleme sind. In diesem Sinne wird in KAPITEL II die Synthese und Charakterisierung des neuen sperrigen  $\text{P(OQuin)}_3$  beschrieben und seine Anwendung als Präkatalysator bei einer metallfreien Transferhydrierung untersucht.  $\text{P(OQuin)}_3$  fördert die Dehydrierung von  $\text{H}_3\text{N}\cdot\text{BH}_3$  (**AB**) und die Reduktion von symmetrischen / asymmetrischen Azoarenen unter Verwendung von **AB** als  $\text{H}_2$ -Quelle und erzielt wirklich gute Ausbeuten (bis zu 95%). Mechanistische Studien legen nahe, dass  $\text{P(OQuin)}_3$  als Präkatalysator fungiert, und kinetische Studien zeigen (DKIEs), dass der Transfer von protischem Wasserstoff und Hydridwasserstoff von **AB** gleichzeitig im Übergangszustand mit einer negativen Reaktionsentropie  $\Delta S^\ddagger = -31$  eu erfolgt. Im Rahmen

einer nachhaltigen Chemie erfüllt das System mindestens 6 von 12 Prinzipien der grünen Chemie.

■ Eintopfreaktion im Multigramm-Maßstab

■ Katalytische Transferhydrierung

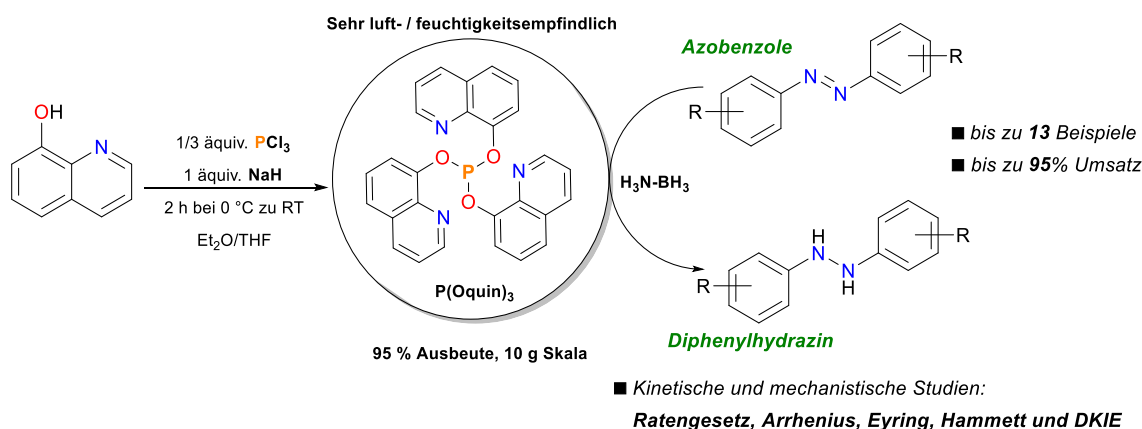


Abbildung Z1. Synthese von  $\text{P}(\text{OQuin})_3$  und seine Anwendung bei der organokatalytischen Reduktion von Azoarenen unter Verwendung von Ammoniakboran als  $\text{H}_2$ -Quelle.

In KAPITEL III wurde ein neuer  $\text{Pd}(\text{II})$ -Metallkomplex mit  $\text{P}(\text{OQuin})_3$  isoliert und vollständig charakterisiert. Eine Röntgenstrukturanalyse zeigt, dass der Ligand  $\text{P}(\text{OQuin})_3$  das erwähnte Metallzentrum als zweizähniges P-N-Chelat bindet.

■ Katalytische lösungsmittelfreie oxidative Kupplung von Aminen

■  $(\text{P},\text{N})$ - $\text{PdCl}_2$  Katalysator hoch luft- / feuchtigkeitsstabil

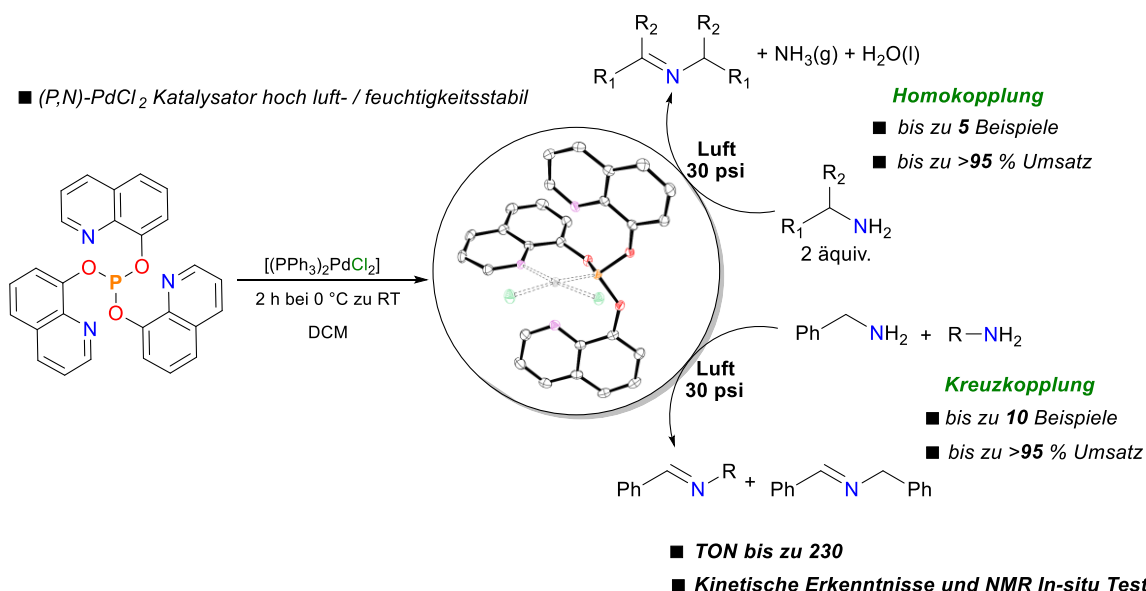


Abbildung Z2. Synthese des neuen  $\text{Pd}(\text{II})$ -Komplexes mit  $\text{P}(\text{OQuin})_3$  und dessen katalytische Anwendung bei der oxidativen Kupplung von primären Aminen.

Die Komplexe  $[\text{Pd}\{\text{P}(\text{OQuin})_3\}\text{Cl}_2]$  sind ein wirksamer Katalysator für die oxidative Kupplung von Benzylamin an N-Benzylidenbenzylamin unter Verwendung von Luft als terminalem Oxidationsmittel. Diese Methode vermeidet die Verwendung gefährlicher

Oxidationsmittel, Additive, hohe Temperaturen und organische Lösungsmittel. Andere primäre Amine können mit moderaten Ausbeuten in ihre entsprechenden Imine umgewandelt werden. Die Kreuzkupplung von Benzylamin mit substituierten Anilinen führt zu Aldiminen. Der Katalysator kann aus dem Reaktionsgemisch zurückgewonnen werden und wurde im nächsten Lauf ohne signifikanten Verlust seiner Aktivität wiederverwendet.

In KAPITEL IV wurden zwei neue Rh(I) -Metallkomplexe mit  $P(OQuin)_3$  isoliert und vollständig charakterisiert.  $[(\kappa^2-P,N)\{P(OQuin)_3\}Rh\{PR_3\}Cl]$  ( $R = Ph, Cy$ ) (PN-RhPh und PN-RhCy) kann aus verschiedenen Rh(I)-Verbindungen erhalten werden. PN-RhPh zeigt ein dynamisches Verhalten bei variabler Temperatur und  $PPh_3$  kann die Koordinationssphäre verlassen. Ein unkoordinierter Chinolinrest von  $P(OQuin)_3$  kann die freie Koordinationsstelle besetzen und einen trikoordinierten Modus von  $P(OQuin)_3$ ,  $[(\kappa^3-N,P,N)RhCl]$  ergeben. PN-RhCy wird durch einen Ligandenaustausch  $PPh_3 / PCy_3$  unter Verwendung von PN-RhPh als Ausgangsmaterial erhalten. PN-RhPh ist ein sehr effizienter Katalysator für die 1,2-chemoselektive Hydroborierung von Pyridinen. Diese Reaktion wird unter milden Bedingungen, 0,5 mol% [Rh], Verhältnis Py / BH 1: 1,1 bei 50 °C durchgeführt, wobei die N-Boryl-1,2-dihydropyridine mit 100% Umwandlung und 95 % Regioselektivität erhalten werden. Diese Methode stellt das beste, bisher bekannte System dar für die durch späte Übergangsmetalle katalysierte Hydroborierung von Pyridinen dar.

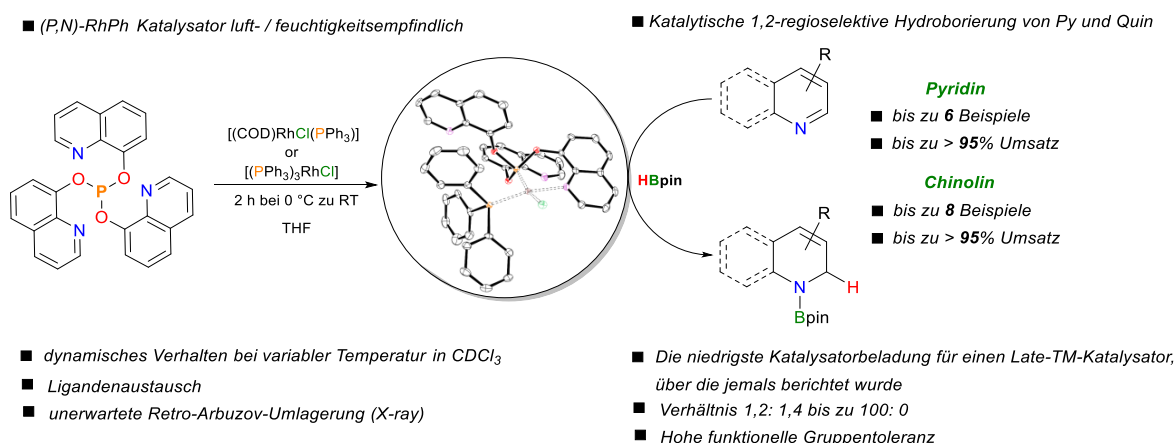


Abbildung Z3. Synthese des neuen Rh(I)-Komplexes mit  $P(OQuin)_3$  und dessen Anwendung bei der 1,2-regioselektiven Hydroborierung substituierter Pyridine und Chinoline.

Schließlich wurden in KAPITEL V zwei neue Ru(II) -Metallkomplexe mit  $P(OQuin)_3$  isoliert und vollständig charakterisiert.  $[(\kappa^3-N,P,N)\{P(OQuin)_3\}Ru\{PPh_3\}Cl_2]$  hatte das gleiche dynamische Verhalten wie die in KAPITEL IV beschriebenen Rh(I)-Komplexe und bildet einen neuen Komplex  $[(\kappa^4-N,N,P,N)RuCl_2]$  ( $PN_3$ -Ru) mit einem tetrakoordinierten Modus von  $P(OQuin)_3$ .  $PN_3$ -Ru erwies sich als effizienter Katalysator für die dehydrierende



Kupplung von Silanen ohne und mit Alkoholen, um Polysilane bzw. Polysiloxane zu erhalten. Hierbei wurden Polymere mit hohem Molekulargewicht in >95% Ausbeute erhalten.  $\text{PN}_3\text{-Ru}$  ist eine interessante Alternative zu frühen Übergangsmetallkatalysatoren, bei denen häufig ein Additiv wie  $n\text{BuLi}$  verwendet werden muss.

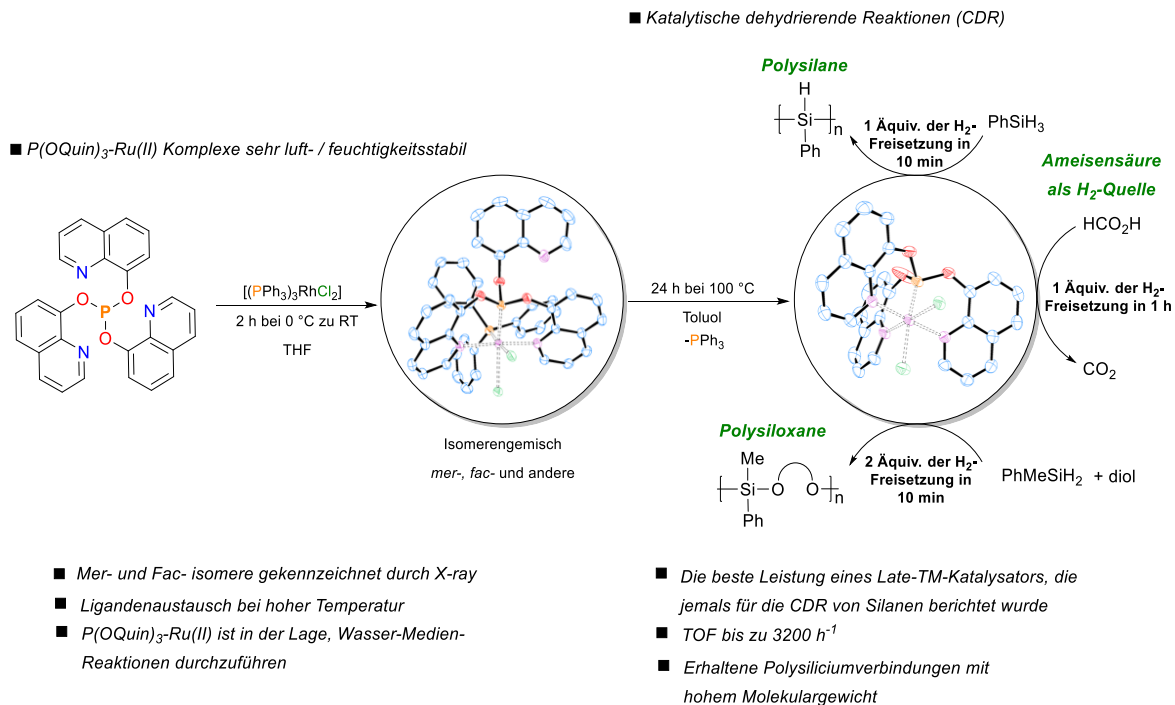


Abbildung Z4. Synthese neuer  $\text{Ru(II)}$ -Komplexe mit  $\text{P}(\text{OQuin})_3$  und Anwendung in dehydrierenden Reaktionen.

## ABBREVIATIONS AND SYMBOLS

MeCN	Acetonitrile	h	Hours
H <sub>3</sub> N•BH <sub>3</sub>	Amineborane	H <sub>2</sub>	Hydrogen
Å	Angstrom	iPr	<i>iso</i> -propyl
BnNH <sub>2</sub>	Benzylamine	MHz	Megahertz
β <sub>n</sub>	Bite angle	mp	Melting point
BCP	Bond critical point	OMe	Methoxy
br	Broad	Me	Methyl
cm	Centimeter	μL	Microliter
δ	Chemical shift in ppm	mg	Milligrams
<i>J</i>	Coupling constant	mL	Milliliter
Cy	Cyclohexane	mmol	Millimol
COD	1,5-Cyclooctadiene	min	Minutes
COE	Cyclooctene	m	Multiplet
DCM	Dichloromethane	nm	Nanometer
Et <sub>2</sub> O	Diethyl ether	<i>n</i> Bu	<i>n</i> -Butyl
°	Degree	NMR	Nuclear magnetic resonance
°C	Degree Celsius	<i>o</i> -Tol	<i>ortho</i> -toluene
K	Degree Kelvin	OQuin	8-oxy-quinoline
iPr <sub>2</sub> N	di-isopropylamine	ppm	Part <i>per</i> million
DMSO	Dimethyl sulfoxide	OPh	Phenoxy
<i>d</i>	Doublet	Ph	Phenyl
DKIE	Deuterated kinetic isotopic effect	Py	Pyridine
EDG	Electron-donating group	RT	Room temperature
EWG	Electron-withdrawing groups	s	Singlet
ν	Frequency in cm <sup>-1</sup>	IR	Spectroscopy infrared
g	Grams	<i>t</i> Bu	<i>tert</i> -Butyl
Hz	Hertz	THF	Tetrahydrofuran

## LIST OF CONTENTS

<b>DEDICATION .....</b>	<b>VII</b>
<b>ACKNOWLEDGEMENTS.....</b>	<b>VIII</b>
<b>ABSTRACT .....</b>	<b>IX</b>
<b>RESUMEN.....</b>	<b>XIII</b>
<b>ZUSAMMENFASSUNG .....</b>	<b>XVII</b>
<b>ABBREVIATIONS AND SYMBOLS.....</b>	<b>XXI</b>
<b>CHAPTER I. Phosphite-Nitrogen Ligands: Preparation, coordination chemistry and applications in homogeneous catalysis.....</b>	<b>34</b>
1.1    General Information. ....	35
1.2    Phosphite ligands. ....	36
1.3    Phosphite-Nitrogen ligands. ....	37
1.4    Coordination chemistry of 8-oxyquinoline containing phosphorus ligands with second-row metal centers of group 8,9 and 10. ....	41
1.5    Catalytic application of Phosphite-Nitrogen ligands. ....	49
1.6    Outline .....	55
1.7    Objectives .....	56
1.7.1    General Aim.....	56
1.7.2    Specific Aim. ....	56
<b>CHAPTER II. Tris(8-quinoliny)phosphite: Synthesis, characterization and its organocatalytic application on transfer hydrogenation of azocompounds.....</b>	<b>57</b>
2.1    Introduction.....	58
2.2    Synthesis of Tris(8-quinoliny)phosphite, P(OQuin) <sub>3</sub> , <b>1</b> .....	60
2.3    Reactivity of Tris(8-quinoliny)phosphite towards H <sub>3</sub> NBH <sub>3</sub> as hydrogen source.....	65
2.4    Reduction of azocompounds catalyzed by P(OQuin) <sub>3</sub> .....	68
2.5    Kinetic studies for the reduction of azocompounds catalyzed by P(OQuin) <sub>3</sub> . ....	75
2.6    Chapter conclusions. ....	84

2.7	Experimental Section .....	85
<b>CHAPTER III. Pd(II)-coordination chemistry of P(OQuin)<sub>3</sub>. Application in the catalytic aerobic oxidation of amines .....</b>		
		91
3.1	Introduction.....	92
3.2	Synthesis and characterization of the Pd(II) complex.....	93
3.3	Oxidative coupling of primary amines catalyzed by the complex Pd-P(OQuin) <sub>3</sub> .	96
3.4	Kinetic studies for the oxidative coupling of primary amines catalyzed by the Pd-P(OQuin) <sub>3</sub> complex. ....	104
3.5	<i>In situ</i> NMR experiments: reactivity of the Pd(II) complex <b>4</b> with benzylamine	108
3.6	Chapter conclusions .....	113
3.7	Experimental section. ....	114
<b>CHAPTER IV. Rh(I)-coordination chemistry of P(OQuin)<sub>3</sub>. Application in the regioselective 1,2-hydroboration of pyridines and quinolines .....</b>		
		122
4.1	Introduction.....	123
4.2	Synthesis and characterization of the Rh(I) complex .....	124
4.3	Reactivity of the Rh(I) complex <b>11</b> toward different external agents (NMR scale).....	130
4.4	Regioselective 1,2-hydroboration of pyridines and quinolines catalyzed by <b>11</b> .	138
4.5	Chapter conclusion.....	146
4.6	Experimental section. ....	147
<b>CHAPTER V. Ru(II)-coordination chemistry of P(OQuin)<sub>3</sub>. Application in dehydrogenative reactions.....</b>		
		153
5.1	Introduction.....	154
5.2	Synthesis and characterization of the Ru(II) complex .....	155
5.3	Hydroamination of alkynes catalyzed by new Ru(II) complexes. ....	170
5.4	Catalytic decomposition of formic acid as H <sub>2</sub> source by new Ru(II) complexes.	170
5.5	Homo-/Heterodehydrocoupling reaction of silanes catalyzed by new Ru(II) complexes. ....	173
5.6	Chapter conclusion.....	178

5.7	Experimental section.....	178
<b>SUMMARY AND OUTLOOK .....</b>		<b>184</b>
<b>REFERENCES .....</b>		<b>186</b>

## LIST OF FIGURE

Figure 1.1 Trivalent phosphorus compounds.....	36
Figure 1.2. a) General reaction for phosphite synthesis (above). b) General structures of symmetric and asymmetric phosphites reported in the literature (below).....	36
Figure 1.3. Cone angle illustration, $\theta$ (left) and the bite angle, $\beta_n$ (right) in a generic organophosphorus-metal complex. ....	37
Figure 1.4. Phosphorus ligands with different coordination modes.....	38
Figure 1.5. A hybrid ligand contains two chemically different donor functions (left). Coordination modes of hybrid ligands (right).....	38
Figure 1.6. a) General characteristics of a ligand P, N. b) <i>Trans</i> effect and its implication on nucleophilic substitution. ....	39
Figure 1.7. Reported phosphorus compounds bearing the 8-oxy-quinoline unit.....	40
Figure 1.8. Structural difference of metal complexes with monofunctional and hybrid phosphorus ligands. ....	41
Figure 1.9. Molecular structure of $[\text{RuCp}(\text{PNquin-BIPOL})(\text{CH}_3\text{CN})]\text{PF}_6 \cdot \frac{1}{2}(\text{C}_2\text{H}_5)_2\text{O}$ ( <b>Rc</b> ) showing 50% displacement ellipsoids (PF <sub>6</sub> , Hydrogens and solvent were omitted for clarity).....	43
Figure 1.10. View of the molecular structure of the complex <b>Ub<sup>a</sup></b> with the atomic numbering system. The ellipsoids are drawn at the 30% probability level.....	45
Figure 1.11. An ORTEP drawing of complex <b>V</b> showing the atom labelling scheme and thermal ellipsoids at 40% probability level. Hydrogen atoms and the BF <sub>4</sub> anion are omitted for clarity.....	47
Figure 1.12. An ORTEP drawing of complex <b>Wa</b> showing the atom labelling scheme and thermal ellipsoids at 40% probability level. Hydrogen atoms are omitted for clarity. ....	49
Figure 1.13. Taddol-based phosphite-oxazoline. Summary of the best results obtained .....	50
Figure 1.14. Phosphite-oxazole/thiazole ligand library.....	51
Figure 1.15. Ferrocenyliminophosphites ligands .....	51
Figure 1.16. Phosphite-oxazoline ligands <b>A1-3</b> .....	52
Figure 1.17. Summary of the best results obtained in the Pd-catalyzed allylic substitution using ligands <b>A1-3a-c</b> . ....	53

Figure 1.18. Cu-catalyzed enantioselective 1,4-addition of diethylzinc to cyclohex-2-enone.	55
Figure 2.1. a) $^{31}\text{P}\{^1\text{H}\}$ NMR and b) $^1\text{H}$ NMR spectra of $\text{P}(\text{OQuin})_3$ at RT in $\text{THF-d}_8$ .	62
Figure 2.2. ORTEP drawing of the molecular structure of the phosphite ligand tris(8-quinoliny)phosphite, $\text{P}(\text{OQuin})_3$ . Thermal ellipsoids are drawn at the 50% probability level. Hydrogen atoms have been neglected for clarity. Two independent molecules <i>per</i> asymmetric unit were found.	63
Figure 2.3. Packing of the molecules in the unit cell: $\pi$ -stacking between proximal <i>N</i> -heterocyclic rings in each one of the independent molecules.	63
Figure 2.4. $^{11}\text{B}$ NMR spectrum of a 1:5 reaction mixture of <b>1</b> + <b>AB</b> after 12 h at 60 °C (blue), isolated $\text{HB}(\text{OQuin})_2$ (green), isolated $\text{H}_2\text{BOQuin}$ (red).	71
Figure 2.5. Azobenzene concentration as a function of time during the first 14 h of reaction.	75
Figure 2.6. Representation of $\text{Ln}([\text{AZB}]/[\text{AZB}]_0)$ vs. time.	76
Figure 2.7. Representation of $\text{Ln}(r)$ as a function of $\text{Ln}[\text{AZB}]$ .	77
Figure 2.8. $\text{Ln}(r)$ as a function of $\text{Ln}[\text{precat}]$ .	78
Figure 2.9. $\text{Ln} [\text{AZB}]$ at different temperatures vs. time.	79
Figure 2.10. Eyring plot for TH of azobenzene catalyzed by $\text{P}(\text{OQuin})_3$ . Based on respective equations, activation thermodynamic parameters were determined.	80
Figure 2.11. Arrhenius plot for TH of azobenzene catalyzed by $\text{P}(\text{OQuin})_3$ . Based on respective equation activation energy was determined.	81
Figure 2.12. Deuterated kinetic isotopic effect (DKIE's) on reaction rate for the TH of azobenzene with deuterated ammonia boranes.	82
Figure 2.13. Representation $\text{Log}(r)$ vs substituent constant ( $\sigma$ ). $\rho = 1.26$ .	83
Figure 2.14. $^1\text{H}$ NMR spectrum (300.1 MHz) of <b>3a</b> in $\text{CD}_3\text{CN}$ .	83
Figure 2.15. $^{13}\text{C}\{^1\text{H}\}$ NMR spectrum (75.5 MHz) of <b>3a</b> in $\text{CD}_3\text{CN}$ .	83
Figure 3.1. a) $^{31}\text{P}\{^1\text{H}\}$ NMR spectrum (121.5 MHz) and b) $^1\text{H}$ NMR spectrum (300.1 MHz) at 298 K of <b>4</b> in $\text{CDCl}_3$ .	94
Figure 3.2. ORTEP drawing of the molecular structure of the complex $[\text{Pd}\{\text{P}(\text{OQuin})_3\}\text{Cl}_2]$ , <b>4</b> . Thermal ellipsoids are drawn at 50% probability level. Hydrogen atoms and a dichloromethane solvate molecule have been removed for clarity.	95

Figure 3.3. Decreasing benzylamine concentration during the first 5 h of reaction. ....	104
Figure 3.4. $\ln([\text{BnNH}_2]/[\text{BnNH}_2]_0)$ vs. time. Conditions: 0.5 mol L <sup>-1</sup> of benzylamine, 1 mol% catalyst, atmospheric pressure, 80 °C, toluene, 1,3,5-trimethoxybenzene (242.2 mg, 1.4 mmol in 5.6 mL) as the internal standard. ....	105
Figure 3.5. Representation $\log([\text{BnNH}_2])$ vs. $\log(r)$ . Conditions: 0.5, 1.0, 1.5 and 4.8 mol L <sup>-1</sup> benzylamine (max. 4.8 mmol), 0.015 mol L <sup>-1</sup> catalyst (9.6 mg, 15 µmol), 130 psi air (98 mL, ca. 7.45 mmol O <sub>2</sub> ), 60 °C, 2 h, toluene, 1,3,5-trimethoxybenzene (84.1 mg, 0.5 mmol in 1.0 mL) as the internal standard. ....	106
Figure 3.6. Representation $\log([4])$ vs. $\log(r)$ . ....	107
Figure 3.7. Representation of $r$ vs. $[\text{BnNH}_2][\text{cat}] = P$ . Conditions: 5 mol L <sup>-1</sup> benzylamine (1.4 mmol in 0.28 mL), 0.05, 0.1, 0.15 and 0.2 mol L <sup>-1</sup> catalyst, 130 psi air (98 mL, ca. 7.45 mmol O <sub>2</sub> ), 60 °C, 2 h, toluene, 1,3,5-trimethoxybenzene (11.8 mg, 0.07 mmol) as the internal standard. ....	108
Figure 3.8. Complex <b>4</b> in neat benzylamine: <i>in situ</i> NMR monitoring by <sup>31</sup> P{ <sup>1</sup> H} NMR (121.5 MHz). a) Inert atmosphere, room temperature, < 5 minutes after mixing <b>4</b> and BnNH <sub>2</sub> ; b) Inert atmosphere, 1 h at 60 °C; c) 40 psi air, 60 °C, < 5 minutes after loading the air pressure; d) 40 psi air, 60 °C, 1 h after loading the air pressure. ....	109
Figure 3.9. Stoichiometric test <b>4</b> + benzylamine: <i>in situ</i> NMR monitoring by <sup>31</sup> P{ <sup>1</sup> H} NMR (121.5 MHz). a) Inert atmosphere, room temperature, < 5 minutes after mixing <b>4</b> and BnNH <sub>2</sub> ; b) Inert atmosphere, 2 h at 60 °C; c) 40 psi air, 60 °C, 4 h after loading the air pressure; d) 40 psi air, 60 °C, 16 h after loading the air pressure. ....	110
Figure 3.10. <sup>31</sup> P{ <sup>1</sup> H} NMR spectrum (121.5 MHz) at 298 K of <b>9</b> in CD <sub>2</sub> Cl <sub>2</sub> . ....	111
Figure 3.11. <sup>1</sup> H NMR spectra of <b>9</b> at variable temperature (600.0 MHz, CD <sub>2</sub> Cl <sub>2</sub> ). ....	111
Figure 3.12. <sup>31</sup> P{ <sup>1</sup> H} NMR spectra of <b>9</b> at variable temperature (121.5 MHz, CD <sub>2</sub> Cl <sub>2</sub> ). ....	112
Figure 3.13. <sup>31</sup> P{ <sup>1</sup> H} NMR spectra of <b>10</b> (121.5 MHz, CD <sub>2</sub> Cl <sub>2</sub> ). ....	113
Figure 3.14. <sup>1</sup> H (300 MHz) NMR spectra at 298 K of isolated <b>6a</b> in CDCl <sub>3</sub> . ....	113
Figure 3.15. <sup>13</sup> C{ <sup>1</sup> H}-APT (75.5 MHz) NMR spectra at 298 K of isolated <b>6a</b> in CDCl <sub>3</sub> . ....	113
Figure 3.16. <sup>1</sup> H (300 MHz) NMR spectra at 298 K of <b>8a</b> crude in CDCl <sub>3</sub> . ....	113
Figure 3.17. <sup>13</sup> C{ <sup>1</sup> H}-APT (75.5 MHz) NMR spectra at 298 K of isolated <b>8a</b> in CDCl <sub>3</sub> . ....	113
Figure 4.1. a) <sup>31</sup> P{ <sup>1</sup> H} NMR spectrum (121.5 MHz) at 298 K of <b>11</b> in CDCl <sub>3</sub> . b) <sup>1</sup> H NMR spectrum (300.1 MHz) at 298 K of <b>11</b> in CDCl <sub>3</sub> . ....	125



Figure 4.2. ORTEP drawing of the molecular structure of the complex $[\kappa^2(P,N)\{P(OQuin)_3\}RhCl(PPh_3)]$ , <b>11<sup>a</sup></b> . Thermal ellipsoids are drawn at 50% probability level. Hydrogen atoms and a dichloromethane solvate molecule have been removed for clarity. .	127
Figure 4.3. ORTEP drawing of the molecular structure of the complex $[\kappa^2(P,N)\{P(OQuin)_3\}RhCl(PPh_3)]$ , <b>11<sup>b</sup></b> . Thermal ellipsoids are drawn at 40% probability level. Hydrogen atoms and THF/Et <sub>2</sub> O solvate molecules have been removed for clarity.....	128
Figure 4.4. $^{31}P\{^1H\}$ NMR spectrum (121.5 MHz) at 323 K of <b>11</b> in CDCl <sub>3</sub> at different time until full conversion on <b>12</b> .....	131
Figure 4.5. ORTEP drawing of the molecular structure of the complex $[\kappa^3(P,N,N)\{OP(OQuin)_2\}RhCl_2(PPh_3)]$ , <b>13</b> . Thermal ellipsoids are drawn at 40% probability level. Hydrogen atoms have been removed for clarity.....	133
Figure 4.6. $^{31}P\{^1H\}$ NMR spectrum (121.5 MHz) at 298 K of a) <b>11</b> , b) reaction mixture of <b>11</b> +PCy <sub>3</sub> after 3 h at RT and c) <b>14</b> in THF-d <sub>8</sub> .....	135
Figure 4.7. $^1H$ NMR spectrum (300.1 MHz) at 298 K of <b>14</b> in THF-d <sub>8</sub> .....	135
Figure 4.8. ORTEP drawing of the molecular structure of the complex $[\kappa^2(P,N)\{P(OQuin)_3\}RhCl(PCy_3)]$ , <b>14</b> . Thermal ellipsoids are drawn at the 50% probability level. Hydrogen atoms and THF solvate molecules have been removed for clarity. Two independent molecules <i>per</i> asymmetric unit were found. The values reported for selected bond distances and angles correspond to the average of both independent molecules.....	137
Figure 4.9. $^{31}P\{^1H\}$ NMR spectrum (121.5 MHz) at 298 K of a) <b>11</b> , b) reaction mixture of <b>11</b> + 1.1 equiv. of NaPF <sub>6</sub> after 3 h at RT and c) reaction mixture of <b>11</b> + 1.1 equiv. of NaPF <sub>6</sub> after 24 h at 50 °C in THF-d <sub>8</sub> .....	135
Figure 5.1. $^{31}P\{^1H\}$ NMR spectrum (121.5 MHz) at 298 K of reaction mixture 1+ [(PPh <sub>3</sub> ) <sub>3</sub> RuCl <sub>2</sub> ] in THF with an inner of C <sub>6</sub> D <sub>6</sub> . ....	156
Figure 5.2. a) $^{31}P\{^1H\}$ NMR spectrum (121.5 MHz) at 298 K of <b>11</b> in CDCl <sub>3</sub> . b) $^1H$ NMR spectrum (300.1 MHz) at 298 K of <b>18</b> in CD <sub>2</sub> Cl <sub>2</sub> . ....	158
Figure 5.3. $^1H$ - $^1H$ COSY NMR spectrum (300.1 MHz) at 298 K of <b>18</b> in CDCl <sub>3</sub> . ....	159
Figure 5.2. a) $^{31}P\{^1H\}$ NMR spectrum (121.5 MHz) at 298 K of <b>19</b> in CDCl <sub>3</sub> . b) $^1H$ NMR spectrum (300.1 MHz) at 298 K of <b>18</b> in CD <sub>2</sub> Cl <sub>2</sub> . ....	166

Figure 5.4. ORTEP drawing of the molecular structure of the complex [ <i>mer</i> - $\kappa^3(N,P,N)\{P(OQuin)_3\}RuCl_2(PPh_3)$ ], <b>18</b> . Thermal ellipsoids are drawn at 40% probability level. Hydrogen atoms and THF solvate molecule have been removed for clarity. ....	163
Figure 5.5. ORTEP drawing of the molecular structure of the complex [ <i>fac</i> - $\kappa^3(N,P,N)\{P(OQuin)_3\}RhCl(PPh_3)$ ], <b>18<sup>B</sup></b> . Thermal ellipsoids are drawn at 50% probability level. Hydrogen atoms and DCM and Et <sub>2</sub> O solvate molecules have been removed for clarity.....	164
Figure 5.5. ORTEP drawing of the molecular structure of the complex [ $\kappa^4(P,N_3)\{P(OQuin)_3\}RhCl(PPh_3)$ ], <b>19</b> . Thermal ellipsoids are drawn at 40% probability level. Hydrogen atoms and THF/Et <sub>2</sub> O solvate molecules have been removed for clarity.....	167
Figure 5.6. Technical set-up for HCO <sub>2</sub> H conversion in an open system. The production of H <sub>2</sub> can be monitored with a gas burette. ....	171
Figure 5.7. The graph displays hydrogen formation from formic acid decomposition (Scheme 5.4).....	172
Figure 5.8. The graph displays hydrogen formation in time from dehydrocoupling of phenylsilane (Scheme 5.5).....	174
Figure 5.9. a) <sup>1</sup> H NMR spectrum (300.1 MHz) and b) <sup>29</sup> Si{ <sup>1</sup> H} NMR spectrum (71.5 MHz) at 298 K of isolated polymeric material in CDCl <sub>3</sub> . ....	176

## LIST OF SCHEME

Scheme 1.1 Synthesis pathway of Ru-complexes <b>Ra-c</b> .	42
Scheme 1.2. Synthesis pathway of Ru-complexes <b>Sa-c</b> .	43
Scheme 1.3. Synthesis pathway of Ru-complexes <b>Ta-b</b> .	44
Scheme 1.4. Synthesis pathway of Pd-complex <b>V</b> .	46
Scheme 1.5. Synthesis pathway of Pd-complex <b>Wa-c</b> .	48
Scheme 1.6. Two classes of asymmetric allylic substitution reactions.	52
Scheme 1.7. Key Pd-Allyl intermediates containing monosubstituted substrates.	53
Scheme 1.8. Suzuki-Miyaura coupling using palladium complexes <b>V</b> and $[(N)PdCl_2]$ .	54
Scheme 2.1. Cyclic phosphorus compounds used in catalytic transfer hydrogenation (TH) from different H <sub>2</sub> sources to unsaturated bonds.	59
Scheme 2.2. General reaction for the synthesis of $P(OQuin)_3$ .	60
Scheme 2.3. a) Reactivity of <b>1</b> toward 20-fold of <b>AB</b> at 60 °C for 12 h in THF-d <sub>8</sub> . b) <sup>31</sup> P { <sup>1</sup> H} NMR spectrum of such reaction mixture (the inset shows a section of the proton-coupled <sup>31</sup> P NMR spectrum). c) <sup>11</sup> B NMR spectrum of such reaction mixture.	66
Scheme 2.4. a) Equimolar reaction of <b>1</b> + <b>AB</b> at 60 °C for 12 h in THF-d <sub>8</sub> . b) <sup>1</sup> H NMR monitoring of such reaction mixture as a function of time, at 60 °C. c) <sup>31</sup> P { <sup>1</sup> H} NMR monitoring of such reaction mixture, every 2 h at 60 °C (the inset shows a section of the proton-coupled <sup>31</sup> P NMR spectrum). d) <sup>11</sup> B NMR spectrum of such reaction mixture after 12 h at 60 °C.	67
Scheme 2.5 a) Reactivity of <b>1</b> toward 5 equiv. of <b>AB</b> at 60 °C for 12 h in THF-d <sub>8</sub> . b) <sup>31</sup> P { <sup>1</sup> H} NMR spectrum of such reaction mixture after 12 h at 60 °C (the inset show the proton-coupled <sup>31</sup> P NMR signal of the species resonating at 6.99 ppm). c) <sup>11</sup> B NMR spectrum of such reaction mixture after 12 h at 60 °C. DADB: diammoniate of diborane	68
Scheme 3.1. Synthesis of the Palladium (II) complex <b>4</b> , $[\kappa^2(P,N)-\{P(OQuin)_3\}PdCl_2]$ .	93
Scheme 3.2. Reaction of complex <b>4</b> with BnNH <sub>2</sub> . Isolation of <b>9</b> or <b>9'</b> .	110
Scheme 3.3. Reaction of complex <b>9/9'</b> with NaPF <sub>6</sub> . Attempt to elucidate <b>9'</b> .	112
Scheme 4.1. Synthesis of the Rhodium (I) complex <b>11</b> , $[\kappa^2(P,N)\{P(OQuin)_3\}RhCl(PPh_3)]$ .	124
Scheme 4.2. PPh <sub>3</sub> dissociation in CDCl <sub>3</sub> solution of <b>11</b> to form <b>12</b> .	130

Scheme 4.3. Retro-Arbuzov-like dearylation reaction performed by <b>11</b> in a not dry CDCl <sub>3</sub> solution. ....	131
Scheme 4.4. Ligand exchange reaction performed by <b>11</b> .....	134
Scheme 4.5. chloride abstraction reaction for <b>11</b> . ....	137
Scheme 4.6. Hydroboration of Py by a rhodium source yielding dehydropyridines (DHP). ....	138
Scheme 4.7. a) hydroboration of 2-vinylpyridine and b) styrene catalyzed by <b>11</b> . ....	146
Scheme 5.1. Synthesis of the Ruthenium (II) complex <b>18</b> , [κ <sup>3</sup> ( <i>N,P,N</i> ){P(OQuin) <sub>3</sub> }RuCl <sub>2</sub> (PPh <sub>3</sub> )]. ....	155
Scheme 5.2. Synthesis of the Ruthenium (II) complex <b>19</b> , [κ <sup>4</sup> ( <i>P,N<sub>3</sub></i> ){P(OQuin) <sub>3</sub> }RuCl <sub>2</sub> ]. ....	166
Scheme 5.3. Hydroamination of phenylacetylene with aniline catalyzed by <b>18</b> or <b>19</b> . ....	170
Scheme 5.4. dehydrogenation of HCO <sub>2</sub> H catalyzed by <b>18</b> or <b>19</b> . ....	171
Scheme 5.5. Transfer hydrogenation of non-active alkyne catalyzed by <b>19</b> using HCO <sub>2</sub> H as H <sub>2</sub> source. ....	172
Scheme 5.5. Dehydrocoupling of phenylsilane to yield polyphenylsilane catalyzed by <b>19</b> ...	173

## LIST OF TABLES

Table 2.1. Screening of base for the synthesis of <b>1</b> .....	60
Table 2.2. Selected bond distance and angles (Å, °) for <b>1</b> and the related compound tris(1-naphthyl) phosphite. ....	64
Table 2.3. Comparison of selected angles for <b>1</b> with related (non-cycle) phosphorus (III) compounds. ....	65
Table 2.4. Metal-free transfer hydrogenation of <b>2a</b> using phosphite <b>1</b> as precatalyst. Screening of catalyst precursors. ....	70
Table 2.5. Optimization process for the TH of azobenzene using different catalyst mixtures.....	72
Table 2.6. Metal-free transfer hydrogenation of azocompounds using phosphite <b>1</b> as precatalyst. Screening of substrates. <sup>[a]</sup> .....	74
Table 2.7. Reaction rates as a function of azobenzene concentration.....	76
Table 2.8. Reaction rates as a function of precatalyst concentration. ....	77
Table 2.9. Reaction rates as a function of the temperature. Ln(r/T) vs. 1/T for Eyring analysis.....	80
Table 2.10. Reaction rates as a function of the temperature. Ln(r) vs. 1/T for Arrhenius analysis.....	80
Table 2.11. Reaction rates for different <i>p</i> -substituted azoarenes. Hammett analysis. ....	83
Table 3.1. Selected geometric parameters (Å, °) for <b>4</b> and the related compounds N-Q. ....	96
Table 3.2. Solvent free oxidative coupling of benzylamine to <i>N</i> -Benzyldenebenzylamine. Screening of catalysts. ....	97
Table 3.3. Palladium catalyzed oxidative coupling of benzylamine to <i>N</i> -Benzyldenebenzylamine. Screening of reaction conditions: solvent. ....	98
Table 3.4. Palladium catalyzed oxidative coupling of benzylamine to <i>N</i> -Benzyldenebenzylamine. Screening of reaction conditions: catalyst loading. ....	98
Table 3.5. Palladium catalyzed oxidative coupling of benzylamine to <i>N</i> -Benzyldenebenzylamine. Screening of reaction conditions: oxidant (ox). ....	99

Table 3.6. Palladium catalyzed oxidative coupling of benzylamine to <i>N</i> -Benzylidenebenzylamine. Screening of reaction conditions: pressure, temperature and time.....	100
Table 3.7. Oxidative coupling of amines to imines. Screening of substrates. ....	101
Table 3.8. Palladium catalyzed oxidative cross-coupling of benzylamine with anilines to imines. <sup>[a]</sup> .....	103
Table 3.9. Rate of reaction (r) as a function of amine concentration [BnNH <sub>2</sub> ]. ....	105
Table 3.10. Rate of reaction r as a function of catalyst concentration ([4]). ....	106
Table 3.11. Rate of reaction r as a function of the product [BnNH <sub>2</sub> ][cat] = P. ....	107
Table 4.1. Selected geometric parameters (Å, °) for <b>11</b> and related compounds.....	129
Table 4.2. Selected geometric parameters (Å, °) for <b>13</b> . ....	134
Table 4.3. Selected geometric parameters (Å, °) for <b>14</b> . ....	136
Table 4.4. Screening of catalyst in the Hydroboration of Py.....	138
Table 4.5. Screening of catalyst loading in the Hydroboration of Py. ....	139
Table 4.6 Screening of Py concentration in the Hydroboration of Py .....	140
Table 4.7. Screening pinBH equivalents in the Hydroboration of Py. ....	141
Table 4.8 Screening of solvent in the Hydroboration of Py. ....	142
Table 4.9. Screening of conditions in the Hydroboration of Py.....	143
Table 4.10. Screening of substrates in the hydroboration of pyridines and quinolines.....	145
Table 5.1. Selected geometric parameters (Å, °) for <b>18</b> , <b>18<sup>b</sup></b> , <b>19</b> and related compounds.....	169

## **Chapter I**

Phosphite-Nitrogen Ligands: Preparation, coordination chemistry and applications in homogeneous catalysis

## 1.1 General Information.

Catalysis is at the heart of modern synthetic chemistry, since 90% of all commercial chemical compounds are obtained by methods that involve at least one catalytic step.<sup>1</sup> Consequently, the global catalyst market has grown steadily in recent decades.<sup>2</sup> Although the history of the development and applications of man-made catalysts goes back to the 19th century, the study of catalytic systems (heterogeneous and homogeneous) is still among the most dynamic fields of chemical research. The increasing pressure to reduce energy consumption, protect the environment and conserve natural resources is challenging synthetic chemicals more than ever. The search for the "ideal" synthetic process, which produces useful compounds with 100% yield and selectivity, economically, environmentally benign and sustainably continues. The development of sustainable synthetic methodologies should be addressed following the so-called "twelve principles of green chemistry".<sup>3a,b</sup> These identify catalysis as one of the main tools for the development and implementation of more environmentally friendly synthetic protocols. In this sense, the design of new catalysts and catalytic systems that reduce or eliminate the use and generation of hazardous substances is of great interest.

The ability of many transition metal complexes to catalyze organic reactions (in the homogeneous phase) is one of the most powerful strategies to address the issue of the "ideal" synthesis. The choice of the transition metal and the possibility of rationally designing a particular ligand, provides the opportunity to adjust the steric and electronic properties of the complex, having a significant relevance on the selectivity and efficiency of a particular reaction.<sup>4</sup> In the last 60 years, the increased interest in the chemistry of transition metals has resulted in a great progress for homogeneous catalysis, making it a fundamental tool both in academia and industry.<sup>5</sup> The leading role that homogeneous catalysis has played in recent times has been demonstrated through the awarded of three Nobel Prizes in the current century: 1.-Noyori, Sharpless and Knowles, 2001; 2.-Grubbs, Schrock and Chauvin, 2005; 3.-Heck, Negishi and Suzuki, 2010.<sup>6</sup>

Phosphorus ligand chemistry has played a key role in the development of an infinite number of catalytic processes.<sup>7</sup> These have contributed strongly to the progress of the field of homogeneous catalysis with relevance for both organic synthesis and industrial production of several chemical products.



## 1.2 Phosphite ligands.

Due to the special properties of metal complexes with phosphorus ligands, trivalent phosphorus compounds have played, and continue playing, an important role as adjusting agents of steric and electronic properties of complexes used in homogeneous catalysis.<sup>7</sup>

In terms of electronic structure, the  $\pi$ -backbonding properties of phosphorus can be strongly modified by replacing the P-C bonds (phosphines) with P-O bonds (Figure 1.1), resulting in phosphinites, phosphonites or phosphites.

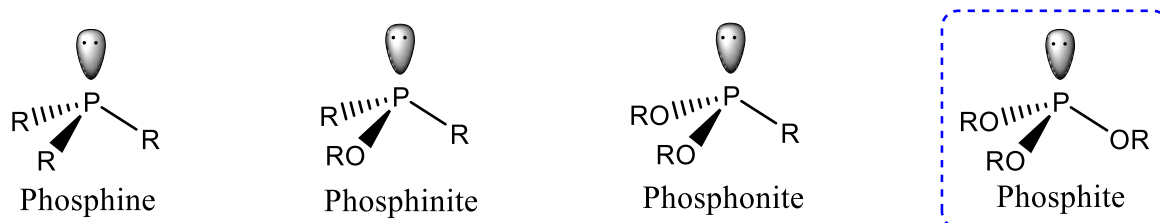
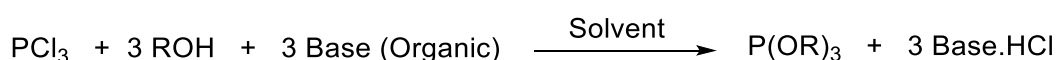


Figure 1.1 Trivalent phosphorus compounds.

In recent decades, phosphite ligands of general formula  $P(OR)_3$  have been of great interest in the field of catalysis, particularly in asymmetric reactions. One of the main advantages of these compounds is that they can be simply prepared from alcohols (Figure 1.2a) in the presence of an organic base, which allows an easy adjustment of their steric and electronic properties (Figure 1.2b). The use of such ligands in coordination chemistry has resulted in many metal complexes that have become catalysts with high selectivity.

a)



b)

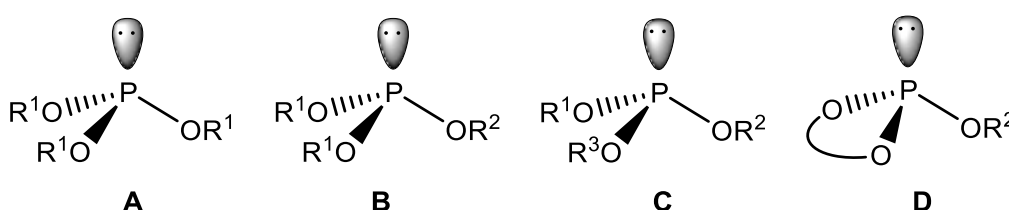


Figure 1.2. a) General reaction for phosphite synthesis (above). b) General structures of symmetric and asymmetric phosphites reported in the literature (below).

Symmetrically substituted phosphite ligands (A) are the simplest components of this family of phosphorus compounds and have been used in catalysis since the 1960s. This  $P(OR^1)_3$  function is present in many phosphorus compounds: alone (trialkyl<sup>8</sup> or triaryl<sup>9</sup>) or mixed with other donor heteroatoms such as nitrogen or sulfur, or other phosphorus functions such as phosphines, phosphites or phosphoramidites.<sup>10</sup> These compounds have been widely used in

homogeneous catalysis as ligands.<sup>8-10</sup> Asymmetrically substituted phosphites are usually prepared by combining an alcohol and a diol (**D**). A variety of organic transformations with high rates of regio- and stereoselectivity are catalyzed by metal complexes with this type of ligands.<sup>11</sup> Phosphites of type (**B**),<sup>12</sup> which contain two different alkoxy substituents, are less common, and so far only a single example of monofunctional phosphites with three different substituents (**C**)<sup>13</sup> has been described.

In general, phosphites are less prone to oxidation than phosphines, but they can be broken down by hydrolysis or alcoholysis and suffer rearrangements such as the Michaelis-Arbuzov reaction.<sup>14</sup> However, it is known that, often, the rate of hydrolysis is low for bulky phosphites.<sup>7,15</sup>

Phosphites have a very wide coordination chemistry, so much so that complexes containing phosphite ligands with most transition metals have been reported.<sup>16</sup> They are strong  $\pi$ -acceptors and form stable complexes with electron-rich transition metals. The strong binding of the M-phosphite bond suggests that  $\pi$ -backbonding prevailing over  $\sigma$ -donation. Steric properties are defined by the cone angle (Tolman angle)<sup>17</sup> in monophosphites and by the bite angle<sup>18</sup> in diphosphites or phosphite mixed with other heteroatoms (Figure 1.3a-b).

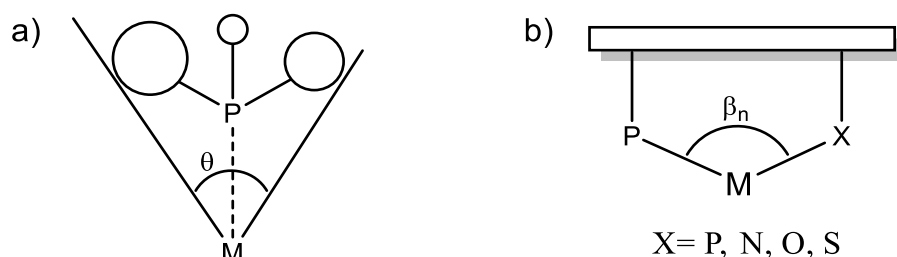


Figure 1.3. Cone angle illustration,  $\theta$  (left) and the bite angle,  $\beta_n$  (right) in a generic organophosphorus-metal complex.

### 1.3 Phosphite-nitrogen ligands.

In general, ligands can be differentiated according to their coordination mode as monodentate, bidentate or polydentate (Figure 1.4). In particular, the hybrid ligands can be bidentate or polydentate ligands. These contain at least two chemically different functions capable of binding to a metal center.<sup>19</sup> Frequently, these two functions are different from each other and each one is linked differently with the metal center. This fact influences the reactivity of the complex against various external substrates, which in a catalytic process could have implications on chemo- or regioselectivity.

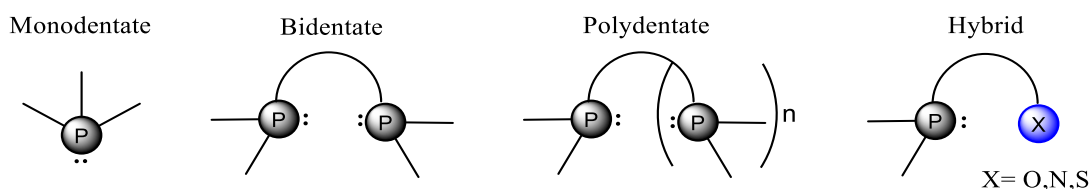


Figure 1.4. Phosphorus ligands with different coordination modes.

A hybrid ligand can be coordinated to a metal in different ways: monodentate, stable chelate, hemilabile chelate, ligand with double or superior coordination capacity and even in bridge mode for the formation of metal dimers with or without  $M \leftrightarrow M$  bonds (Figure 1.5).<sup>20</sup>

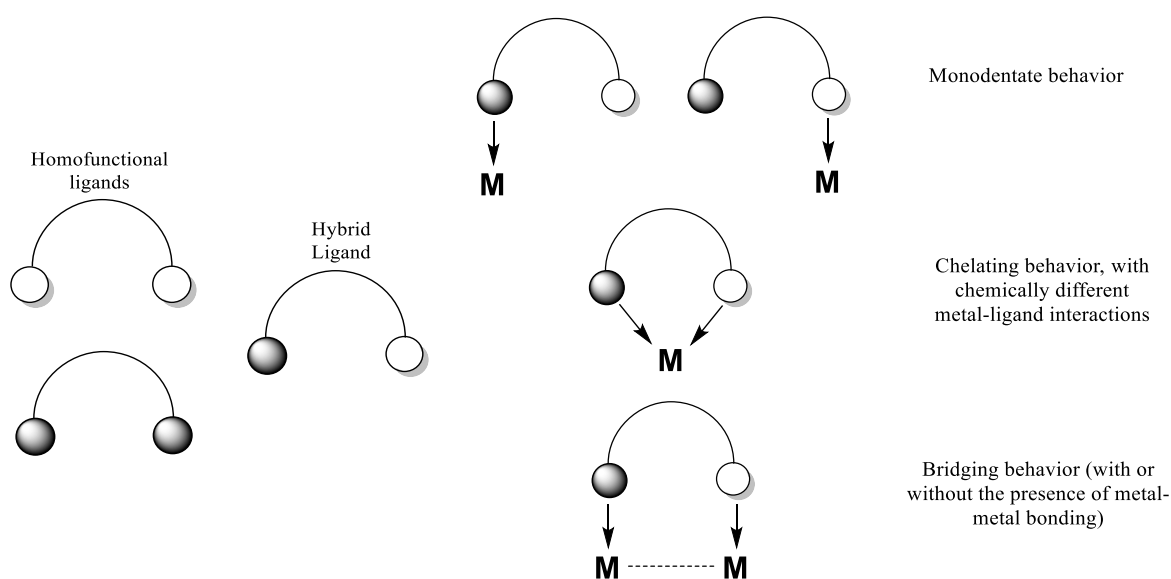


Figure 1.5. A hybrid ligand contains two chemically different donor functions (left). Coordination modes of hybrid ligands (right).

One of the most prominent classes of bidentate ligands are the  $P,N$  hybrid ligands.<sup>21</sup> The  $P,N$  ligands combine in their structure two very diverse chemical functions, such as those of a hard donor (nitrogen) and a soft donor (phosphorus) according to Pearson's definition (Figure 1.6a). The  $\pi$ -acceptor character of phosphorus can stabilize a metal center in a low oxidation state, while the  $\sigma$ -donor capacity of nitrogen makes the metal more susceptible to oxidative addition reactions. This combination might help to stabilize the intermediate oxidation states that could be implicated in a catalytic cycle. In addition, the  $P,N$  ligands can exert a degree of regiocontrol by a phenomenon known as the trans effect (Figure 1.6b). This occurs when the position trans to the donor atom that has a greater  $\pi$ -acceptor capacity (phosphorus) is more electrophilic than that trans to the  $\sigma$ -donor (nitrogen).<sup>22</sup> As an example, the nucleophilic substitution of an olefin will take place at the allyl end trans to phosphorus in a complex with  $\pi$ -allyl-metal bond (Figure 1.6b).

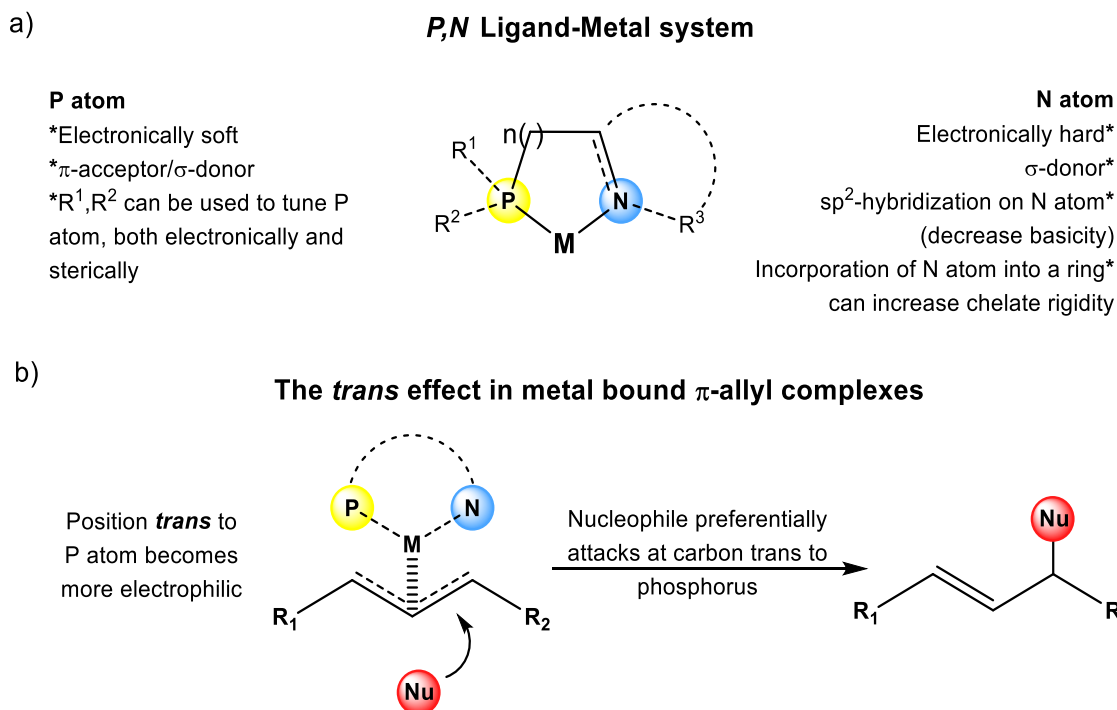


Figure 1.6. a) General characteristics of a ligand *P,N*. b) *trans* effect and its implication on nucleophilic substitution.

The design of *P,N* ligands has proven to be a powerful tool to obtain catalytic precursors with certain properties<sup>23</sup> and has been the subject of study by many research groups. With these ligands a control can be exercised in the metal coordination sphere, making it possible to observe new catalytic properties in the resulting complexes.

Pfaltz,<sup>24a</sup> Helmchen,<sup>24b</sup> and Williams,<sup>24c</sup> developed independently a new class of ligands, the phosphinoxazoline (PHOX) ligands. The combination of a P-ligand fragment and a chiral N ligand part is another way to build up non- $C_2$ -symmetric, chelating ligands, wherein the two ligand parts are more fundamentally distinguished, compared to the modified diphosphine ligands.<sup>24a-c</sup> Here, the “soft” P-ligand exhibits  $\pi$ -acceptor properties, while the “hard” N-ligand is dominantly acting as a  $\sigma$ -donor. The beneficial effect of the combination of two ligands with different electronic properties is well illustrated in the palladium catalyzed allylic alkylation.<sup>24b</sup> Crystal structure and NMR data confirmed that palladium-allyl-PHOX complexes exhibit a strong electronic differentiation of the allylic fragment, and it was observed that these complexes are predisposed to be attacked at the allylic carbon atom *trans* to the phosphine group.<sup>24b</sup> Electronic differentiation of this type has also been calculated and demonstrated by Moberg *et al.* using pseudo- $C_2$ -symmetric ligands, *i.e.* with sterical symmetry and electronic asymmetry.<sup>24d</sup>

Since then, a variety of ligands have been developed with P, N coordination mode, using oxazoline, imines, amines units, etc.<sup>16,25</sup> Most of the known examples have been applied in the generation of catalysts based on Rh, Ir and Pd, showing excellent chemoselectivity. Phosphites containing the quinoline unit (**E-Q**; Figure 1.7),<sup>26</sup> have been used successfully in catalytic systems with Rh and Pd in hydroformylation reactions of olefins obtaining high regioselectivities.

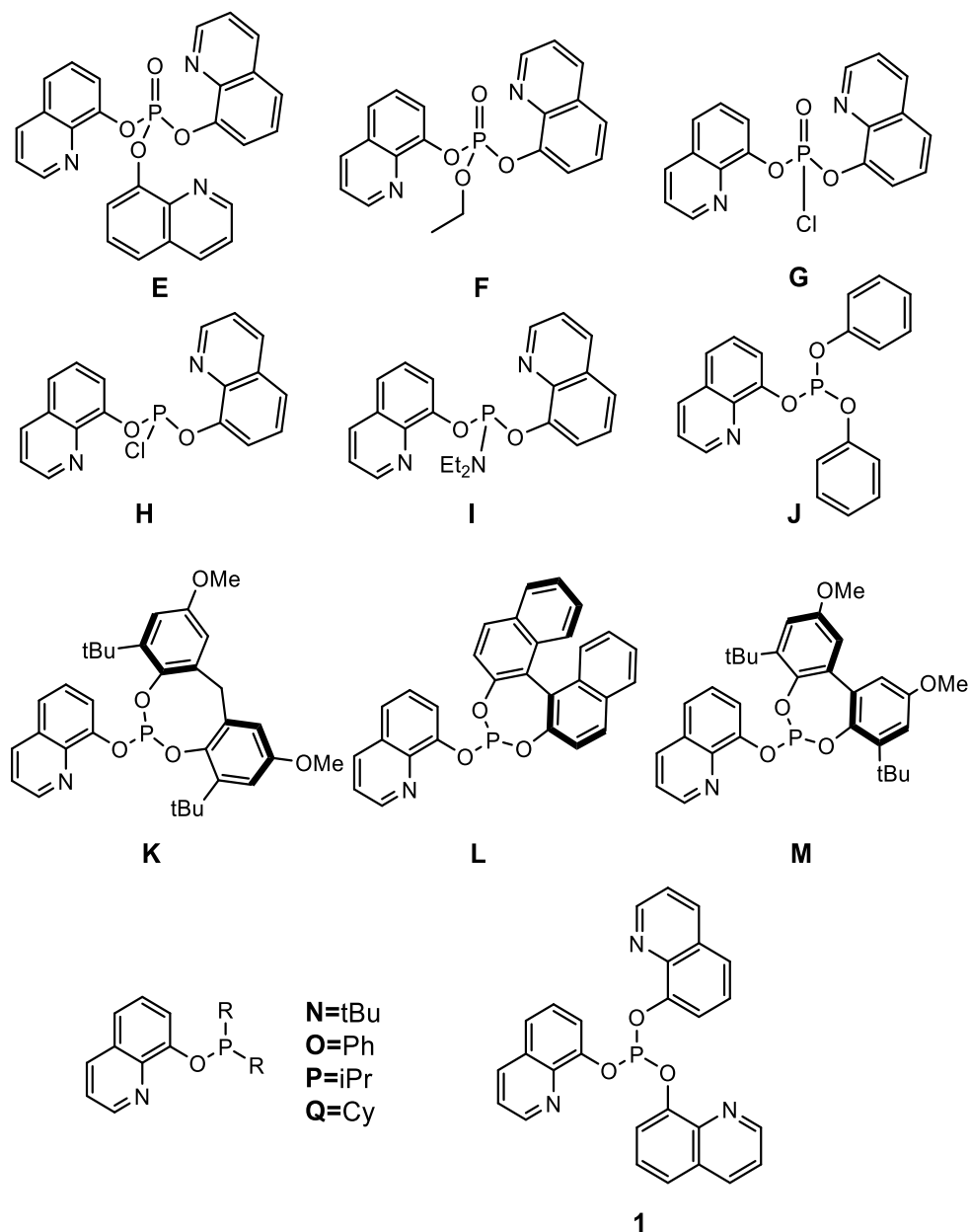


Figure 1.7. Reported phosphorus compounds bearing the 8-oxy-quinoline unit.

An extensive literature review on the subject showed that there are no precedents for the synthesis of the acyclic phosphorus compound (III) tris(8-quinolinyl)phosphite,  $P(OQuin)_3$ , (**1**; Figure 1.7), and therefore, there are no examples of studies of their reactivity against metal complexes or their application in catalysis.

The incorporation of the quinoline unit in the formation of a phosphite type ligand would allow a monofunctional ligand to be transformed into a hybrid ligand. In addition, coordination of the type  $\kappa^2\text{-}P,N$  would be possible, which could generate a particular reactivity in various types of reactions catalyzed by transition metals containing  $\text{P}(\text{OQuin})_3$ . The incorporation of the quinolinic function as a substituent group(s) around the phosphorus could generate bi- or polydentate chelate-like metal species that present a strong steric hindrance around the coordination sphere. This fact would prevent, for example, the free rotation of the metal-ligand bond (Figure 8), thus generating greater structural rigidity in the complex. Such rigidity would force certain substrates to coordinate in a specific way, which would be expected to translate into regioselectivity and / or enantioselectivity.<sup>27</sup>

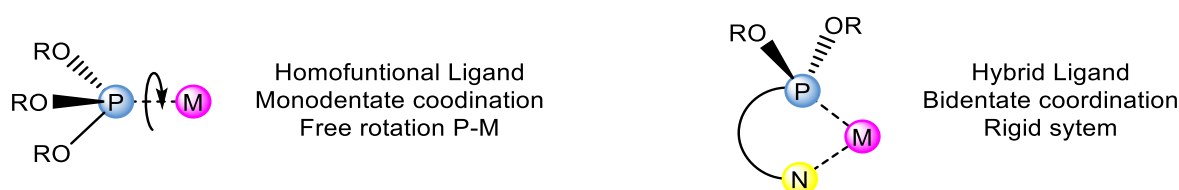


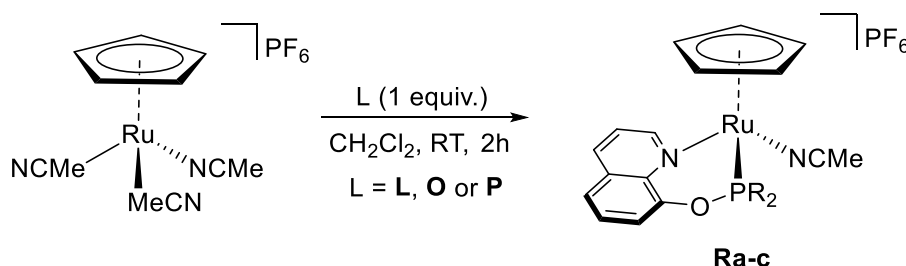
Figure 1.8. Structural difference of metal complexes with monofunctional and hybrid phosphorus ligands.

#### 1.4 Coordination chemistry of 8-oxyquinoline containing phosphorus ligands with second-row metal centers of group 8,9 and 10.

Systems containing an electron-donating center of a different nature, apart from the phosphorus center, are being vigorously studied.  $P,N$ -Bidentate ligands are highly important. They simultaneously exhibit properties of both soft and hard bases and promote redistribution of functions in a catalytic cycle, formation of bimetallic structures and a specific arrangement of the metal coordination sphere. Thus  $P,N$ -bidentate ligands can provide *cis*- or *trans*-chelation, bridging binding in either the ‘head-to-tail’ or ‘head-to-head’ fashions (in particular, in structures with metal-metal bonds) and  $P$ -monodentate coordination.<sup>28</sup> The type of coordination depends, first of all, on the length of the bridge linking the donor atoms. Systems with two binding points are typical chelating agents. The bridging type coordination is barely known for them, whereas ligands with three binding points are capable of bridging coordination. Coordination of a  $P,N$ -system to a central atom gives rise to two moieties differing in kind, containing electron-donating centers with different steric and electronic characteristics. Being structurally asymmetric,  $P,N$ -bidentate ligands also possess clear-cut electronic asymmetry. In addition, both steric and electronic parameters of the electron-donating centers and the nature of the bridge linking them can be varied over a wide range.<sup>29</sup>

In this section, an overview about the coordination chemistry of phosphorus ligands bearing a 8-oxyquinoline moiety is presented. Herein, highlights of the reactivity of such ligands towards metal centers as Ru, Rh and Pd is provided.

Garagorri *et al.*<sup>30</sup> studied the reaction of  $[\text{RuCp}(\text{CH}_3\text{CN})_3]\text{PF}_6$  with 1 equiv. of  $\text{R}_2\text{POQuin}$  ligands (**L**, **O** or **P**; Figure 1.7) in  $\text{CH}_2\text{Cl}_2$  at room temperature for 2 h. The synthesis yielded the half-sandwich complexes  $[\text{RuCp}(\text{R}_2\text{POQuin})(\text{CH}_3\text{CN})]\text{PF}_6$  (**Ra-c**) in 80–94% isolated yields (Scheme 1.1). Complexes **Ra-c** are orange solids which are air-stable both in the solid state and in solution for several days. In the  $^{31}\text{P}$  NMR spectra of **Ra-c** exhibit a singlet at 160.0, 194.3, and 175.6 ppm, respectively.



Scheme 1.1 Synthesis pathway of Ru-complexes **Ra-c**.

The solid-state structure of **Rc** was determined by single-crystal X-ray diffraction. An ORTEP diagram is depicted in Figure 1.9. Complex **Rc** adopts a typical three-legged piano stool conformation with  $\text{CH}_3\text{CN}$  and the N and P atoms of the PNquin ligand as the legs. The Ru–N1, Ru–N2, and Ru–P1 distances are 2.149(2), 2.059(2), and 2.1681(4) Å, respectively, with P1–Ru–N1, P1–Ru–N2, and N1–Ru–N2 angles of 89.02(4)°, 95.63(4)°, and 84.34(6)°. The Ru–C distances range from 2.163(2) to 2.257(2) Å (mean 2.206 Å). The chelate ring Ru1–P1–O1–C13–C14–N1 is notably non-planar and the quinoline moiety remarkably twisted (non-planarity 0.065 Å, interplanar angle between its two 6-membered rings 7.0(1)°. Ru1, P1, and O1 deviate by 0.77, 0.37, and -0.42 Å from the mean plane through quinoline.

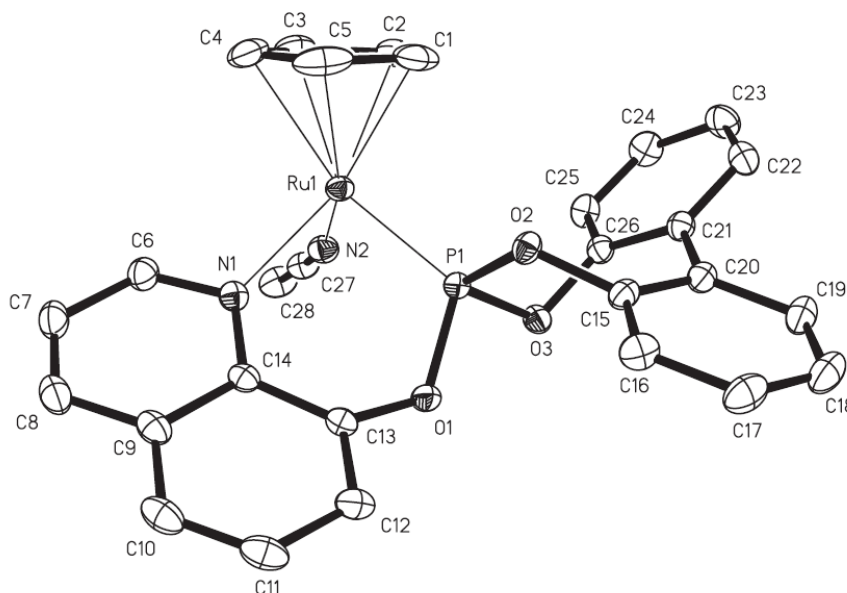
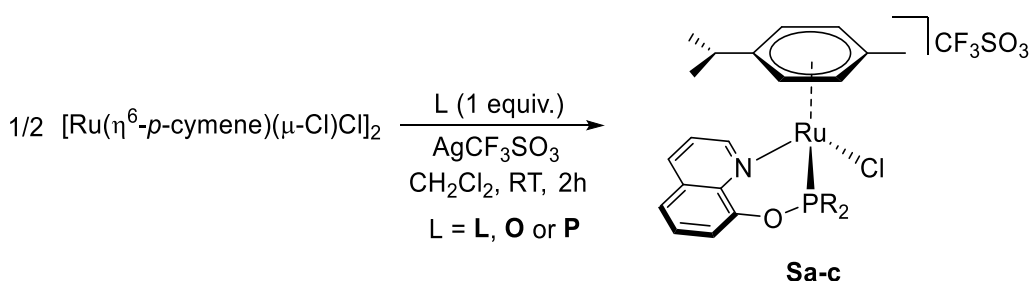


Figure 1.9. Molecular structure of  $[\text{RuCp}(\text{PNquin-BIPOL})(\text{CH}_3\text{CN})]\text{PF}_6 \cdot \frac{1}{2}(\text{C}_2\text{H}_5)_2\text{O}$  (**Rc**) showing 50% displacement ellipsoids ( $\text{PF}_6$ , H atoms and solvent solvate were omitted for clarity).

Also, treatment of  $[\text{Ru}(\eta^6\text{-}p\text{-cymene})(\mu\text{-Cl})\text{Cl}]_2$  with 2 equiv. of  $\text{R}_2\text{POQuin}$  ligands (**L**, **O** or **P**; Figure 7) in the presence of 2 equiv. of  $\text{AgCF}_3\text{SO}_3$  in  $\text{CH}_2\text{Cl}_2$  at room temperature for 2 h affords the half-sandwich complexes  $[\text{Ru}(\eta^6\text{-}p\text{-cymene})(\text{R}_2\text{POQuin})\text{Cl}]\text{CF}_3\text{SO}_3$  (**Sa-c**) in 85–86% isolated yields as orange air-stable complexes (Scheme 1.2).



Scheme 1.2. Synthesis pathway of Ru-complexes **Sa-c**.

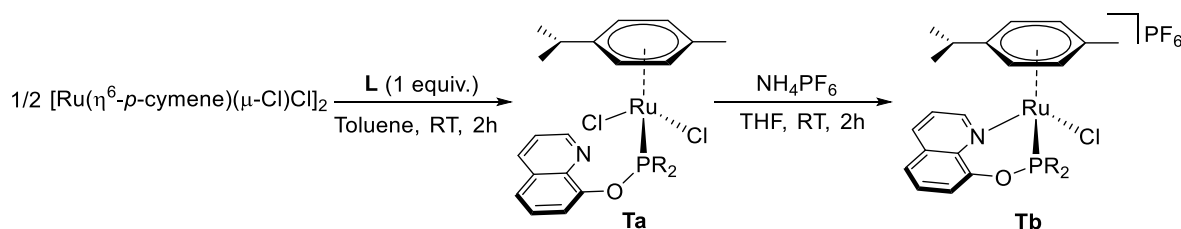
Complexes **Sa-c** have been characterized by  $^1\text{H}$ ,  $^{13}\text{C}$  and  $^{31}\text{P}$  NMR spectroscopy, and elemental analysis. In the  $^{31}\text{P}$  NMR spectrum, **Sa-c** exhibit singlets at 126.2, 160.2, and 153.8 ppm, respectively.

In other work, Francio *et al.*<sup>260</sup> report the reactions between the ligands phosphite-N (**L**; Figure 1.7) and the complexes  $[\text{Ru}(\eta^6\text{-}p\text{-cymene})(\mu\text{-Cl})\text{Cl}]_2$  and  $[\text{Rh}(\eta^5\text{-C}_5\text{Me}_5)(\mu\text{-Cl})\text{Cl}]_2$ , which lead to the expected pseudo-tetrahedral organometallic compounds of the type **Ra-c** or **Sa-c**. The asymmetric induction and the configurational stability at the metal center of the synthesized isoelectronic half-sandwich ruthenium and rhodium complexes was also discussed by these authors. The absolute configuration of one *P,N*-rhodium (III) complex was determined



by X-ray diffractometry. Rhodium (I), palladium (II), and platinum (II) complexes have previously been synthesized using the chiral ligand **L**.<sup>26q</sup>

In fact, on coordination to a metal center, **L** can form a six-chelate metallic-ring, and this feature strongly influences the outcome when it reacts with  $[\text{Ru}(\eta^6\text{-}p\text{-cymene})(\mu\text{-Cl})\text{Cl}]_2$  or  $[\text{Rh}(\eta^5\text{-C}_5\text{Me}_5)(\mu\text{-Cl})\text{Cl}]_2$ . The reaction of **L** with  $[\text{Ru}(\eta^6\text{-}p\text{-cymene})(\mu\text{-Cl})\text{Cl}]_2$  in a 2:1 molar ratio in toluene afforded the complex  $[\text{Ru}(\eta^6\text{-}p\text{-cymene})(\text{L})\text{Cl}_2]$  (**Ta**), in which the **L** ligand is monodentate P-bonded to the ruthenium center (Scheme 1.3).



Scheme 1.3. Synthesis pathway of Ru-complexes **Ta-b**.

Acetone solutions of **Ta** are not conducting, indicating that **Ta** is a neutral species. The  $^{31}\text{P}\{^1\text{H}\}$  NMR ( $\text{C}_6\text{D}_6$ ) spectrum exhibits one singlet at  $\delta$  130.1 ppm. In the  $^1\text{H}$  NMR spectrum no shift to lower field with regard to the free ligand was observed for the signal of the proton ortho to the nitrogen. The addition of  $\text{NH}_4\text{PF}_6$  to a THF solution of **Ta** promoted the chelation process of the P-coordinated ligand **L**. After several days the cationic chelate complex  $[\text{Ru}(\eta^6\text{-}p\text{-cymene})(\text{L})\text{Cl}]\text{PF}_6$  (**Tb**) was obtained as a pair of diastereoisomers differing in the configuration at the metal center. A ratio of 10:1 between the diastereoisomers **Tb<sup>α</sup>** and **Tb<sup>β</sup>** was estimated by integration of the singlets observed in the  $^{31}\text{P}\{^1\text{H}\}$  NMR ( $\text{C}_6\text{D}_6$ ) spectrum at  $\delta$  155.1 and 143.1 ppm, respectively. Unfortunately, Francio *et al.* were unable to separate **Tb<sup>α</sup>** and **Tb<sup>β</sup>** by crystallization or chromatographic techniques, due to their low stability in solution over prolonged time or on silica. Moreover, mixtures of **Tb<sup>α</sup>** and **Tb<sup>β</sup>** in various solvents rapidly decompose on warming, thus preventing the possibility to obtain information about the configurational stability of the metal stereocenter.

Similarly, the reaction of  $[\text{Rh}(\eta^5\text{-C}_5\text{Me}_5)(\mu\text{-Cl})\text{Cl}]_2$ , with **L** afforded the compound  $[\text{Rh}(\eta^5\text{-C}_5\text{Me}_5)(\text{L})\text{Cl}_2]$  (**Ua**) as an orange solid which is air-stable in the solid state for a long time.<sup>31</sup> Complex **Ua** is not stable in chlorinated solvents and in methanol. The structure of **Ua** in which **L** is monodentate through phosphorus was confirmed by conductivity measurements in acetone, which showed the complex to be neutral. Furthermore,  $^1\text{H}$  NMR exhibited no chemical shift difference between the proton ortho to the quinolinic nitrogen and the free ligand **L**.<sup>32</sup> When  $\text{NH}_4\text{PF}_6$  was added to **Ua** in THF, the cationic chelate complex  $[\text{Rh}(\eta^5\text{-}$

$\text{C}_5\text{Me}_5(\text{L})\text{Cl}]\text{PF}_6$  (**Ub**) was formed, as confirmed by analytical, conductivity, and  $^1\text{H}$  NMR spectroscopic data. Complex **Ub** was obtained as a pair of diastereoisomers, **Ub $^\alpha$**  and **Ub $^\beta$** , in the molar ratio 15:1, as estimated by the integration of the doublets respectively at  $\delta$  146.5 ( $^1J_{\text{RhP}} = 237$  Hz) and  $\delta$  135.7 ppm ( $^1J_{\text{RhP}} = 217$  Hz) in the  $^{31}\text{P}\{^1\text{H}\}$  NMR ( $\text{C}_6\text{D}_6$ ) spectrum. The diastereoisomers **Ub $^\alpha$**  and **Ub $^\beta$**  have opposite configurations at rhodium. Since the molar ratio between the diastereoisomers does not change on refluxing for 36 h in methanol, thus the epimerization does not occur. Crystallization of the diastereomeric mixture from dichloromethane-methanol afforded orange crystals after several days. These crystals corresponded to the major diastereoisomer **Ub $^\alpha$** , as was established by  $^{31}\text{P}\{^1\text{H}\}$  NMR spectroscopy. An X-ray crystallographic study proved that the absolute configuration of this diastereoisomer is  $S_{\text{Rh}}S_{\text{Ub}}^\alpha$ . They further confirmed that **Ub $^\alpha$**  is configurationally stable in refluxing methanol over 24 h. DCM solvation molecules were found in the crystals of complex **Ub $^\alpha$** . A view of the structure of **Ub $^\alpha$**  is shown in Figure 1.10.

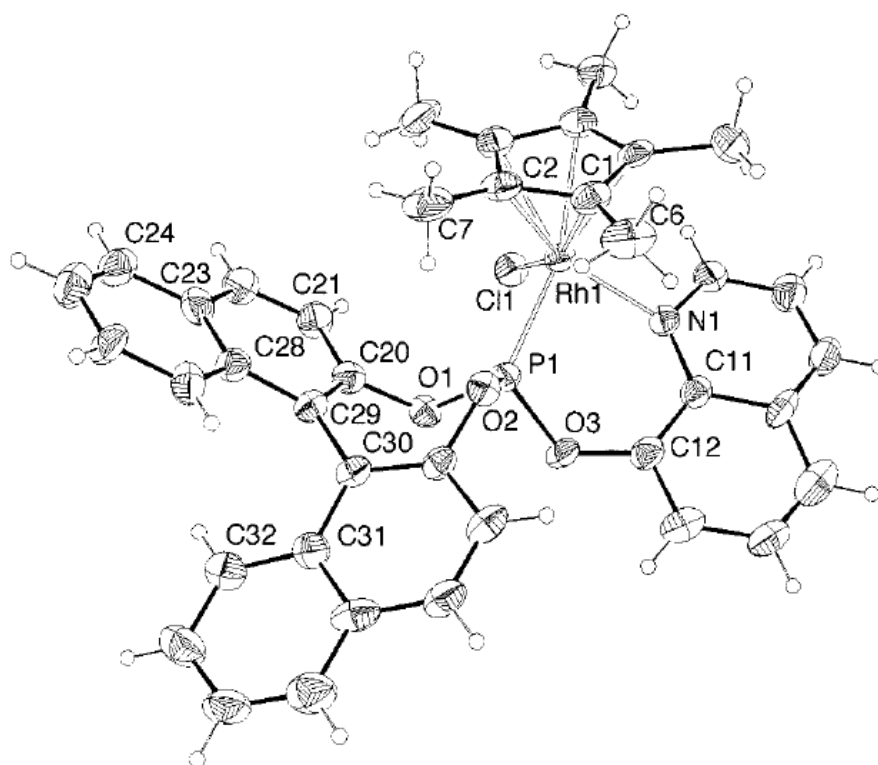
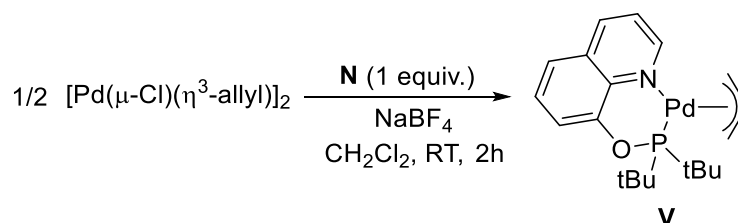


Figure 1.10. Molecular structure of the complex **Ub $^\alpha$**  with the atomic numbering system. The ellipsoids are drawn at the 30% probability level.

The metal displays a three-legged piano-stool type of coordination involving an  $\eta^5$ -coordinated pentamethylcyclopentadienyl group (the five Rh-C bond distances are within the range 2.165(9)-2.252(9) Å), a Cl atom, and the P and N atoms of the phosphite chelate **L** ligand. If the centroid of the Cp\* ring is considered as a single site, the coordination geometry can also

be described as pseudotetrahedral. The six-membered Rh1-N1-C11-C12-O3-P1 ring shows a roughly boat-shaped conformation, while the O3 and N1 atoms are displaced by 0.408(6) and 0.519(7) Å, respectively, from the mean plane through the other four atoms. The bite angle P1-Rh1-N1 is 89.1(2)° and the Rh1-P1, Rh1-C11, and Rh1-N1 bond distances are 2.209(2), 2.397(2), and 2.149(7) Å, respectively. In the **L** ligand, the coordinated-quinoline moiety is slightly twisted. The P-O(1-3) bond distances, 1.597(6), 1.598(5), and 1.604(6) Å, are practically identical, the O-P-O angles are within the range 94.8(3)-122.5(2)°, and the two naphthyl groups are planar and form a dihedral angle of 54.5(2)°.

Two reports concern the Pd-coordination chemistry of 8-hydroxyquinoline containing phosphorus ligands, Crociani *et al.* reported the preparation of a phosphinite ligand, namely 8-(di-tert-butylphosphinoxy)quinoline, (**N**; Figure 1.7) and its palladium(II) coordination chemistry (Scheme 1.4) in 2008,<sup>26s</sup>. This ligand contains a phosphinito group and, like other phosphinites,<sup>33</sup> is rather unstable as it decomposes quickly even when stored at -20 °C under N<sub>2</sub> atmosphere. This prevented any further purification and characterization by elemental analysis. Nevertheless, as shown by its <sup>1</sup>H and <sup>31</sup>P{<sup>1</sup>H} NMR spectroscopy, the raw product is sufficiently pure to be used in Pd-coordination chemistry. The complex [(<sup>t</sup>Bu<sub>2</sub>POQuin)Pd(η<sup>3</sup>-allyl)]BF<sub>4</sub> (**V**) appear thermally stable and no decomposition was observed after prolonged time at ambient temperature both in the solid state and in solution.



Scheme 1.4. Synthesis pathway of Pd-complex **V**.

*P,N* ligands with an 8-oxyquinoline group have already been studied,<sup>34</sup> but this is the first example of a phosphinite–quinoline compound. Complex **V** was isolated as BF<sub>4</sub> salt, and its ionic nature is confirmed by conductivity measurements in CH<sub>2</sub>Cl<sub>2</sub> solution. As suggested by the downfield shifts of the <sup>1</sup>H NMR signal of the H (*ortho* to N atom) quinoline proton and of the <sup>31</sup>P NMR signal upon coordination, **N** acts as a *P,N*-bidentate ligand in this complex. The chelating nature of **N** is clearly indicated by the X-ray structural analysis of **V**. (Figure 1.11)

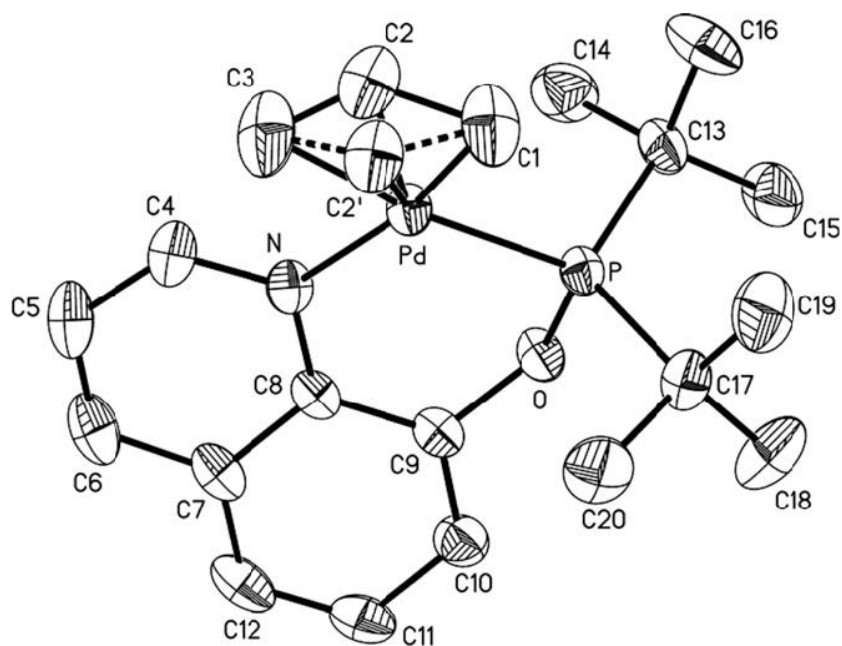


Figure 1.11. Molecular structure of complex **V** showing the atom labelling scheme and thermal ellipsoids at 40% probability level. Hydrogen atoms and the  $\text{BF}_4$  anion are omitted for clarity.

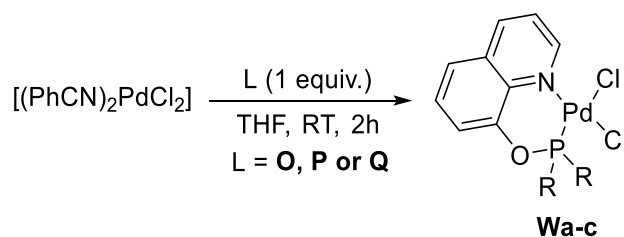
The orientation around the central metal is distorted square-planar with the allylic carbons and the P and N donor atoms comprising the immediate coordination sphere. The bite angle P–Pd–N of  $92.8(2)^\circ$  is close to the idealized value of  $90^\circ$  and in line with the presence of a flexible six-membered chelate ring. The quinoline plane is twisted, N–C4–C5–C6–C7–C8–C9–C10–C11–C12 makes a dihedral angle of  $30.2(1)^\circ$  with the P–Pd–N plane and the oxygen atom being at a distance of  $0.152(4)$  Å from this plane.

The central carbon of the allyl ligand is disordered in two positions with an occupancy factor of 0.60 for C2 and 0.40 for C2'. Such structural disorder seems to be a common feature for cationic complexes of the type  $[\text{Pd}(\eta^3\text{-C}_3\text{H}_5)(\text{P},\text{N})]^+$  (P,N= iminophosphine or phosphino-oxazoline),<sup>35</sup> although it was not found for the complex where P,N is a phosphinito-oxazoline.<sup>36</sup> In both orientations, the three allylic carbon atoms are bonded to palladium. In the C1–C2–C3 unit the C–C bond distances are of comparable values [ $1.36(2)$  and  $1.34(2)$  Å], whereas in the C1–C2'–C3 unit the C–C bond lengths are significantly different [ $1.39(2)$  and  $1.26(3)$  Å]. The longer Pd–C3 bond *trans* to phosphorus [ $2.208(9)$  Å], compared to Pd–C1 *trans* to nitrogen [ $2.111(6)$  Å], reflects the greater *trans* influence of the P donor atom. The dihedral angles between the allyl planes C1–C2–C3, C1–C2'–C3 and the P–Pd–N plane are  $128(2)^\circ$  and  $121(2)^\circ$ , respectively.

In 2010, Xia *et al.*<sup>26t</sup> reported the synthesis of 8-quinolinyl-phosphinite ligands  $\text{R}_2\text{POQuin}$ , (R = Ph, iPr, Cy) (**O-Q**; Figure 1.7) with a similar fashion as those reported by Crociani *et al.* (*vide supra*). Xia showed the synthesis, characterization, and catalytic

applications of three new palladium complexes containing 8-quinolylphosphinites (Scheme 1.5). Due to their air-sensitive nature,<sup>26s,33</sup> the phosphinites were used directly without further purification to react them with bis(benzonitrile)dichloropalladium(II) affording the corresponding palladium quinolylphosphinite complexes (**Wa-c**). All the complexes can be stored and handled in air. They were also thermally robust, showing no sign of decomposition under 200 °C in air. They were characterized by <sup>1</sup>H and <sup>31</sup>P NMR spectroscopy and infrared (IR) spectroscopy. The solid-state structures of the palladium complexes (**Wa-c**) were determined through X-ray diffraction studies. The elemental analysis results matched well with the expected values.

The <sup>1</sup>H NMR spectra of the three palladium complexes exhibited chemical shifts for the quinolyl hydrogen (*ortho* to N atom) around 10.5 ppm. This reflects a downfield shift of 1.5 ppm with respect the same resonance for the reported free ligands.<sup>26s</sup> The rest of the quinolyl hydrogens showed smaller shifts in comparison with the ligand. The methyl groups in the isopropyl moieties in complex **Wb** became nonequivalent, reflecting the restriction of rotation of the isopropyl in the palladium complexes. The <sup>31</sup>P signals ranged from 115 to 162 ppm.



Scheme 1.5. Synthesis pathway of Pd-complex **Wa-c**.

Suitable crystals of **Wa-c** for X-ray analysis were grown by slow evaporation of dichloromethane and hexane solutions. The molecular structures of the complexes were almost identical. A representative structure of **Wa** is shown in Figure 1.12. The structure of **Wa** showed a distorted square-planar geometry around the palladium ion, which is bonded to the P and N atoms from the quinolylphosphinite as well as two Cl atoms. The bond angles of N–Pd–Cl1 and P–Pd–Cl2 are 175.58 and 170.88, respectively. The bond lengths for Pd–P (2.177 Å) and Pd–N (2.080 Å), are comparable to the reported values by Crociani *et al.* in related di-*tert*-butyl quinolylphosphinite palladium complex.<sup>26s</sup> The Pd–Cl2 distance *trans* to the phosphorus is slightly longer than the Pd–Cl1 distance *trans* to the nitrogen atom, suggesting a stronger *trans* effect of the phosphinite donor.

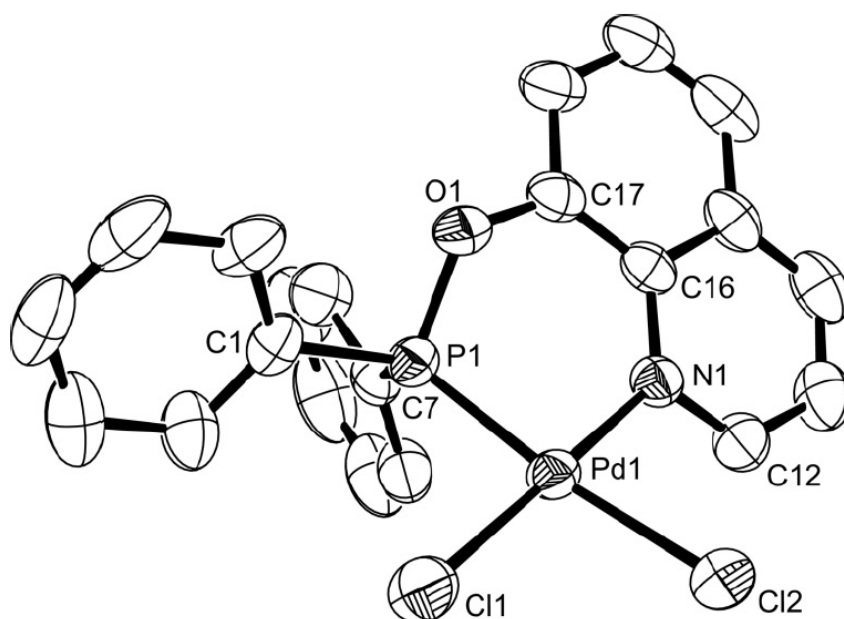


Figure 1.12. Molecular structure of complex **Wa** showing the atom labelling scheme and thermal ellipsoids at 40% probability level. Hydrogen atoms are omitted for clarity.

### 1.5 Catalytic application of phosphite-nitrogen ligands.

To achieve the highest levels of reactivity and selectivity in catalysis, several reaction parameters must be optimized, but one of the most crucial is perhaps the design of the ligand.<sup>37</sup> In this context, in the early 1990s, phosphites emerged as suitable ligands for asymmetric Rh-catalyzed hydroformylation<sup>38</sup> and Cu-catalyzed 1,4-additions.<sup>39</sup> In recent years, their use has been successfully extended to other catalytic reactions. The most noteworthy of phosphite-containing ligands are the important breakthroughs achieved using it in the asymmetric hydrogenation of functionalized and unfunctionalized olefins, asymmetric allylic substitution, and the Heck reaction, among others. The capacity of this kind of ligand to mediate catalytic processes with a high degree on regio- and stereocontrol have motivated many research groups around the world the continuous development in this regard. As stated before, phosphite ligands are extremely attractive for catalysis because they are easy to prepare from readily available alcohols, which enables the synthesis and screening of ligand series in the search for high activities and selectivities for each particular reaction. For this reason, phosphite ligands have not been often used in non-asymmetric catalysis and its contribution to this field has remained largely unexplored.

Excellent activities and enantioselectivities have been achieved for the asymmetric hydrogenation of dehydroamino acids and other functionalized alkenes and ketones. For the hydrogenation of unfunctionalized olefins and imines, iridium complexes containing *P,N* ligands have become the most successful catalysts.<sup>40</sup>

Several phosphite-oxazoline ligands have recently been developed for the Ir-catalyzed hydrogenation of minimally functionalized olefins.<sup>41</sup> Taddol based phosphite-oxazoline ligands, developed by Pfaltz *et al.*, represented the first successful application of such ligands. These ligands provided enantioselectivities up to 95% in the hydrogenation of several E and Z-trisubstituted alkenes (Figure 1.13).<sup>41a</sup>

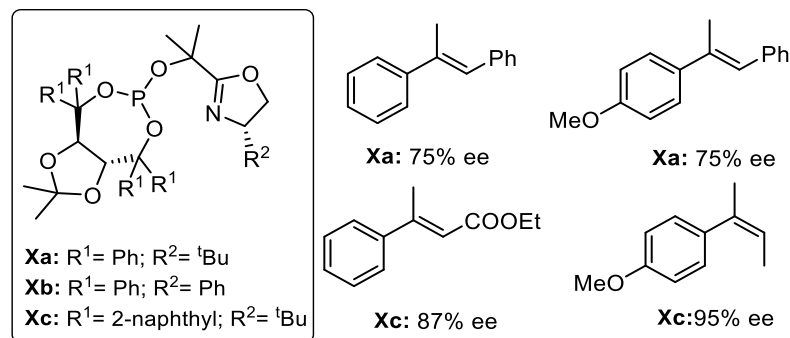


Figure 1.13. Taddol-based phosphite-oxazoline. Summary of the best results obtained.

More recently, two large libraries of phosphite-oxazoline ligands derived from hydroxyl-amino acid derivatives<sup>41b,c</sup> and D-glucosamine<sup>41d</sup> have been developed. These libraries are highly modular, and thus, several ligand parameters that are known to be important in catalytic performance can be studied. By carefully selecting the ligand components, high activities and enantioselectivities were obtained in the hydrogenation of several E- and Z-trisubstituted and 1,1-disubstituted olefins. It should be noted that the introduction of a bulky biaryl phosphite moiety in the ligand design is highly advantageous in the product outcome. Therefore, such ligands provided higher enantioselectivities than their Taddol-based phosphite-oxazoline **Y** analogues.

Very recently, a library of readily available phosphite-oxazole/thiazole ligands (**Ya-g**; Figure 1.14) was applied in the Ir-catalyzed asymmetric hydrogenation of several largely unfunctionalized E- and Z-trisubstituted and 1,1-disubstituted terminal alkenes.<sup>41e</sup> The ligand library combines the advantages of the oxazole/thiazole moieties with those of the phosphite scaffold. They are more stable than their oxazoline counterparts, less sensitive to air and other oxidizing agents than phosphines and phosphinites, and easy to synthesize from readily available alcohols. Dieguez and co-workers again found that the effectiveness at transferring the chiral information in the product can be tuned by choosing suitable ligand components, and in this way enantioselectivities can be maximized for each substrate as required. Enantioselectivities were therefore excellent (*ee* values up to >99%) in a wide range of E- and Z-trisubstituted and 1,1-disubstituted terminal alkenes.<sup>41e</sup>



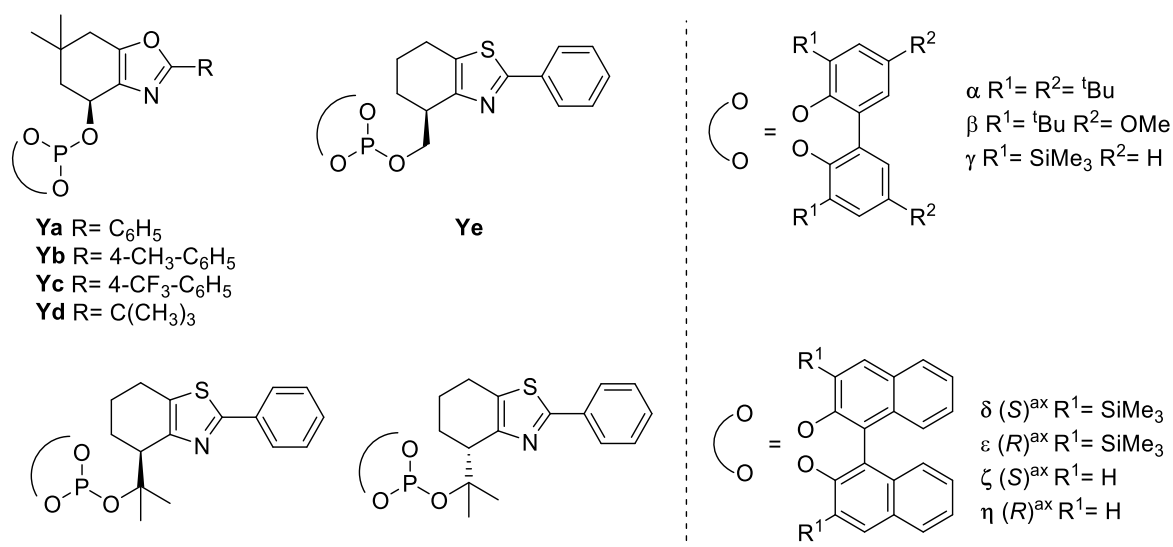


Figure 1.14. Phosphite-oxazole/thiazole ligand library.

Other heterodonor phosphite-N ligands applied in asymmetric hydrogenation are the ferrocenyliminophosphites **Z** (Figure 1.15). These ligands provided moderate-to-good enantioselectivities (up to 97%) in the Rh-catalyzed hydrogenation of R-dehydroamino acid derivatives<sup>41f</sup> and very poor *ee*'s in the Pd-catalyzed reduction of R-ketophosphonates.<sup>41g</sup>

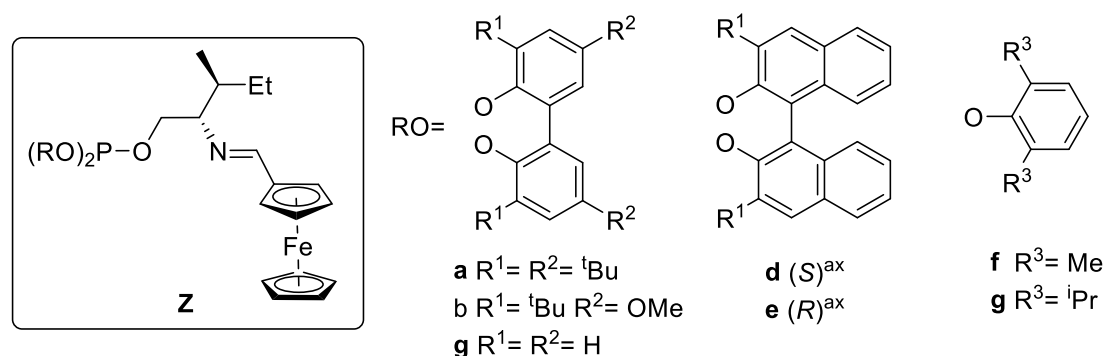
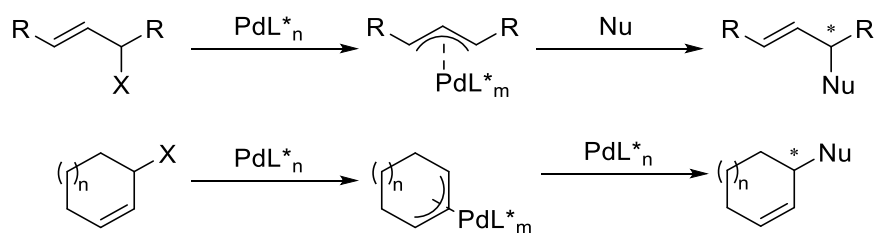
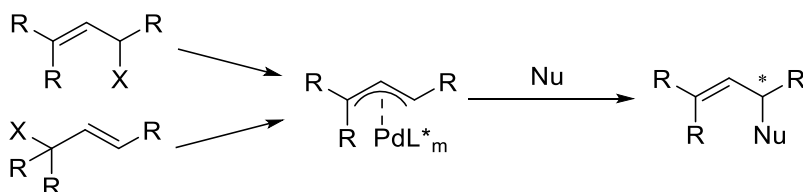


Figure 1.15. Ferrocenyliminophosphites ligands.

Several phosphite-oxazoline ligands have been applied in the Pd-catalyzed allylic substitution reactions of several substrate types (Scheme 1.6).<sup>42</sup> Phosphite-oxazoline ligands (**A1-3a-c**) were first successfully applied in this process by Pfaltz *et al.* (Figure 1.16).<sup>42d</sup>



**Type A****Type B**

Scheme 1.6. Two classes of asymmetric allylic substitution reactions.

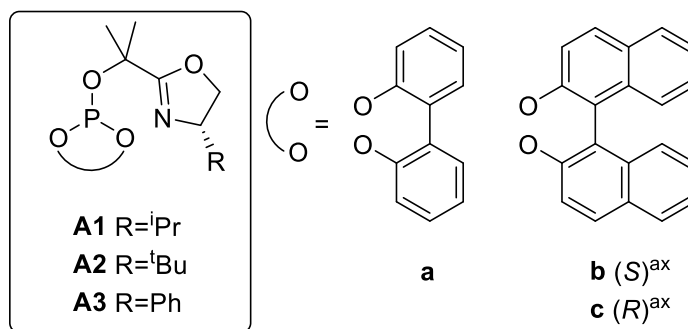
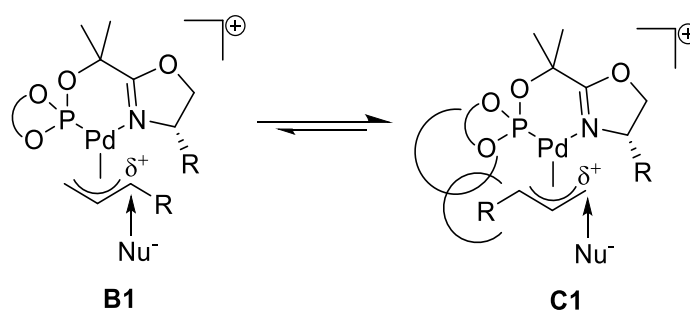


Figure 1.16. Phosphite-oxazoline ligands **A1-3**.

Ligands **A1-3a-c** were designed to overcome the problem of regioselectivity in the allylic alkylation of monosubstituted linear substrates. Pfaltz *et al.* found that regio- and enantioselectivities were affected by substituents in the oxazoline moiety and by the substituents/configuration of the phosphite moiety. The best results were obtained with ligand **A2b**, which provides an excellent combination of regioselectivities (up to 95%) in the desired branched isomer and enantioselectivities (up to 94%). These ligands were successful because of the combination of two ligand parameters that directed the nucleophilic attack to the most substituted allyl terminus (Scheme 1.7).<sup>42d</sup>



Scheme 1.7. Key Pd-Allyl intermediates containing monosubstituted substrates.

The first of these parameters is the  $\pi$ -acceptor capacity of the phosphite moiety, which decreases the electron density of the most substituted allylic terminal carbon atom via the *trans*-influence, favoring the nucleophilic attack to this carbon atom (**B1**; Scheme 1.7). The second is the introduction of a bulky biaryl phosphite moiety, which shifts the equilibrium to the desired Pd-allyl (**C1**; Scheme 1.7) intermediate.

The application of such ligands in the asymmetric Pd-catalyzed allylic substitution reactions was very successful. Therefore, excellent activities (TOF's > 2400 mol<sup>-1</sup>.h<sup>-1</sup>, and regio- (up to 99%) and enantioselectivities (*ee*'s up to >99%) were obtained for hindered and unhindered disubstituted and monosubstituted substrates (Figure 1.17). It is noteworthy that these ligands are more versatile than their phosphine-oxazoline PHOX analogues. The excellent results are consistent with the presence of a  $\pi$ - acceptor flexible bulky biphenyl phosphite moiety. The results indicate that the enantioselectivity is affected by both the substituents in the biphenyl phosphite and in the oxazoline moieties. The best enantioselectivities are obtained using a bulky tetra-*tert*-butyl-biphenyl phosphite moiety. It should be noted that the choice of the oxazoline substituent depends on the substrate. Thus, for hindered linear substrates, a phenyl substituent is required, while for unhindered ones more sterically demanding substituents (*t*Bu or *i*Pr) are needed.

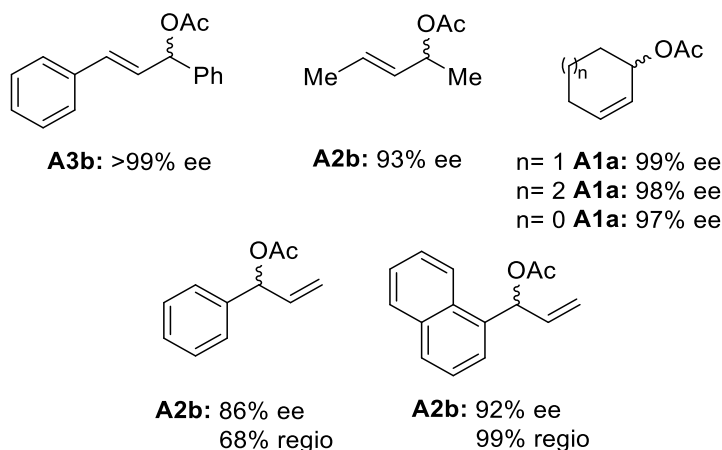
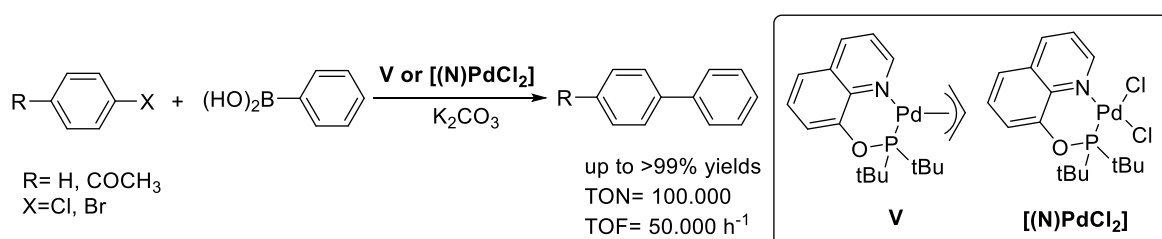


Figure 1.17. Summary of the best results obtained in the Pd-catalyzed allylic substitution using ligands **A1-3a-c**.

In summary, several heterodonor phosphite-containing ligands have been described and found to be very efficient in many catalytic systems. The most successful ligands combine the phosphite moiety with a nitrogen donor group. An examination of the literature about heterodonor phosphite-nitrogen ligands reveals that three main scaffold types have been investigated: phosphite-oxazoline,<sup>43</sup> phosphite-pyridine,<sup>44</sup> and phosphite-amine<sup>45</sup> ligand combinations. Among the phosphite-pyridine ligand type are the 8-oxyquinoline-containing phosphorus compounds which have been scarcely studied in catalytic applications.

One example, is the report by Crociani *et al.*<sup>26s</sup> in 2008. There, the Pd(II)-complex **V** (see above, Scheme 1.4) and its chlorine analogue bearing ligand **N** ( $[(\mathbf{N})\text{PdCl}_2]$ ) were employed as precatalyst in reactions leading to C–C bond formation such as the Suzuki–Miyaura reaction. The catalytic activity of those complexes in the coupling of phenylboronic acid with aryl bromides and chlorides were tested. (Scheme 1.8) The initial experiments were carried out with complex  $[(\mathbf{N})\text{PdCl}_2]$ , in toluene using an aryl bromide/palladium ratio of 100000:1 in the presence of  $\text{K}_2\text{CO}_3$  as the base. While at temperatures lower than 90 °C the reaction with *p*-bromoacetophenone proceeds at modest rates, above 100 °C the catalyst activity becomes impressive (TON= 100.000, TOF=50.000 h<sup>-1</sup>), so that a complete substrate conversion is achieved in two hours.



Scheme 1.8. Suzuki-Miyaura coupling using palladium complexes **V** and  $[(\mathbf{N})\text{PdCl}_2]$ .

Such high reaction rates are observed even in the coupling of phenylboronic acid with bromobenzene a substrate lacking an activating electron-withdrawing group (EWG). Encouraged by these results, Crociani *et al.* extended the substrate scope to the more challenging coupling of phenylboronic acid with aryl chlorides. Under the same reaction conditions and with a substrate/catalyst ratio of 200:1, the coupling of *p*-chloroacetophenone with phenylboronic acid proceeds to completion in two hours. Likewise, the less activated chlorobenzene is coupled with phenylboronic in high yield (85% yield, TON=200, TOF= 85). Further experiments showed that also the cationic allyl complex **X** is active in promoting the Suzuki coupling of phenylboronic acid with the same aryl halides (best result, >99% yield, TON= 90.000, TOF=45.000 h<sup>-1</sup>). Considering that the reaction conditions were not optimized, the catalytic potential of complexes  $[(\mathbf{N})\text{PdCl}_2]$  and **V** appears of particular interest. As a matter

of fact, the coupling of aryl chlorides with boronic acids is usually carried out using 1–3 mol% of catalyst<sup>46</sup> and only a small number of catalysts<sup>46b-h</sup> are able to activate aryl chloride substrates at loading lower than 1 mol% in short reaction time.

Finally, Arena *et al.*<sup>47</sup> reported the efficiency of the catalytic system formed by Cu(OTf)<sub>2</sub> and the ligands **L** (Figure 1.7) in the enantioselective conjugate addition of Et<sub>2</sub>Zn to 2-cyclohexenone (Scheme 1.9). The most promising result was obtained using a Cu(OTf)<sub>2</sub>/**L** molar ratio of 0.03 at -15 °C, in CH<sub>2</sub>Cl<sub>2</sub> as a solvent. Under these conditions the conversion is almost complete (95%) within 2 h and (S)-3-ethylcyclohexanone was obtained in 51% *ee*, while in toluene the corresponding *ee* value was lowered to 35%. The reaction proceeded more slowly and less selectively when the catalyst loading was reduced.

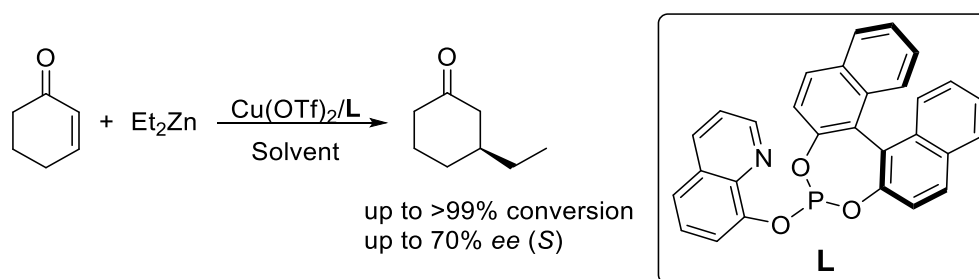


Figure 1.18. Cu-catalyzed enantioselective 1,4-addition of diethylzinc to cyclohex-2-enone.

## 1.6 Outline

The main focus of this work is the synthesis of tris(8-quinolynyl)phosphite, P(OQuin)<sub>3</sub>, (**1**; Figure 1.7) and its reactivity against metallic precursors of groups 8, 9 and 10. Both **1** and the resulting compounds with transition metals will be evaluated in selected catalytic transformations, in particular leading to nitrogen compounds of interest (imines, diphenylhydrazines, hydropyridines). P(OQuin)<sub>3</sub> has a phosphorus atom that can be coordinated to a metal as well as three quinoline groups, in which nitrogen atoms can also be coordinated. It is expected that **1**, will be a hemilabile ligand due to competition between the three quinoline groups with the same coordination ability. Also, given the known lability of certain metal-nitrogen bonds, the generation / exchange of a vacant site in the metal center would be possible. This hybrid character of **1** could be relevant both in the activity and selectivity of the reactions involving it as catalyst, as well as in the stabilization of cationic or anionic metallic (intermediate) species.

## 1.7 Objectives

### 1.7.1 General Aim

- Study the synthesis, characterization, coordination chemistry and catalytic properties of the new compound tris(8-quinolinyl)phosphite,  $\text{P(OQuin)}_3$ , **1**. Evaluate the potential of **1** as ligand will be investigated through its reactivity against metallic precursors from groups 8, 9 and 10. Evaluate **1** and the resulting species with transition metals in selected catalytic transformations, in particular leading to nitrogen compounds of interest (imines, diphenylhydrazines, hydropyridines).

### 1.7.2 Specific Aim.

- Synthesize and characterize **1** based on synthetic protocols already reported for similar phosphites.
- Optimize the procedure for the synthesis of **1**, changing different reaction conditions such as: temperature, solvent, nature of the base, reaction time, among others.
- Evaluate the catalytic potential of **1** in the reduction of azocompounds.
- Study the reactivity of the synthesized ligand against metal precursors of groups 8, 9 and 10 such as Ru (II), Rh (I) and Pd (II).
- Evaluate the catalytic potential of a Pd (II) metal complex bearing the ligand **1** in the oxidative coupling of primary amines to yield imines.
- Evaluate the catalytic potential of a Rh (I) metal complex bearing the ligand **1** in the hydroboration of pyridines.
- Evaluate the catalytic potential of a Ru (II) metal complex bearing the ligand **1** in dehydrogenative transformations.
- Optimize each catalytic reaction by varying different reaction conditions such as: temperature, solvent, catalyst / substrate ratio, reaction time, among others.
- Evaluate the scope and limitations of the optimized catalyst systems by varying the substrates.

## Chapter II

Tris(8-quinolinyl)phosphite: Synthesis, characterization and its organocatalytic application on transfer hydrogenation of azocompounds.

Reproduced with permission from M. A. Chacón-Terán, R. E. Rodríguez-Lugo, R. Wolf, V. R. Landaeta, «Metal-Free Transfer Hydrogenation of Azocompounds with Ammonia Borane using a Simple Acyclic Phosphite Precatalyst», *Eur. J. Inorg. Chem.* **2019**, 4336–4344.

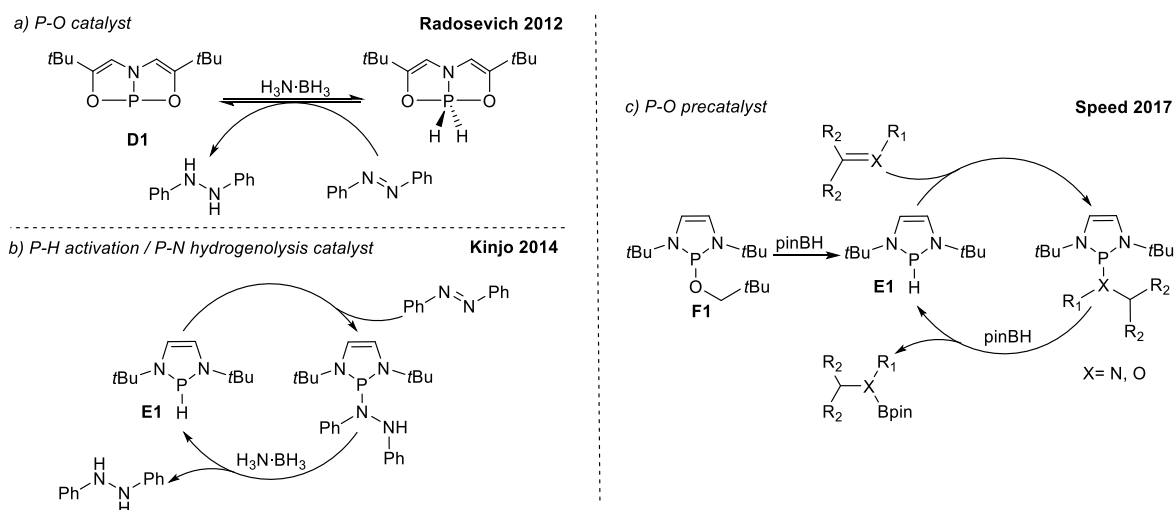
## 2.1 Introduction

Hydrogenation is one of the most fundamental transformations in organic synthesis, and its industrial applications are broad, particularly in the production of fine chemicals to pharmaceuticals.<sup>48</sup> Considering that using H<sub>2</sub> gas requires special reaction (pressure) vessels and particular safety measures, researchers have dedicated substantial effort to develop simpler and safer alternatives for the reduction of unsaturated moieties. In this sense, transfer hydrogenation (TH) has become a practical and useful tool in reduction chemistry in the last decade.<sup>49</sup> TH-reactions using precious-metal catalysts have been intensively investigated.<sup>50</sup> However, for these, abundance, cost, and toxicity are significant issues. Furthermore, considering that for large-scale applications a catalyst for the release/transfer of hydrogen must be cheap and based on abundant materials, the use of platinum-group metals should be avoided. In this respect, organocatalytic-TH using main-group compounds is currently undergoing great development.<sup>51</sup>

Among the broad variety of potential hydrogen storage materials, ammonia-borane (**AB**) has attracted particular interest due to its high weight percent of available hydrogen (19.6%), high stability in air, high portability and the fact that its dehydrogenation is thermodynamically favorable ( $\Delta H = -5.1$  kcal/mol).<sup>52</sup> Although rapid H<sub>2</sub>-release from **AB** has been widely demonstrated by metal-based catalysts,<sup>53,54</sup> latest focus on the hydrogen transfer from **AB** (or amine-boranes in general) has been directed to organocatalyzed dehydrogenation using, for example, *p*-block based systems.<sup>55,56</sup> Cornella *et al.* have addressed the use of pnictogen-based compounds for TH reactions from **AB**, *e.g.* a bismuth<sup>57</sup> and several phosphorus-based catalysts.<sup>58-52</sup> DFT calculations have revealed an energetically feasible pathway for a concerted double hydrogen transfer (concerted metathesis) from **AB**, using a phosphorus catalyst.<sup>44</sup>

Studies by Radosevich and co-workers<sup>59</sup> have shown that a highly-strained T-shaped phosphorus (III) compound **D1** (Scheme 2.1a) promotes the TH of azobenzene (**2a**) with yields up to 98% of 1,2-diphenylhydrazine (**3a**). Reduction of **2a** with quantitative yields was also achieved by Kinjo and co-workers<sup>60,61</sup> using diazaphospholene **E1** (Scheme 2.1b).<sup>62</sup> In addition, these authors also investigated the potential of such compounds as transfer hydrogenation/hydroboration catalysts for the reduction of unsaturated bonds using **AB** and HBpin respectively, through a hydrophosphination/metathesis mechanism.<sup>47</sup> Similarly, Speed *et al.* described the reduction of imines and conjugated C=C bonds using HBpin and the diazaphospholene **F1** as precatalyst (Scheme 2.1c).<sup>48,63</sup> Treatment of **F1** with HBpin (1 equiv.) resulted in the formation of **E1**. The authors remarked that, after the hydrophosphination

reaction, the initial metathesis occurred only at the exocyclic P-N or P-O bond (whichever the case). Prolonged exposure of **B** to **AB** or HBpin initiates further *P-N* bond cleavage, and the generation of  $\text{PH}_3$  was observed.<sup>64,65</sup>



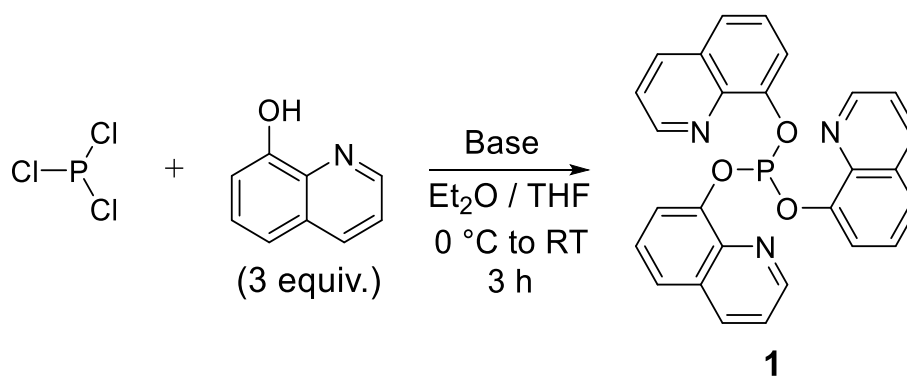
Scheme 2.1. Cyclic phosphorus compounds used in catalytic transfer hydrogenation (TH) from different  $\text{H}_2$  sources to unsaturated bonds.

Lately, reports by the groups of Radosevich,<sup>50</sup> Kinjo<sup>51</sup> and Speed<sup>66</sup> proved that it is possible to extend this application to challenging reduction reactions such as stereoselective reduction of imines and  $\alpha,\beta$ -unsaturated aldehydes, chemoselective reduction of C=C bonds in  $\alpha,\beta$ -unsaturated esters and hydroboration of pyridines. Additionally, diazaphospholene **E1** catalyzes C-C coupling reactions,<sup>51b</sup> and an analogue of **F1** has been used to promote reductive Claisen rearrangement in presence of boranes.<sup>67</sup> These investigations suggest the possibility to further expand the scope of phosphorus compounds and their catalytic reactivity.



## 2.2 Synthesis of tris(8-quinolinyl)phosphite, P(OQuin)<sub>3</sub>, **1**.

Upon reaction of PCl<sub>3</sub> with a slight excess of 8-hydroxy-quinoline, in the presence of base, the new trivalent phosphorus compound tris(8-quinolinyl)phosphite, P(OQuin)<sub>3</sub>, **1**, was obtained (Scheme 2.2). The product was isolated as a white microcrystalline solid in high yield (95%) and can be prepared on a multigram scale (10 g). Elemental analysis, HR-MS and NMR spectroscopic data (<sup>1</sup>H, <sup>13</sup>C{<sup>1</sup>H}, and <sup>31</sup>P{<sup>1</sup>H}) are according to the proposed formulation. Protons and carbons were assigned using 2D NMR analysis such as HMQC and HMBC. P(OQuin)<sub>3</sub> is very sensitive to air and moisture but can be stored at room temperature for months in a glovebox under an inert atmosphere.



Scheme 2.2. General reaction for the synthesis of P(OQuin)<sub>3</sub>, **1**.

The formation of **1** was monitored by <sup>31</sup>P{<sup>1</sup>H} NMR in order to investigate the effect of aspects such as reaction temperature, time and solvent on the reaction yield. Over the temperature range 0-60 °C, time range 3-16 h and Et<sub>2</sub>O, THF or CH<sub>2</sub>Cl<sub>2</sub> as solvents, not significant differences on the productivity and selectivity of the reaction were observed. Nevertheless, the selection of the base is critical as described in Table 1. For example, the synthesis of P(OQuin)<sub>3</sub> can proceed with a high excess of 8-hydroxy-quinoline (8 equiv. regard to PCl<sub>3</sub>), yielding only 45% of the desired product (entry 2, Table 2.1).

Table 2.1. Screening of base for the synthesis of **1**. <sup>a</sup>

Entry	Base	Yield <sup>b</sup>
1	NEt <sub>3</sub>	85
2 <sup>c</sup>	8-Hidroxyquinoline	45
3	<sup>n</sup> BuLi	90
4	NaH	95

[a] PCl<sub>3</sub> (2.10 g, 15.3 mmol), 8-hydroxyquinoline (6.88 g, 47.4 mmol), base (47.4 mmol), THF (50 mL) and Et<sub>2</sub>O (100 mL), argon atmosphere, RT, 3 h. [b] Isolated yield. [c] 8-hydroxyquinoline (17.76 g, 122.3 mmol) w/o additional base.

When the reaction proceeds in the presence of  $\text{NEt}_3$  or  $n\text{BuLi}$ , the product can be obtained with high yield and “sufficiently clean” based on spectroscopic analysis ( $^1\text{H}$  and  $^{31}\text{P}\{^1\text{H}\}$  NMR) but not analytically pure as confirmed by elemental analysis, which revealed the existence of some impurities. The problem lies in the difficulties to eliminate the formed  $\text{NEt}_3\cdot\text{HCl}$  or  $\text{LiCl}$  in an efficient way. For this reason, an alternative base for the synthesis of **1** was employed, namely sodium hydride. Following a reported procedure for the preparation of the lithium quinolate salt,  $\text{NaH}$  readily reacts with 8-hydroxy-quinoline to get the sodium analogue as a bright yellow solid. Moreover, the sodium quinolate can be prepared *in-situ* and reacted with  $\text{PCl}_3$ . The formed- $\text{NaCl}$  can be separated more easily than  $\text{NEt}_3\cdot\text{HCl}$  or  $\text{LiCl}$ . An analytically pure batch of phosphite was obtained in 95% yield after recrystallization from dichloromethane and diethyl ether.

$^{31}\text{P}\{^1\text{H}\}$  NMR in  $\text{THF-d}_8$  spectrum shows a singlet resonance at  $\delta$  130 ppm, as depicted in Figure 2.1a. This value is shifted downfield, as already described for similar compounds<sup>68,69</sup>. In the  $^1\text{H}$  NMR ( $\text{THF-d}_8$ ) four sets of signals that integrate to 6 or 18 protons are found (Figure 2.1b), which means that a magnetic equivalence is observed between these three quinoline moieties. The resonances represent two set of separate spin systems. The first of them, an AMX-type system, corresponds to the pyridine scaffold. The signals exhibit a doublet of doublet multiplicity with a chemical shift of 8.30 ( $^3J_{\text{HH}} = 4.2$  Hz,  $^4J_{\text{HH}} = 1.7$  Hz), 8.20 ( $^3J_{\text{HH}} = 8.3$  Hz,  $^4J_{\text{HH}} = 1.7$  Hz) and 7.29 ( $^3J_{\text{HH}} = 8.4$  Hz,  $^3J_{\text{HH}} = 4.2$  Hz) ppm, respectively. The large shift on a signal ( $\delta$  8.30 ppm) corresponds to the H atom *ortho* to the N atom, as confirmed by 2D NMR experiments (COSY, HSQC and HMBC). The second set of resonances, a multiplet between 7.59-7.49 ppm, shows an ABC-type spin system. Such signals are assigned to the phenolate group.

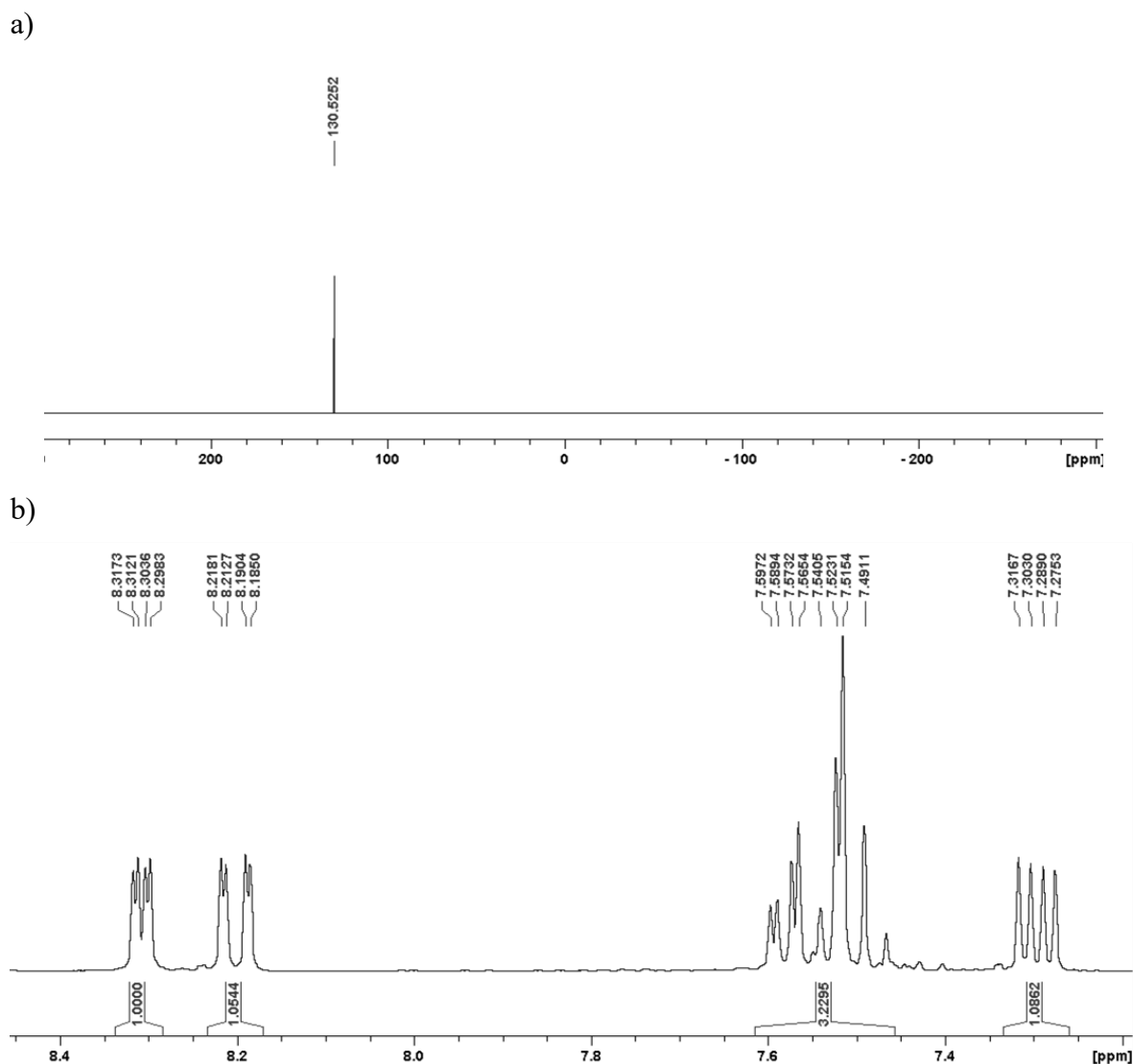


Figure 2.1. a)  $^{31}\text{P}\{^1\text{H}\}$  NMR and b)  $^1\text{H}$  NMR spectra of  $\text{P}(\text{OQuin})_3$  at RT in  $\text{THF-d}_8$ .

Crystals suitable for X-ray diffraction analysis were obtained *via* slow evaporation of a THF solution of **1**. The molecular structure of **1** is shown in Figure 2.2. Two independent molecules are observed in the asymmetric unit, with a distorted trigonal-pyramidal geometry around the P atom (pseudo-tetrahedral taking the phosphorus lone-pair into account). The heterocyclic rings are oriented in a way that the O–C bonds are directed toward the electron lone pair of the P atom. In this scenario, two nitrogen centers (N3/N2 and N5/N6) are pointing toward the vertex of the pyramid (P1 and P2, correspondingly) while the third nitrogen is directed away from the phosphorus center (N1 and N4, correspondingly). Indeed, each of the nitrogen atoms N2 and N6 shows a short contact with the oxygen O1 and O4, correspondingly. The N–O interatomic distance is in average 3.03(4) Å.

An interesting feature in the crystal packing of **1** is the existence of  $\pi$ -stacking between proximal N-heterocyclic rings in each one of the independent molecules (Figure 2.3). The

centroid–centroid distance is 3.765 Å. This value is within the equilibrium distances calculated by Sherrill<sup>70</sup> for  $\pi$ -stacking, *i.e.* 3.45–3.95 Å.

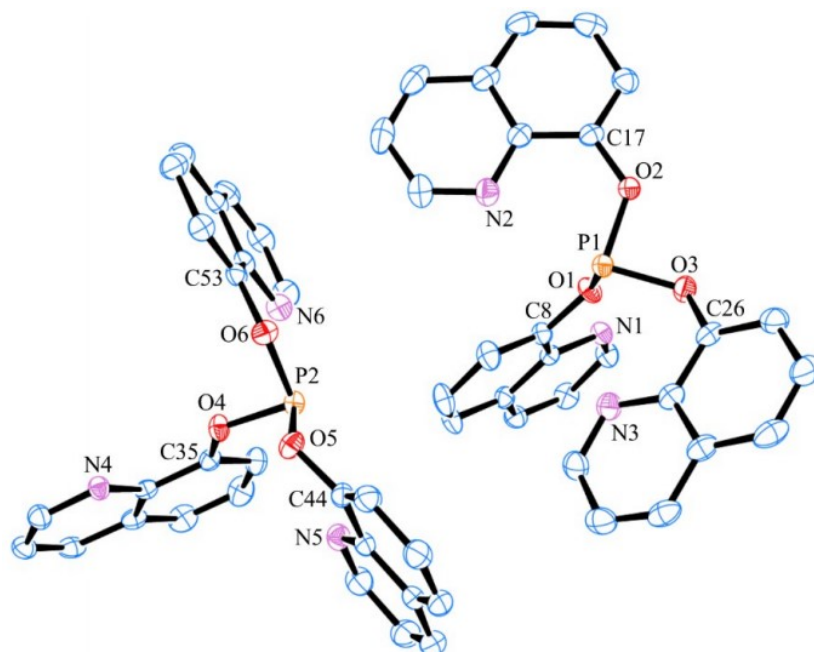


Figure 2.2. ORTEP drawing of the molecular structure of the phosphite ligand tris(8-quinoliny)phosphite, P(OQuin)<sub>3</sub>. Thermal ellipsoids are drawn at the 50% probability level. Hydrogen atoms have been neglected for clarity. Two independent molecules *per* asymmetric unit were found.

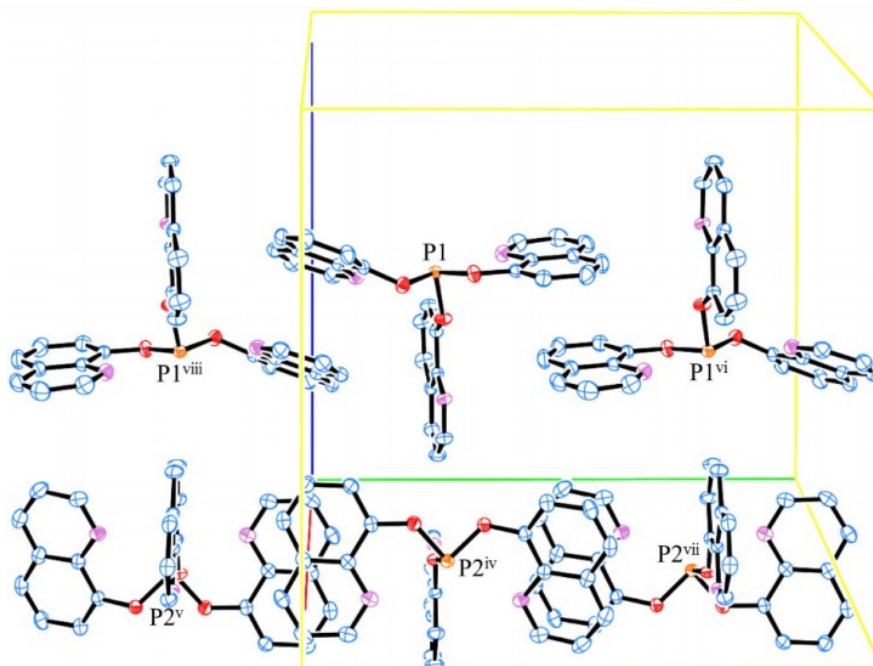


Figure 2.3. Packing of the molecules in the unit cell:  $\pi$ -stacking between proximal *N*-heterocyclic rings in each one of the independent molecules

Several contacts are present in the asymmetric unit of **1**: P···H, O···H, N···H and C–H···C–H interactions. The average of the interatomic distances and angles around the phosphorus atoms are listed in Table 2.2 and 2.3. The P–O bond lengths are significantly longer in **1** than those in the related compound tris(1-naphthyl)phosphite,<sup>68</sup> as shown in Table 2.2.

Table 2.2. Selected distances [Å] for **1** and the related compound tris(1-naphthyl) phosphite.

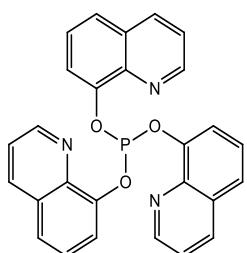
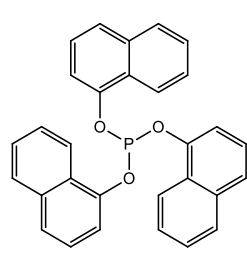
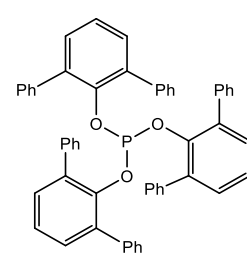
Bond	<b>1</b> <sup>a</sup>	Tri(1-naphthyl)phosphite
P-O	1.6406(11)	1.6086(11)
	1.6526 (12)	1.6376(11)
	1.6558 (12)	1.6425(11)
C-O	1.3752(18)	1.3889(17)
	1.3767(19)	1.3906(18)
	1.3799(18)	1.4026(17)

<sup>a</sup> Average of the two independent molecules in the unit cell.

The C–O distances and the O–P–O angles are significantly shorter in **2** than the analogous distances for tris(1-naphthyl)phosphite.<sup>68</sup> As a matter of fact, to the best of our knowledge, in average the O–P–O angles (93.5°) in **1** are shorter than the values previously obtained for any other phosphite ligand, cyclic or acyclic. The shortest average value for this kind of angle, 95.6° (Table 2.3), was the one reported for tris((2,6-diphenyl)phenyl)phosphite.<sup>69</sup> Such small bond angles are attributed to the steric hindrance of the substituents surrounding the P-atom. In average, the O–P–O angles of phosphite ligands are in the range of 97–98°.

Unlike **D1–F1**, which require several synthetic steps, **1** is quickly prepared in a one-pot reaction from commercial products on a gram scale, rendering it convenient for catalytic applications. P(OQuin)<sub>3</sub> presents intramolecular interactions in the solid-state that restrain the structure and originate a distorted geometry around the P atom (with an average O–P–O bond angle of 93.5 degrees) which, being acyclic, could somehow get a similar reactivity to the strained or cyclic P<sup>III</sup> compounds previously mentioned.

Table 2.3. Comparison of selected angles for **1** with related (acycle) phosphorus (III) compounds.

<b>1</b> <sup>a</sup>		Tri(1-naphthyl)phosphite		Tris((2,6-diphenyl)phenyl)phosphite	
O <sub>1</sub> -P-O <sub>2</sub>	88.07(3)	O <sub>1</sub> -P-O <sub>2</sub>	94.73(5)	O <sub>1</sub> -P-O <sub>2</sub>	94.91(2)
O <sub>1</sub> -P-O <sub>3</sub>	94.79(2)	O <sub>1</sub> -P-O <sub>3</sub>	98.02(6)	O <sub>1</sub> -P-O <sub>3</sub>	96.33(2)
O <sub>2</sub> -P-O <sub>3</sub>	97.27(3)	O <sub>2</sub> -P-O <sub>3</sub>	101.91(6)	O <sub>2</sub> -P-O <sub>3</sub>	95.65(2)
$\bar{\chi}_\alpha$	<b>93.37</b>	$\bar{\chi}_\alpha$	<b>98.22</b>	$\bar{\chi}_\alpha$	<b>95.63</b>

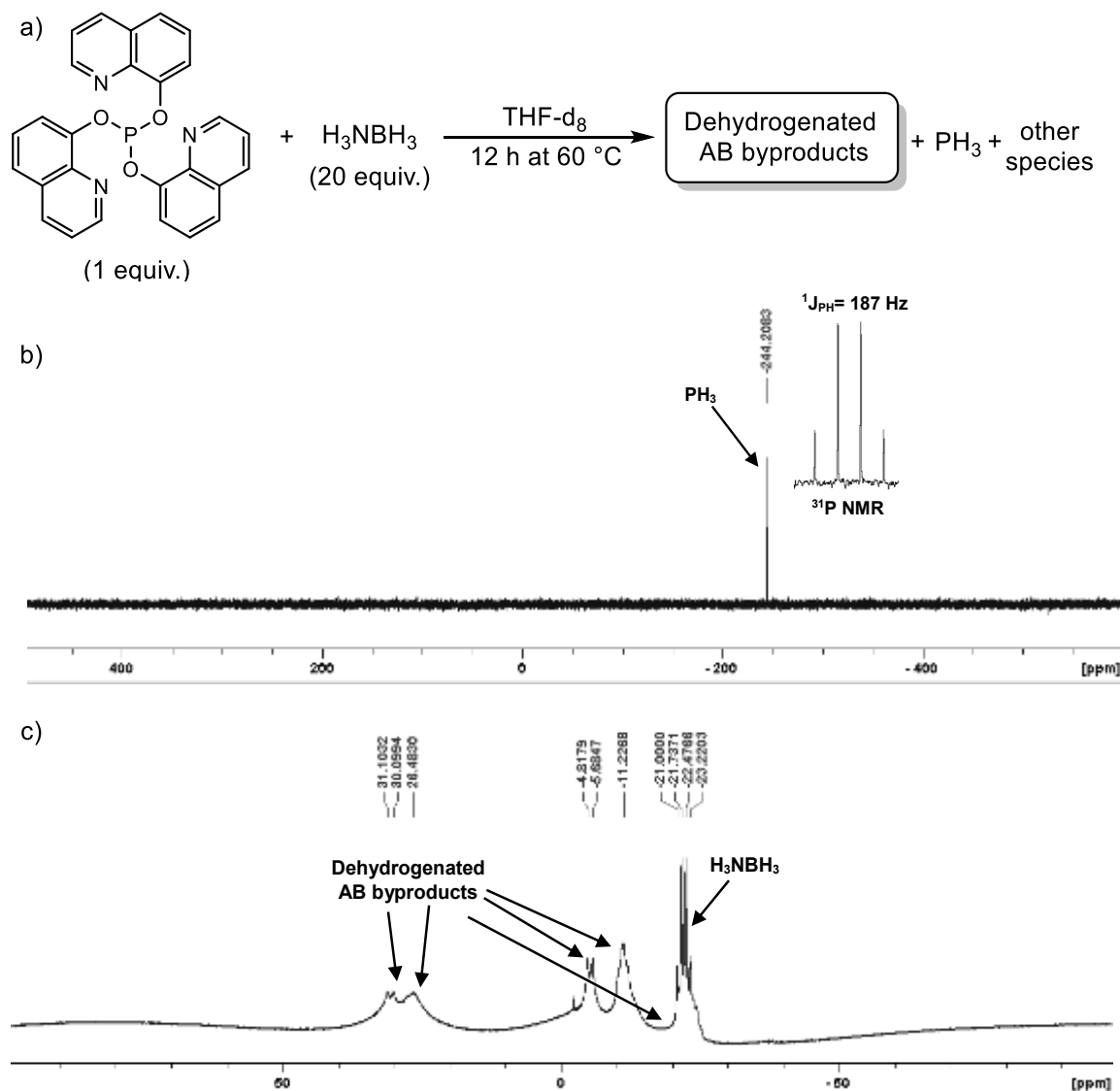
<sup>a</sup> Average of the two independent molecules in the unit cell.

### 2.3 Reactivity of Tris(8-quinolynyl)phosphite towards H<sub>3</sub>N·BH<sub>3</sub> as hydrogen source.

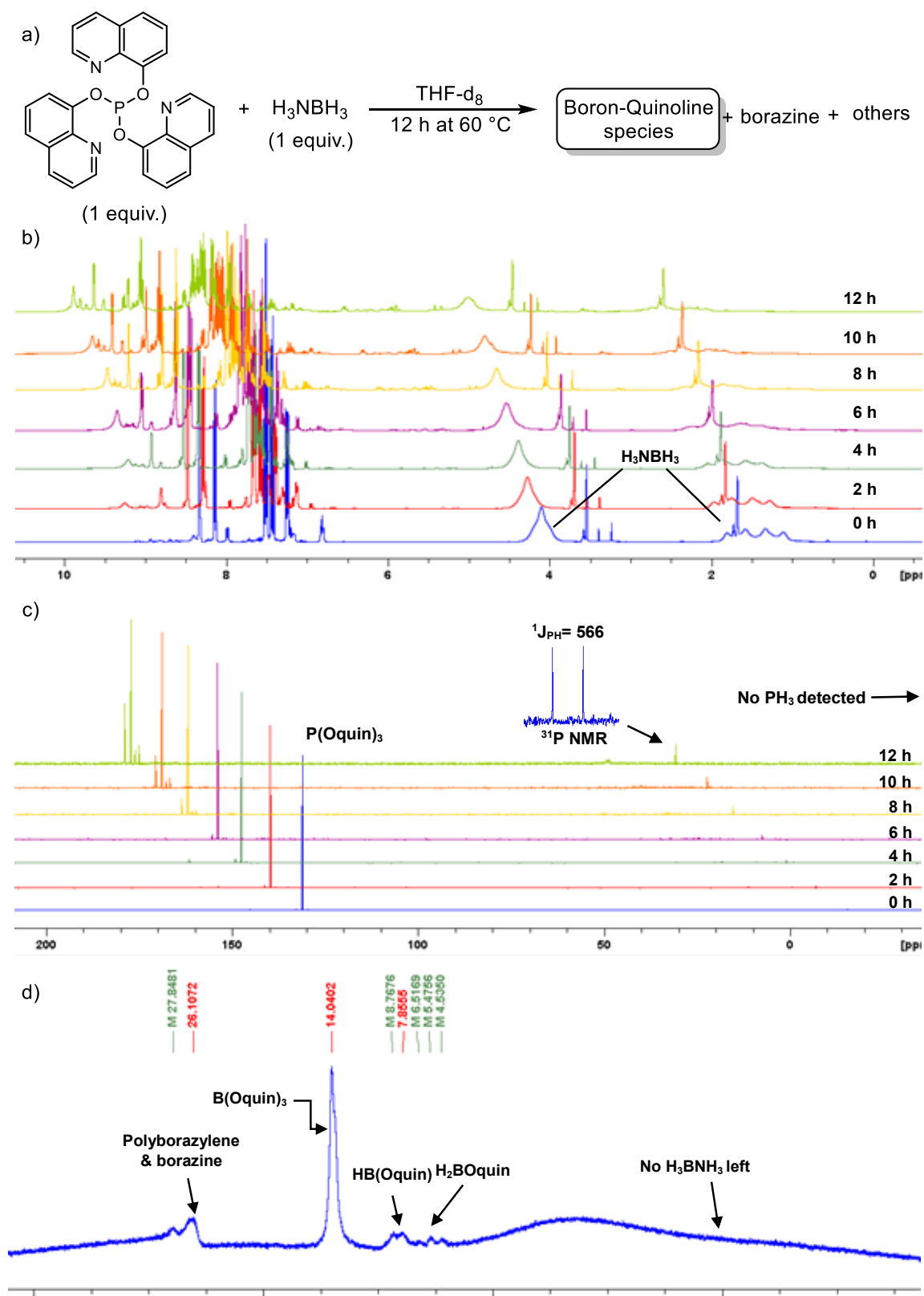
Considering the studies by Radosevich,<sup>59</sup> Kinjo<sup>60</sup> and Speed,<sup>63</sup> it becomes interesting to explore the potential of the p-block compound **1** as an organocatalyst in similar transformations. Thus, initially, it was important to study the reactivity of **1** toward **AB**. To this end, a test using a twenty-fold excess of **AB** was carried out (Scheme 2.3a). The selective formation of PH<sub>3</sub> (<sup>31</sup>P δ = −242 ppm, <sup>1</sup>J<sub>PH</sub> = 180 Hz; Scheme 2.3b) along with dehydrogenated ammonia borane species, such as borazine and polyborazylene,<sup>53</sup> was observed (Scheme 2.3c) by <sup>31</sup>P and <sup>11</sup>B NMR spectroscopy.

These findings evidence the dehydrogenation of ammonia borane along with a chemical transformation of **1**. To evaluate the effect of the amount of AB complex on the reaction with **1**, the ratio **1**/**AB** was reduced to 1:1 (Scheme 2.4) and 1:5 (Scheme 2.5). The stoichiometric or pseudo-stoichiometric reaction were conducted as independent tests. Although in such cases the reaction is less selective, producing several phosphorus- and boron-containing species (identified by <sup>31</sup>P or <sup>11</sup>B NMR, respectively), it was possible to observe products of the interaction of **1** with **AB** and to confirm that **1** is a hydrogen acceptor, which is transformed into other compounds. In particular, the presence of quinoline-based boron compounds, such as the corresponding borinate ester BH<sub>2</sub>(OQuin) (<sup>11</sup>B NMR δ = 5.9 ppm, <sup>1</sup>J<sub>BH</sub> = 122 Hz) and the boronate ester BH(OQuin)<sub>2</sub> (<sup>11</sup>B NMR δ = 8.8 ppm, <sup>1</sup>J<sub>BH</sub> = 135 Hz), was determined (Scheme 2.4d and 2.5c). Also, an-other (major) signal at 14 ppm in <sup>11</sup>B NMR, attributed to the *in-situ*

formation of B(OQuin)<sub>3</sub>, was identified, along with the common **AB** dehydrogenation product polyborazylene.

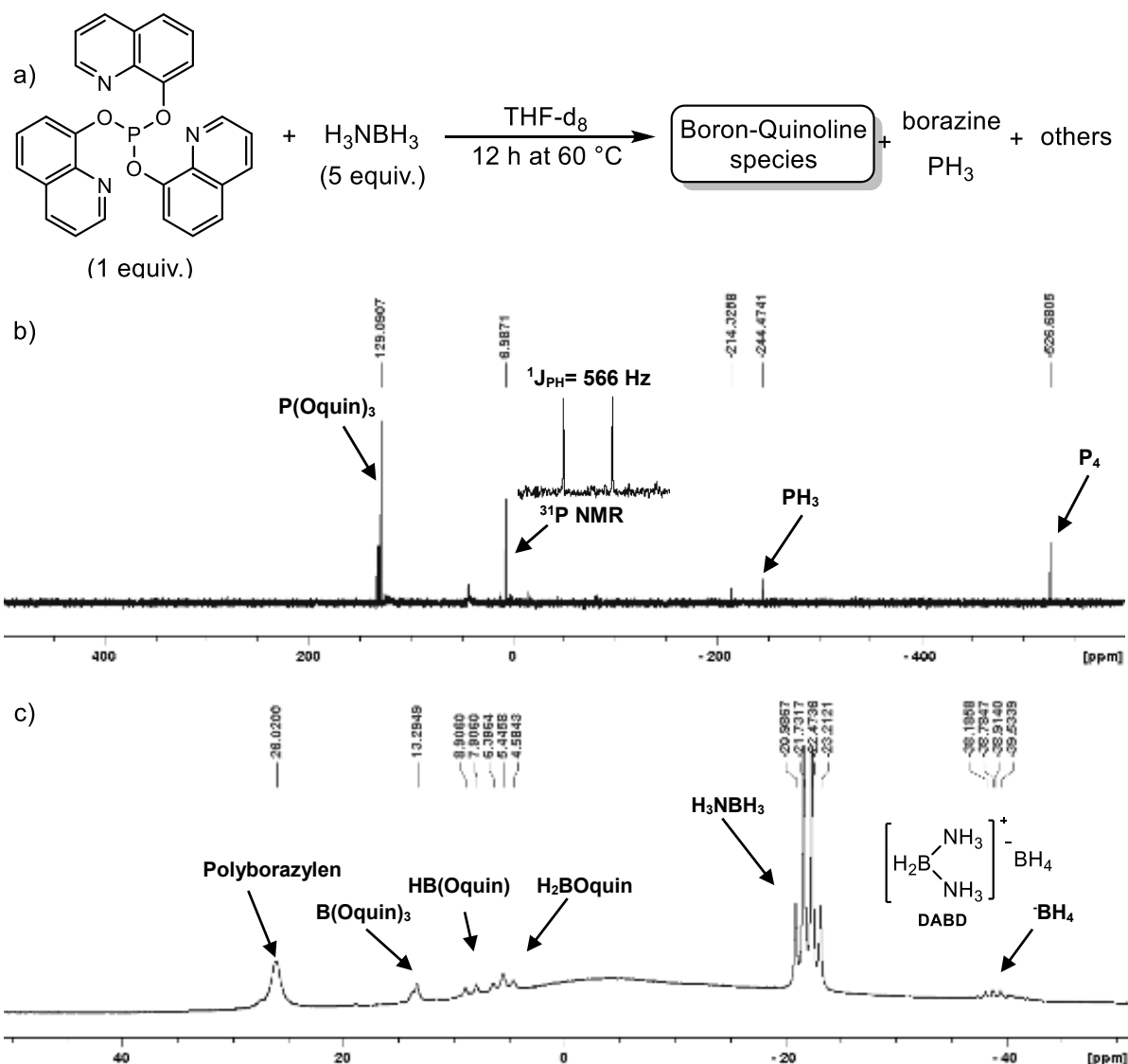


Scheme 2.3. a) Reactivity of **1** toward 20-fold of **AB** at 60 °C for 12 h in THF-d<sub>8</sub>. b) <sup>31</sup>P {<sup>1</sup>H} NMR spectrum of such reaction mixture (the inset shows a section of the proton-coupled <sup>31</sup>P NMR spectrum). c) <sup>11</sup>B NMR spectrum of such reaction mixture.



Scheme 2.4. a) Equimolar reaction of **1** + **AB** at 60 °C for 12 h in THF- $d_8$ . b)  $^1\text{H}$  NMR monitoring of such reaction mixture as a function of time, at 60 °C. c)  $^{31}\text{P}$   $\{^1\text{H}\}$  NMR monitoring of such reaction mixture, every 2 h at 60 °C (the inset shows a section of the proton-coupled  $^{31}\text{P}$  NMR spectrum). d)  $^{11}\text{B}$  NMR spectrum of such reaction mixture after 12 h at 60 °C.





Scheme 2.5 a) Reactivity of **1** toward 5 equiv. of **AB** at 60 °C for 12 h in THF- $d_8$ . b)  $^{31}\text{P}$   $\{^1\text{H}\}$  NMR spectrum of such reaction mixture after 12 h at 60 °C (the inset show the proton-coupled  $^{31}\text{P}$  NMR signal of the species resonating at 6.99 ppm). c)  $^{11}\text{B}$  NMR spectrum of such reaction mixture after 12 h at 60 °C. DADB: diammoniate of diborane<sup>[71]</sup>

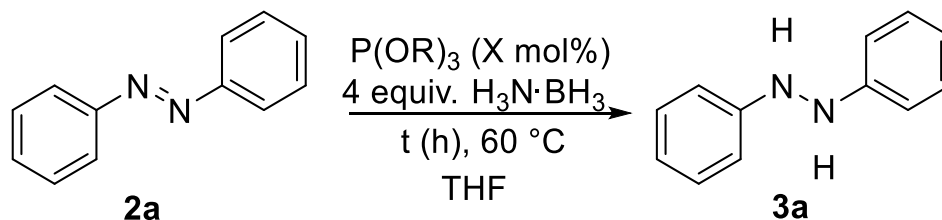
Regardless of such lack of selectivity, after determining the reactivity of **1** as hydrogen acceptor from **AB**, it was important then to study its potential to promote transfer hydrogenation reactions or, more specifically, to determine whether the phosphite or its products after dehydrogenation of **AB** could engage in the transfer of hydrogen to an unsaturated substrate.

## 2.4 Reduction of azocompounds catalyzed by $\text{P}(\text{OQuin})_3$ .

The hydrogenation of azobenzene (**2a**) in the presence of **1** to yield 1,2-diphenylhydrazine (**3a**), was tested as a model reaction (Table 2.4). For the sake of comparison, other analogous phosphite compounds were also tested as catalyst precursors. The reduction of **2a** in THF at 60 °C produces **3a** in high yields (>95% after 16 h; entry 1). By using stoichiometric amounts of

**AB** (1.1 equiv. relative to azobenzene) at the highest catalyst loading studied (*i.e.* 30 mol%), the reaction proceeded without significant loss in yield, but a longer reaction time was required (>95% after 24 h; entry 2). However, when stoichiometric amounts of **AB** were used at catalysts loadings between 20 mol% and 5 mol%, the catalytic activity dropped significantly (entries 4, 6, 9 and 11 compared to entries 3, 5, 8 and 10, respectively). The observed effect is more pronounced for lower catalyst loadings. Good conversion was achieved using 10 mol% of **1** and a four-fold excess of **AB** (80% after 24 h; entry 8). Moderate activity was observed for loadings below 5 mol% of **1** (57%; entry 10). Lowering the pre-catalyst loading to 12.5 mol% still gave high conversions of **2a** when compared to higher catalysts loadings (ca. 90%; entries 3 or 5 *vs* entry 7). Compounds similar to **1**, *e.g.* ((*R*)-binaphthol)-P(8-OQuin)<sup>26q</sup> and P(1-O-Naphthyl)<sub>3</sub>,<sup>68</sup> or the aromatic phosphite P(OPh)<sub>3</sub>, were inefficient catalyst precursors under the studied conditions, yielding **3a** in only 63%, 17% or 40%, respectively (entries 13 and 14). In the absence of a catalyst precursor, a very poor conversion was observed, thus highlighting the catalytic nature of the transformation (entry 15). In a screening of solvents, high activity was also obtained in acetonitrile, benzene, and toluene. In particular, the latter two apolar hydrocarbons gave a quantitative reduction of **2a** after 24 h. However, THF was selected as the solvent for the rest of the studies to avoid interference with aromatic signals at quantifying steps on the <sup>1</sup>H NMR spectra.

Table 2.4. Metal-free transfer hydrogenation of **2a** using the phosphite **1** as precatalyst. Screening of catalyst precursors. <sup>a</sup>



Entry	Catalyst Precursor P(OR) <sub>3</sub>	Time (h)	Catalyst loading (mol%)	Conversion (%) <sup>c</sup>
1	1	16	30	>95
2	1 <sup>b</sup>	24	30	>95
3	1	24	20	>95
4	1 <sup>b</sup>	24	20	78
5	1	24	15	94 ± 1 (91) <sup>d</sup>
6	1 <sup>b</sup>	24	15	75 ± 3
7	1	24	12.5	87 ± 3
8	1	24	10	80 ± 2
9	1 <sup>b</sup>	24	10	57 ± 2
10	1	24	5	57 ± 2
11	1 <sup>b</sup>	24	5	20 ± 1
12	P(OPh) <sub>3</sub>	64	30	40
13	((R)-1,1'-binaphthane-2,2'-diyl)P(8-OQuin)	64	30	63
14	P(1-O-Naphthyl) <sub>3</sub>	64	30	17
15	None	64	0	<5

[a] **2a** (54.7 mg, 0.3 mmol), **AB** (37.0 mg, 1.2 mmol, 4 equivalents), 1,3,5-trimethoxybenzene (16.7 mg, 99.0 μmol, internal standard), THF (1.25 mL), argon atmosphere, 60 °C, 24 h. [b] **AB** (10.2 mg, 0.33 mmol, 1.1 equivalents). [c] Conversions determined by <sup>1</sup>H NMR using the internal standard. Values with errors are the result of at least two independent experiments. Triplicates were performed when the deviation of two experiments was larger than ±5. [d] Values in parenthesis correspond to isolated yield.

Considering the spectroscopic evidence obtained from the reactivity tests (*i.e.* the formation of PH<sub>3</sub>, BH<sub>2</sub>(OQuin), BH(OQuin)<sub>2</sub> and HOQuin) it was important then to determine the

influence of such compounds on the model reaction (Table 2.5) and, thus, to shed some light into the possible mechanism and/or catalytic species involved in the transformation. Initially, the catalytic activity of 8-quinolinol (HOQuin) was tested. 70% conversion was achieved with 30 mol% of 8-quinolinol after 24 h. Longer reaction time (64 h) did not increase the conversion in this case (entry 1 and 2, respectively; Table 2.5). Also, NaPH<sub>2</sub> was independently examined as a PH<sub>3</sub> source. No conversion of **2a** to **3a** was observed, using either NaPH<sub>2</sub> or combining NaPH<sub>2</sub> with HCl (10 mol%, 1.0 M in Et<sub>2</sub>O) to produce PH<sub>3</sub> *in situ*. (entry 3 and 4, respectively; Table 2.5). Subsequently, the catalytic performance of a 1:3 mixture of NaPH<sub>2</sub> and 8-quinolinol was investigated. This mixture yielded a conversion to **3a** of >95% after 24 h, thus reproducing the performance (in terms of product yield) achieved by **1**. The substrate to **AB** ratio could be lowered to 2:1 and the reduction of **2a** still occurred effectively (>95%, entry 8; Table 2.5).

Finally, to investigate the possible role of the boron-containing species generated *in situ* from the system **1** + **AB**, separate TH reactions were performed using some of the boron-esters observed in the reactivity tests. In fact, H<sub>2</sub>BOQuin and HB(OQuin)<sub>2</sub> were among such boron compounds detected on the NMR scale experiments (Figure 2.4a).

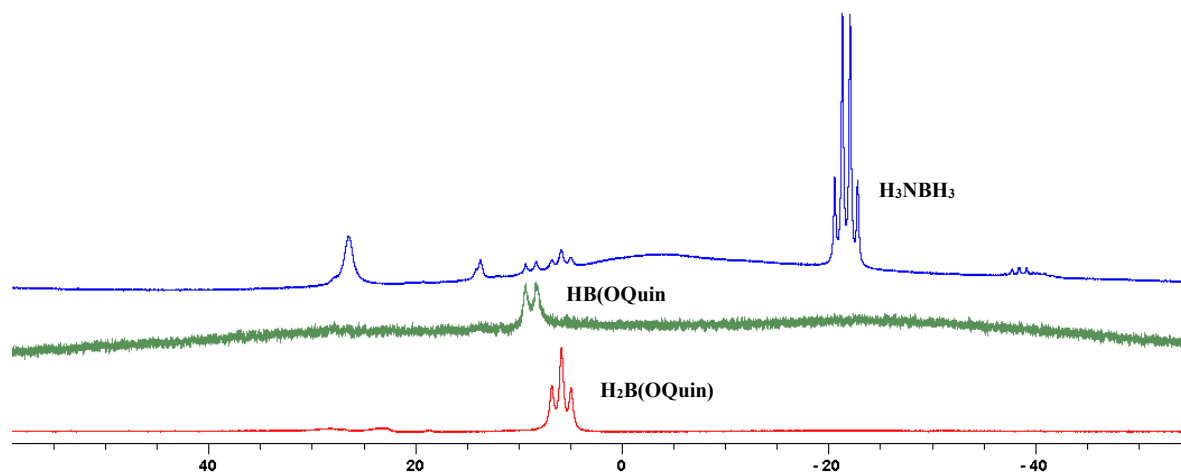


Figure 2.4. <sup>11</sup>B NMR spectrum of a 1:5 reaction mixture of **1** + **AB** after 12 h at 60 °C (blue), isolated HB(OQuin)<sub>2</sub> (green), isolated H<sub>2</sub>BOQuin (red).

These were also independently synthesized<sup>72</sup> (Figure 2.4b,c) to be used on the catalytic tests, yielding 70% and >95% conversion of **2a** to **3a**, respectively. The use of H<sub>2</sub>B(OQuin) as catalyst<sup>72</sup> in the reaction led to a yield of the diphenylhydrazine product **3a** lower than with the system **1** + **AB**. This seems to indicate that H<sub>2</sub>B(OQuin) is not the (*sole*) species responsible for the catalysis in this case. Unfortunately, it was impossible to assess the role of B(OQuin)<sub>3</sub> on the reaction. Attempts to isolate pure B(OQuin)<sub>3</sub> (which was assigned to a signal at 14 ppm in the <sup>11</sup>B NMR spectra, *vide supra*) yielded a mixture of H<sub>x</sub>B(OQuin)<sub>3-x</sub> (x = 0,1,2) that could

not be separated. Steric crowding on the boron atom, due to the presence of the three “OQuin” moieties, could be responsible for the impossibility to isolate such compound.

Table 2.5. Optimization process for the TH of azobenzene using different catalyst mixtures.

Entry	[Cat]	Equiv. AB	Time	Conversion (%) <sup>n</sup>
1 <sup>a,b</sup>	30 mol% 8-OH-Quinoline	4	64	70
2 <sup>a,b</sup>	30 mol% 8-OH-Quinoline	4	24	70
3 <sup>a,c</sup>	10 mol% NaPH <sub>2</sub>	4	64	<2
4 <sup>a,c,d</sup>	10 mol% NaPH <sub>2</sub> + 10 mol% HCl	4	64	<2
5 <sup>a-c</sup>	10 mol% NaPH <sub>2</sub> + 30 mol% 8-OH-Quinoline	4	24	>95
6 <sup>a-c</sup>	10 mol% NaPH <sub>2</sub> + 30 mol% 8-OH-Quinoline	4	16	>95
7 <sup>a-c,e</sup>	10 mol% NaPH <sub>2</sub> + 30 mol% 8-OH-Quinoline	1	16	>95
8 <sup>a-c,f</sup>	10 mol% NaPH <sub>2</sub> + 30 mol% 8-OH-Quinoline	0.5	16	>95
9 <sup>a-c,g</sup>	10 mol% NaPH <sub>2</sub> + 30 mol% 8-OH-Quinoline	0.25	24	45
10 <sup>a,c,h</sup>	10 mol% NaPH <sub>2</sub> + 10 mol% 8-OH-Quinoline	4	24	>95
11 <sup>a-d</sup>	10 mol% NaPH <sub>2</sub> + 10 mol% HCl + 30 mol% 8-OH-Quinoline	4	16	>95
12 <sup>a,b,i</sup>	10 mol% PMe <sub>3</sub> + 30 mol% 8-OH-Quinoline	4	64	<10
13 <sup>a,c,j</sup>	10 mol% NaPH <sub>2</sub> + 30 mol% 1-Naphtol	4	64	2
14 <sup>a,b,k</sup>	10 mol% LiNH <sub>2</sub> + 30 mol% 8-OH-Quinoline	4	64	58
15 <sup>a,l</sup>	30 mol% H <sub>2</sub> BOQuin	4	24	70
16 <sup>a,m</sup>	30 mol% HB(OQuin) <sub>2</sub>	4	24	>95

[a] **2a** (36.4 mg, 0.2 mmol), **AB** (24.7 mg, 0.8 mmol, 4 equivalents), 1,3,5-trimethoxybenzene (11.1 mg, 66.0 μmol, internal standard), THF (1 mL), argon atmosphere, 60 °C, 24 h. [b] 8-hydroxyquinoline (8.7 mg, 60.0 μmol). [c] NaPH<sub>2</sub> (1.1 mg, 30.0 μmol). [d] HCl (0.7 mg, 20 μl, 20.0 μmol, 1 M in Et<sub>2</sub>O). [e] **AB** (6.1 mg, 0.2 mmol). [f] **AB** (3.1 mg, 0.1 mmol). [g] **AB** (1.6 mg, 50.0 μmol). [h] 8-hydroxyquinoline (2.9 mg, 20.0 μmol). [i] Trimethylphosphine (1.5 mg, 20.0 μmol). [j] 1-Naphtol (8.7 mg, 60.0 μmol). [k] LiNH<sub>2</sub> (1.4 mg, 60.0 μmol). [l] H<sub>2</sub>BOQuin (9.4 mg, 60.0 μmol). [m] HB(OQuin)<sub>2</sub> (18.0 mg, 60.0 μmol). [n] Conversions determined by <sup>1</sup>H NMR using the internal standard.

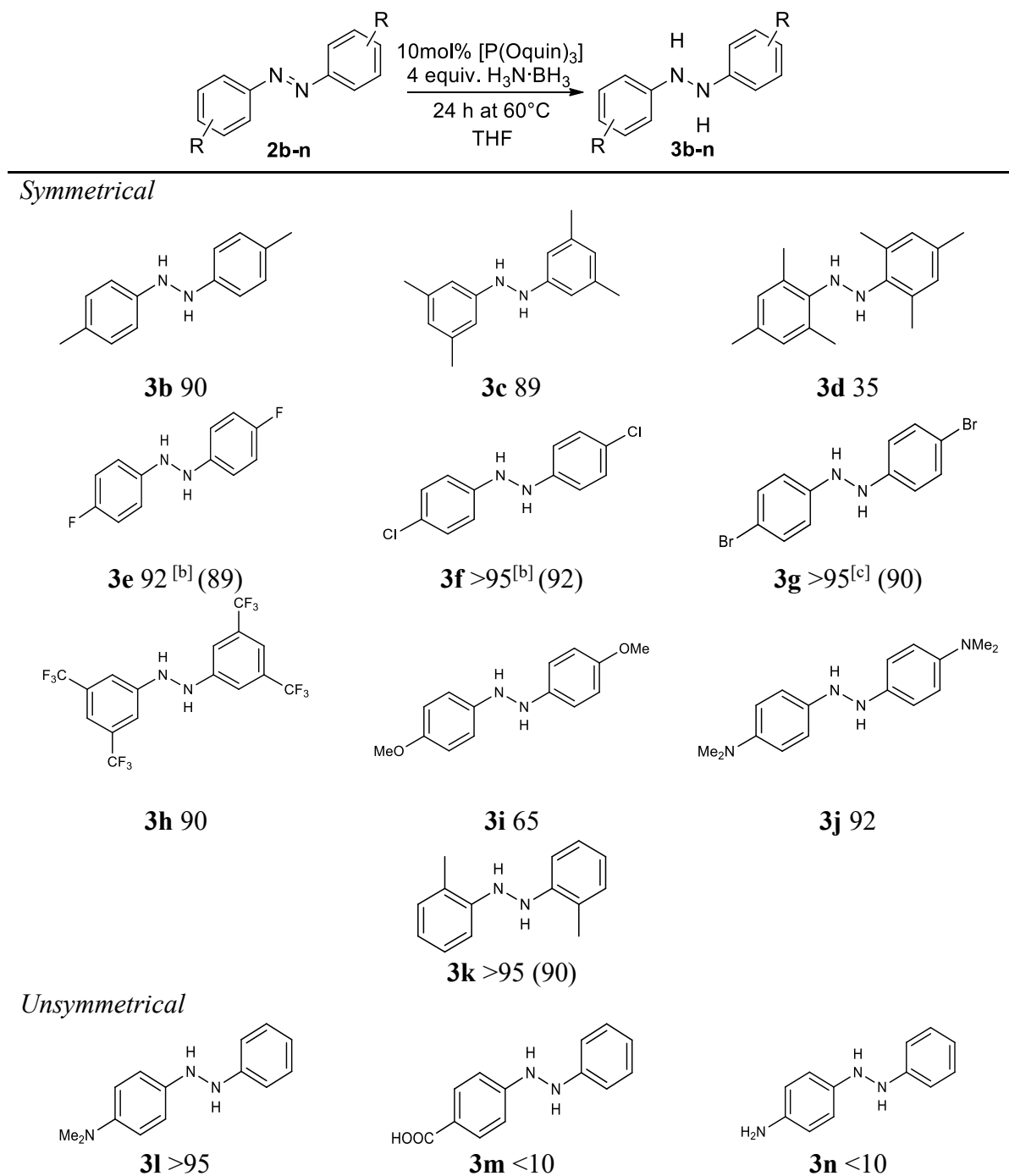
The findings from the reactivity tests strongly suggest that **1** is indeed a catalyst precursor, which serves as an appropriate source of the actual catalyst(s). While the identity of the true catalyst(s) presently remains unknown, both the phosphorus source and the “OQuin” moiety are required for the catalytic TH of **2a** from **AB**. Furthermore, although NaPH<sub>2</sub>/8-quinolinol and HB(OQuin)<sub>2</sub> (entry 16, Table 2.5) also worked effectively in converting **2a** into **3a** in the

presence of **AB**, the use of these catalytic systems would be more inconvenient. NaPH<sub>2</sub> is hard to prepare, difficult to handle and pyrophoric.<sup>73</sup> HB(OQuin)<sub>2</sub> (as well as H<sub>2</sub>B(OQuin)<sup>72</sup>) is thermally unstable and needs to be stored cold under inert atmosphere. For all the above, **1** was chosen as catalyst precursor for the rest of the study.

The following were selected as optimized conditions to examine the scope of the catalytic system with a series of symmetrical and unsymmetrical (*E*)-diazenes (Table 2.6): 10 mol% of catalyst precursor **1**, 4 equivalents of **AB**, 60 °C, 24 h (unless otherwise stated). Although the best conversion for substrate **2a** was achieved using 15 mol% of phosphite **1** as catalyst, for the rest of the azoarenes studied the use of catalytic loadings of 10 mol%, 12.5 mol% or 15 mol% did not significantly affect the conversion obtained. Thus, the catalyst loading was kept to the lowest possible to achieve the observed yields (Table 2.4). Symmetrical azoarenes bearing electron-donating groups (EDG) such as methyl in different relative positions (*p*-, *m*- and/or *o*-, **2b-d**, **k**), were converted into the corresponding phenylhydrazine compounds with good yields. The bulky compound **2d** is the only exception, for which 35% of the corresponding product was achieved after 24 h. Steric hindrance around the N=N bond might explain the low yield for such a compound.

In the case of *p*-dimethylamino derivatives (**2j** and **2l**, symmetrical and unsymmetrical, respectively) a quantitative conversion was achieved. For *p*-methoxy (**2i**) a moderate conversion was obtained. Likewise, symmetrical and unsymmetrical azoarenes bearing electron-withdrawing groups (EWG) in the *para* position, such as fluoro (**2e**), chloro (**2f**), and bromo (**2g**) derivatives, were reduced with good to excellent yields. In addition, a derivative substituted with trifluoromethyl groups (**2h**) in the *m*-position was tested, and a conversion of 90% was achieved. (*E*)-diazenes bearing a *p*-NH<sub>2</sub> (**2n**) or *p*-COOH (**2m**) gave very poor yields of the corresponding hydrazine after 24 h. Increasing the reaction time up to 64 h in these cases did not improve the conversion, suggesting that the system does not tolerate groups that have acidic protons.

Table 2.6. Metal-free transfer hydrogenation of azocompounds using the phosphite **1** as precatalyst. Screening of substrates.<sup>a</sup>



[a] **2b-n** (0.3 mmol), **1** (13.9 mg, 30.0  $\mu\text{mol}$ ), **AB** (37.0 mg, 1.2 mmol), 1,3,5-trimethoxybenzene (16.7 mg, 99.0  $\mu\text{mol}$ , internal standard) THF (1.25 mL), Argon atmosphere, 60  $^\circ\text{C}$ , 24 h. [b] 16 h. [c] 12 h. Given conversions (%) determined by  $^1\text{H}$  NMR spectroscopy. Values in parentheses (%) correspond to isolated yields.

## 2.5 Kinetic studies for the reduction of azocompounds catalyzed by P(OQuin)<sub>3</sub>.

The kinetics for the catalytic TH of **2a** to yield **3a** were examined. The progress of the reaction as a function of time was monitored by <sup>1</sup>H NMR spectroscopy (Figure 2.5). Plotting  $\ln ([\text{AZB}]/[\text{AZB}]_0)$  vs. time (h) returned a straight line (Figure 2.6). Here, [AZB] is the molar concentration of azobenzene at each given time and [AZB]<sub>0</sub> is the initial molar concentration of azobenzene. This simple experiment suggested a pseudo-first-order rate equation with regard to the azobenzene concentration in the presence of an excess of **AB**. Additionally, an induction period was observed, which needed to be considered for the analysis of the kinetic data. This period might be related to the time required for the activation of the precatalyst **1**, thus forming the actual active species, as evidenced by the reactivity tests (*vide supra*).

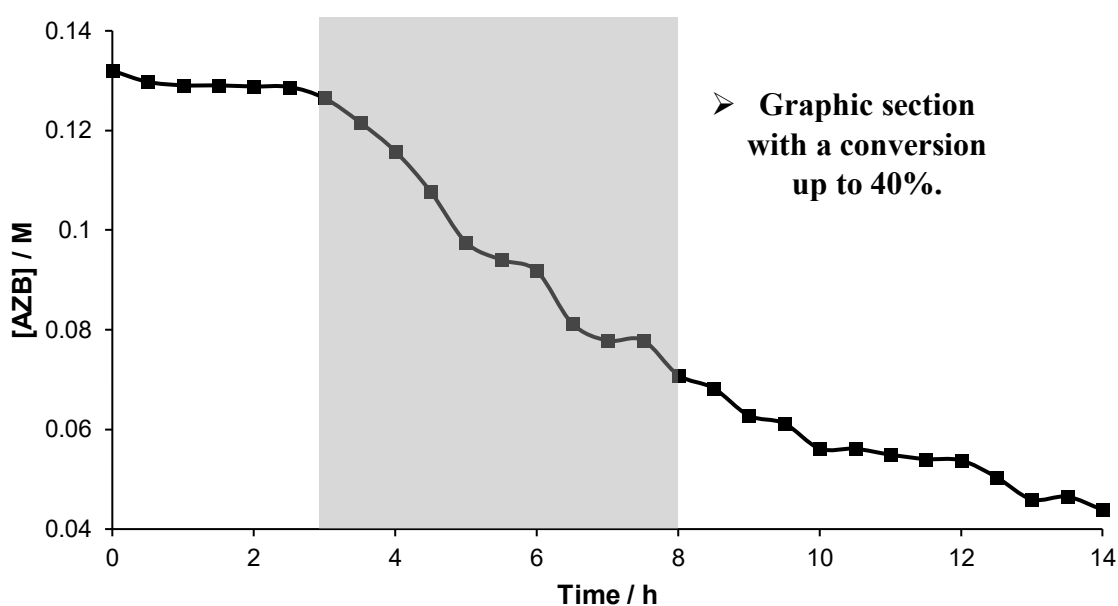


Figure 2.5. Azobenzene concentration as a function of time during the first 14 h of reaction.



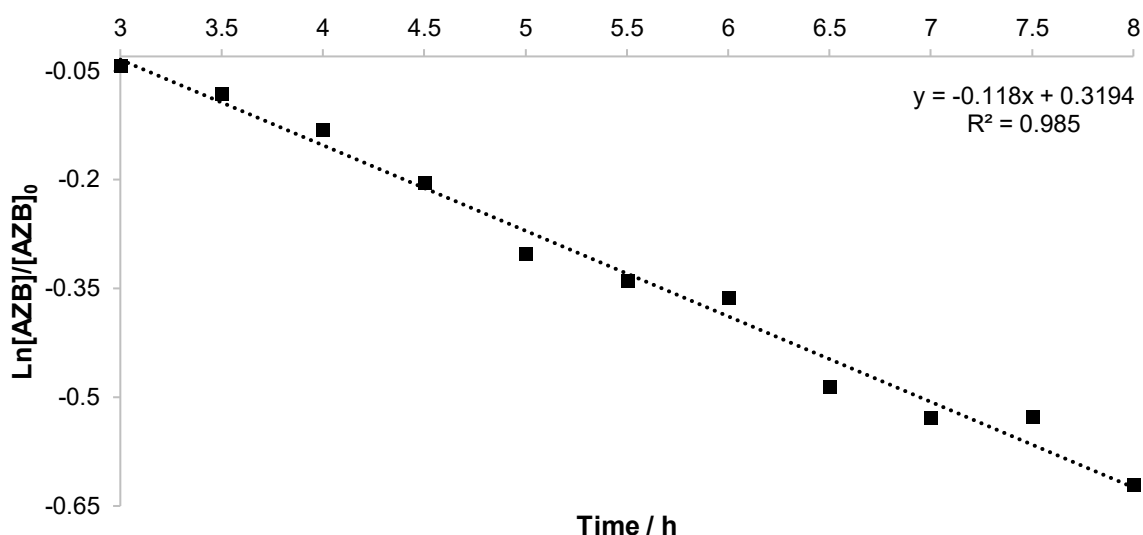


Figure 2.6. Representation of  $\text{Ln}([\text{AZB}]/[\text{AZB}]_0)$  vs. time

The evaluation of the reaction order with regard to the other individual components of the system was also carried out. A generic rate law for the TH of azobenzene is shown in equation 1 (Eq. 1). From this, the values  $\alpha$ ,  $\beta$ , and  $\gamma$  were determined by measuring the influence of the concentration for each respective component on the reaction rate.

$$r = k \cdot [\text{AZB}]^\alpha \cdot [\text{cat}]^\beta \cdot [\text{AB}]^\gamma \quad (\text{Eq. 1})$$

The rate of the reaction was measured as a function of the concentration of azobenzene, ranging between 0.044 M and 0.220 M, while the concentration of precatalyst and **AB**, temperature and time were kept constant (Table 2.7). The representation of  $\ln r$  vs.  $\ln [\text{AZB}]$  (Figure 2.7) returned a straight line with a slope of 1.02, indicating a first-order dependence on the concentration of azobenzene. This confirmed the result from the monitoring of the reaction as a function of time (*vide supra*).

Table 2.7. Reaction rates as a function of azobenzene concentration.

[AZB](mol.L <sup>-1</sup> )	Ln [AZB]	r (mol.L <sup>-1</sup> .s <sup>-1</sup> )	R <sup>2</sup>	Ln r
0.044	-3.1235656	8.205E-06	0.994	-11.710767
0.088	-2.4304185	1.993E-05	0.976	-10.823284
0.132	-2.0249534	2.937E-05	0.985	-10.435537
0.176	-1.7372713	3.692E-05	0.983	-10.206757
0.220	-1.5141277	4.638E-05	0.970	-9.9786422

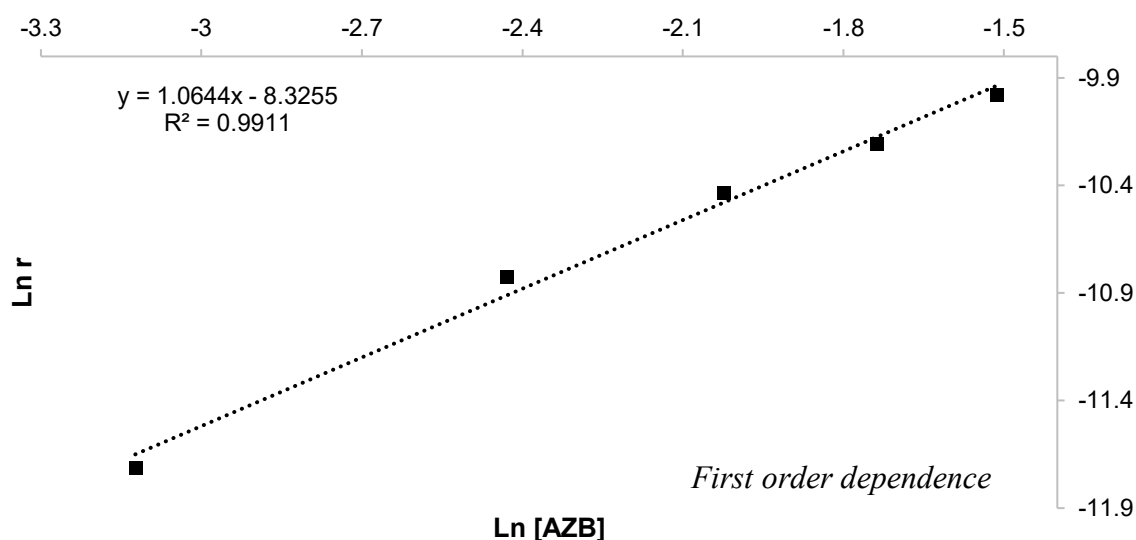


Figure 2.7. Representation of  $\text{Ln}(r)$  as a function of  $\text{Ln}[\text{AZB}]$ .

Likewise, the rate of reaction was measured depending on the catalyst concentration, ranging from 0.004 M to 0.025 M, while the concentration of azobenzene, concentration of **AB**, temperature and reaction time were kept constant. (Table 2.8) A fractional order (1/2) dependence on catalyst concentration can be observed from the plot of  $\ln r$  vs.  $\ln [\text{cat}]$  with a slope value of 0.48 (Figure 2.8). The kinetic data was also analyzed using the graphical method described by Burés *et al.*,<sup>74</sup> thus confirming our findings for catalyst loadings higher than 10 mol%. This result suggests that there is a complex relationship between the catalyst concentration and the reaction rate and confirms that **1** act as a precatalyst. The fractional order could be a consequence of the induction time required to form the actual catalyst or could also be related to the fact that more than one catalytically active species is involved.

Table 2.8. Reaction rates as a function of precatalyst concentration.

[precat] mol%	[precat] M	$\text{Ln} [\text{precat}]$	$r$ $\text{mol.L}^{-1}.\text{s}^{-1}$	$R^2$	$\text{Ln } r$
2.5	0.004	-5.52146092	1.598E-05	0.972	-11.0441726
5	0.007	-4.96184513	2.162E-05	0.977	-10.7418917
10	0.013	-4.34280592	2.689E-05	0.985	-10.5237561
15	0.019	-3.9633163	3.296E-05	0.977	-10.3202159
20	0.025	-3.68887945	3.920E-05	0.972	-10.1468338

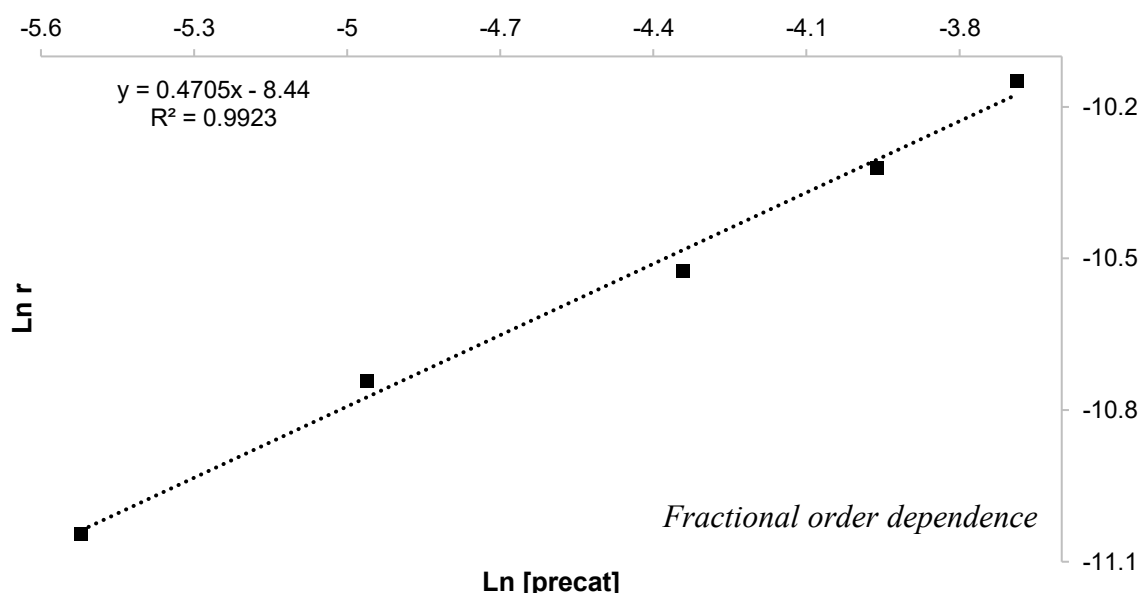


Figure 2.8. Ln(r) as a function of Ln[precat].

Given the fact that an excess of **AB** (4 equivalents respect AZB, formally up to 12 eq. H<sub>2</sub>) has been used, its concentration is higher than needed at any time and, thus, it can be considered constant. Consequently, **AB** concentration disappears from the rate law equation (Eq. 1) and it is integrated into the rate constant  $k$ , leading to an apparent rate constant  $k_{app} = k[AB]^{\gamma}$ . Once the order of reaction with respect [AZB] and [1] were determined, the magnitude of  $k_{app}$  could be calculated ( $0.029 \pm 0.005 \text{ s}^{-1} \cdot \text{L}^{0.5} \cdot \text{mol}^{-0.5}$ ). These kinetic experiments indicate that the rate law can be represented as in equation 2 (Eq. 2) at constant temperature (60 °C) and using a four-fold excess of **AB** (formally 12 equivalents of H<sub>2</sub>).

$$r = k_{app} \cdot [AZB] \cdot [1]^{1/2} \quad (\text{Eq. 2})$$

The temperature dependence on the rate of reaction was evaluated using temperature ranges between 40 °C and 80 °C, at 10 °C intervals. The representation of the ln [AZB] vs. time gave a straight line (Figure 2.9). An induction time caused by precatalyst activation was observed, which was inversely proportional to the temperature and the substrate concentration. Points representing the induction time were discarded from the graph, to obtain a better fit on linearity.

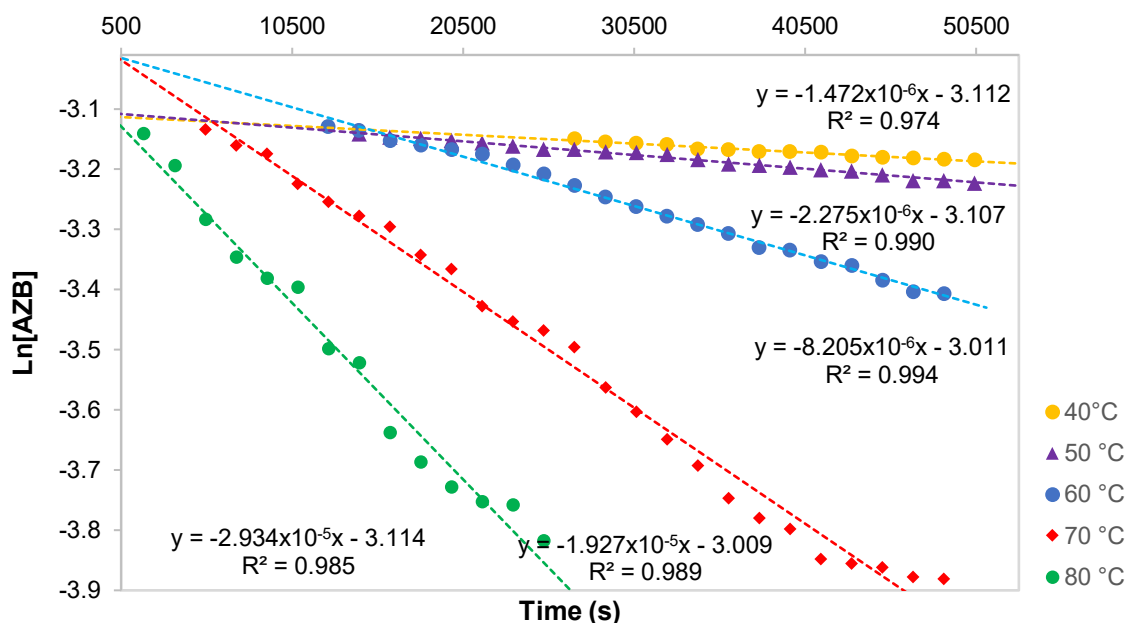


Figure 2.9. Ln [AZB] at different temperatures vs. time.

After determination of the temperature influence on the reaction rate, both Eyring and Arrhenius analysis were performed (Table 2.9 and 2.10, Figure 2.10 and 2.11, respectively). The  $\ln(r/T)$  was plotted against the inverse of the temperature ( $1/T$ ) (Figure 2.10) yielding a straight line in accordance with the corresponding equation (Eq. 3).

$$\ln\left(\frac{r}{T}\right) = \left(\frac{-\Delta H^\ddagger}{R}\right) \cdot \left(\frac{1}{T}\right) + \ln\left(\frac{kB}{h}\right) + \ln\left(\frac{\Delta S^\ddagger}{R}\right) \quad (\text{Eq. 3})$$

From the slope and the intercept, values of  $\Delta H^\ddagger = 17.1 \pm 2.6$  kcal/mol,  $\Delta S^\ddagger = -31 \pm 7$  e.u and  $\Delta G^\ddagger_{(298.15 \text{ K})} = 26.4 \pm 5.7$  kcal/mol were calculated. The sign and magnitude of the entropy of activation are consistent with a reaction step involving a transition structure typical of a bimolecular reaction. This might be in agreement with an associative mechanism, in which at least two reaction partners form a single activated complex.<sup>55a-c,64,75</sup> Then, The  $\ln r$  was plotted against  $1/T$  (Figure 2.11) and from the Arrhenius analysis, an activation energy of  $17.8 \pm 4.1$  kcal/mol was obtained using the corresponding equation (Eq. 4).

$$\ln(r) = \left(-\frac{Ea}{R}\right) \cdot \left(\frac{1}{T}\right) + \ln A \quad (\text{Eq. 4})$$

Table 2.9. Reaction rates as a function of the temperature. Ln(r/T) vs. 1/T for Eyring analysis.

T / K	1/T	r / mol.L <sup>-1</sup> .s <sup>-1</sup>	r / T	Ln (r/T)
313.15	0.00319336	1.472E-06	4.701E-09	-19.175571
323.15	0.00309454	2.275E-06	7.040E-09	-18.771647
333.15	0.00300165	8.205E-06	2.463E-08	-17.519360
343.15	0.00291418	1.927E-05	5.616E-08	-16.695129
353.15	0.00283166	2.952E-05	8.359E-08	-16.297335

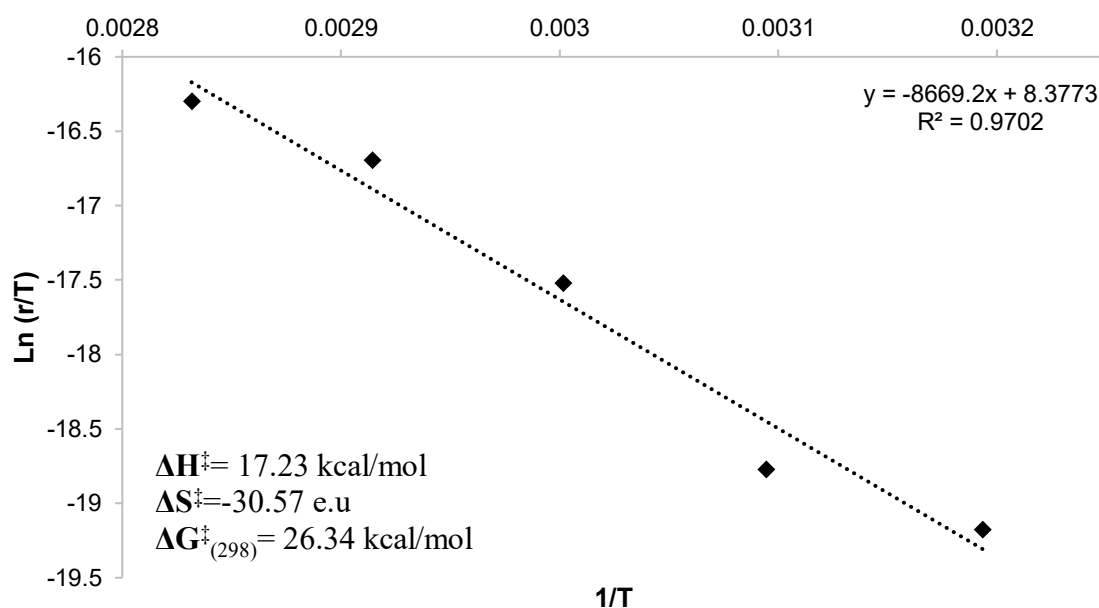
Figure 2.10. Eyring plot for TH of azobenzene catalyzed by P(OQuin)<sub>3</sub>. Based on respective equations, activation thermodynamic parameters were determined.

Table 2.10. Reaction rates as a function of the temperature. Ln(r) vs. 1/T for Arrhenius analysis.

T / K	1/T	K / mol.L <sup>-1</sup> .s <sup>-1</sup>	Ln r
313.15	0.00319336	1.472E-06	-13.428889
323.15	0.00309454	2.275E-06	-12.993531
333.15	0.00300165	8.205E-06	-11.710767
343.15	0.00291418	1.927E-05	-10.856961
353.15	0.00283166	2.952E-05	-10.430443

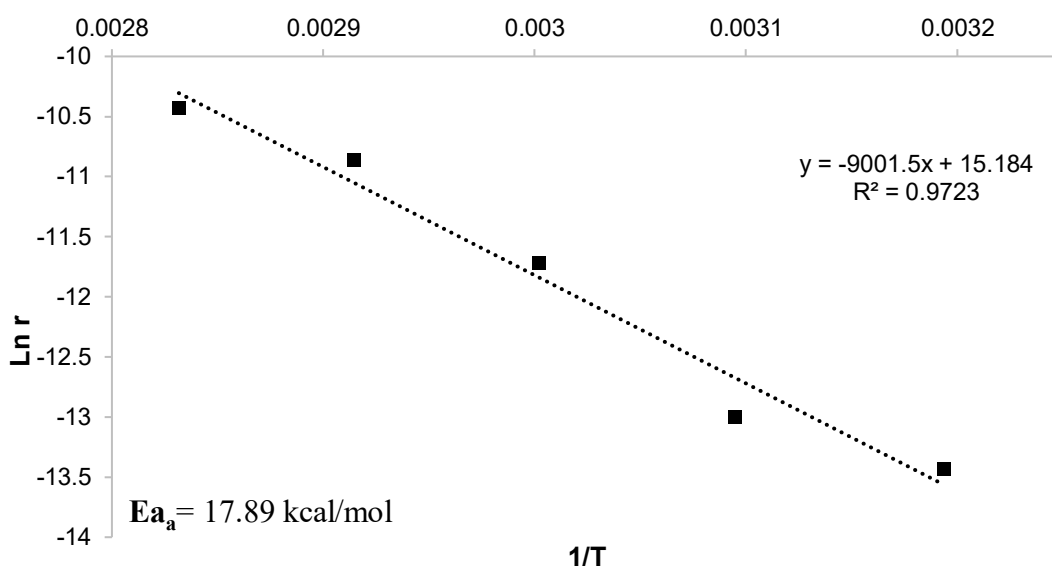


Figure 2.11. Arrhenius plot for TH of azobenzene catalyzed by P(OQuin)<sub>3</sub>. Based on respective equation activation energy was determined.

To the best of our knowledge, only two examples of kinetic experiments have been reported for the TH of azobenzene involving **AB** as the hydrogen source. Kinjo and co-workers studied the kinetics for the TH of azobenzene using the diazaphospholene catalyst **E1** (Scheme 2.1b).<sup>60,61</sup> Their results also suggest a first-order rate equation with regard to the substrate. Radosevich and co-workers<sup>59</sup> carried out kinetic experiments for the TH of azobenzene catalyzed by species **D1** (Scheme 2.1a). Also, in this case, in the presence of an excess of azobenzene, the reaction follows a pseudofirst-order kinetics. Furthermore, Eyring analyses were performed obtaining the following activation thermodynamics parameters:  $\Delta H^\ddagger = 21.8$  kcal/mol,  $\Delta S^\ddagger = -11.6$  e.u and  $\Delta G^\ddagger_{(298.15)} = 25.2$  kcal/mol, for Kinjo's system;  $\Delta H^\ddagger = 12.4$  kcal/mol,  $\Delta S^\ddagger = -36$  e.u and  $\Delta G^\ddagger_{(298.15)} = 23.13$  kcal/mol, for Radosevich's system. The sign of the enthalpy of activation ( $+\Delta H^\ddagger$ ) and the sign and magnitude of the entropy of activation ( $-\Delta S^\ddagger$ ) in the present work agree with the results cited before. Moreover, the magnitudes of the free-energy of activation ( $+\Delta G^\ddagger$ ) are very similar in all cases. This might suggest that the nature of the transition state of the rate-determining step is related in these cases.

Further kinetic analysis using deuterated ammonia boranes was carried out to examine deuterium kinetic isotope effects (Figure 2.12). The DKIEs values were determined based on the ratio of the reaction constants ( $k_{AB}/k_{DAB}$ ), where  $k_{AB}$  corresponds to the reaction constant with the protic and hydride ammonia borane and  $k_{DAB}$  is the reaction constant of each of the respective deuterated ammonia boranes.

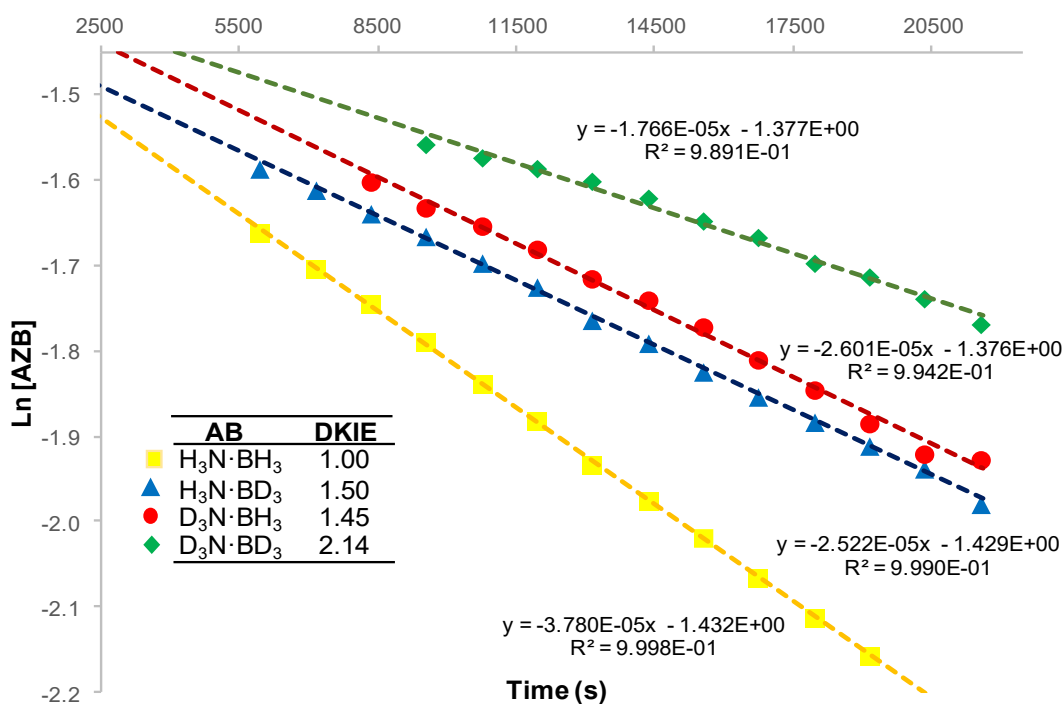


Figure 2.12. Deuterated kinetic isotopic effect (DKIE's) on reaction rate for the TH of azobenzene with deuterated ammonia boranes.

Normal DKIEs values of 1.45 and 1.50 were observed for the reaction of azobenzene with  $\text{D}_3\text{N}\cdot\text{BH}_3$  and  $\text{H}_3\text{N}\cdot\text{BD}_3$ , respectively, and a DKIE of 2.14 in the case of the fully-deuterated compound. The group of Kinjo reported a trend similar to the one found in this investigation for the kinetic isotope effect (KIE) in their system, i.e.  $k_{\text{AB}} > k_{\text{AB(D)}} > k_{\text{A(D)B}} > k_{\text{A(D)B(D)}}$  ( $\text{AB(D)} = \text{H}_3\text{N}\cdot\text{BD}_3$ ;  $\text{A(D)B} = \text{D}_3\text{N}\cdot\text{BH}_3$ ;  $\text{A(D)B(D)} = \text{D}_3\text{N}\cdot\text{BD}_3$ ), determined by experimental and theoretical means. The overall KIE was associated with the cleavage of both B–H and N–H bonds in the rate determining step of the reaction, in a double-hydrogen transfer concerted mechanism.<sup>60,61</sup> For the TH of azobenzene catalyzed by 1, as expected, the DKIE obtained with perdeuterated **AB** ( $\text{D}_3\text{N}\cdot\text{BD}_3$ ,  $k_{\text{AB}}/k_{\text{A(D)B(D)}} = 2.14$ ), corresponds to the product of the individual KIEs (within the experimental error,  $k_{\text{AB}}/k_{\text{A(D)B(D)}} = 1.45$ ,  $k_{\text{AB}}/k_{\text{AB(D)}} \times 1.50$ ,  $k_{\text{AB}}/k_{\text{A(D)B}} = 2.18$ ). This suggests that B–H and N–H bonds are simultaneously broken and are probably relevant to the rate-determining step (RDS). Similar observations have been previously made for other homogeneous catalytic systems of **AB** dehydrogenation.<sup>57,76</sup> In the literature,<sup>50d,57,60,61,75-77</sup>  $k_{\text{AB}}/k_{\text{A(D)B(D)}}$  values ranging from 1.39<sup>75</sup> to 7.05<sup>57</sup> have been considered as significant and a clear indication of both B–H/N–H bond breaking as the rate-determining step.

Finally, a Hammett study was performed to investigate the effect of different substituents in *p*-position on the aryl ring. THF solutions (0.132 M) of different *p*-substituted azobenzene compounds were chosen as follow: two of them bearing electron- donating groups (Me and

OMe, Table 2.11), and two with electron-withdrawing groups (Cl and F; Table 2.11). The reaction rate ( $r$ ) for each substrate (2a–b, e–f, i) was obtained from the slope of the plot of the natural logarithm of the substrate concentration  $\ln ([p\text{-FG-AZB}])$  against time. Once the reaction rate for the  $p$ -substituted azobenzene series was known, a Hammett analysis was carried out.  $\log k$  was plotted against the substituted constant ( $\sigma$ ) as depicted in Figure 2.13 using the corresponding equation (Eq.5).

Table 2.11. Reaction rates for different  $p$ -substituted azoarenes. Hammett analysis.

$p$ -Substituent	Substituent constant ( $\sigma$ )	$r$ (mol.L <sup>-1</sup> .s <sup>-1</sup> )	$R^2$	$\log r$	$\ln r$	$\Delta G^\ddagger_{(333.15)}$ Kcal/mol
OMe	-0.268	1.308x10 <sup>-5</sup>	0.970	-4.883	-11.244	27.020
Me	-0.170	2.071E-05	0.965	-4.683	-10.784	26.715
H	0.000	2.689E-05	0.981	-4.570	-10.523	26.543
F	0.062	3.630E-05	0.990	-4.440	-10.223	26.344
Cl	0.227	5.932E-05	0.953	-4.226	-9.732	26.019

$$\text{Log}(r) = \rho \cdot \sigma + \text{Log}(r^\circ) \quad (\text{Eq. 5})$$

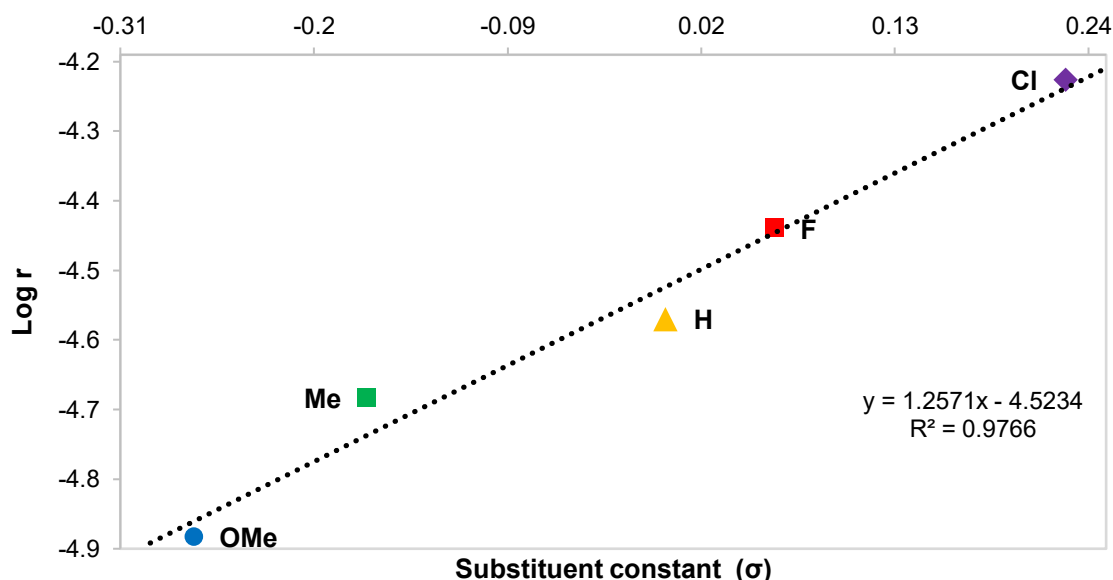


Figure 2.13. Representation  $\text{Log}(r)$  vs substituent constant ( $\sigma$ ).  $\rho = 1.26$ .

The Hammett plot returns a straight line and reveals a linear free-energy relationship ( $\Delta G^\ddagger$ ) between the  $p$ -substituted azobenzene compounds. In other words,  $\Delta H^\ddagger$  is nearly constant for the series whereas  $\Delta S^\ddagger$  is proportional to the substituent constant  $\sigma$ . The azocompound series studied followed the linear-free energy relationship (LFER) equation (Eq. 6) with a reaction



constant ( $\rho$ ) of 1.294. The sign of the reaction constant indicates that the transition state of the rate-determining step presumably carries a negative charge, while the magnitude means that this system is less sensitive to functional groups around the aryl ring than related systems.<sup>60,61</sup>

$$\Delta G_{(T)}^{\ddagger} = RT \cdot \left\{ \ln \left( \frac{k_B \cdot T}{h} \right) - \ln(r) \right\} \quad (\text{Eq.6})$$

The experimental evidence and results obtained, along with the kinetic data (rate of reaction, activation thermodynamics parameters, DKIE, and LFER) confirm that **AB** suffers dehydrogenation initiated by the acyclic phosphite (1), thus generating catalytically active species which perform the transfer hydrogenation of azobenzenes. The system is very efficient, and a variety of substituted phenylhydrazines were obtained. However, it is not possible to make a mechanistic outline or to propose a catalytic cycle for the system since the identity of the active species (catalyst) could not be unequivocally determined. Regardless of that, it becomes clear that: 1) P(OQuin)<sub>3</sub> is a precatalyst, and its use is more convenient than the *in situ* catalytic system NaPH<sub>2</sub> + 8-HOQuin, 2) the mechanism is probably associative, as reflected in the  $\Delta S_{\ddagger}^{\ddagger}$  which indicates a more ordered (concerted TH) transition state, and 3) deuteration of **AB** significantly affects the reaction rate and suggests a simultaneous N-H and B-H bond cleavage that (directly or indirectly) influences the rate-determining step.

## 2.6 Chapter conclusions.

The new phosphite P(OQuin)<sub>3</sub>, based on 8-hydroxy-quinoline, was prepared on a multigram scale and fully characterized. The phosphorus (III) compound **1** reacts with **AB** generating a catalytically active system which was exploited to perform the transfer hydrogenation of apolar N=N bonds in azoarenes. The corresponding hydrazines were obtained in high yields. The reaction conditions were studied for a model reaction (azobenzene as substrate) and the hydrazine formation proceeds under mild reaction conditions: 10 mol% of **1** as catalyst precursor, 60 °C, 24 h and 4 equivalents of **AB**.

Kinetic measurements indicate that the best approximation for the rate law is  $r = 0.029 \pm 0.005 \text{ s}^{-1} \cdot \text{L}^{0.5} \cdot \text{mol}^{-0.5} \cdot [\text{AZB}] \cdot [\text{1}]^{1/2}$  at a constant concentration of **AB** and temperature (60 °C). The analysis of KIEs indicated that the cleavage of B-H and N-H bonds of **AB** is either part of the rate-determining step or at least has a significant indirect effect in the reaction rate. Activation thermodynamic parameters were obtained from both Eyring and Arrhenius analysis, and suggest that the reaction proceeds through an organized transition state, consistent with an associative mechanism. A Hammett plot showed a linear free-energy relationship ( $\Delta G^{\ddagger}$ ) among the *p*-substituted azobenzene compounds studied. The kinetic and mechanistic investigations

do not provide enough evidence on the identity of the catalytically active species, formed from **1**, but suggest that **AB** is involved in more than one reaction step (at least in the reaction with phosphite **1** and in the hydrogen transfer to the substrates).

The potential of **1** to promote novel transformations via bond activation in small molecules will certainly be an ongoing area of interest in our group. Additional efforts are also being directed to the synthesis of alternative  $\sigma^3$ -P compounds for the reduction of even less reactive, nonpolar covalent bonds.

## 2.7 Experimental Section

### Synthesis of P(OQuin)<sub>3</sub>:

• **Using NEt<sub>3</sub> or <sup>n</sup>BuLi as base:** To a solution of 8-hydroxyquinoline (3.28 g, 22.6 mmol) in Et<sub>2</sub>O (50 mL) a solution of triethylamine (2.36 g, 23.3 mmol) in Et<sub>2</sub>O (50 mL) was added dropwise, while stirring. Then, a solution of phosphorus trichloride (635  $\mu$ L, *ca.* 1g, 7.3 mmol) in Et<sub>2</sub>O (100 mL) was added dropwise at 5 °C (ice bath) for 1 h. Once the addition was finished, the mixture was left to warm up to room temperature for 3 h. A colorless solid was formed (product **2** plus NEt<sub>3</sub>•HCl) and the mother liquors were analyzed by <sup>31</sup>P{<sup>1</sup>H} NMR. Typically, PCl<sub>3</sub> reacts within 3-5 h. Depending on the amount of moisture/air present during the reaction a yellow or reddish solution could be formed. The solid was filtered off and washed twice with Et<sub>2</sub>O (30 mL) in order to eliminate unreacted 8-hydroxyquinoline, hydrolyzed product, NEt<sub>3</sub> and the yellow/reddish side product. Then CH<sub>2</sub>Cl<sub>2</sub> (50 mL) was added two times to extract the phosphite from the residual ammonium salt. The solvent was removed under reduced pressure to obtain a white powder (2.85 g, 85% yield). <sup>1</sup>H NMR (300.1 MHz, CD<sub>2</sub>Cl<sub>2</sub>, 25°C):  $\delta$  = 8.36 (dd, <sup>3</sup>J<sub>HH</sub> = 4.2 Hz, <sup>4</sup>J<sub>HH</sub> = 1.7 Hz, 1H, H2), 8.17 (dd, <sup>3</sup>J<sub>HH</sub> = 8.3 Hz, <sup>4</sup>J<sub>HH</sub> = 1.7 Hz, 1H, H4), 7.60-7.49 (m, 3H, H5-7), 7.30 (dd, <sup>3</sup>J<sub>HH</sub> = 8.4 Hz, <sup>3</sup>J<sub>HH</sub> = 4.2 Hz, 1H, H3). <sup>13</sup>C{<sup>1</sup>H} NMR (75.5 MHz, CD<sub>2</sub>Cl<sub>2</sub>, 25°C):  $\delta$  = 150.5 (s, C<sup>quat</sup>), 148.8 (s, C2), 140.9 (s, C<sup>quat</sup>), 135.7 (s, C4), 129.6 (s, C<sup>quat</sup>), 126.8, 122.2 (s, C5 & C6), 121.4 (s, C3), 118.8 (d, <sup>3</sup>J<sub>PC</sub> = 5.5 Hz, C7). <sup>31</sup>P{<sup>1</sup>H} NMR (121.5 MHz, CD<sub>2</sub>Cl<sub>2</sub>, 25°C):  $\delta$  = 129.0 ppm (s). Analytically pure samples were obtained by using <sup>n</sup>BuLi (3.05 equiv., 85% yield) as base upon several recrystallizations. Anal. Calcd. for C<sub>27</sub>H<sub>18</sub>N<sub>3</sub>O<sub>3</sub>P•0.5CH<sub>2</sub>Cl<sub>2</sub> C, 65.29; H, 3.79; N, 8.31. Found: C, 65.78; H, 3.95; N, 8.26. ATR IR ( $\nu$  in cm<sup>-1</sup>): 3036 w, 3008 w, 1614 w, 1594 w, 1568 w, 1497 m, 1466 m, 1421 w, 1389 w, 1371 w, 1312 m, 1243 s, 1165 w, 1089 s, 1055 s, 1027 w, 962 w, 913 w, 892 s, 844 m, 821 s, 810 s, 788 m, 767 s, 751 s, 711 m, 680 s, 658 m, 632 w, 607 w, 588 w, 573 w, 559 w, 544 m, 532 w, 505 w, 481 w, 465 w, 432 m, 431 m, 415 w.

- **Using NaH as base:** Step 1: To a suspension of NaH (0.813 g, 33.9 mmol) in Et<sub>2</sub>O (25 mL) a solution of 8-hydroxyquinoline (5.41 g, 37.3 mmol) in Et<sub>2</sub>O (50 mL) was added dropwise while stirring at -20 °C for 2 h. A yellowish fluorescent solid was formed, identified as NaOQuin, and the solvent was filtered off. More Et<sub>2</sub>O (50 mL) was added in order to remove unreacted 8-hydroxyquinoline and the solution was filtered off again. The remaining solid was dried under vacuum. NaOQuin can be isolated in high yield (5.22g, 93%). Step 2: A solution of NaOQuin (3.26 g, 18.9 mmol) in THF (50 mL) was charged into a dropping funnel. The solution was added dropwise to a solution of phosphorus trichloride (0.850 g, 6.2 mmol) in Et<sub>2</sub>O (100 mL) at -20 °C for 1 h. Once the addition was finished, the mixture was allowed to reach room temperature, during a period of 3 h. A colorless solid was formed (product 1 plus NaCl). The solvent was removed under reduced pressure and then extracted twice with CH<sub>2</sub>Cl<sub>2</sub> (2 x 50 mL) to separate the phosphite from the residual sodium salt and unreacted NaOQuin. The combined CH<sub>2</sub>Cl<sub>2</sub> extract was evaporated to dryness under vacuum to afford a white powder (2.70 g, 94% yield). If necessary, the phosphite can be recrystallized from dichloromethane and diethyl ether. Alternatively, the 8-quinolinol sodium salt can be generated *in situ* and reacted then, without isolation and purification, with PCl<sub>3</sub>. Using this methodology, a spectroscopically and analytically pure compound is typically obtained with only one recrystallization step. <sup>1</sup>H NMR (400.1 MHz, THF-d<sub>8</sub>, 25 °C): δ [ppm] = 8.28 (dd, <sup>3</sup>J<sub>HH</sub> = 4.1 Hz, <sup>4</sup>J<sub>HH</sub> = 1.7 Hz, 1H, H2), 8.16 (dd, <sup>3</sup>J<sub>HH</sub> = 8.3 Hz, <sup>4</sup>J<sub>HH</sub> = 1.7 Hz, 1H, H4), 7.56-7.44 (m, 3H, H5-7), 7.26 (dd, <sup>3</sup>J<sub>HH</sub> = 8.4 Hz, <sup>3</sup>J<sub>HH</sub> = 4.1 Hz, 1H, H3). <sup>13</sup>C{<sup>1</sup>H} NMR (100.6 MHz, THF-d<sub>8</sub>, 25 °C): δ [ppm] = 150.5 (s, C<sup>quat</sup>), 148.8 (s, C2), 140.9 (s, C<sup>quat</sup>), 135.7 (s, C4), 129.6 (s, C<sup>quat</sup>), 126.8, 122.2 (s, C5 & C6), 121.4 (s, C3), 118.8 (d, <sup>3</sup>J<sub>PC</sub> = 5.5 Hz, C7). <sup>31</sup>P{<sup>1</sup>H} NMR (162.0 MHz, THF-d<sub>8</sub>, 25 °C): δ [ppm] = 130.9 (s). HRMS (MALDI): m/z calc. for C<sub>27</sub>H<sub>18</sub>N<sub>3</sub>O<sub>3</sub>PNa 486.0978 [M+Na]<sup>+</sup>; found 486.0974. Anal. Calcd. for C<sub>27</sub>H<sub>18</sub>N<sub>3</sub>O<sub>3</sub>P•0.5CH<sub>2</sub>Cl<sub>2</sub>: C, 65.29; H, 3.79; N, 8.31. Found: C, 65.78; H, 3.95; N, 8.26.

**Catalytic TH of azo compounds:** Compound 1 (13.9 mg, 0.030 mmol), the corresponding azocompound 2a–n (0.300 mmol), ammonia borane (37.0 mg, 1.20 mmol), the internal standard 1,3,5- trimethoxybenzene (16.7 mg, 0.099 mmol) and THF (1.25 mL) were loaded in a Schlenk tube under argon atmosphere. The Schlenk tube was sealed, placed in an oil bath, and heated at 60 °C. The reaction was monitored by <sup>1</sup>H NMR spectroscopy. Products 3a–n were purified by flash column chromatography on silica gel (9:1 = petroleum ether/ethyl acetate) or simply extracted from the reaction mixture with n-hexane when quantitative conversion was achieved.

## Spectroscopic data of hydrazine products

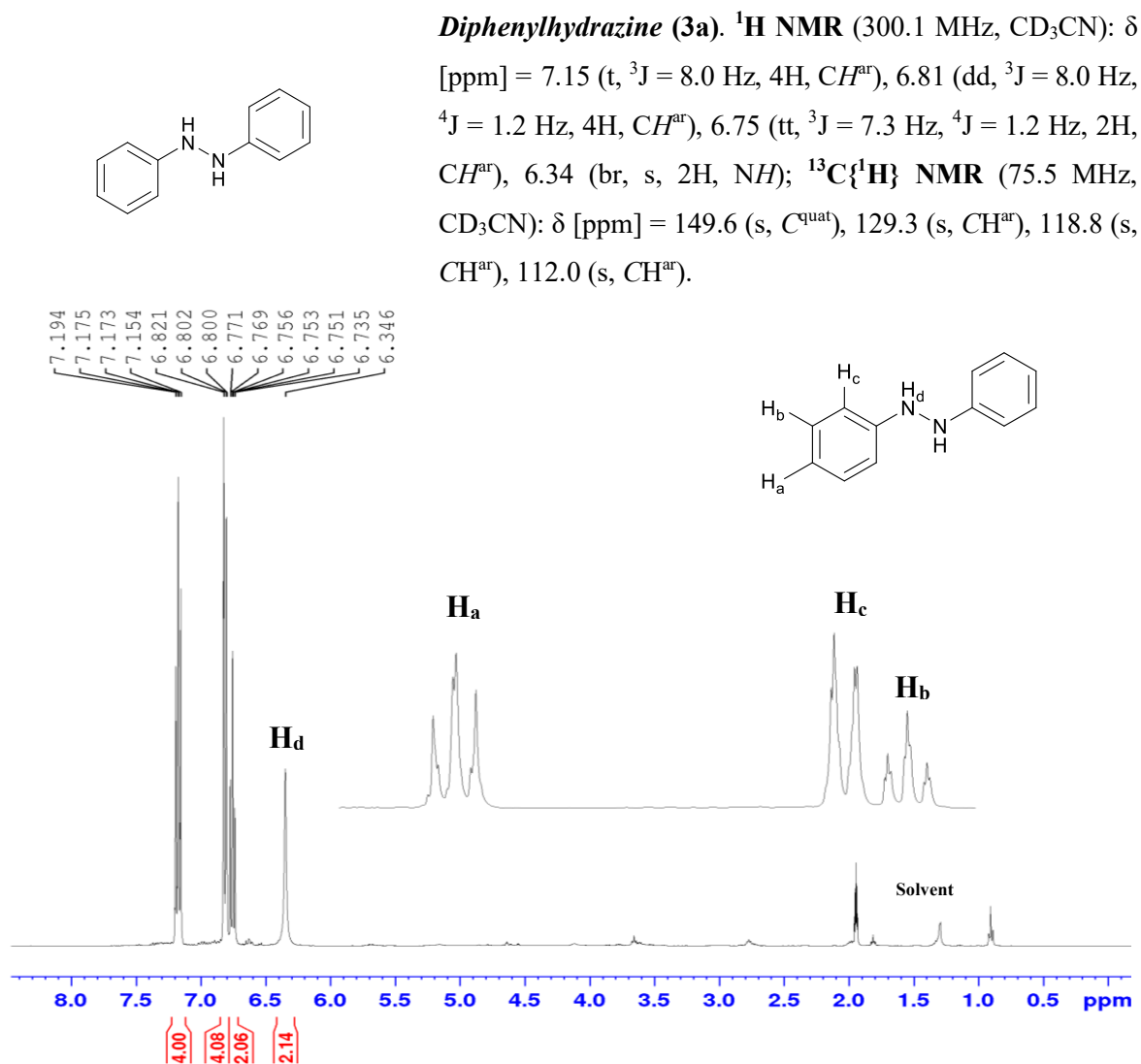


Figure 2.14.  $^1\text{H}$  NMR spectrum (300.1 MHz) of **3a** in  $\text{CD}_3\text{CN}$ .

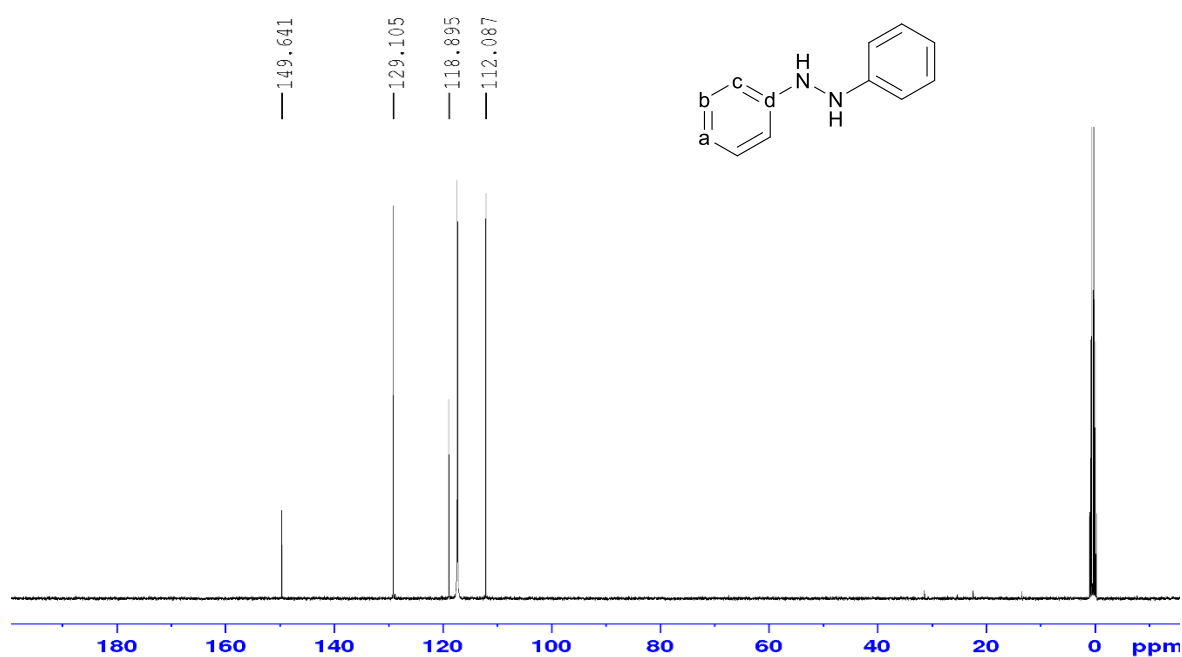
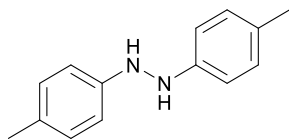
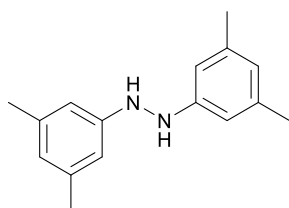


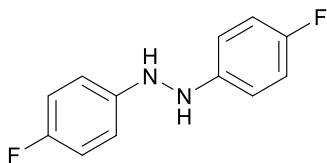
Figure 2.15.  $^{13}\text{C}\{^1\text{H}\}$  NMR spectrum (75.5 MHz) of **3a** in  $\text{CD}_3\text{CN}$ .



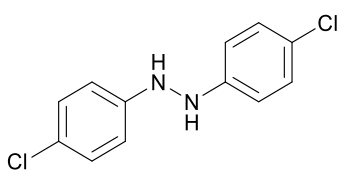
**Bis(4-methylphenyl)hydrazine (3b).**  $^1\text{H}$  NMR (300.1 MHz,  $\text{CD}_3\text{CN}$ ):  $\delta$  [ppm] = 7.79 (d,  $^3J$  = 8.5 Hz, 4H,  $\text{CH}^{\text{ar}}$ ), 7.37 (d,  $^3J$  = 8.5 Hz, 4H,  $\text{CH}^{\text{ar}}$ ), 2.42 (s, 6H,  $\text{CH}_3$ ), 2.14 (s, 2H, NH);  $^{13}\text{C}\{^1\text{H}\}$  NMR (75.5 MHz,  $\text{CD}_3\text{CN}$ ):  $\delta$  [ppm] = 161.3 (s,  $\text{NC}^{\text{quat}}$ ), 129.5 (s,  $\text{CH}^{\text{ar}}$ ), 122.1 (s,  $\text{C}^{\text{quat}}$ ), 116.6 (s,  $\text{CH}^{\text{ar}}$ ), 20.6 (s,  $\text{CH}_3$ ).



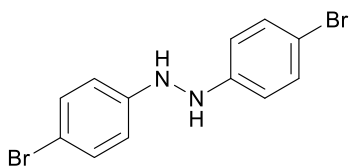
**Bis(3,5-di(methyl)phenyl)hydrazine (3c).**  $^1\text{H}$  NMR (400.1 MHz,  $\text{CD}_3\text{CN}$ ):  $\delta$  [ppm] = 6.51 (s, 6H,  $\text{CH}^{\text{ar}}$ ), 5.46 (s, 2H, NH), 2.25 (s, 12H,  $\text{CH}_3$ );  $^{13}\text{C}\{^1\text{H}\}$  NMR (100.6 MHz,  $\text{CD}_3\text{CN}$ ):  $\delta$  [ppm] = 149.4 (s,  $\text{NC}^{\text{quat}}$ ), 139.3 (s,  $\text{C}^{\text{quat}}$ ), 121.9 (s,  $\text{CH}^{\text{ar}}$ ), 110.2 (s,  $\text{CH}^{\text{ar}}$ ), 21.6 (s,  $\text{CH}_3$ ).



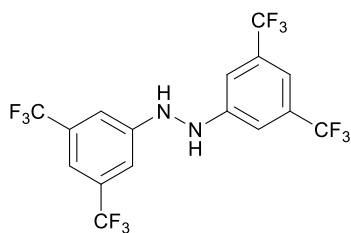
**Bis(4-fluorophenyl)hydrazine (3e).**  $^1\text{H}$  NMR (400.1 MHz,  $\text{CD}_3\text{CN}$ ):  $\delta$  [ppm] = 6.93 (t,  $^3J$  = 9.0 Hz, 4H,  $\text{CH}^{\text{ar}}$ ), 6.81 – 6.78 (m, 4H,  $\text{CH}^{\text{ar}}$ ), 5.55 (s, 2H, NH);  $^{13}\text{C}\{^1\text{H}\}$  NMR (100.6 MHz,  $\text{CD}_3\text{CN}$ ):  $\delta$  [ppm] = 157.3 (d,  $^1J_{\text{CF}}$  = 236.4 Hz,  $\text{FC}^{\text{quat}}$ ), 145.0 (s,  $\text{NC}^{\text{quat}}$ ), 116.0 (d,  $^2J_{\text{CF}}$  = 22.6 Hz,  $\text{CH}^{\text{ar}}$ ), 113.5 (d,  $^3J_{\text{CF}}$  = 7.5 Hz,  $\text{CH}^{\text{ar}}$ );  $^{19}\text{F}$  NMR (376.5 MHz,  $\text{CD}_3\text{CN}$ ):  $\delta$  [ppm] = –128.4.



**Bis(4-chlorophenyl)hydrazine (3f).**  $^1\text{H}$  NMR (400.1 MHz,  $\text{CD}_3\text{CN}$ ):  $\delta$  [ppm] = 6.95 (d,  $^3J$  = 8.7 Hz, 4H,  $\text{CH}^{\text{ar}}$ ), 6.57 (d,  $^3J$  = 8.7 Hz, 4H,  $\text{CH}^{\text{ar}}$ ), 6.28 (br., 2H, NH);  $^{13}\text{C}\{^1\text{H}\}$  NMR (100.6 MHz,  $\text{CD}_3\text{CN}$ ):  $\delta$  [ppm] = 148.2 (s,  $\text{NC}^{\text{quat}}$ ), 128.9 ( $\text{CH}^{\text{ar}}$ ), 122.9 (s,  $\text{ClC}^{\text{quat}}$ ), 113.4 ( $\text{CH}^{\text{ar}}$ ).

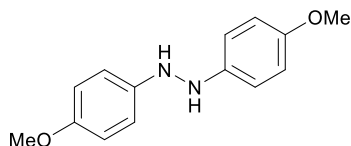


**Bis(4-bromophenyl)hydrazine (3g).**  $^1\text{H}$  NMR (400.1 MHz,  $\text{CD}_3\text{CN}$ ):  $\delta$  [ppm] = 7.28 (d,  $^3J$  = 8.9 Hz, 4H,  $\text{CH}^{\text{ar}}$ ), 6.76 (d,  $^3J$  = 8.9 Hz, 4H,  $\text{CH}^{\text{ar}}$ ), 6.48 (s, 2H, NH);  $^{13}\text{C}\{^1\text{H}\}$  NMR (100.6 MHz,  $\text{CD}_3\text{CN}$ ):  $\delta$  [ppm] = 148.6 (s,  $\text{NC}^{\text{quat}}$ ), 131.8 (s,  $\text{CH}^{\text{ar}}$ ), 114.0 (s,  $\text{CH}^{\text{ar}}$ ), 110.0 (s,  $\text{BrC}^{\text{quat}}$ ).



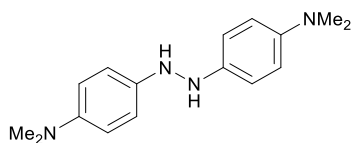
***Bis(3,5-di(trifluoromethyl)phenyl)hydrazine (3h).***

$^1\text{H}$  NMR (400.1 MHz, THF/ $\text{C}_6\text{D}_6$  capillary):  $\delta$  [ppm] = 8.22 (s, 2H,  $\text{CH}^{\text{ar}}$ ), 7.65 (s, 4H,  $\text{CH}^{\text{ar}}$ ), 1.60 (s, 2H, NH). This compound could not be isolated as a pure product.



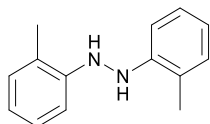
***Bis(4-methoxyphenyl)hydrazine (3i).***

$^1\text{H}$  NMR (400.1 MHz, THF/ $\text{C}_6\text{D}_6$  capillary):  $\delta$  [ppm] = 8.13 (d,  $^3J_{\text{HH}} = 8.7$  Hz, 4H,  $\text{CH}^{\text{ar}}$ ), 7.30 (d,  $^3J_{\text{HH}} = 8.7$  Hz, 4H,  $\text{CH}^{\text{ar}}$ ), 6.25 (br., 2H, NH), 4.11 (s, 6H,  $\text{OCH}_3$ ). This compound could not be isolated as a pure product.



***Bis(4-dimethylaminophenyl)hydrazine (3j).***

$^1\text{H}$  NMR (400.1 MHz, THF/ $\text{C}_6\text{D}_6$  capillary):  $\delta$  [ppm] = 7.67 (d,  $^3J_{\text{HH}} = 9.7$  Hz, 4H,  $\text{CH}^{\text{ar}}$ ), 6.78 (s, 2H, NH), 6.70 (d,  $^3J_{\text{HH}} = 9.7$  Hz, 4H,  $\text{CH}^{\text{ar}}$ ), 2.96 (s, 12H,  $\text{NCH}_3$ ). This compound could not be isolated as a pure product.



***Bis(2-methylphenyl)hydrazine (3k).***  $^1\text{H}$  NMR (300.1 MHz,  $\text{CD}_3\text{CN}$ ):  $\delta$  [ppm] = 7.07 (d,  $^3J = 7.3$  Hz, 2H,  $\text{CH}^{\text{ar}}$ ), 7.01 (t,  $^3J = 7.7$  Hz, 2H,  $\text{CH}^{\text{ar}}$ ), 6.77 (d,  $^3J = 7.3$  Hz, 2H,  $\text{CH}^{\text{ar}}$ ), 6.68 (t,  $^3J = 7.7$  Hz, 2H,  $\text{CH}^{\text{ar}}$ ), 6.08 (br., 2H, NH), 2.23 (s, 6H,  $\text{CH}_3$ );  $^{13}\text{C}\{^1\text{H}\}$  NMR (75.5 MHz,  $\text{CD}_3\text{CN}$ ):  $\delta$  [ppm] = 146.7 (s,  $\text{NC}^{\text{quat}}$ ), 130.1 (s,  $\text{CH}^{\text{ar}}$ ), 126.7 (s,  $\text{CH}^{\text{ar}}$ ), 121.4 (s,  $\text{C}^{\text{quat}}$ ), 118.5 (s,  $\text{CH}^{\text{ar}}$ ), 110.6 (s,  $\text{CH}^{\text{ar}}$ ), 16.5 (s,  $\text{CH}_3$ ).

**Kinetic study:** In a dry 25 mL Schlenk tube with a silicone septa-screw-cap and under argon atmosphere a THF solution of azobenzene (0.500 mmol, 0.132 M), 1 (23.2 mg, 0.050 mmol), ammonia borane (72.1 mg, 2.00 mmol), and 1,3,5-trimethoxybenzene (28.0 mg, 0.165 mmol) were loaded and heated at 60 °C. Aliquots (0.2 mL) for NMR sample were transferred with a syringe and the NMR tubes were filled with dry THF and a  $\text{C}_6\text{D}_6$  capillary. Reaction progress was monitored as consumption of azobenzene, by  $^1\text{H}$  NMR, every 30 minutes for 14 h.

**Rate of reaction as a function of substrate or precatalyst concentration.**

**Dependence on the concentration of substrate:** The general procedure was applied using the following concentration ( $\text{mol.L}^{-1}$ ) of azobenzene: 0.044, 0.088, 0.132, 0.176 and 0.220. The

concentration of precatalyst and **AB**, as well as temperature and time, were kept constant during such experiments.

**Dependence on the concentration of precatalyst:** The general procedure was applied using the following concentration ( $\text{mol.L}^{-1}$ ) of **1**: 0.004, 0.007, 0.013, 0.019 and 0.025. The concentration of substrate and **AB**, as well as temperature and time, were kept constant during such experiments.

**Rate of reaction as a function of temperature (Eyring and Arrhenius study):** The general procedure was followed for the range of temperatures 40–80 °C, rising the temperature in 10 °C intervals. The concentration of substrate, **1** and **AB**, as well as time, were kept constant during such experiments. The Eyring plot was obtained based on the representation of  $\ln(r/T)$  against the inverse of temperature ( $1/T$ ). With this, activation thermodynamic parameters were calculated. The Arrhenius plot was obtained from  $\ln(r)$  vs. inverse of temperature ( $1/T$ ), which returned the activation energy.

**Hammett study:** The general procedure was applied using different *p*-substituted azobenzenes, bearing either electron-donating or electron-withdrawing groups (OMe, Me, F and Cl). The Hammett plot was obtained by representing graphically  $\text{Log}(r)$  against the corresponding substituent coefficient  $\sigma$  for each substrate individually.

**Deuterium kinetic isotope effect (DKIE's).** A  $[\text{D}_8]\text{THF}$  solution of azobenzene (27.3 mg, 0.150 mmol, 0.220 M), **1** (7.0 mg, 0.015 mmol), ammonia borane  $\text{H}_3\text{N}\cdot\text{BH}_3$  (18.5 mg, 0.600 mmol), and 1,3,5-trimethoxybenzene (8.3 mg, 0.049 mmol) were loaded in a dry J-Young-Tube, under argon atmosphere. The tube was sealed and heated at 60 °C. The reaction progress, as consumption of azobenzene, was monitored by  $^1\text{H}$  NMR spectroscopy in-situ at 20-minute intervals for 6 h. This procedure was repeated for different deuterated ammonia borane adducts ( $\text{D}_3\text{N}\cdot\text{BH}_3$ ,  $\text{H}_3\text{N}\cdot\text{BD}_3$ , and  $\text{D}_3\text{N}\cdot\text{BD}_3$ , 0.600 mmol). The DKIE values were determined based on the ratio of reaction rates ( $k_{\text{AB}}/k_{\text{DAB}}$ ).

### Chapter III

Pd(II)-coordination chemistry of P(OQuin)<sub>3</sub>.

Application in the catalytic aerobic oxidation of amines

Reproduced with permission from R. E. Rodríguez-Lugo, M. A. Chacón-Terán, S. De León, M. Vogt, A. J. Rosenthal, V. R. Landaeta, «Synthesis, characterization and Pd(II)-coordination chemistry of the ligand tris(8-quinolinyl)phosphite. Application in the catalytic aerobic oxidation of amines». *Dalton Trans.* **2018**,47, 2061–2072.



### 3.1 Introduction

Imines and their derivatives are important building blocks for the synthesis of heterocyclic compounds and fine chemicals of pharmaceutical and biological relevance. These are usually prepared through effective Lewis acid-catalyzed condensation reactions between amines and carbonyl compounds in the presence of dehydrating agents, but other protocols have also attracted considerable attention.<sup>78</sup> Among them, one-pot oxidative processes are interesting alternatives since these reduce energy consumption, waste emission, and the number of operating stages and purification steps compared to traditional methodologies.<sup>79</sup> Three kinds of oxidative processes for imine formation have been described:<sup>80</sup>

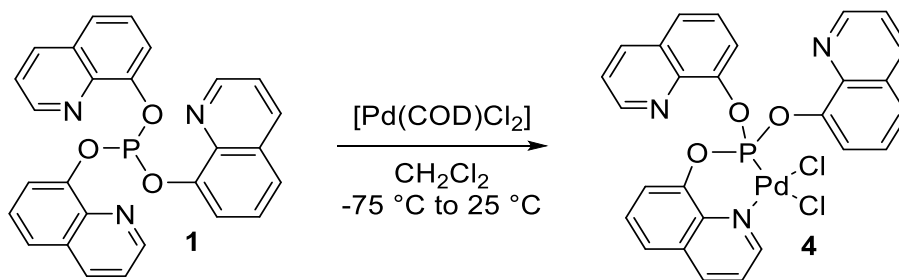
- a) (Dehydrogenative) Oxidative couplings of alcohols with amines.<sup>81</sup>
- b) Self-coupling of primary amines.<sup>82</sup>
- c) Oxidative dehydrogenation of secondary amines.<sup>83</sup>

All these are based on metal,<sup>84</sup> metal-free,<sup>85</sup> photo-,<sup>86</sup> and bioinspired<sup>87</sup> catalysts. The atmospheric oxidation of amines mediated by transition metals has been described. Copper salts, in combination with additives or simply CuCl alone, have been used as a method for imine formation.<sup>88</sup> Ogawa<sup>89</sup> and Gao<sup>90</sup> reported the use of vanadium complexes for the green oxidation of primary amines into the corresponding imines. Other homogeneous systems based on Zn,<sup>91</sup> Co,<sup>92</sup> Fe,<sup>93</sup> Ag,<sup>94</sup> Pd,<sup>95,96</sup> Au<sup>97</sup> and Ir<sup>98</sup> coordination compounds have been described as catalysts for the aerobic oxidation of amines to imines.

Here the synthesis and characterization of a coordination compound of Pd<sup>(II)</sup> bearing the phosphite ligand 1 is described. The application of such metal complex as a homogeneous catalyst for the oxidative coupling of primary amines to yield imines is also discussed, along with kinetic measurements. To the best of our knowledge, no examples of Pd complexes bearing phosphite ligands have been reported as catalysts for this type of reaction.

### 3.2 Synthesis and characterization of the Pd(II) complex

The reaction of **1** with the metal precursor [Pd(COD)Cl<sub>2</sub>] (COD = 1,5-cyclooctadiene, C<sub>8</sub>H<sub>12</sub>) was studied. The complex [κ<sup>2</sup>P,N-{P(OQuin)<sub>3</sub>}PdCl<sub>2</sub>], (**4**), is accessible by treating such a metal precursor in dichloromethane with a solution of the ligand in the same solvent at -75 °C (Scheme 3.1). When the reaction mixture was allowed to reach room temperature, the coordination compound precipitated as a pale-yellow solid in 79% yield. The complex is remarkably stable toward air and moisture.



Scheme 3.1. Synthesis of the palladium (II) complex **4**, [κ<sup>2</sup>(P,N)-{P(OQuin)<sub>3</sub>}PdCl<sub>2</sub>].

IR, UV-Vis spectra, elemental analysis and NMR spectroscopic data (<sup>1</sup>H, <sup>13</sup>C{<sup>1</sup>H}, and <sup>31</sup>P{<sup>1</sup>H}) of **4** are in accordance with the proposed formulation. Protons and carbons were assigned using 2D NMR analysis such as COSY, HMQC and HMBC. The resonance of the <sup>31</sup>P{<sup>1</sup>H} NMR in the free ligand is strongly shifted to lower frequencies (high field) upon coordination to the palladium center (130 ppm for **1** vs. 32 ppm for **4**; Figure 3.1a).

The opposite effect is observed for the resonances of the protons in the ortho and para positions with regard to the N atom. Upon coordination, such protons are significantly shifted to higher frequencies compared with those of the free ligand (Figure 3.1b). (see page 55), “*It is expected that **1** will be a hemilabile ligand due to competition between the three quinoline groups with the same coordination ability*”. A set of four signals that integrate to 6 or 18 protons are found in the <sup>1</sup>H NMR spectrum. That means that there is a hemilability behavior of **1** in a DCM solution of **4**. This dynamic process is possibly so fast that at room temperature the NMR device records these three quinoline moieties as a single one (equivalency).

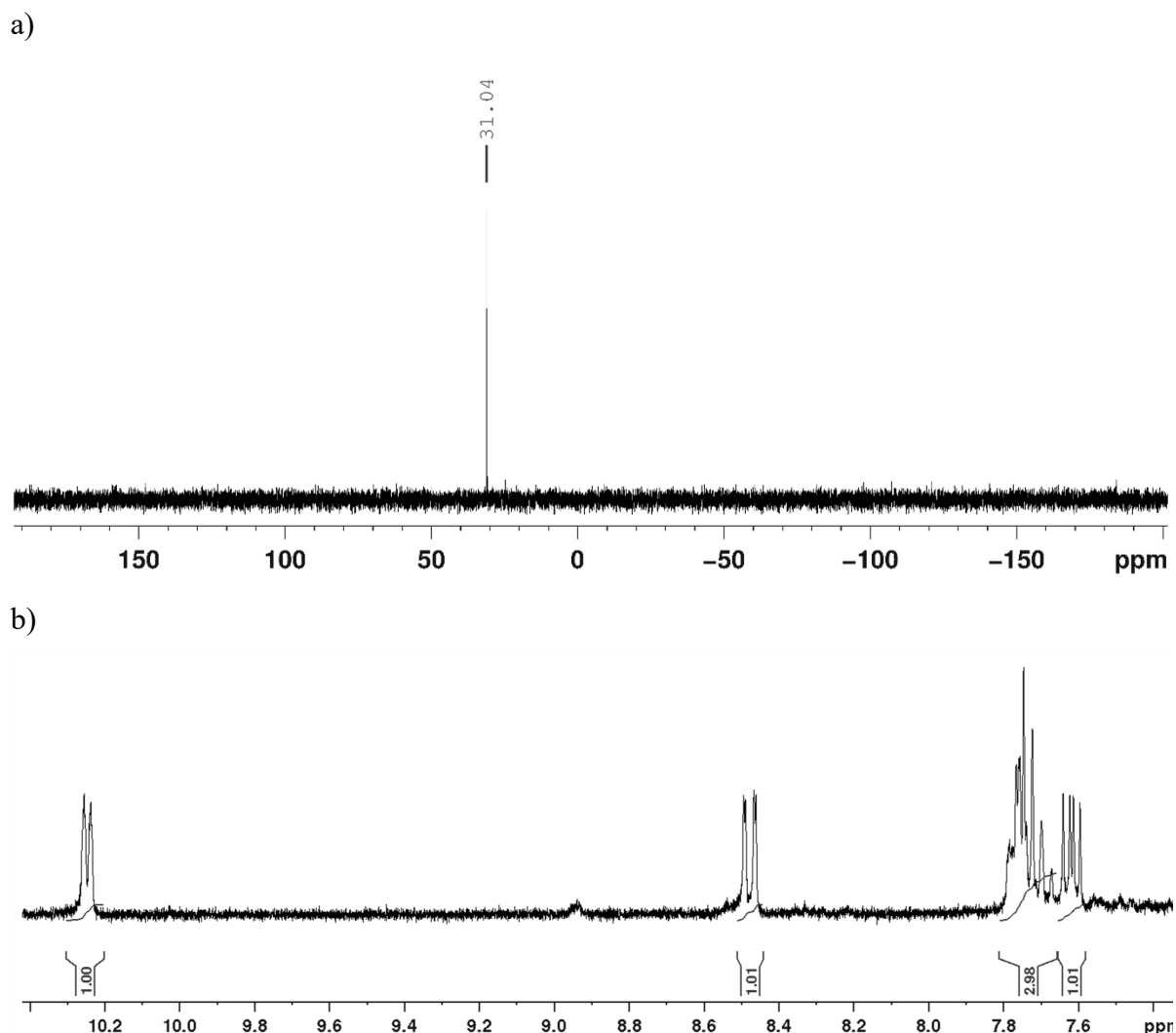


Figure 3.1. a)  $^{31}\text{P}\{^1\text{H}\}$  NMR spectrum (121.5 MHz) and b)  $^1\text{H}$  NMR spectrum (300.1 MHz) at 298 K of **4** in  $\text{CDCl}_3$ .

Crystals suitable for X-ray diffraction analysis were obtained from dichloromethane. (Figure 3.2) The solid state structure of **4** reveals that the ligand **1** binds the metal center as a bidentate chelate through the P atom and one of the N atom donors of the heterocycles (N1 in Figure 3.2a) confirming a  $\kappa^2(\text{P},\text{N})$  coordination mode of **1**. The other two quinoline units are oriented in such a way that a short contact is established between the N atoms (N2 and N3) and the O atom center (O1) of the chelating quinoline fragment. The N–O distance for this interaction is, in average, 3.01(6) Å. The complex exhibits a slightly distorted square planar geometry, since the chelate (plane P1/Pd1/N1) is not co-planar with the chlorine atoms (plane Cl1/Pd1/Cl2). The deviation from co-planarity between the planes P1/Pd1/N1 and Cl1/Pd1/Cl2 is only 5.06 degrees. The two aromatic units of the coordinated quinoline moiety are twisted, as indicated by the C19–C7–N1–C11 and C19–C7–C17–C25 torsion angles (Table 3.1, numbering scheme in Figure 3.2a). Such twisting of the quinoline ring has been also described for the related compounds, N-Q.<sup>26s,t</sup> (Chapter I; Figure 7) By applying  $\pm 3\sigma$  criterium, the

lengths Pd–P, P–O and Pd–Cl (*trans* to the P center) in **4** are significantly shorter than in the related compounds **N–Q**. The Pd–Cl bond length (*trans* to the N atom) is similar to the one observed in **P**,<sup>26t</sup> while the interatomic distance Pd–N is similar to that observed in **N**.<sup>26s</sup>

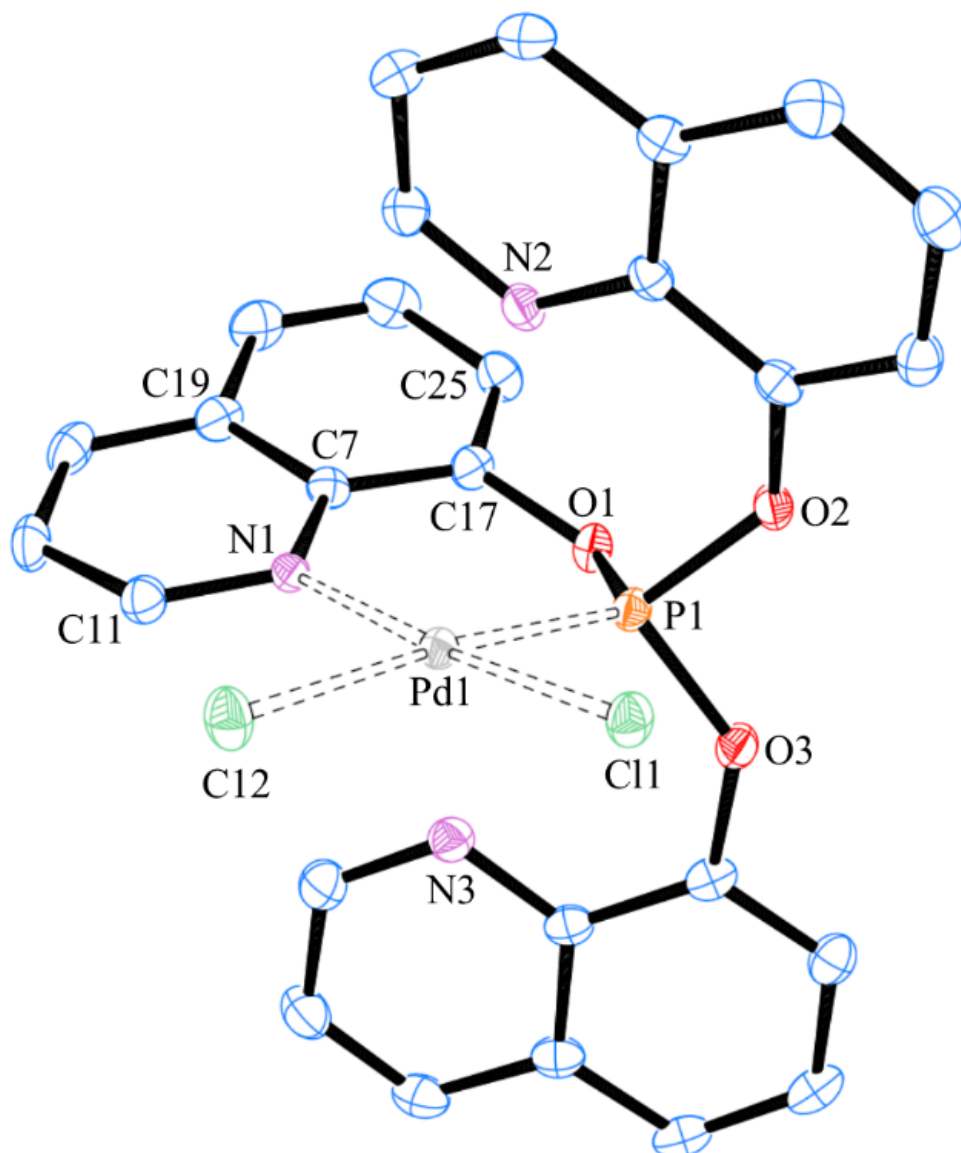
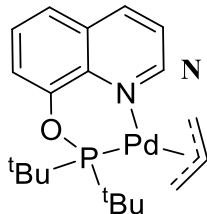
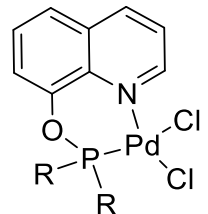


Figure 3.2. ORTEP drawing of the molecular structure of the complex  $[\text{Pd}\{\text{P}(\text{OQuin})_3\}\text{Cl}_2]$ , **4**. Thermal ellipsoids are drawn at 50% probability level. Hydrogen atoms and a dichloromethane solvate molecule have been removed for clarity.

Table 3.1. Selected geometric parameters (Å, °) for **4** and the related compounds **N-Q**.<sup>50</sup>





**O:** R = C<sub>6</sub>H<sub>5</sub> (Ph)  
**P:** R = C<sub>3</sub>H<sub>7</sub> (<sup>i</sup>Pr)  
**Q:** R = C<sub>6</sub>H<sub>11</sub> (Cy)

	<b>4</b>	<b>N</b>	<b>O</b>	<b>P<sup>a</sup></b>	<b>Q</b>
Pd—P	2.1513 (6)	2.2554 (14)	2.1765 (6)	2.1835 (6)	2.1804 (7)
Pd—N	2.1275 (19)	2.137 (5)	2.0803 (18)	2.0615 (18)	2.072 (2)
Pd—Cl ( <i>trans</i> to N)	2.3027 (6)	-	2.2880 (7)	2.2982 (6)	2.3000 (7)
Pd—Cl ( <i>trans</i> to P)	2.3756 (6)	-	2.3809 (6)	2.3993 (6)	2.4130 (7)
	1.5773 (16)	1.632 (4)	1.6176 (16)	1.6236 (16)	1.6244 (8)
P—O	1.5846 (17)	-	-	-	-
	1.5962 (15)	-	-	-	-
P—Pd—N	91.07 (5)	92.79 (13)	86.28 (5)	86.74 (5)	86.64 (6)
Cl—Pd—Cl	88.67 (2)	-	89.68 (2)	92.35 (2)	92.86 (3)
<i>cis</i> P—Pd—Cl	85.00 (2)	-	91.65 (2)	91.43 (2)	91.32 (3)
<i>cis</i> N—Pd—Cl	95.43 (5)	-	93.00 (5)	90.20 (5)	90.78 (6)
P—Pd—Cl	172.91 (2)	-	170.84 (2)	170.21 (2)	167.88 (2)
N—Pd—Cl	174.91 (5)	-	175.48 (5)	175.06 (5)	171.60 (6)
C19-C7-N1-C11	9.05	-6.72	-4.76	-10.62, 11.21	5.73
C19-C7-C17-C25	7.17	-4.38	-1.58	-10.56, 9.27	6.86

[a] Average of the two independent molecules in the unit cell.

### 3.3 Oxidative coupling of primary amines catalyzed by complex **4**.

Compound **4** was tested as a catalyst precursor for the oxidative homo-coupling of benzylamine to *N*-benzylidenebenzylamine, as a model reaction (Table 3.2). Other Pd sources, such as [Pd(COD)Cl<sub>2</sub>] or PdCl<sub>2</sub>, were not efficient catalyst precursors for this reaction under the studied conditions (entries 2 and 3). Moreover, other phosphorus-containing compounds, *e.g.* [Pd(PPh<sub>3</sub>)<sub>2</sub>Cl<sub>2</sub>] and [Pd(P(OPh)<sub>3</sub>)<sub>2</sub>Cl<sub>2</sub>], were not as efficient as **4** for the oxidative homo-coupling of benzylamine (entries 4 and 5). The mercury test suggests that metallic palladium or nanoparticles are not likely to be responsible for the activity observed (entry 6). In fact, no

palladium black is formed. In the absence of the catalyst (blank run) a very poor yield was achieved (entry 7) confirming the catalytic nature of the transformation.

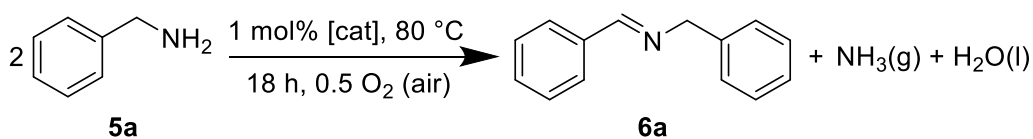
Table 3.2. Solvent free oxidative coupling of benzylamine to *N*-Benzyldenebenzylamine. Screening of catalysts. <sup>a</sup>

<p style="text-align: center;"> <math display="block">2 \text{ Ph-CH}_2\text{NH}_2 \xrightarrow[18 \text{ h, } 0.5 \text{ O}_2 \text{ (air)}]{1 \text{ mol\% [cat], } 80 \text{ }^\circ\text{C}} \text{ Ph-CH=CH-Ph} + \text{NH}_3(\text{g}) + \text{H}_2\text{O}(\text{l})</math> </p> <p style="text-align: center;"> <b>5a</b> <span style="margin-left: 200px;"><b>6a</b></span> </p>			
Entry	Catalyst [Pd]	Yield <sup>b</sup> (%)	TON/TOF (h <sup>-1</sup> )
1	<b>4</b>	>99	100/5.6
2	[Pd(COD)Cl <sub>2</sub> ]	5	5/0.3
3	[PdCl <sub>2</sub> ]	4	4/0.2
4	[Pd(PPh <sub>3</sub> ) <sub>2</sub> Cl <sub>2</sub> ]	52	52/3.0
5	[Pd(P(OPh) <sub>3</sub> ) <sub>2</sub> Cl <sub>2</sub> ]	11	11/0.6
6	<b>4</b> / Hg(l)	90	90/5
7	None	2	-

[a] Reaction conditions: Benzylamine (154.3 mg, 1.44 mmol), [Pd] (9.2 mg, 14 μmol, 1 mol%), open to atmosphere, 80 °C, 18 h. [b] Yield determined by <sup>1</sup>H NMR.

The effect of selected solvents on the oxidative coupling of benzylamine to *N*-benzyldenebenzylamine catalyzed by **4** was studied (Table 3.3). Under solvent-free conditions and in toluene the yield is high, >99% and 87% respectively (entries 1 and 2). Acetonitrile and 2-propanol were not efficient as reaction media for this system, evidenced by the diminished catalytic activity (entries 3 and 4). These experiments were carried out in an open atmosphere and identical flasks were used in order to prevent problems of air (oxygen) diffusion into the reaction mixture.

Table 3.3. Palladium catalyzed oxidative coupling of benzylamine to *N*-Benzylidenebenzylamine. Screening of reaction conditions: solvent. <sup>a</sup>

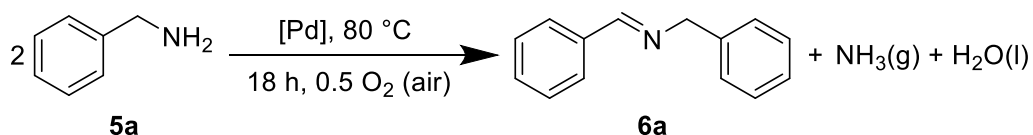


Entry	Solvent	Yield <sup>b</sup> (%)	TON/TOF (h <sup>-1</sup> )
1	None	>99	100/5.6
2	Toluene	87	87/4.8
3	2-Propanol	18	18/1
4	Acetonitrile	8	8/0.4

[a] Reaction conditions: Benzylamine (154.3 mg, 1.44 mmol), **4** (9.2 mg, 14 μmol, 1 mol%), solvent (1.4 mL, 1 mol/L amine), open to atmosphere, 80 °C, 18 h. [b] Yield determined by <sup>1</sup>H NMR.

Different catalyst loadings were evaluated (Table 3.4). Under the established reaction conditions, the yield drops significantly for catalyst loadings below 0.5 mol% (entries 4–6 vs. entries 1–3).

Table 3.4. Palladium catalyzed oxidative coupling of benzylamine to *N*-Benzylidenebenzylamine. Screening of reaction conditions: catalyst loading. <sup>a</sup>



Entry	Catalyst loading, <b>4</b> (mol%)	Yield <sup>b</sup> (%)	TON/TOF (h <sup>-1</sup> )
1	1	>99	100/5.6
2	0.75	>99	100/5.6
3	0.6	70	70/3.9
4	0.5	55 <sup>c</sup>	55/3.1
5	0.25	21	21/1.2
6	0.1	9	9/0.5

[a] Reaction conditions: Benzylamine (154.3 mg, 1.44 mmol), open to atmosphere, 80 °C, 18 h. [b] Yield determined by <sup>1</sup>H NMR. [c] Average of two experiments (55±4%).

The model reaction was carried out using different oxidants (Table 3.5). Oxygen, pure or present in air, is a suitable oxidant (entries 1–2), while nitrous oxide or organic oxidants (quinones) are not appropriate (entries 3–5). Under an inert atmosphere (N<sub>2</sub>; entry 6) the benzylamine homo-coupling does not occur, thus demonstrating the need for oxidizing

conditions. entries 1 and 2 formally correspond to experiments under different oxidant (O<sub>2</sub>) pressures, but the long reaction time (18 h) masked its effect on the reaction performance. The same experiments were conducted by shortening the reaction time (entries 3 and 4) to address the role of the oxygen pressure. The yield drops significantly when the reaction is carried out for 4 h in an open atmosphere (61%) compared with the almost quantitative oxidation of the amine under 50 psi air (*ca.* 10 psi O<sub>2</sub>) and the same period of time.

Table 3.5. Palladium catalyzed oxidative coupling of benzylamine to *N*-Benzylidenebenzylamine. Screening of reaction conditions: oxidant (ox). <sup>a</sup>

Nc1ccccc1 (5a)  $\xrightarrow[18\text{h, } 80\text{ }^{\circ}\text{C, oxidant (ox)}]{1\text{ mol\% [Pd]}}$  c1ccccc1=C(Nc2ccccc2) (6a) + NH<sub>3</sub>(g) + H<sub>2</sub>ox

Entry	Oxidant (ox)	Yield <sup>b</sup> (%)	TON/TOF (h <sup>-1</sup> )
1	Air	>99	100/5.6
2	Oxygen	>99 <sup>c</sup>	100/5.6
3	N <sub>2</sub> O	<1	-
4	DDQ	-	-
5	Naphthoquinone	-	-
6	None (N <sub>2</sub> atmosphere)	<1	-

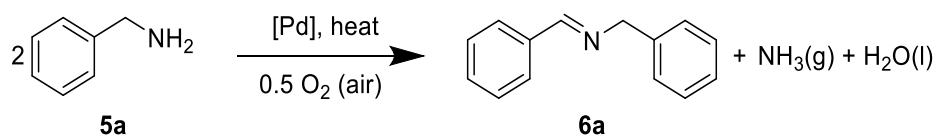
[a] Reaction conditions: Benzylamine (154.3 mg, 1.44 mmol), **4** (9.2 mg, 14 μmol, 1 mol%), 80 °C, 18 h. H<sub>2</sub>ox is the reduced form of the oxidant (ox). [b] Yield determined by <sup>1</sup>H NMR. [c] 10 psi O<sub>2</sub> in 98 mL autoclave, *ca.* 2.73 mmol O<sub>2</sub>.

Once the appropriate oxidant, catalyst precursor, and reaction media (solvent-free) were identified, the effect of other variables on the model reaction was studied (Table 3.6). Under atmospheric pressure, the yield drops significantly if the reaction is performed at room temperature (entries 1 vs. 2). In an autoclave (30 psi air, *ca.* 1.72 mmol O<sub>2</sub>) the reaction time can be shortened up to one third if the catalytic reaction is carried out at 80 °C (entries 1, 3 and 4). Under these conditions (30 psi air, 80 °C and 6 h) the catalyst loading can be lowered to 0.5 mol% without a significant loss of activity (entries 4 vs. 5). Likewise, with this catalyst loading the reaction time was shortened to 4 h and the yield remained very high (entry 6), but the attempts to further reduce the reaction time (entry 7) caused a significant drop in product formation. When the temperature was reduced to 60 °C while the catalyst loading remained low (0.5 mol%) and the reaction time was relatively short (6 h), a high yield was obtained (entry 8). The need of longer reaction times and higher temperatures when the reaction is carried out under atmospheric pressure was confirmed by performing the reaction at 60 °C and only 6 h,



which gave the product in moderate yields (entry 9). At 60 °C, the reaction time cannot be further shortened to 4 h without significantly affecting the activity (entries 6 and 10). In conclusion, these experiments indicate that the optimal reaction conditions are: no solvent, 0.5–1 mol% [Pd{(P(OQuin)<sub>3</sub>)Cl<sub>2</sub>}] as the catalyst precursor, at 60 °C for 6 h and using air as a terminal oxidant (30 psi, in a 98 mL autoclave, *ca.* 1.72 mmol O<sub>2</sub>, 1.2 equivalents). Under these conditions, the amine was cleanly converted into the imine and neither benzaldehyde nor benzonitrile were detected as side products. Ammonia formation was qualitatively proved by bubbling the gas phase of the reaction through a basic mixture of KI and HgI<sub>2</sub> (Nessler's reagent), upon which a brown precipitate immediately formed.

Table 3.6. Palladium catalyzed oxidative coupling of benzylamine to *N*-Benzyldenebenzylamine. Screening of reaction conditions: pressure, temperature and time. <sup>a</sup>



Entry	Pressure (psi), temperature (°C), time (h)	Yield <sup>b</sup> (%)	TON/TOF (h <sup>-1</sup> )
1	Atmospheric, 80, 18	>99	100/5.6
2	Atmospheric, 25, 18	4	4/0.2
3 <sup>c</sup>	30, 80, 12	>99	100/8.3
4 <sup>c</sup>	30, 80, 6	>99	100/16.7
5 <sup>c,d</sup>	30, 80, 6	>99	200/33.3
6 <sup>c,d</sup>	30, 80, 4	>99	200/50
7 <sup>c,d</sup>	30, 80, 2	36	72/36
8 <sup>c,d,e</sup>	30, 60, 6	>99	200/33.3
9	Atmospheric, 60, 6	68	68/11.3
10 <sup>c,d</sup>	30, 60, 4	50	100/25
11 <sup>f</sup>	300, 80, 4	23	230/57.5

[a] Reaction conditions: Benzylamine (154.3 mg, 1.44 mmol), **4** (9.2 mg, 14 μmol, 1 mol%), 80 °C, 18 h.

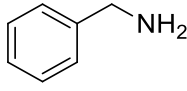
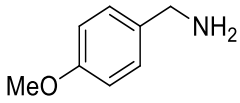
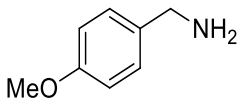
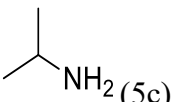
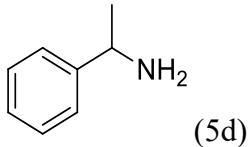
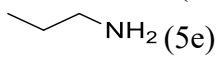
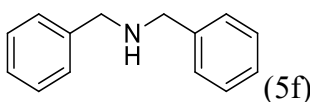
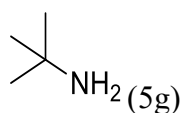
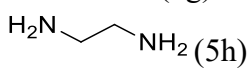
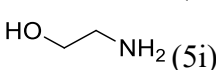
[b] Yield determined by <sup>1</sup>H NMR. [c] 30 psi air, 21 % O<sub>2</sub>, 98 mL autoclave, *ca.* 1.72 mmol O<sub>2</sub>. [d] Catalyst loading: 0.5 mol%. [e] Average of two experiments. [f] Catalyst loading: 0.1 mol%, 300 psi air, *ca.* 17.2 mmol O<sub>2</sub>.

Finally, the oxidative coupling of benzylamine to *N*-benzyldenebenzylamine was also tested under more drastic conditions to aim at a higher TON and TOF (*i.e.*, higher pressure and temperature, shorter reaction time and lower catalyst loading). Although only 23% of **5a** was achieved, a TON of 230 was reached and almost 60 molecules of the substrate were converted *per* molecule of catalyst in one hour (entry 11; Table 3.6).

Under the optimized reaction conditions, a screening of several amines was performed to explore the scope and limitations of the catalytic system studied (Table 3.7). As shown before, benzylamine is converted into *N*-benzylidenebenzylamine with excellent yield (entry 1).

Table 3.7. Oxidative coupling of amines to imines. Screening of substrates.<sup>a</sup>

$$\begin{array}{ccc}
 2 \text{ } \begin{array}{c} \text{R}_2 \\ | \\ \text{R}_1\text{---CH---NH}_2 \\ \text{5a-i} \end{array} & \xrightarrow[\substack{6 \text{ h, } 60^\circ\text{C} \\ 30 \text{ psi air}}]{[\text{cat}]} & \begin{array}{c} \text{R}_2 \quad \text{R}_2 \\ \diagdown \quad \diagup \\ \text{R}_1\text{---C=N---C---R}_1 \\ \text{6a-i} \end{array} + \text{NH}_3(\text{g}) + \text{H}_2\text{O}(\text{l})
 \end{array}$$

Entry	Amine	Yield <sup>b</sup> (%)	TON/TOF (h <sup>-1</sup> )
1	 (5a)	>99	100/16.7
2	 (5b)	28	28/4.7
3 <sup>c</sup>	 (5b)	89	89/14.8
4	 (5c)	59	59/9.8
5	 (5d)	60	60/10
6	 (5e)	47	47/7.8
7	 (5f)	-	-
8	 (5g)	-	-
9	 (5h)	-	-
10	 (5i)	-	-

[a] Reaction conditions: amine (1.44 mmol), [Pd{(P(OQuin)<sub>3</sub>)Cl<sub>2</sub>}] (9.2 mg, 14 μmol, 1 mol%), 30 psi air (98 mL autoclave, ca. 1.72 mmol O<sub>2</sub>), 60 °C, 6 h. [b] Yield determined by <sup>1</sup>H NMR. [c] 18 h.

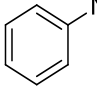
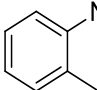
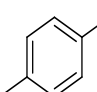
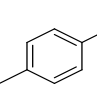
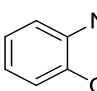
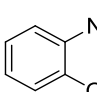
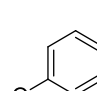
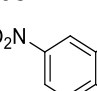
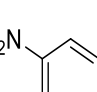
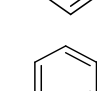
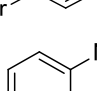
Under the same conditions, the related 4-methoxy-benzylamine gave the corresponding imine with low yield (entry 2). However, at a longer reaction time (18 h) the activity increased significantly (entry 3). Other primary amines bearing only one alpha hydrogen, 2-propylamine and α-methyl-benzylamine are oxidatively homo-coupled with moderate yields (entries 4 and 5). With the aliphatic primary amine n-propylamine moderate activity was observed (entry 6). The role of the amine hydrogen atom(s) in the alpha position was investigated in two simple

experiments using *N,N*-dibenzylamine and *tert*-butylamine as substrates. In both cases, no imine formation was detected and only the starting amines were observed by  $^1\text{H}$  NMR or GC-MS. Hence, it can be concluded that this system of oxidative homo-coupling of amines to imines works best for primary amines (entry 7) bearing at least one hydrogen in the  $\alpha$  position (entry 8). Likewise, functionalized aliphatic primary amines (ethanolamine and ethylenediamine) gave only the starting substrate and no imine formation was observed by  $^1\text{H}$  NMR or GC-MS (entries 9 and 10).

The cross-coupling of benzylamine with aromatic primary amines (substituted anilines) was also investigated (Table 3.8). Anilines were chosen to avoid any additional competitive homo-coupling and the formation of E/Z isomers. Unfortunately, the selectivity for the cross-coupled products **8a–j** is low and, instead, the product from benzylamine homocoupling (**6a**) is predominantly obtained. Imines **8b**, **8e**, **8h** and **8j** (entries 2, 6, 9 and 11, respectively) were not observed. The best results in this screening were obtained for the imines **8c** (21%, entry 4), **8f** (24%, entry 7) and **8g** (36%, entry 8). In an attempt to improve the ratio of **8/6a**, a three-fold excess of *p*-toluidine was used but no significant improvement in the yield of **8c** was achieved (entries 3 and 4). Some substrates, such as aniline itself (entry 1), *ortho*-substituted anilines (entries 2 and 6) and those bearing nitro groups (entries 8 and 9), might deactivate the catalyst since the conversion of benzylamine drops considerably. In a final attempt to obtain cross-coupled products, *tert*-butyl amine was used instead of aniline(s). Unfortunately, once again the reaction only returned the product of benzylamine homocoupling (62%).

Although several homogeneous systems for the aerobic oxidation of amines to imines have been described, to the best of our knowledge only two examples of Pd complexes have been reported as catalysts for this type of reaction.<sup>94,95</sup> Both systems employ Pd compounds with photoactivity and the oxidation of amines (only secondary amines) takes place under photochemical conditions. No records were found in the literature for the aerobic oxidation of amines catalyzed by metal complexes bearing phosphite ligands. The methodology described here is simple: one pot reaction of the neat amine with air in the presence of the catalyst, applying relatively short times, moderate temperatures and moderate pressures. The catalyst can be recovered from the reaction mixture by precipitation with hexanes and it can be reused in a next run without a significant loss of activity.

Table 3.8. Palladium catalyzed oxidative cross-coupling of benzylamine with anilines to imines. <sup>a</sup>

$  \begin{array}{c}  \text{Ph-CH}_2\text{-NH}_2 + \text{R-NH}_2 \xrightarrow[\text{30 psi air}]{\text{[Pd]}} \text{Ph-CH=N-R} + \text{Ph-CH=N-CH}_2\text{Ph} \\  \text{5a} \qquad \text{7a-j} \qquad \qquad \text{6 h, 60 }^\circ\text{C} \\  \text{8a-j} \qquad \qquad \text{6a}  \end{array}  $				
Entry	Amine	Conversion of 5a <sup>b</sup> (%)	8 (%) <sup>c</sup>	6a (%) <sup>c</sup>
1	 (7a)	3	9	91
2	 (7b)	53	-	>99
3	 (7c)	>99	19	81
4 <sup>d</sup>	 (7c)	>99	21	79
5	 (7d)	>99	15	85
6	 (7e)	16	-	>99
7	 (7f)	65	24	76
8	 (7g)	20	36	64
9	 (7h)	31	-	>99
10	 (7i)	82	9	91
11	 (7j)	>99	-	>99

[a] Reaction conditions: benzylamine (1.44 mmol), amine (1.44 mmol), **4** (9.2 mg, 14  $\mu$ mol, 1 mol%), 30 psi air (98 mL autoclave, *ca.* 1.72 mmol O<sub>2</sub>), 60  $^\circ$ C, 6 h. [b] Conversion of **5a** to either **8** or **6a** determined by <sup>1</sup>H NMR (residual signal of **5a** vs. internal standard). [c] Yield determined by <sup>1</sup>H NMR (8 or 6a vs. internal standard). [d] 3 equivalents of *p*-toluidine were used.

### 3.4 Kinetic studies for the oxidative coupling of primary amines catalyzed by the Pd-P(OQuin)<sub>3</sub> complex.

The kinetics for the oxidative coupling of benzylamine (BnNH<sub>2</sub>) to *N*-benzylidenebenzylamine (model reaction) was examined. Although this reaction proceeds well under solvent free conditions, toluene was used as a solvent to perform the kinetic measurements to study the effect of changing the amine concentration. The progress of the reaction as a function of time was monitored by <sup>1</sup>H NMR. (Figure 3.3) The T1 relaxation times of benzylamine and *N*-benzylidenebenzylamine in toluene were determined to set a relaxation delay (*d*<sub>1</sub> = 15 s) long enough to obtain reliable integrals. The reaction was monitored for the first 5 hours and was carried out under atmospheric pressure, at 80 °C, with 1 mol% catalyst and 0.5 mol L<sup>-1</sup> of benzylamine.

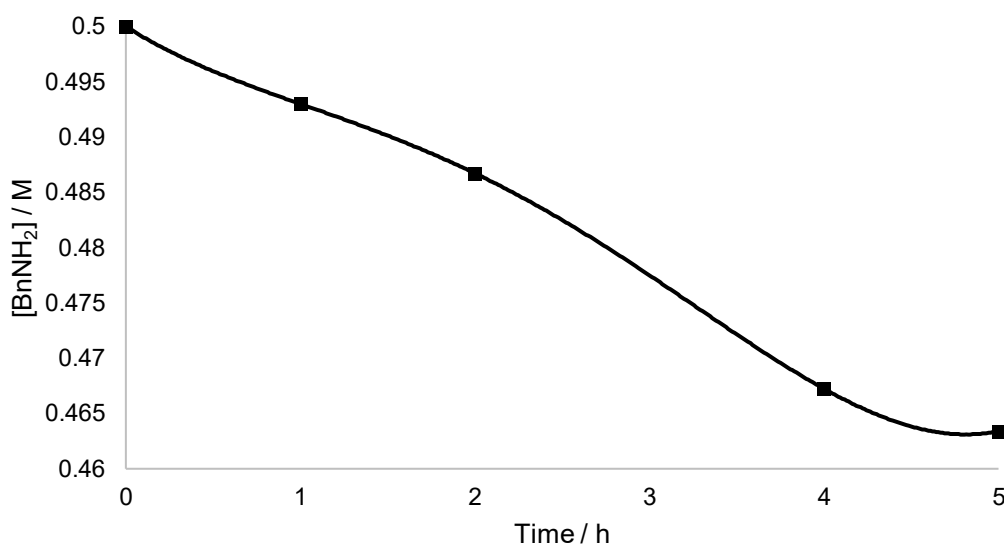


Figure 3.3. Decreasing benzylamine concentration during the first 5 h of reaction.

The representation of  $\ln([BnNH_2]/[BnNH_2]_0)$  vs. time returns a straight line (Figure 3.4). Here  $[BnNH_2]$  is the molar concentration of benzylamine at any “t” time and  $[BnNH_2]_0$  is the initial molar concentration of benzylamine. This suggests a first order rate equation with regard to the amine concentration and a rate constant of 0.016 h<sup>-1</sup>. Considering that very low conversion was achieved under these conditions, it might lead to errors in the conversion determined by <sup>1</sup>H NMR. Further kinetic experiments were carried out under pressure and by increasing the amine and catalyst concentration.

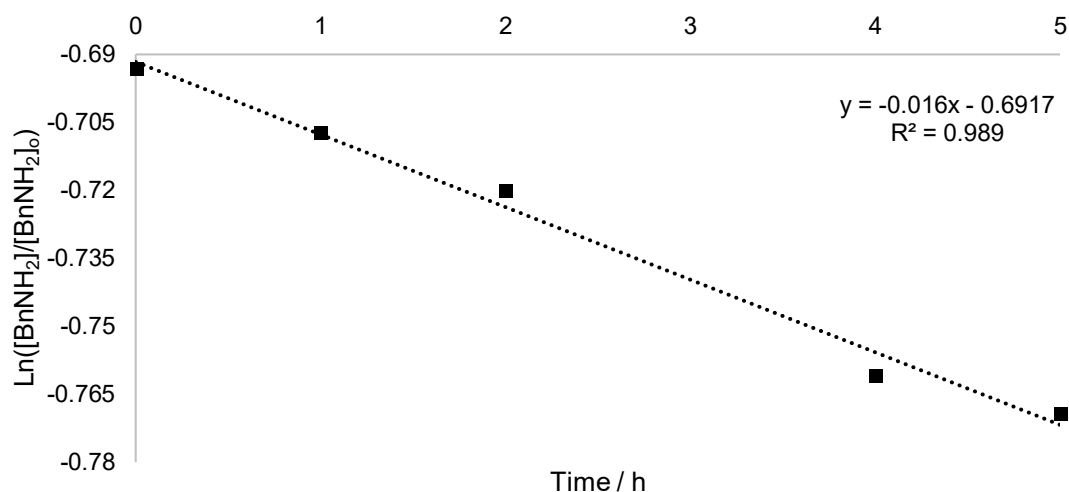


Figure 3.4.  $\ln([BnNH_2]/[BnNH_2]_0)$  vs. time. Conditions: 0.5 mol L<sup>-1</sup> of benzylamine, 1 mol% catalyst, atmospheric pressure, 80 °C, toluene, 1,3,5-trimethoxybenzene (242.2 mg, 1.4 mmol in 5.6 mL) as internal standard.

In general, the rate law for this system can be expressed as:

$$r = k \cdot [BnNH_2]^\alpha \cdot [cat]^\beta \cdot [O_2]^\gamma \quad (\text{Eq. 7})$$

where  $\alpha$ ,  $\beta$  and  $\gamma$  are the partial reaction orders on the amine, catalyst and oxygen concentrations, respectively.

In this sense, the rate of reaction ( $r$ , mol.L<sup>-1</sup>.h<sup>-1</sup>) was measured as a function of the amine concentration, while the concentration of the catalyst, air pressure, temperature and time were kept constant (Table 3.9). The representation of  $\ln(r)$  vs.  $\ln([BnNH_2])$  (Figure 3.5) gives a straight line with a slope of 1.06, thus indicating a first-order dependence on the concentration of benzylamine.

Table 3.9. Rate of reaction ( $r$ ) as a function of amine concentration  $[BnNH_2]$ .

Volume from 10 mol/L BnNH <sub>2</sub> stock solution (mL)	[BnNH <sub>2</sub> ] (mol L <sup>-1</sup> )	$r$ (mol L <sup>-1</sup> h <sup>-1</sup> )	$\ln([BnNH_2])$	$\ln(r)$
2.0	7.0	1.809	1.946	0.593
2.2	8.0	1.973	2.079	0.679
2.4	8.5	2.125	2.140	0.753
2.8	10.0	2.627	2.303	0.965

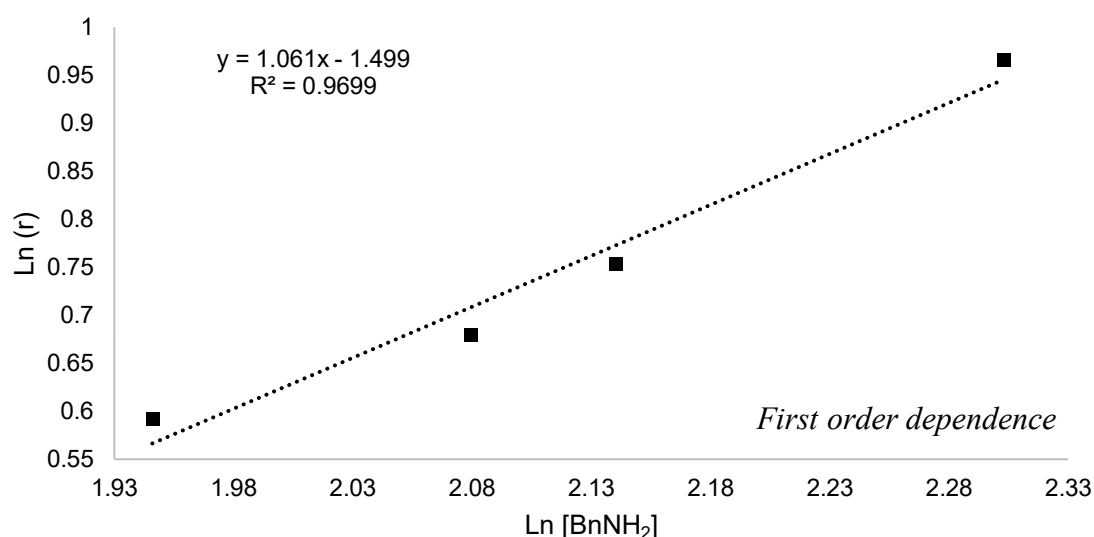


Figure 3.5. Representation  $\log([\text{BnNH}_2])$  vs.  $\log(r)$ . Conditions: 0.5, 1.0, 1.5 and 4.8 mol L<sup>-1</sup> benzylamine (max. 4.8 mmol), 0.015 mol L<sup>-1</sup> catalyst (9.6 mg, 15  $\mu\text{mol}$ ), 130 psi air (98 mL, *ca.* 7.45 mmol O<sub>2</sub>), 60 °C, 2 h, toluene, 1,3,5-trimethoxybenzene (84.1 mg, 0.5 mmol in 1.0 mL) as internal standard.

Likewise, the rate of reaction  $r$  was measured as a function of the catalyst concentration, while the concentration of the amine, air pressure, temperature and time were kept constant (Table 3.10). A first order dependence on the catalyst concentration is observed by the plot  $\log(r)$  vs.  $\log([\text{cat}])$  with a slope value of 1.04 (Figure 3.6).

Table 3.10. Rate of reaction  $r$  as a function of catalyst concentration ([4]).

Mass of complex <b>4</b> (mg)	[4] (mol L <sup>-1</sup> )	$r$ (mol L <sup>-1</sup> h <sup>-1</sup> )	Ln([4])	Ln( $r$ )
9.0	0.05	0.194	-2.996	-1.639
18.0	0.10	0.343	-2.302	-1.070
27.0	0.15	0.558	-1.897	-0.583
36.0	0.20	0.710	-1.609	-0.342

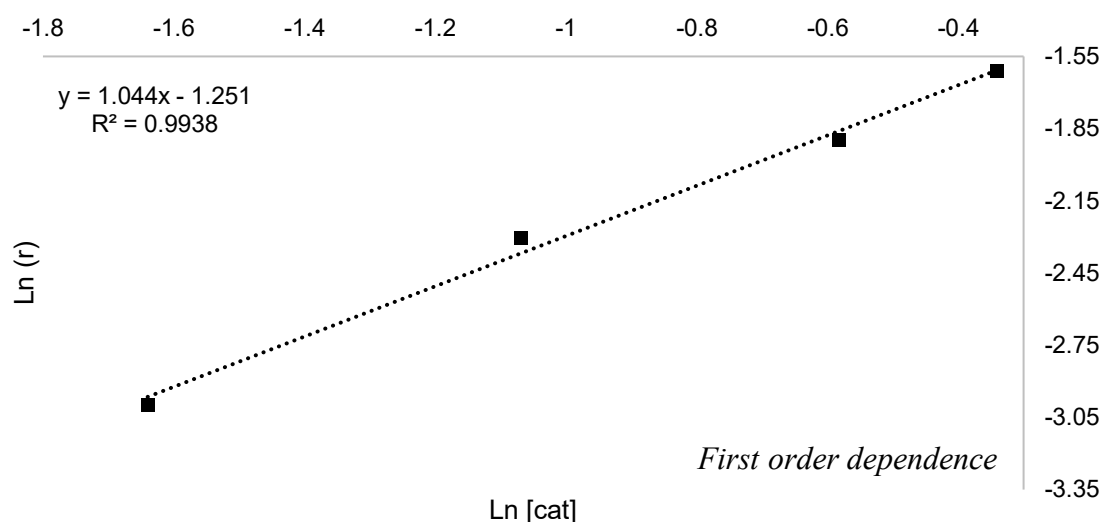


Figure 3.6. Representation  $\log([4])$  vs.  $\log(r)$ .

Although several efforts were made to measure the rate of reaction  $r$  under different air pressures, unfortunately the reaction order with regard to the oxygen partial pressure could not be accurately determined due to technical difficulties. These kinetic experiments indicate that the rate law can be represented as in (Eq. 8), where  $k_{app} = k[O_2]^{\gamma}$ . The apparent rate constant  $k_{app}$  was calculated by measuring the rate of reaction as a function of the product  $[BnNH_2][cat]=P$ , *i.e.*,  $r = k_{app}P$  (Table 3.11 and Figure 3.7).

$$r = k_{app} \cdot [BnNH_2] \cdot [4] \quad (\text{Eq. 8})$$

The plot  $r$  vs.  $P$  depicts a straight line that almost intercepts the origin ( $-0.008$ ) and the slope is the value for  $k = 0.756 \text{ L} \cdot \text{mol}^{-1} \cdot \text{h}^{-1}$ .

Table 3.11. Rate of reaction  $r$  as a function of the product  $[BnNH_2][cat] = P$ .

$[4]$ (mol L <sup>-1</sup> )	$[BnNH_2]$ (mol L <sup>-1</sup> )	$[BnNH_2][cat] = P$ (mol <sup>2</sup> L <sup>-2</sup> )	$r$ (mol L <sup>-1</sup> h <sup>-1</sup> )
0.05	5.0	0.218	0.154
0.10	5.0	0.467	0.343
0.15	5.0	0.729	0.558
0.20	5.0	1.000	0.740



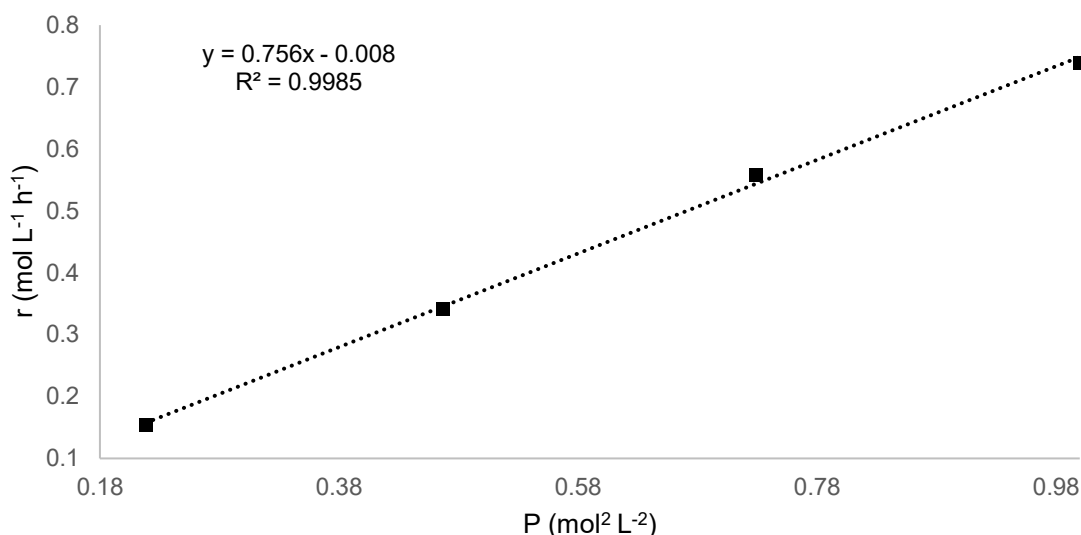


Figure 3.7. Representation of  $r$  vs.  $[\text{BnNH}_2][\text{cat}] = P$ . Conditions: 5 mol L<sup>-1</sup> benzylamine (1.4 mmol in 0.28 mL), 0.05, 0.1, 0.15 and 0.2 mol L<sup>-1</sup> catalyst, 130 psi air (98 mL, *ca.* 7.45 mmol O<sub>2</sub>), 60 °C, 2 h, toluene, 1,3,5-trimethoxybenzene (11.8 mg, 0.07 mmol) as internal standard.

In consequence, the best estimation obtained for the rate law is  $r = 0.756 \text{ L mol}^{-1} \text{ h}^{-1} [\text{BnNH}_2][\text{cat}]$  at a constant air pressure (130 psi, 98 mL, *ca.* 7.45 mmol O<sub>2</sub>) and temperature (60 °C). To the best of our knowledge, no kinetic experiments have been reported for the homocoupling of primary amines to yield imines under homogeneous conditions. Suib *et al.* have performed kinetic experiments for the atmospheric oxidation of 4-methoxybenzylamine to the corresponding imine using a heterogeneous catalyst (meso Cs/MnOx).<sup>83a</sup> Their results suggest a first-order rate equation with regard to the amine concentration and a rate constant of 0.42 min<sup>-1</sup> (0.007 h<sup>-1</sup>).

### 3.5 *In situ* NMR experiments: reactivity of the Pd(II) complex 4 with benzylamine

The reaction of the metal complex **4** in neat BnNH<sub>2</sub> (in the absence and presence of air) and stoichiometric reactions of complex **4** with two equivalents of benzylamine in CDCl<sub>3</sub> (in the absence and presence of air) were carried out and monitored by both <sup>1</sup>H and <sup>31</sup>P{<sup>1</sup>H} NMR). The free phosphite ligand, its corresponding oxide or its hydrolytic product were not detected in any of the <sup>31</sup>P{<sup>1</sup>H} spectra. This might indicate that ligand dissociation does not take place, although it does not exclude the possibility of (fast) N dissociation (hemilability).

In neat benzylamine in the absence of air, the characteristic <sup>31</sup>P{<sup>1</sup>H} resonance of complex **4** (δ = 32.0 ppm) was not observed and, instead, two new resonances (formed in the time scale of the experiment's setup) were identified (δ = 48.4 and 44.8 ppm). (Figure 3.8) After heating for 1 h (60 °C) five new resonances were detected (δ = 23.1, 19.7, 17.7, 7.5 and 2.7

ppm, singlets). Air (40 psi) was charged into the reactor. After 1 h at 60 °C, the homo-coupling product **6a** was detected ( $^1\text{H}$  NMR), while in the  $^{31}\text{P}$  NMR the resonance at 7.5 ppm was predominant. Additional heating (overnight) yielded only *ca.* 3% of imine **5a** ( $^1\text{H}$  NMR) and a featureless  $^{31}\text{P}\{^1\text{H}\}$  NMR.

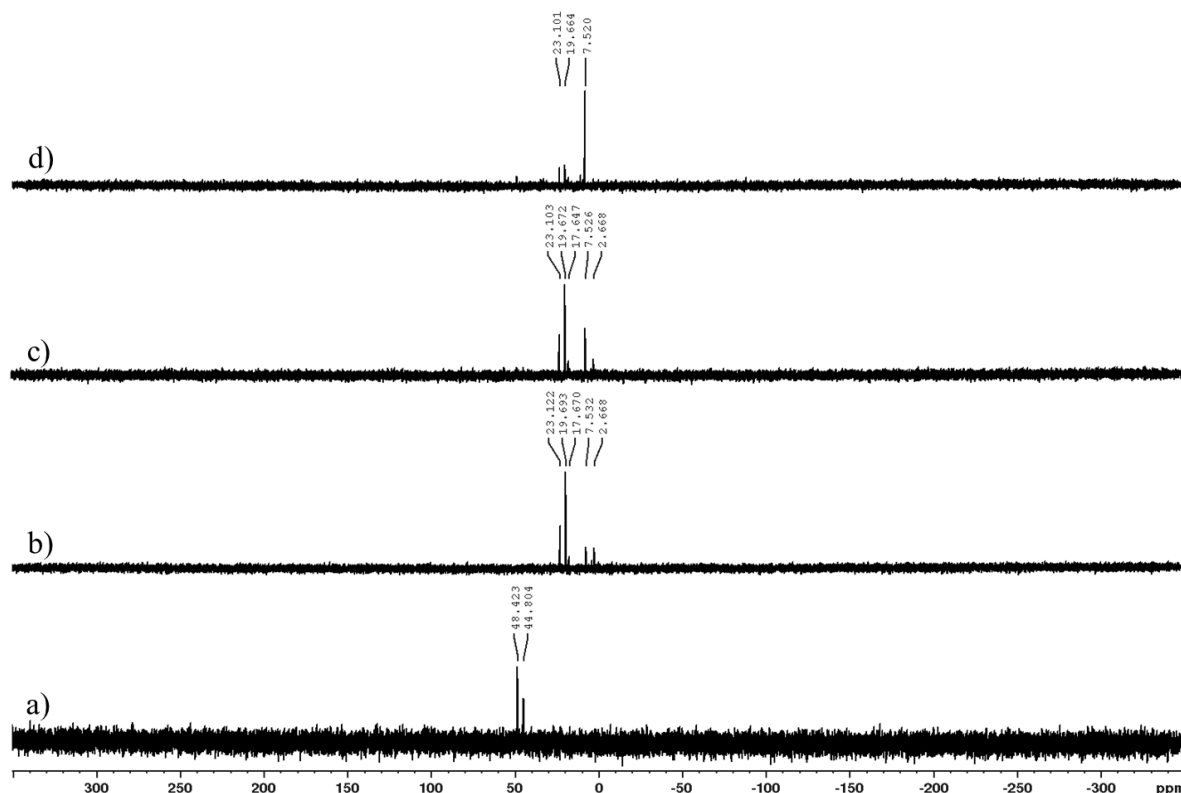


Figure 3.8. Complex **4** in neat benzylamine: *in situ* NMR monitoring by  $^{31}\text{P}\{^1\text{H}\}$  NMR (121.5 MHz). a) Inert atmosphere, room temperature, < 5 minutes after mixing **4** and  $\text{BnNH}_2$ ; b) Inert atmosphere, 1 h at 60 °C; c) 40 psi air, 60 °C, < 5 minutes after loading the air pressure; d) 40 psi air, 60 °C, 1 h after loading the air pressure.

In the stoichiometric *in situ* experiment, the signal at 44.1 ppm was observed upon addition of  $\text{BnNH}_2$  to a  $\text{CDCl}_3$  suspension of **4**. In this case, the characteristic  $^{31}\text{P}\{^1\text{H}\}$  resonance of complex **4** ( $\delta = 32.0$  ppm) persisted up to 1 h at room temperature and disappeared after heating (2 h, 60 °C). (Figure 3.9) In contrast to the experiment in neat benzylamine, a single phosphorus-containing species was detected. Air (40 psi) was added to the sample and only after 2 h at 60 °C a new signal ( $\delta = 53.0$  ppm) appeared and persisted for 4 h. Remarkably, after 16 h under these conditions, imine **6a** and complex **4** were quantitatively formed.

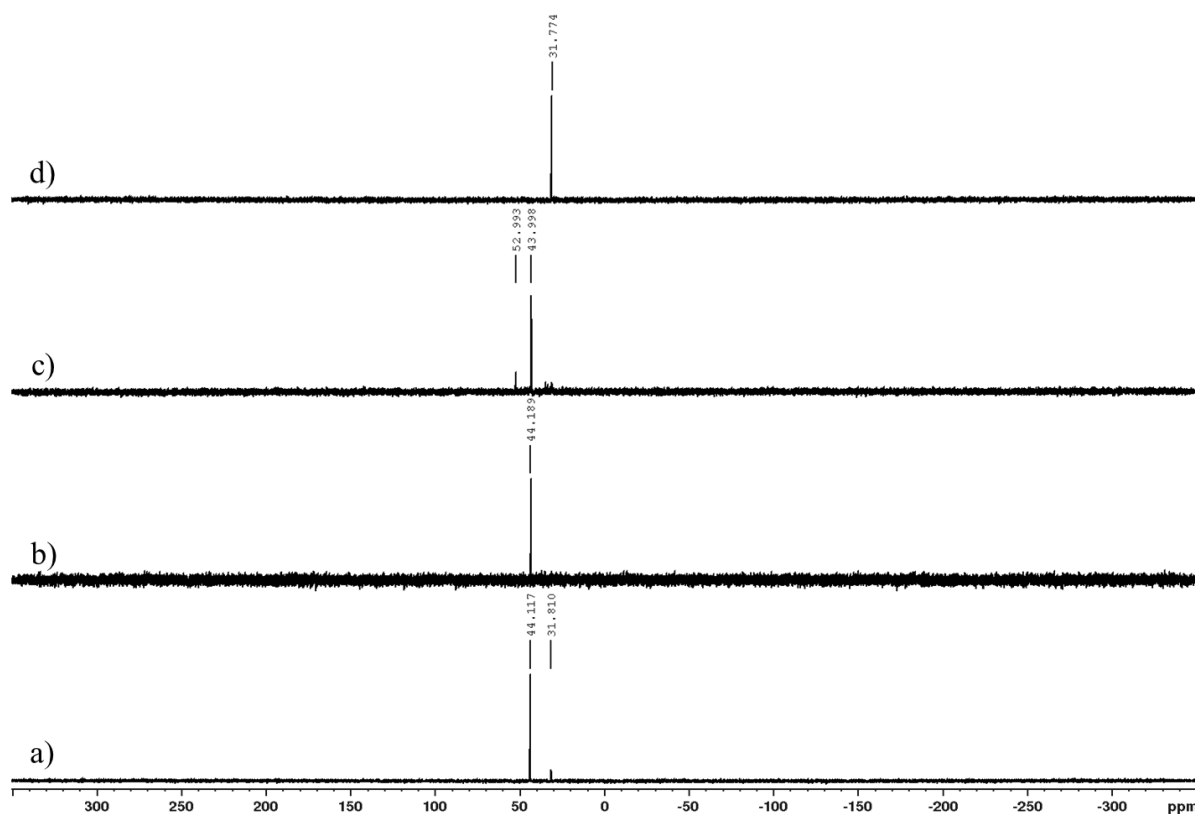
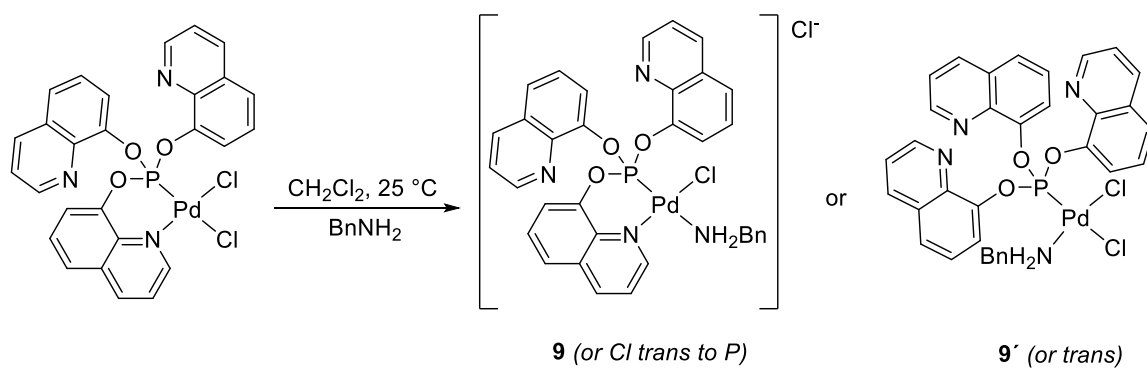


Figure 3.9. Stoichiometric test **4** + benzylamine: *in situ* NMR monitoring by  $^{31}\text{P}\{^1\text{H}\}$  NMR (121.5 MHz). a) Inert atmosphere, room temperature, < 5 minutes after mixing **4** and  $\text{BnNH}_2$ ; b) Inert atmosphere, 2 h at 60 °C; c) 40 psi air, 60 °C, 4 h after loading the air pressure; d) 40 psi air, 60 °C, 16 h after loading the air pressure.

Based on these results, the isolation of the specie observed at 44.1 ppm in the  $^{31}\text{P}\{^1\text{H}\}$  spectra was attempted. Complex **4** was treated with 8 equivalents of benzylamine in dichloromethane under an inert atmosphere (Scheme 3.2).



Scheme 3.2. Reaction of complex **4** with  $\text{BnNH}_2$ . Isolation of **9** or **9'**.

Stirring of the reaction mixture (RT, 1 h) yields a complete conversion of **4** into a new complex **9/9'** ( $\delta = 44.1$  ppm) as can be seen on the  $^{31}\text{P}\{^1\text{H}\}$  spectrum (Figure 3.10). Filtration of the reaction mixture, followed by treatment of the clear solution with hexanes, yielded a

bright yellow solid. The  $^1\text{H}$  NMR spectrum suggests the presence of benzylamine in the compound assigned as **9/9'**, based on the characteristic resonance of the methylene group (3.84 ppm) and the integral value of aromatic signals.

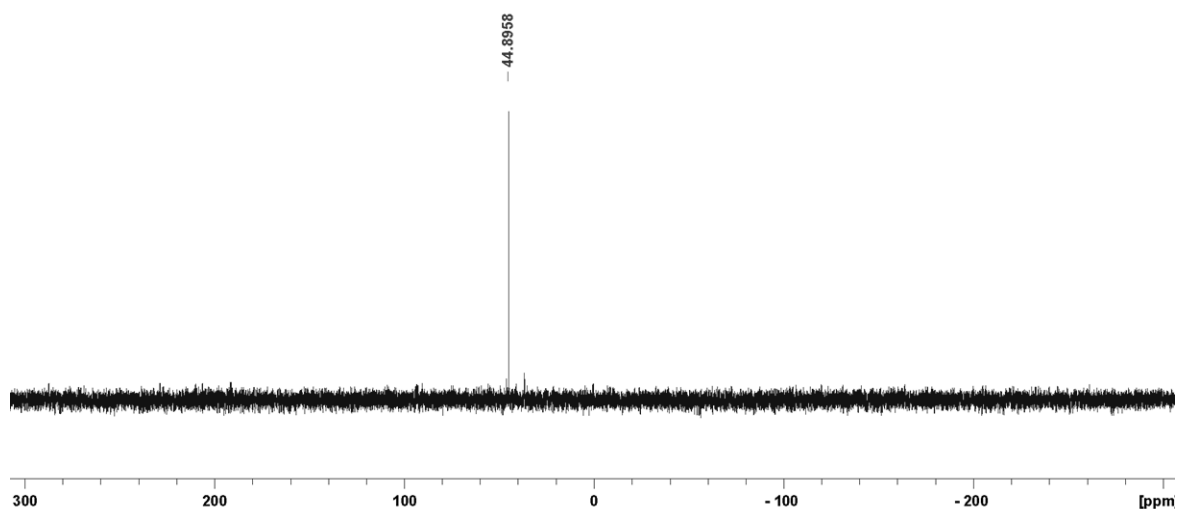


Figure 3.10.  $^{31}\text{P}\{^1\text{H}\}$  NMR spectrum (121.5 MHz) at 298 K of **9** in  $\text{CD}_2\text{Cl}_2$ .

Variable temperature NMR measurements, both for  $^1\text{H}$  and  $^{31}\text{P}\{^1\text{H}\}$ , reveal the existence of a dynamic process (fluxionality) associated with the rotation of the Pd–N bond in the coordinated benzylamine (Figures 3.11 and 3.12).

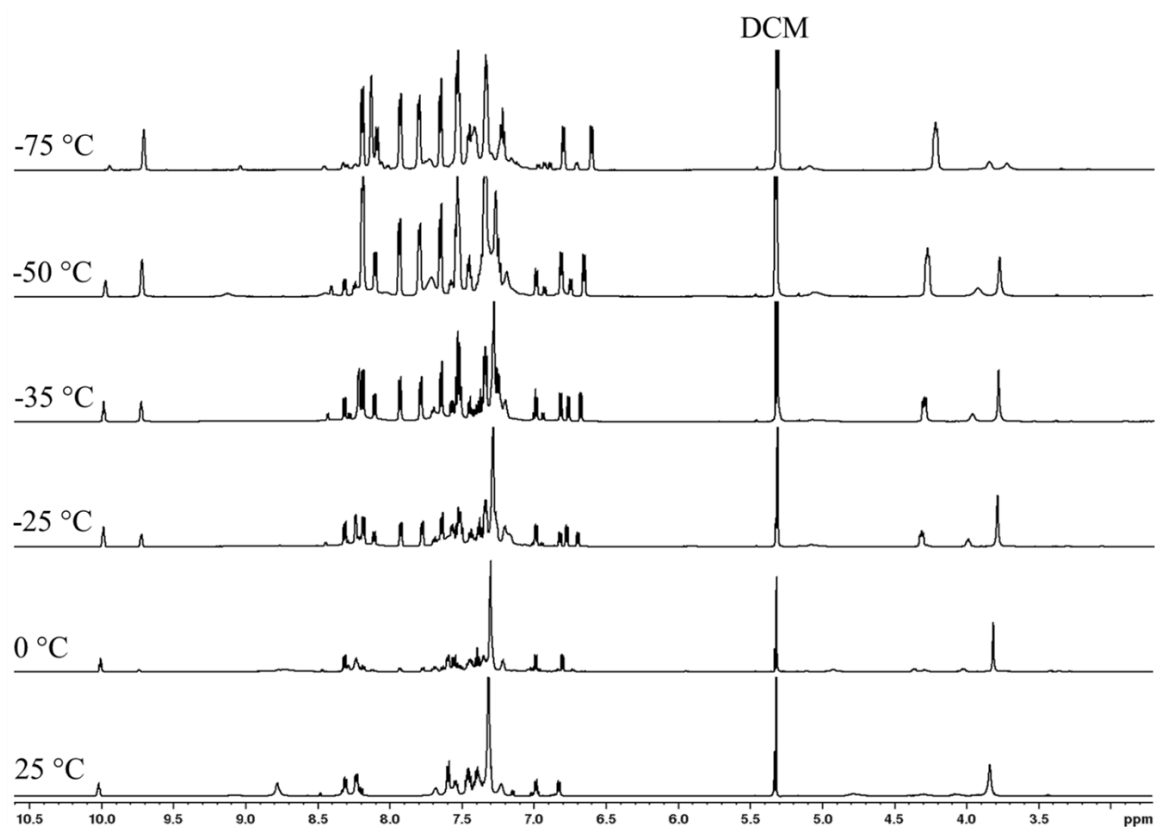


Figure 3.11.  $^1\text{H}$  NMR spectra of **9** at variable temperature (600.0 MHz,  $\text{CD}_2\text{Cl}_2$ ).

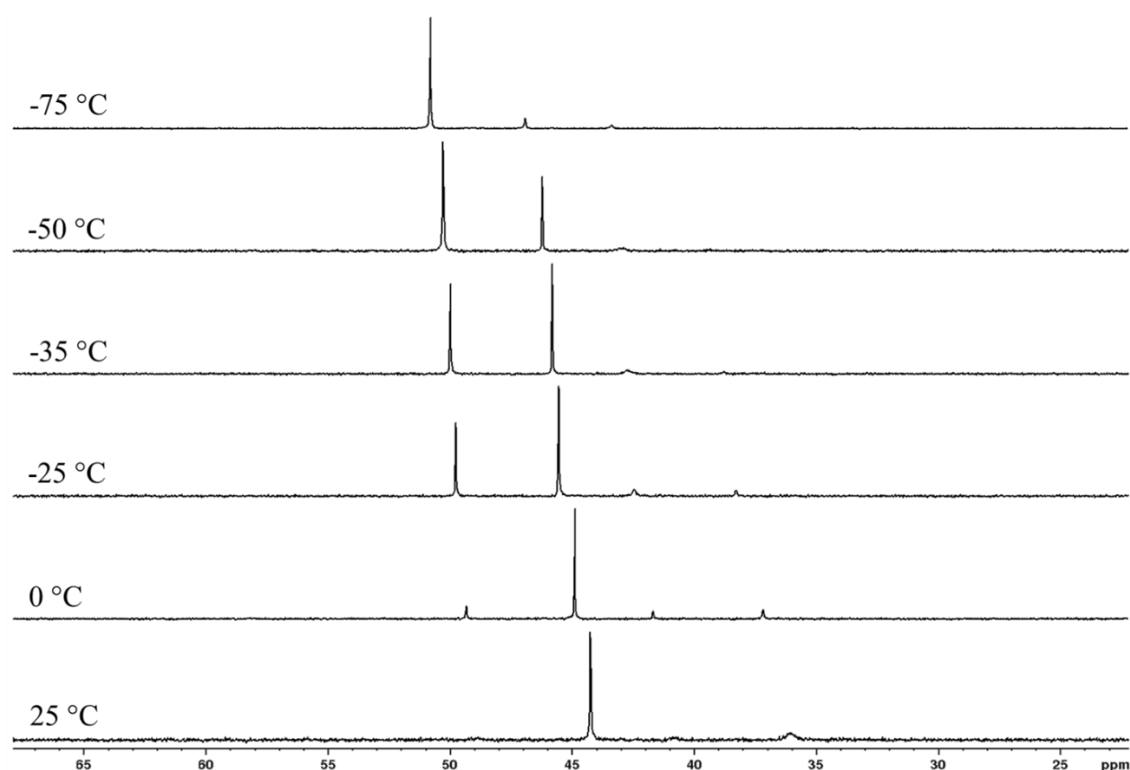
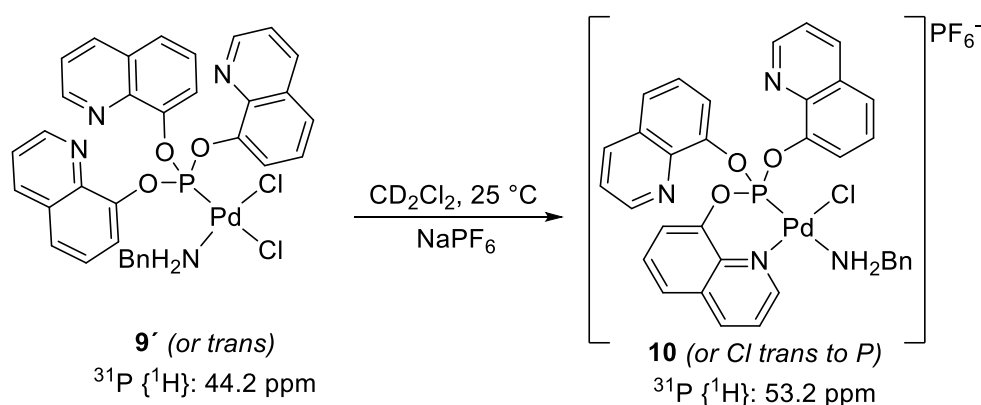


Figure 3.12.  $^{31}\text{P}\{^1\text{H}\}$  NMR spectra of **9** at variable temperature (121.5 MHz,  $\text{CD}_2\text{Cl}_2$ ).

Careful analysis of the relative ratio of the integrals (aromatics/methylene) at different temperatures indicates that complex **9/9'** contains only one coordinated  $\text{BnNH}_2$ . Thus, the formula of **9/9'** would be  $[\text{Pd}(\text{BnNH}_2)\{\text{P}(\text{OQuin})_3\}\text{Cl}_2]/[\text{Pd}(\text{BnNH}_2)\{\text{P}(\text{OQuin})_3\}\text{Cl}]\text{Cl}$  respectively. To find out whether the  $\text{Cl}^-$  or the N arm of the chelate  $\text{P}(\text{OQuin})_3$  dissociates from the  $\text{Pd}(\text{II})$  center (leading to the cationic complex **9** or the neutral **9'**) **9/9'** was reacted with  $\text{NaPF}_6$ . The reaction proceeds cleanly to a unique species **10** (Scheme 3.3).



Scheme 3.3. Reaction of complex **9/9'** with  $\text{NaPF}_6$ . Attempt to elucidate **10**.

The significant shift in  $^{31}\text{P}\{^1\text{H}\}$  NMR ( $\Delta\delta = 9$  ppm, toward higher frequencies; Figure 3.13) suggests that **9'** is more likely to be formed. Given the inherent *trans* influence of the phosphorus atom (as evidenced by the different  $\text{Pd}-\text{Cl}$  distances in the solid-state structure of

4) one of the chloride ligands should be more labile than the other, and the N-arm could dissociate generating an hemilabile ligand. Crystals of **9/9'** suitable for X-ray diffraction analysis could not be isolated. Attempts to perform an elemental analysis of this compound have so far been unsuccessful since the coordinated BnNH<sub>2</sub> is eliminated from **9/9'** under vacuum to yield back **4**, as confirmed by <sup>31</sup>P{<sup>1</sup>H} NMR (vacuum was required to remove residual solvents, CH<sub>2</sub>Cl<sub>2</sub> and Et<sub>2</sub>O from the synthesis).

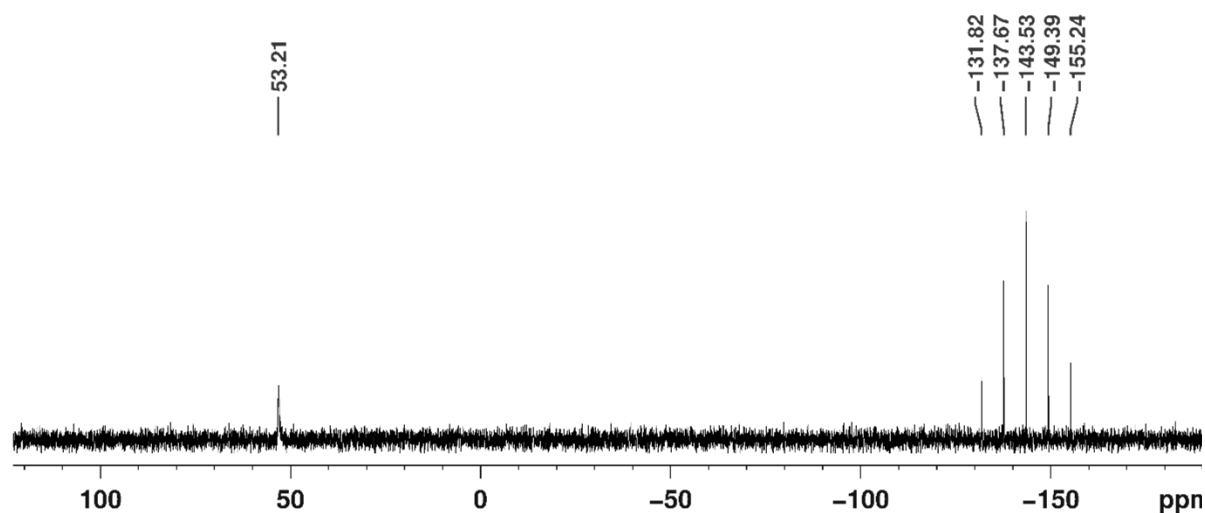


Figure 3.13. <sup>31</sup>P{<sup>1</sup>H} NMR spectra of **10** (121.5 MHz, CD<sub>2</sub>Cl<sub>2</sub>).

MS analyses of **9/9'** revealed the species [Pd(NH<sub>2</sub>){P(OQuin)<sub>3</sub>}]<sup>+</sup> (585.0302 μm, LIFDI-MS) and [Pd(ND<sub>3</sub>){P(OQuin)<sub>3</sub>}Cl]<sup>+</sup> (624.01 μm, HESI-MS, deuterium from NMR solvents) along with the decomposition products from the Arbuzov reaction. These analyses would indicate that compound **9/9'** decomposes/reacts under the conditions of the MS analysis. Thus, the observed species would bear either ammonia or amide ligands, confirming the finding of NH<sub>3</sub> evolution in the catalytic reactions. Although these experiments do not provide solid evidence of the mechanism that governs the oxidative coupling of primary amines catalyzed by **4**, two facts are clear:

- (1) Dissociation of the phosphite ligand under the studied conditions appears to be unlikely.
- (2) Amine pre-coordination takes place. Furthermore, once the amine is coordinated to the Pd center, its transformation into the corresponding imine only happens in the presence of an appropriate oxidant (O<sub>2</sub>).

### 3.6 Chapter conclusions

P(OQuin)<sub>3</sub> ligand binds Pd(II) as a bidentate P–N chelate, as confirmed by X-ray diffraction analysis of the compound [Pd{P(OQuin)<sub>3</sub>}Cl<sub>2</sub>]. This Pd(II) complex is a suitable catalyst or

precatalyst for the solvent-free oxidative coupling of primary amines to imines. The reaction conditions were optimized for a model reaction (benzylamine as the substrate) and the imine formation can proceed under mild conditions: 0.5 mol% [Pd{(P(OQuin)<sub>3</sub>)Cl<sub>2</sub>}] as the catalyst precursor, 60 °C, 6 h and 30psi of air as the terminal oxidant (*ca.* 1.72 mmol O<sub>2</sub>, 1.2 equivalents). TONs up to 230 were reached and almost 60 molecules of the substrate were converted *per* molecule of catalyst in one hour. Kinetic measurements indicate that the rate law is  $r = 0.756 \text{ L}\cdot\text{mol}^{-1}\cdot\text{h}^{-1} [\text{BnNH}_2]\cdot[\text{cat}]$  at a constant air pressure (130 psi, 25 mL, *ca.* 1.90 mmol O<sub>2</sub>) and temperature (60 °C). The partial order regard to the oxygen concentration could not be accurately determined. *In situ* and variable temperature NMR experiments suggest that the dissociation (and oxidation) of the phosphite ligand does not take place under the studied conditions. Coordination of the amine moiety to the Pd atom was concluded from the NMR experiments. The cross-coupling of benzylamine with aromatic primary amines (substituted anilines) was studied but the selectivity toward the asymmetric imines was found to be low.

### 3.7 Experimental section.

#### Preparation of *cis*-dichloro-(*P,N*)-tris(8-quinolinyl)phosphite palladium (II), 4.

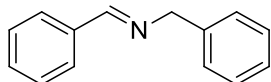
To a solution of [PdCl<sub>2</sub>(COD)] (242.0 mg, 0.84 mmol) in CH<sub>2</sub>Cl<sub>2</sub> (10 mL) was added a solution of **1** (397.0 mg, 0.85 mmol) in CH<sub>2</sub>Cl<sub>2</sub> (10 mL) at -75 °C, and the mixture was stirred for 30 min. Then, the mixture was left to warm up to room temperature and was stirred for additional 3 h. All volatile materials were removed under reduced pressure. The complex was washed twice with dried Et<sub>2</sub>O (20 mL) and twice with dried hexane (20 mL). The solid was dried under vacuum to obtain a pale-yellow solid (426.0 mg, 79% yield). <sup>1</sup>H NMR (300.2 MHz, CDCl<sub>3</sub>, 25°C): δ = 10.26 (d, <sup>3</sup>J<sub>HH</sub> = 5.4 Hz, 1H, H2), 8.48 (dd, <sup>3</sup>J<sub>HH</sub> = 8.3 Hz, <sup>4</sup>J<sub>HH</sub> = 1.4 Hz, 1H, H4), 7.79-7.68 (m, 3H, H5-7), 7.62 (dd, <sup>3</sup>J<sub>HH</sub> = 8.3 Hz, <sup>3</sup>J<sub>HH</sub> = 5.4 Hz, 1H, H3). Given the low solubility of **4** in CDCl<sub>3</sub>, the <sup>13</sup>C resonances are poorly resolved. <sup>31</sup>P{<sup>1</sup>H} NMR (121.5 MHz, CDCl<sub>3</sub>, 25°C): δ = 31.8 ppm (s). <sup>1</sup>H NMR (600.1 MHz, DMSO-*d*<sub>6</sub>, 25°C): δ = 10.11 (d, <sup>3</sup>J<sub>HH</sub> = 5.1 Hz, 1H, H2), 8.94 (dd, <sup>3</sup>J<sub>HH</sub> = 8.3 Hz, <sup>4</sup>J<sub>HH</sub> = 1.4 Hz, 1H, H4), 8.08 (dd, <sup>3</sup>J<sub>HH</sub> = 7.8 Hz, <sup>4</sup>J<sub>HH</sub> = 1.8 Hz, 1H, H5), 7.93 (dd, <sup>3</sup>J<sub>HH</sub> = 8.3 Hz, <sup>3</sup>J<sub>HH</sub> = 5.3 Hz, 1H, H3), 7.90-7.85 (m, 2H, H6-7). <sup>13</sup>C{<sup>1</sup>H} NMR (150.9 MHz, DMSO-*d*<sub>6</sub>, 25°C): δ = 159.1 (s, C2), 142.5 (s, C4), 129.0 (s, C6), 126.2 (s, C5), 123.0 (s, C3), 122.4 (d, <sup>3</sup>J<sub>PC</sub> = 5.5 Hz, C7), quaternary carbons (C8-10) are poorly resolved. <sup>31</sup>P{<sup>1</sup>H} NMR (121.5 MHz, DMSO-*d*<sub>6</sub>, 25°C): δ = 32.3 ppm (s). LRMS (ESI): *m/z* calc. for C<sub>28</sub>H<sub>21</sub>N<sub>3</sub>O<sub>4</sub>PPdNa 692.96 [M•MeOH+Na]<sup>+</sup>; found 692.96. Analytically pure samples were obtained upon recrystallization in CHCl<sub>3</sub>. Anal. Calcd. for C<sub>27</sub>H<sub>18</sub>N<sub>3</sub>O<sub>3</sub>Cl<sub>2</sub>PPd•3.5CHCl<sub>3</sub>: C, 34.61; H, 2.05; N, 3.97. Found: C, 34.44; H, 1.99; N, 3.58. IR (KBr disk, ν in cm<sup>-1</sup>): 1634

m, 1593 w, 1579 w, 1511 m, 1502 w, 1466 m, 1385 m, 1377 m, 1307 m, 1253 m, 1240 w, 1196 m, 1098 m, 923 m, 854 m, 826 m, 760 m, 753 m, 721 m, 603 w, 575 w, 459 w. UV-Vis (CHCl<sub>3</sub>,  $\lambda_{\text{max}}$  in nm): 246, 328.

### General procedure for catalytic oxidative homo-coupling of amines to imines.

A glassware flask (5 mL) or Parr reactor (98 mL) was charged with the catalyst precursor (Table 3, 0.014 mmol, 1 mol%) and the corresponding amine (Table 2-8, 1.4 mmol). If applicable, see Table 4, the corresponding solvent was added (1.4 mL, 1 mol/L). If applicable, an oxidant (Table 6) was added or the autoclave was pressurized at the specified pressure. (see Table 7). The reaction mixture was stirred at the specified temperatures and during the time stated. (see Table 7). If applicable, the system was cooled to room temperature and the pressure of gas was carefully released. The yield was determined by <sup>1</sup>H NMR using 1, 3, 5-trimethoxybenzene as internal standard. Hexanes were added to the crude of reaction in order to precipitate the catalyst and the solution was flash chromatographed through silica. The imines **6a-e** were thus obtained upon evaporation of the eluent (hexane and ethyl acetate).

### Spectroscopic data of homo-coupling products



**N-Benzylidenebenzylamine (6a).** Yellow liquid. <sup>1</sup>H NMR (300 MHz, CDCl<sub>3</sub>):  $\delta$  8.38 (s, 1H), 7.79-7.77 (m, 2H), 7.41-7.40 (m, 3H), 7.33 (d,  $J$  = 4.5 Hz, 4H), 7.27-7.23 (m, 1H), 4.82 (s, 2H). <sup>13</sup>C NMR (125.4 MHz, CDCl<sub>3</sub>):  $\delta$  162.0, 139.4, 136.3, 130.8, 128.7, 128.6, 128.3, 128.0, 127.0, 65.1. MS (ESI):  $m/z$  196 [M + 1].

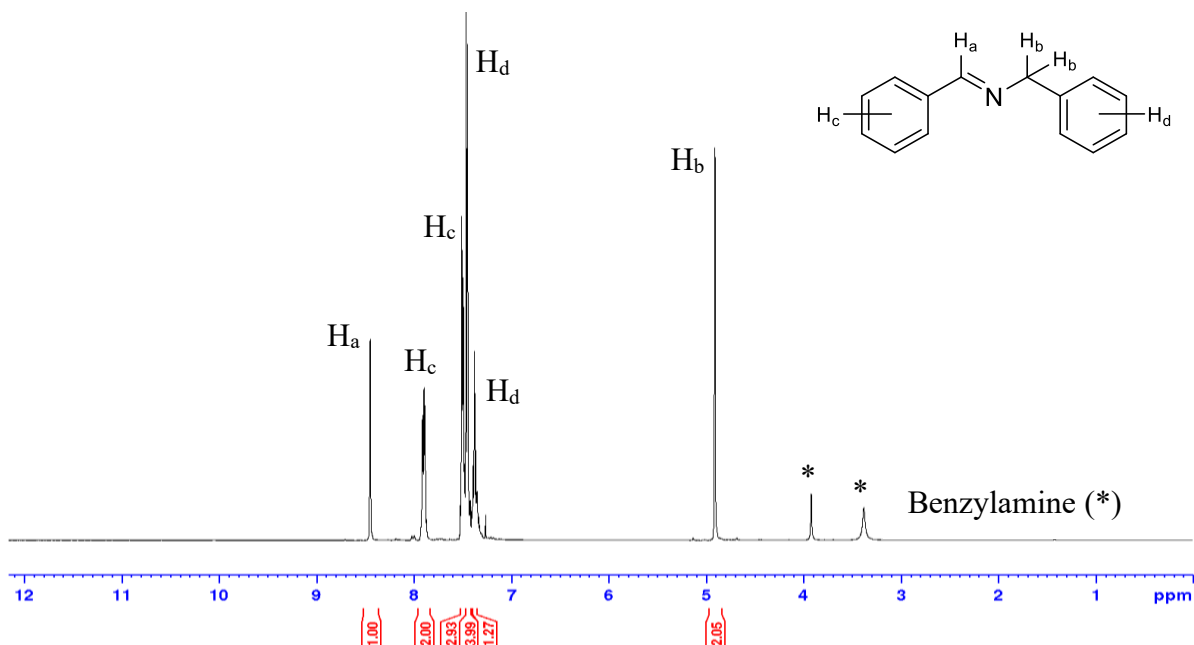


Figure 3.14. <sup>1</sup>H (300 MHz) NMR spectra at 298 K of isolated **6a** in CDCl<sub>3</sub>.



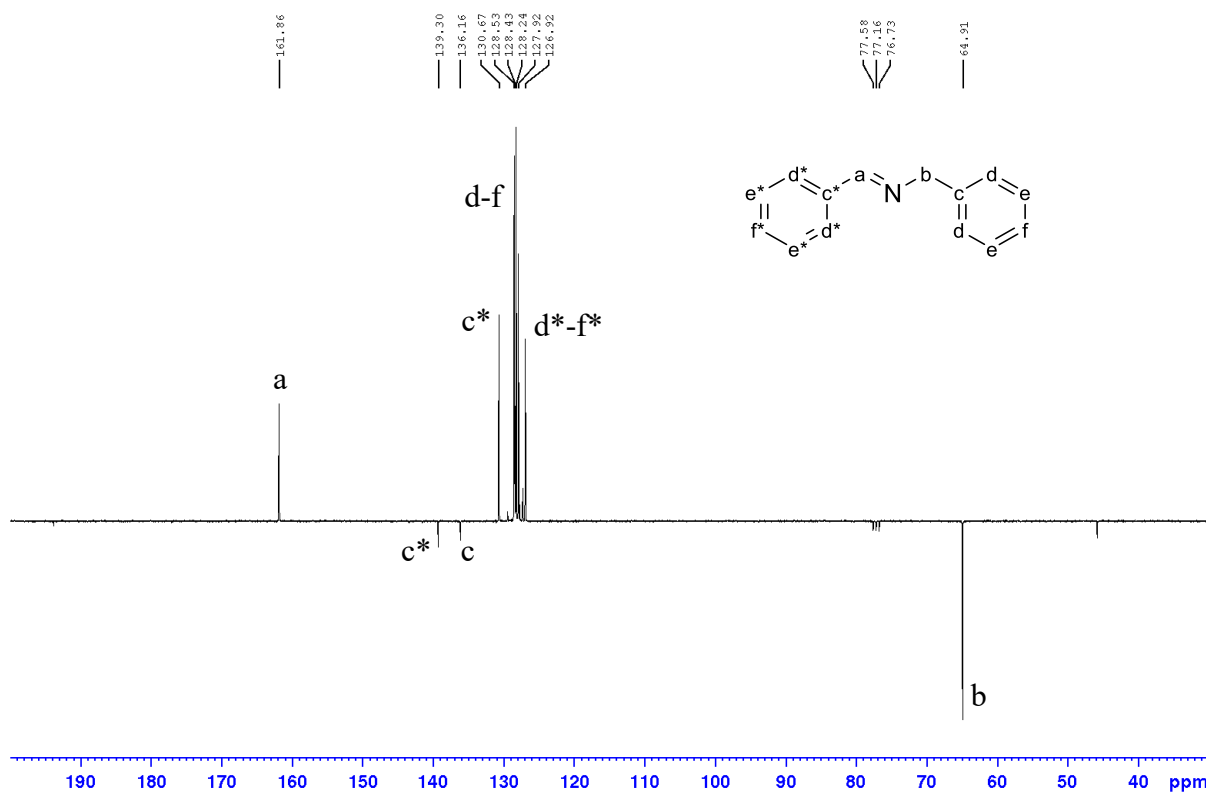
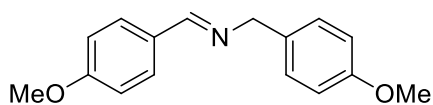
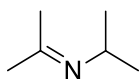


Figure 3.15.  $^{13}\text{C}\{^1\text{H}\}$ -APT (75.5 MHz) NMR spectra at 298 K of isolated **6a** in  $\text{CDCl}_3$ .

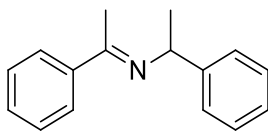


***N*-(4-methoxy)Benzylidene-4-methoxybenzylamine**

**(6b).** Yellow liquid.  $^1\text{H}$  NMR (300 MHz,  $\text{CDCl}_3$ ):  $\delta$  8.27 (s, 1H), 7.80 (d, 2H), 7.23 (d, 2H), 6.88 (dd, 4H), 4.70 (s, 2H), 3.81 (s, 3H), 3.77 (s, 3H).  $^{13}\text{C}$  NMR (125.4 MHz,  $\text{CDCl}_3$ ):  $\delta$  160.9, 158.6, 131.9, 131.7, 129.8, 129.1, 114.0, 64.38, 55.86. **MS** (ESI):  $m/z$  256.16 [ $M + 1$ ].

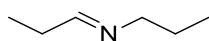


***N*-Isoprpylidenepropylamine (6c).** Yellow liquid.  $^1\text{H}$  NMR (300 MHz,  $\text{CDCl}_3$ ):  $\delta$  3.36 (m, 1H), 1.73(s, 3H), 1.59 (s, 3H), 0.86 (d, 6H).  $^{13}\text{C}$  NMR (125.4 MHz,  $\text{CDCl}_3$ ):  $\delta$  00.0, **MS** (ESI):  $m/z$  100 [ $M + 1$ ].



***N*-(Methyl-Benzylidene)Methylbenzylamine (6d).**

Yellow liquid.  $^1\text{H}$  NMR (300 MHz,  $\text{CDCl}_3$ ):  $\delta$  7.00-7.09 (m, 10H), 4.33 (q, 1H), 1.54 (s, 3H), 1.21 (d, 3H).  $^{13}\text{C}$  NMR (125.4 MHz,  $\text{CDCl}_3$ ):  $\delta$  165.68, 147.06, 145.74, 128.18, 128.09, 126.51, 126.40, 126.23, 125.56, 59.03, 30.33, 25.16. **MS** (ESI):  $m/z$  224.31 [ $M + 1$ ].

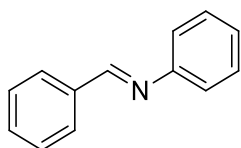


**N-Propyldienepropylamine (6e).** Yellow liquid.  $^1\text{H}$  NMR (300 MHz,  $\text{CDCl}_3$ ):  $\delta$  3.08 (t, 1H), 2.06 (s, 2H), 1.90 (s, 2H), 1.72 (s, 3H), 1.55 (m, 2H), 0.83 (t, 3H).  $^{13}\text{C}$  NMR (125.4 MHz,  $\text{CDCl}_3$ ):  $\delta$  53.21, 43.93, 26.60, 11.90, 11.35. **MS** (ESI):  $m/z$  100  $[\text{M} + 1]$ .

### General procedure for catalytic oxidative cross-coupling of amines to imines.

A Parr reactor (98 mL) was charged with **4** (0.01 mmol, 1 mol%), benzylamine (150 mg, 1.4 mmol), and the corresponding aniline (1.4 mmol). For solid anilines (see Table 9), toluene was added as solvent (1.4 mL, 1 mol/L). The Parr reactor was pressurized at 30 psi of air and the reaction mixture was stirred at 60 °C for 6h. The system was cooled to room temperature and the pressure of gas was carefully released. The yield was determined by  $^1\text{H}$  NMR using 1, 3, 5-trimethoxybenzene as internal standard. Hexanes were added to the crude of reaction in order to precipitate the catalyst and the solution was flash chromatographed through silica. The imines **8a**, **8c**, **8d**, **8f**, **8g** and **8i** were thus obtained upon evaporation of the eluent (hexane and ethyl acetate).

### Spectroscopic data of cross-coupling products



**N-Benzylideneaniline (8a).** Yellow liquid.  $^1\text{H}$  NMR (300 MHz,  $\text{CDCl}_3$ ):  $\delta$  8.37 (s, 1H), 7.81-7.79 (m, 2H), 7.36-7.18(m, 8H).

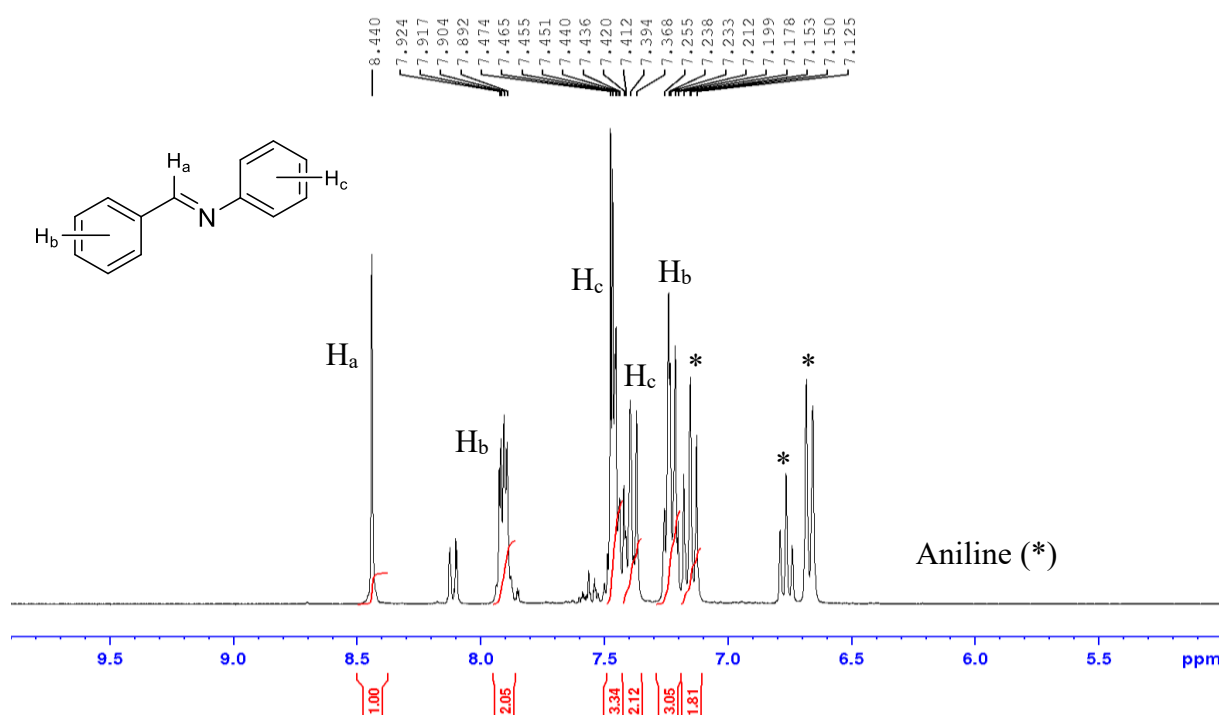


Figure 3.16.  $^1\text{H}$ (300 MHz) NMR spectra at 298 K of **8a** crude in  $\text{CDCl}_3$ .

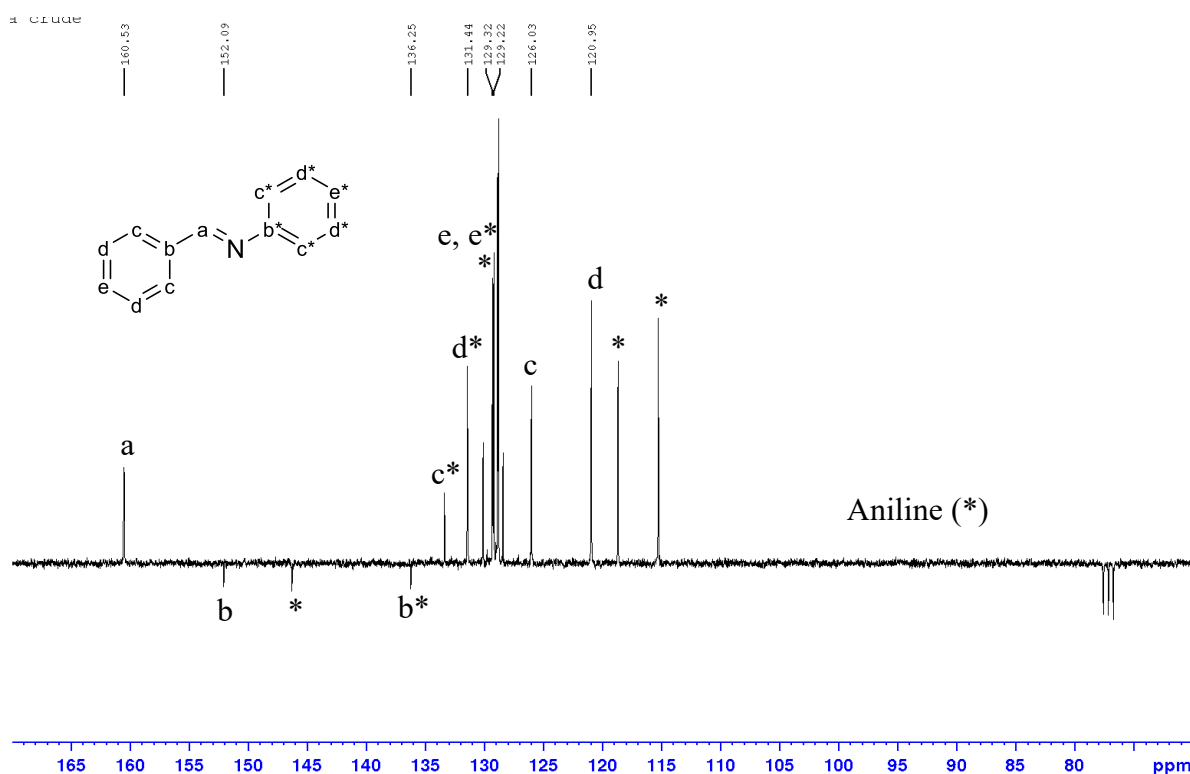
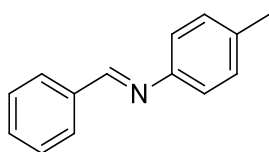
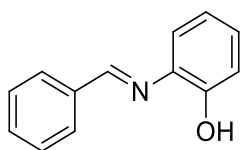


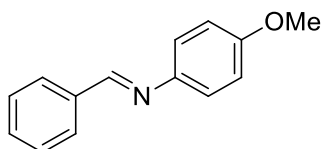
Figure 3.17.  $^{13}\text{C}\{^1\text{H}\}$ -APT (75.5 MHz) NMR spectra at 298 K of **8a** crude in  $\text{CDCl}_3$ .



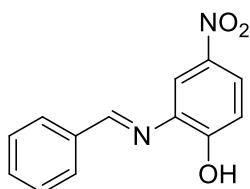
**4-methyl-*N*-Benzylideneaniline (8c).** Yellow liquid.  $^1\text{H}$  NMR (300 MHz,  $\text{CDCl}_3$ ):  $\delta$  8.38 (s, 1H), 7.90-7.87 (m, 2H), 7.48-7.25 (m, 3H), 7.33 (d,  $J = 4.5$  Hz, 4H), 7.27-7.23 (m, 1H), 4.82 (s, 2H).  $^{13}\text{C}$  NMR (125.4 MHz,  $\text{CDCl}_3$ ):  $\delta$  162.0, 139.4, 136.3, 130.8, 128.7, 128.6, 128.3, 128.0, 127.0, 65.1.



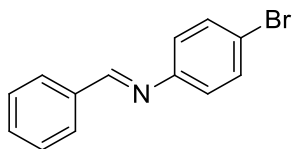
**2-hydroxy-*N*-Benzylideneaniline (8d).** Yellow liquid.  $^1\text{H}$  NMR (300 MHz,  $\text{CDCl}_3$ ):  $\delta$  8.38 (s, 1H), 7.79-7.77 (m, 2H), 7.41-7.40 (m, 3H), 7.33 (d,  $J = 4.5$  Hz, 4H), 7.27-7.23 (m, 1H), 4.82 (s, 2H).  $^{13}\text{C}$  NMR (125.4 MHz,  $\text{CDCl}_3$ ):  $\delta$  162.0, 139.4, 136.3, 130.8, 128.7, 128.6, 128.3, 128.0, 127.0, 65.1.



**4-methoxy-*N*-Benzylideneaniline (8f).** Yellow liquid.  $^1\text{H}$  NMR (300 MHz,  $\text{CDCl}_3$ ):  $\delta$  8.38 (s, 1H), 7.79-7.77 (m, 2H), 7.41-7.40 (m, 3H), 7.33 (d,  $J = 4.5$  Hz, 4H), 7.27-7.23 (m, 1H), 4.82 (s, 2H).  $^{13}\text{C}$  NMR (125.4 MHz,  $\text{CDCl}_3$ ):  $\delta$  162.0, 139.4, 136.3, 130.8, 128.7, 128.6, 128.3, 128.0, 127.0, 65.1.



**2-hydroxy-5-nitro-*N*-Benzylideneaniline (8g).** Yellow liquid.  $^1\text{H}$  NMR (300 MHz,  $\text{CDCl}_3$ ):  $\delta$  8.38 (s, 1H), 7.79-7.77 (m, 2H), 7.41-7.40 (m, 3H), 7.33 (d,  $J = 4.5$  Hz, 4H), 7.27-7.23 (m, 1H), 4.82 (s, 2H).  $^{13}\text{C}$  NMR (125.4 MHz,  $\text{CDCl}_3$ ):  $\delta$  162.0, 139.4, 136.3, 130.8, 128.7, 128.6, 128.3, 128.0, 127.0, 65.1.



**4-bromo-*N*-Benzylideneaniline (8i).** Yellow liquid.  $^1\text{H}$  NMR (300 MHz,  $\text{CDCl}_3$ ):  $\delta$  8.41 (s, 1H), 7.90-7.87 (m, 2H), 7.48-7.25 (m, 7H).  $^{13}\text{C}$  NMR (125.4 MHz,  $\text{CDCl}_3$ ):  $\delta$  162.0, 139.4, 136.3, 130.8, 128.7, 128.6, 128.3, 128.0, 127.0, 65.1.

## General procedure for the kinetic experiments

### *In situ* progress of the reaction as a function of time

In a round-bottom flask the complex **4** (0.03 mmol, 1 mol%) and a solution of benzylamine in toluene (5.6 mL from stock solution 0.499 mol/L, 300 mg, 2.8 mmol) were placed. The round flask was connected to a short condenser and the mixture was heated to 80 °C. 1, 3, 5-trimethoxybenzene was used as internal standard. Samples of 0.4 mL were taken every hour during 5 h and analyzed by  $^1\text{H}$  NMR. Under these conditions, the amine was cleanly converted into imine and neither benzaldehyde nor benzonitrile were detected as side-products. The progress of reaction, as consumption of benzylamine, was followed on time (Figure 3.3). The representation of  $\text{Ln}([\text{BnNH}_2]/[\text{BnNH}_2]_0)$  vs. time returns a straight line (Figure 13). Here  $[\text{BnNH}_2]$  is the molar concentration of benzylamine at any “t” time and  $[\text{BnNH}_2]_0$  is the initial molar concentration of benzylamine.

### Rate of reaction *r* as a function of $[\text{BnNH}_2]$ at constant catalyst concentration ( $[\mathbf{4}] = 0.01$ mol/L), reaction time, temperature and pressure.

A Parr reactor (98 mL) was charged with the complex **4** (18.4 mg, 28  $\mu\text{mol}$ , 0.01 mol/L) and an appropriate volume from a stock solution of benzylamine in toluene (10 mol/L, final volume: 2.8 mL, Table 3.8). The Parr reactor was pressurized at 130 psi of air and the reaction mixture was stirred at 60 °C for 2h. The system was cooled to room temperature and the pressure of gas was carefully released. The yield was determined by  $^1\text{H}$  NMR using 1, 3, 5-trimethoxybenzene as internal standard. The rate of reaction *r* ( $\text{mol L}^{-1} \text{h}^{-1}$ ) was calculated by means of the amount of imine (mmol) formed divided by the total volume (2.8 mL) and the time of reaction (2 h). The representation of  $\log(r)$  vs.  $\log([\text{BnNH}_2])$  gives a straight line with a slope of 1.06 (Table 3.9 and Figure 3.5).

**Rate of reaction  $r$  as a function of [4] at constant benzylamine concentration ( $[\text{BnNH}_2] = 5 \text{ mol/L}$ ), reaction time, temperature and pressure.**

A Parr reactor (98 mL) was charged with a solution of benzylamine in toluene (0.14 mL from stock solution 10.0 mol/L, final volume: 0.28 mL) and an appropriate amount of the complex **4** (0.05, 0.1, 0.15 and 0.2 mol/L, Table 3.10). The Parr reactor was pressurized at 130 psi of air and the reaction mixture was stirred at 60 °C for 2h. The system was cooled to room temperature and the pressure of gas was carefully released. The yield was determined by  $^1\text{H}$  NMR using 1, 3, 5-trimethoxybenzene as internal standard. The rate of reaction  $r$  ( $\text{mol L}^{-1} \text{ h}^{-1}$ ) was calculated by means of the amount of imine (mmol) formed divided by the total volume (2.8 mL) and the time of reaction (2 h). The representation of  $\log(r)$  vs.  $\log([\text{4}])$  gives a straight line with a slope of 1.15 (Table 3.10 and Figure 3.6).

**Rate of reaction as a function of the product  $[\text{BnNH}_2][\text{cat}] = \text{P}$  at constant reaction time, temperature and pressure. Determination of the apparent rate constant  $k_{\text{app}}$ .**

A Parr reactor (98 mL) was charged with a solution of benzylamine in toluene (0.14 mL from stock solution 10.0 mol/L, final volume: 0.28 mL) and an appropriate amount of the complex **4** (0.05, 0.1, 0.15 and 0.2 mol/L, Table 3.11). The Parr reactor was pressurized at 130 psi of air and the reaction mixture was stirred at 60 °C for 2h. The system was cooled to room temperature and the pressure of gas was carefully released. The yield was determined by  $^1\text{H}$  NMR using 1, 3, 5-trimethoxybenzene as internal standard. The rate of reaction  $r$  ( $\text{mol L}^{-1} \text{ h}^{-1}$ ) was calculated by means of the amount of imine (mmol) formed divided by the total volume (2.8 mL) and the time of reaction (2 h). The representation of  $\log(r)$  vs.  $\log([\text{P}])$  gives a straight line with a slope of 0.756  $\text{L mol}^{-1} \text{ h}^{-1}$  (Table 3.11 and Figure 3.7).

***In situ* experiments**

**In neat benzylamine.**

Under inert atmosphere, the complex **4** (10.0 mg, 16  $\mu\text{mol}$ ), benzylamine (*ca.* 0.4 mL) and a sealed inner tube filled with DMSO- $d_6$  (*ca.* 0.1 mL) were placed in a young NMR tube. The mixture was immediately analyzed by  $^1\text{H}$  and  $^{31}\text{P}\{^1\text{H}\}$  NMR and then after 0.5 and 1 h. The sample was heated to 60 °C and analyzed twice (1 and 2 h). The tube was pressurized with air (40 psi) and spectra were recorded every hour for two hours. The system was heated to 60 °C and analyzed four times (1, 2, 4 and 16 h). Selected  $^{31}\text{P}\{^1\text{H}\}$  and  $^1\text{H}$  NMR spectra are shown in Figure 3.8.

### ***In situ* stoichiometric experiment.**

Under inert atmosphere, the complex **4** (10.0 mg, 16  $\mu$ mol), benzylamine (4.2 mg, 39  $\mu$ mol, 2.4 equivalents) and  $\text{CDCl}_3$  (*ca.* 0.5 mL). were placed in a young NMR tube. The mixture was immediately analyzed by  $^1\text{H}$  and  $^{31}\text{P}\{^1\text{H}\}$  NMR and then after 0.5 and 1 h. The sample was heated to 60  $^\circ\text{C}$  and analyzed twice (1 and 2 h). The tube was pressurized with air (40 psi) and spectra were recorded every hour for two hours. The system was heated to 60  $^\circ\text{C}$  and analyzed four times (1, 2, 4 and 16 h). Selected  $^{31}\text{P}\{^1\text{H}\}$  and  $^1\text{H}$  NMR spectra are shown in Figure 3.9.

### **Isolation of the species observed in the stoichiometric experiments.**

To a suspension of **4** (50.0 mg, 0.078 mmol) in  $\text{CH}_2\text{Cl}_2$  (3 mL) was added a solution of benzylamine (66.9 mg, 0.62 mmol) in  $\text{CH}_2\text{Cl}_2$  (3 mL) and the mixture was stirred for 1 h. The reaction mixture was filtered-off in order to remove any unreacted **4**. The clear filtrate was concentrated to *ca.* 1 mL and  $\text{Et}_2\text{O}$  (5 mL) was added. A bright yellow solid was formed. The product was washed with  $\text{Et}_2\text{O}$  (3 x 5 mL) and was dried under vacuum to obtain a yellow solid (53.0 mg, 90% yield).  $^1\text{H}$  NMR (600.0 MHz,  $\text{CD}_2\text{Cl}_2$ , 25 $^\circ\text{C}$ ):  $\delta$  = 10.02 (t,  $^3J_{\text{HH}} = 4.2$  Hz, 1H), 8.78 (br., 2.34H), 8.33-8.19 (m, 5.52 H), 7.68-7.23 (m, 32.08 H), 7.02-6.97 (m, 1.45 H), 6.87-6.82 (m, 1.35 H), 3.84 (br., 3.81 H,  $\text{CH}_2$ ). Ratio  $\text{CH}^{\text{ar}} / \text{CH}_2 = 43.74 / 3.81 = 11.48 / 1 = 22.96 / 2 \sim 23 / 2$ .  $^{13}\text{C}\{^1\text{H}\}$  NMR (150.9 MHz,  $\text{CD}_2\text{Cl}_2$ , 25 $^\circ\text{C}$ ):  $\delta$  = 165.9 (s,  $\text{C}^{\text{quat}}$ ), 152.3 (s,  $\text{CH}^{\text{ar}}$ ), 151.5 (s,  $\text{CH}^{\text{ar}}$ ), 147.2 (s,  $\text{C}^{\text{quat}}$ ), 145.9 (s,  $\text{C}^{\text{quat}}$ ), 139.5 (s,  $\text{CH}^{\text{ar}}$ ), 138.5 (s,  $\text{CH}^{\text{ar}}$ ), 131.5 (s,  $\text{C}^{\text{quat}}$ ), 130.4 (s,  $\text{CH}^{\text{ar}}$ ), 130.3 (s,  $\text{CH}^{\text{ar}}$ ), 128.7 (s,  $\text{CH}^{\text{ar}}$ ), 127.5 (s,  $\text{CH}^{\text{ar}}$ ), 127.0 (s,  $\text{CH}^{\text{ar}}$ ), 124.8 (s,  $\text{C}^{\text{quat}}$ ), 124.1 (s,  $\text{CH}^{\text{ar}}$ ), 121.8 (s,  $\text{CH}^{\text{ar}}$ ), 121.6 (s,  $\text{CH}^{\text{ar}}$ ), 114.6 (s,  $J_{\text{PC}} = 6.4$  Hz,  $\text{CH}^{\text{ar}}$ ), 111.8 (s,  $\text{CH}^{\text{ar}}$ ), 46.6 (s,  $\text{CH}_2$ ).  $^{31}\text{P}\{^1\text{H}\}$  NMR (121.5 MHz,  $\text{CD}_2\text{Cl}_2$ , 25 $^\circ\text{C}$ ):  $\delta$  = 44.2 ppm (s). IR (KBr disk,  $\nu$  in  $\text{cm}^{-1}$ ): 3454 m, 2997 m, 2890 m, 1573 m, 1499 s, 1467 s, 1395 m, 1323 m, 1260 m, 1237 m, 1083 m, 1010 w, 901 w, 797 m, 746 m, 695 m, 611 w, 553 m, 513 m, 483 m. UV-Vis ( $\text{CHCl}_3$ ,  $\lambda_{\text{max}}$  in nm): 249, 323.

## **Chapter IV**

Rh(I)-coordination chemistry of  $\text{P}(\text{OQuin})_3$ .

Application in the 1,2-regioselective hydroboration of pyridines and quinolines

## 4.1 Introduction

There has been much interest in the dearomatizing transformations of pyridine derivatives, which lead to the synthesis of six-membered nitrogen-containing cyclic compounds directly.<sup>99,100</sup> These transformations are particularly attractive for obtaining partially unsaturated cyclic compounds such as 1,2-dihydropyridine (DHP) derivatives, which are useful synthetic intermediates for the synthesis of nitrogen-containing organic molecules.<sup>100,101</sup> As exemplified by Fowler's NaBH<sub>4</sub> reduction of *N*-(alkoxycarbonyl)pyridinium chloride,<sup>102</sup> such dearomatizing transformations have been achieved mainly through the formation of pyridinium salts,<sup>100</sup> in which nucleophilic attack to the pyridine ring is facilitated.<sup>103</sup>

Transition metal-catalyzed addition reactions to pyridines are also an attractive strategy for the reduction of pyridine rings without stoichiometric activation to form pyridinium salts, but such simple additions to pyridine derivatives are still relatively unexplored. Although hydrogenation is the simplest reaction to reduce pyridine rings, the harsh reaction conditions and overreduction to form piperidine derivatives are often problematic.<sup>104,105</sup> Alternatively, catalytic hydrosilylations have been developed to obtain di- and tetrahydropyridines.<sup>106,107</sup> However, it should be noted that existing hydrosilylation systems have encountered low product selectivity,<sup>106</sup> overreaction,<sup>107a,b</sup> and a narrow substrate scope.<sup>107c</sup> Therefore, it is highly desirable to develop an efficient catalytic addition to pyridines that allows selective partial reduction to dihydropyridine derivatives.

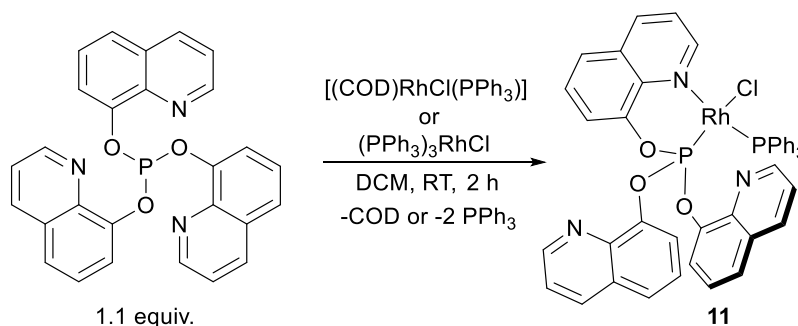
In 2011, Suginome *et al.* found that pyridine derivatives undergo addition of silylboronic esters in the presence of a palladium catalyst to give *N*-boryl-4-silyl-1,4-dihydropyridines.<sup>108</sup> This reaction was the first catalytic addition to pyridine derivatives to introduce non-hydrogen elements onto the carbon atoms of the pyridine ring. There, it was assumed that one of the driving forces of the reaction is the formation of the boron–nitrogen bond, which is known to be a stable covalent bond. Then, it was envisioned that the use of boron-containing reagents would promote the addition to pyridine rings by virtue of the formation of a strong B–N bond. Recently, Marks *et al.*<sup>109</sup> and Suginome *et al.*<sup>110</sup> described the first early (lanthanide) and late (rhodium) transition-metal-catalyzed hydroboration of pyridines<sup>111</sup> giving *N*-boryl-1,2-dihydropyridines in a regioselective manner. It should be noted that magnesium-catalyzed hydroboration of pyridine derivatives has just been reported in the literature.<sup>112</sup>

Here the synthesis and characterization of a Rh(I) complex bearing the ligand **1** is described. The application of this coordination compound as a homogeneous catalyst for the 1,2-regioselective hydroboration of pyridines is also discussed. No Rh-complexes bearing phosphite ligands have been previously reported as catalysts for this type of reaction.



## 4.2 Synthesis and characterization of the Rh(I) complex

The reaction of **1** with the precursors complexes  $[(\text{COD})\text{RhCl}(\text{PPh}_3)]$  (COD = 1,5-cyclooctadiene,  $\text{C}_8\text{H}_{12}$ ) and  $[(\text{PPh}_3)_3\text{RhCl}]$  (Wilkinson catalyst) was studied. The complex  $[\kappa^2P,N\text{-}\{\text{P}(\text{OQuin})_3\}\text{RhCl}(\text{PPh}_3)]$ , (**11**), is accessible by treating such a metal precursor in dichloromethane (DCM) with a solution of the ligand in the same solvent at  $-75^\circ\text{C}$  (Scheme 4.1). When the reaction mixture was allowed to reach room temperature, compound **11** was obtained after solvent evaporation and a washing step with diethyl ether. The product is a pale-orange solid sensitive to air/moisture and was isolated in high yield (80%). LIFDI-MS, elemental analysis and NMR spectroscopic data ( $^1\text{H}$ ,  $^{13}\text{C}\{^1\text{H}\}$ , and  $^{31}\text{P}\{^1\text{H}\}$ ) of **11** are in accordance with the proposed formulation. Proton and carbon signals were assigned using 2D NMR analysis such COSY, HMQC and HMBC.



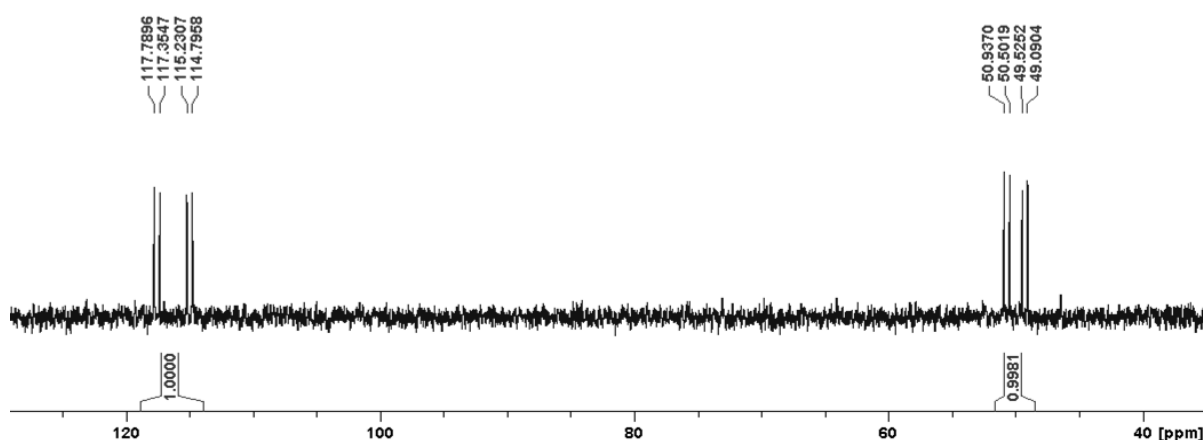
Scheme 4.1. Synthesis of the rhodium (I) complex **11**,  $[\kappa^2(P,N)\{\text{P}(\text{OQuin})_3\}\text{RhCl}(\text{PPh}_3)]$ .

The  $^{31}\text{P}\{^1\text{H}\}$  NMR spectrum shows two sets of doublet of doublet (*dd*) resonances at  $\delta$  116.3 ppm (**1**) and 50.0 ppm ( $\text{PPh}_3$ ) with their respective coupling constants  $^1J_{\text{PRh}} = 311.0$  Hz,  $^2J_{\text{PP}} = 52.8$  Hz and  $^1J_{\text{PRh}} = 171.1$  Hz,  $^2J_{\text{PP}} = 52.8$  Hz (Figure 4.1a). The phosphorus resonance is upfield shifted for **1** and downfield shifted for  $\text{PPh}_3$  with regard to the corresponding value for the free ligands. The chemical shifts and coupling constants ( $^nJ_{\text{PP}}$  and  $^nJ_{\text{PRh}}$ ) are similar to the ones observed for analogous rhodium (I) complexes bearing phosphine and phosphite moieties at “*cis*” configuration. For instance: a)  $[\text{Rh}(\text{acac})(R,R\text{-BINAPHOS})]^{113}$ ,  $^{31}\text{P}\{^1\text{H}\}$  NMR (121 MHz,  $\text{CDCl}_3$ )  $\delta$  152.5 ppm (*dd*,  $^1J_{\text{PRh}} = 325.1$  Hz,  $^2J_{\text{PP}} = 80.8$  Hz,  $\text{P}(\text{OR})_3$ ) and 51.9 ppm (*dd*,  $^1J_{\text{PRh}} = 178.5$  Hz,  $^2J_{\text{PP}} = 80.8$  Hz,  $\text{PPh}_2$ ), where *R,R*-BINAPHOS = (*R*)-(2-(diphenylphosphino)-1,1'-binaphthalen-2-yl)-(*R*)-1,1'-binaphthalen-2,2'-diylphosphite.; b)  $[\text{Rh}(\text{COD})(\text{P-OP})]^{114}$ ,  $^{31}\text{P}\{^1\text{H}\}$  NMR (162 MHz,  $\text{CD}_2\text{Cl}_2$ ):  $\delta$  132.3 ppm (*dd*,  $^1J_{\text{PRh}} = 267$  Hz,  $^2J_{\text{PP}} = 61$  Hz,  $\text{P}(\text{OR})_3$ ) and 16.4 ppm (*dd*,  $^1J_{\text{PRh}} = 136$  Hz,  $^2J_{\text{PP}} = 61$  Hz,  $\text{PPh}_2$ ), where P-OP = (*R*)-{2-[Di(1-naphthyl)phosphino]phenyl}-1,1'-(5,5',6,6'-tetramethyl)biphenyl-2,2'-diyl phosphite.; c)  $[(\text{P}(\text{OPh})_3)\text{Rh}(\text{PPh}_3)_2]^{115}$ ,  $^{31}\text{P}\{^1\text{H}\}$  NMR (121 MHz,  $\text{CDCl}_3$ )  $\delta$  114.8 ppm (*dd*,  $^1J_{\text{PRh}} = 310.8$  Hz,  $^2J_{\text{PP}} = 44.6$  Hz,  $\text{P}(\text{OPh})_3$ ) and 36.6 ppm (*dd*,  $^1J_{\text{PRh}} = 134.4$  Hz,  $^2J_{\text{PP}} = 44.6$  Hz,

PPh<sub>3</sub>). Based on such literature examples, the spectroscopic data recorded for **11** strongly indicates that in solution there is a “*cis*” spatial configuration for the phosphorus ligands.

The <sup>1</sup>H NMR spectrum confirms the κ<sup>2</sup>(P,N) coordination mode of the tris(8-quinolyl)phosphite ligand, as indicated by the presence of downfield shifted signals corresponding to the coordinate pyridine scaffold of the quinoline group. The four set of signals, δ 9.10, 8.22, 7.56 and 7.09 ppm, that correspond to **1** are clearly resolved from the resonances that belong to the triphenylphosphine, and the integral values exhibit a 18/15 (or 6/5) ratio (Figure 4.1b).

a)



b)

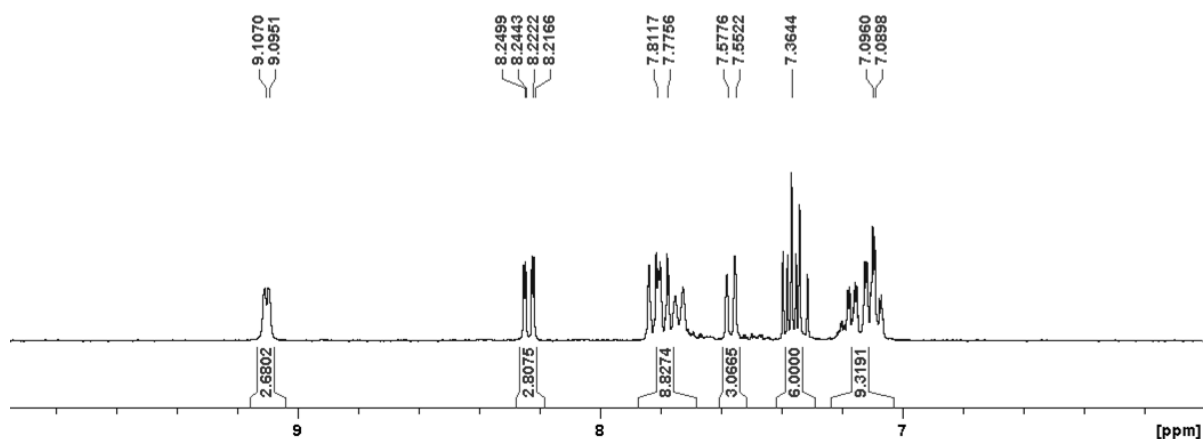


Figure 4.1. a) <sup>31</sup>P{<sup>1</sup>H} NMR spectrum (121.5 MHz) and b) <sup>1</sup>H NMR spectrum (300.1 MHz) at 298 K of **11** in CD<sub>2</sub>Cl<sub>2</sub>.

As well as in the Pd-P(OQuin)<sub>3</sub> complex (Chapter III), the <sup>1</sup>H NMR spectrum for **1** in **11** shows two separate spin systems (Figure 4.1b). The first of them, an AMX-type system arise from the pyridine scaffold. The signals exhibit a doublet and doublet of doublet multiplicity with a chemical shift of 9.10 (*d*, <sup>3</sup>J<sub>HH</sub> = 3.6 Hz), 8.23 (*dd*, <sup>3</sup>J<sub>HH</sub> = 8.3 Hz, <sup>3</sup>J<sub>HH</sub> = 3.2 Hz) and 7.56 (*d*, <sup>3</sup>J<sub>HH</sub> = 8.1 Hz) ppm. The largest shift on a signal (δ 9.10 ppm) corresponds to the H

*ortho* to the N atom, as confirmed by 2D NMR experiments (COSY, HSQC and HMBC). This spectroscopic data suggests that ligand **1** is hemilabile in a CD<sub>2</sub>Cl<sub>2</sub> solution of **11**. Such a dynamic process is possibly so fast that the NMR device records the three quinoline moieties as a single one (equivalency), as similarly observed for the palladium complex in the previous chapter. The second set of resonances, a multiplet between 7.85-7.71 (m, 9H) ppm, shows an ABC spin system. Such signals are assigned to the phenolate group. Finally, the multiplets between 7.38-7.34 (m, 6H) and 7.15-7.05 (m, 9H) ppm are assigned to the phenyl groups of PPh<sub>3</sub>.

Two types of crystals, **11**<sup>α</sup> and **11**<sup>β</sup>, with different unit cell parameters were obtained by different crystallization methods and both were suitable for X-ray diffraction analysis. The crystals denoted as **11**<sup>α</sup> (Figure 4.2) were grown by layering hexane over a DCM solution of **11**. On the other hand, **11**<sup>β</sup> (Figure 4.3) was obtained by slow diffusion of Et<sub>2</sub>O over a THF solution of **11**. The solid-state structures of **11**<sup>α</sup> and **11**<sup>β</sup> reveals in both cases that the ligand **1** binds the Rh center as a bidentate chelate. The X-ray diffraction analysis confirms the  $\kappa^2(P,N)$  coordination mode of **1** observed by <sup>1</sup>H NMR in solution, as well as the “*cis*” spatial configuration between both phosphorus ligands expected from the <sup>2</sup>J<sub>PP</sub> coupling constants from the <sup>31</sup>P{<sup>1</sup>H} NMR. Selected bond distances and angles are listed in Table 4.1.

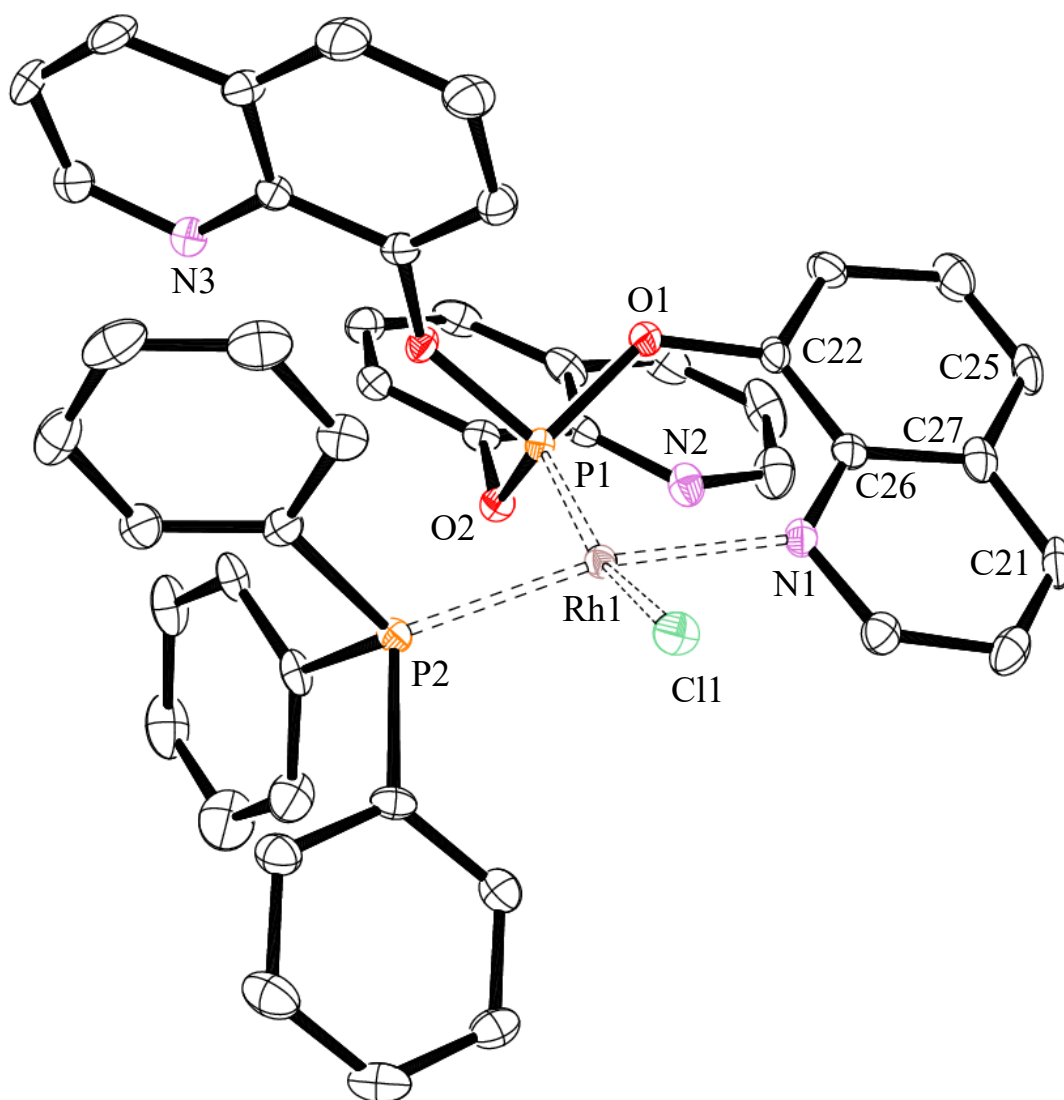


Figure 4.2. ORTEP drawing of the molecular structure of the complex  $[\kappa^2(P,N)\{P(OQuin)_3\}RhCl(PPh_3)]$ , **11<sup>a</sup>**. Thermal ellipsoids are drawn at 50% probability level. Hydrogen atoms and dichloromethane solvate molecule have been removed for clarity.

In **11<sup>a</sup>**, the Rh–P1, Rh–N1, Rh–P2 and Rh–Cl1 distances are 2.095(2), 2.151(2), 2.235(4) and 2.412(1) Å, respectively, with an angle between both phosphorus atoms P1–Rh–P2 of 93.16(4)°. The six-membered ring defined by Rh–N1–C22–C26–O1–P1 shows a roughly half-chair-shaped conformation, where the P1 atom is displaced by 1.21 Å from the mean plane through the other 5 atoms. The bite angle P1–Rh–N1 is 90.22(2)°. The P1–O(1-3) bond distances, 1.629(6), 1.598(5), and 1.618(6) Å, are quite shortened with regard to the free ligand, likely due to the strong  $\sigma$ -donation from the phosphite to the metal center. The O–P–O angles are within the range 95.36(3)–104.48(2)°. Concerning **11<sup>b</sup>**, the bond distances and angles around the metal center are almost identical to those in **11<sup>a</sup>**. Interestingly, in both cases the *trans* angles P1–Rh–Cl1 are around 160°, illustrating the strong geometry distortion around the rhodium atom, probably caused by the sterical hindrance of **1**.

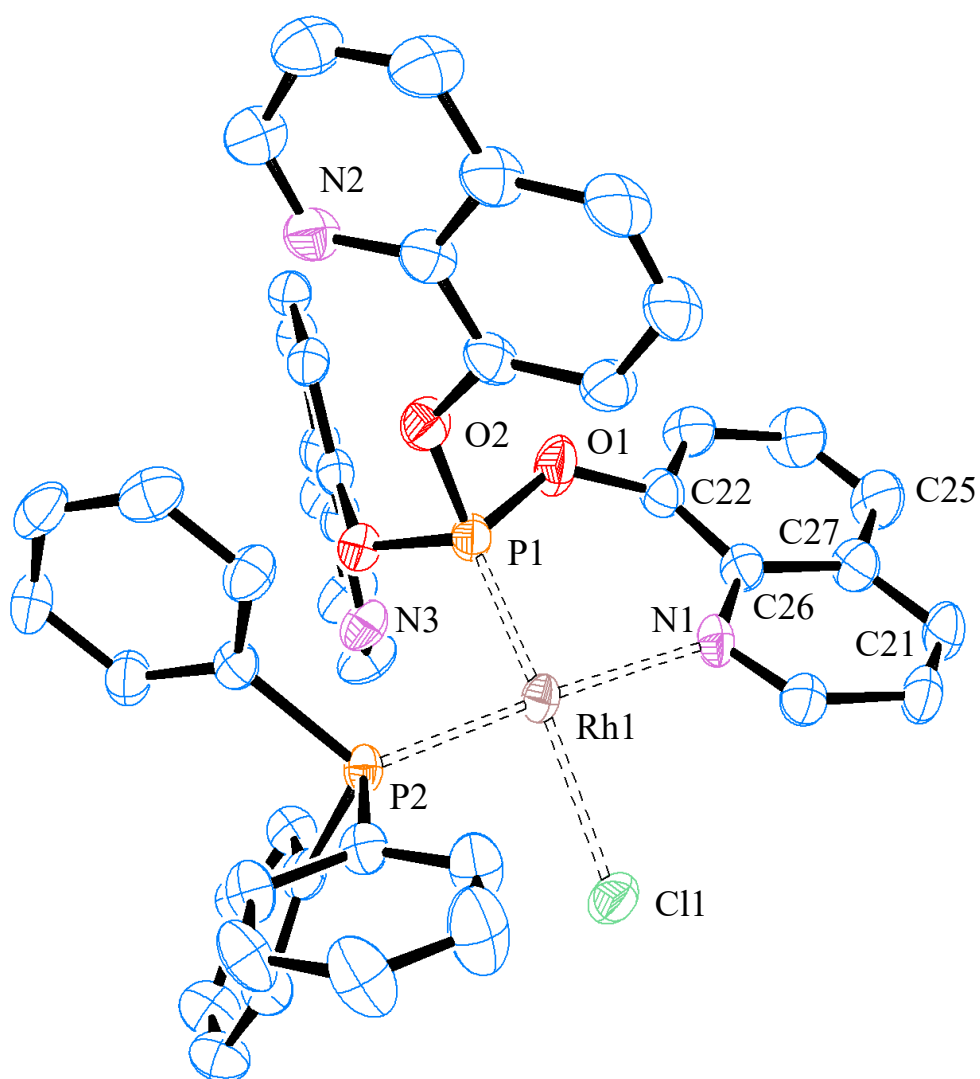


Figure 4.3. ORTEP drawing of the molecular structure of the complex  $[\kappa^2(P,N)\{P(OQuin)_3\}RhCl(PPh_3)]$ , **11<sup>b</sup>**. Thermal ellipsoids are drawn at 40% probability level. Hydrogen atoms and THF/Et<sub>2</sub>O solvate molecules have been removed for clarity.

The complex **11<sup>a</sup>** exhibits a considerable distorted square planar geometry, since the chelate (plane P1/Rh1/N1) is not co-planar with the other phosphorus atom (PPh<sub>3</sub>) and chlorine (plane P2/Rh1/Cl1). The deviation from co-planarity between the planes P1/Rh1/N1 and P2/Rh1/Cl1 is 21.68 degrees. The two aromatic units of the coordinated quinoline moiety are slightly twisted, as indicated by the C21–C27–C26–N1 and C22–C26–C27–C25 torsion angles (0.12°).

Table 4.1. Selected geometric parameters (Å, °) for **11** and related compounds

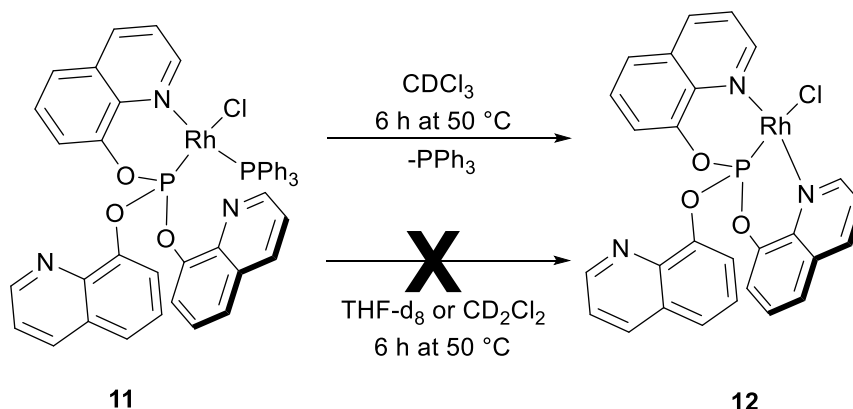
	<b>11<sup>α</sup></b>	<b>11<sup>β</sup></b>	<b>Ua<sup>31</sup></b>	<b>G1</b>
<i>Bond distance (Å)</i>				
Rh—P1	2.095(2)	2.101 (4)	2.209 (2)	2.215 (7)
Rh—P2	2.235(4)	2.236 (5)	-	-
Rh—N1	2.151(2)	2.155 (2)	2.149 (6)	2.123 (18)
Rh—Cl	2.412(1)	2.392 (3)	2.397(6)	2.393 (7)
P—O	1.629(6)	1.607(4)	1.597 (6)	-
	1.598(5)	1.605(5)	1.598 (5)	-
	1.618(6)	1.626(4)	1.604 (6)	-
<i>Angles (°)</i>				
P1—Rh—N1	90.22 (5)	90.93 (4)	89.09 (17)	92.93 (5)
P1—Rh—P2	93.16 (2)	93.90 (1)	-	-
P2—Rh—Cl1	90.57 (2)	87.44 (3)	-	-
N1—Rh—Cl1	90.62 (5)	88.86 (4)	85.60 (17)	89.76 (5)
P1—Rh—Cl1	160.74 (2)	164.81 (2)	93.70 (3)	176.96 (2)
<i>Torsion angles of coordinate quinoline moiety (°)</i>				
C21—C27—C26—N1	9.05	3.01	-	-
C22—C26—C27—C25	7.17	6.96	-	-

<sup>a</sup> Average of the two independent molecules in the unit cell.

In **11<sup>β</sup>** the distorted square planar geometry is also observed, but the deviation from coplanarity between the planes P1/Rh1/N1 and P2/Rh1/Cl1 (35.9°) is considerably larger than the one in **11<sup>α</sup>**. The two aromatic units of the coordinated quinoline moiety are slightly twisted as indicated by the C21—C27—C26—N1 and C22—C26—C27—C25 torsion angles (3.05°) and it is also bigger than in **11<sup>α</sup>**. The twisting of the coordinated quinoline scaffold has been also observed in related compounds, for example the complex **Ua**<sup>30</sup> (Table 4.1). The bond distances P—O, Rh—N, and Rh—Cl in **11<sup>α-β</sup>** are slightly shorter than in the related compound **Ua**. The bond distances Rh—P in **11<sup>α-β</sup>** are significantly shorter than in **Ua** and in **G1**.<sup>116</sup> Meanwhile, the bite angles P—Rh—N in **11<sup>α-β</sup>** are quite similar to the one in **Ua** but shorter than in **G1**.

### 4.3 Reactivity of the Rh(I) complex **11** toward different external agents (NMR scale).

The reactivity of the new complex **11** toward different external agents was investigated. The reactions were performed *in situ* at NMR scale. The stability in solution of **11** in selected solvents and at different temperatures was first examined. In particular, the dissociation of the triphenylphosphine and subsequent coordination of one quinoline moiety was expected (Scheme 4.2).



Scheme 4.2.  $\text{PPh}_3$  dissociation from **11** in a  $\text{CDCl}_3$  solution of **11** to form **12**.

A THF solution of **11** is stable over the course of 6 h at room temperature, as evidenced by  $^{31}\text{P}\{^1\text{H}\}$  NMR spectroscopy. The same behavior was observed both at lower and higher temperatures, namely 0 and 50 °C. In  $\text{CDCl}_3$ , the stability of **11** in solution is completely different. By  $^{31}\text{P}\{^1\text{H}\}$  NMR monitoring of a  $\text{CDCl}_3$  solution of **11** at 50 °C was possible to observe the gradual dissociation of  $\text{PPh}_3$  (*s*,  $\delta$  -5 ppm) and subsequent formation of the complex **12** (*d*,  $\delta$  90.8 ppm,  $J_{\text{PRh}} = 161.6$  Hz) (Figure 4.4). After 6 h, the phosphine dissociation was completed. Such a reaction also takes place at room temperature but within 24 h, while at low temperature (0 °C) the chloroform solution of **11** seems to be stable. Complex **12** represents the first example of a phosphite ligand coordinated to Rh (I) in a NPN pincer-fashion. This compound might open new research opportunities in the already rich NPN ligand chemistry. Likewise, this example demonstrates the polydentacity of **1**. Unfortunately, after many attempts to determine the molecular structure of **12**, it was not possible to obtain monocrystals of sufficient quality for X-ray diffraction analysis.

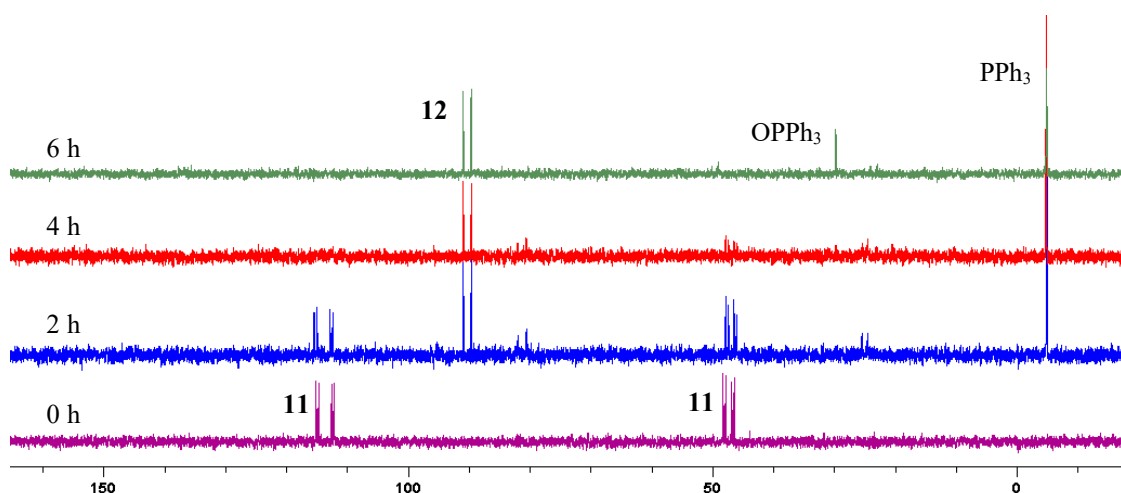
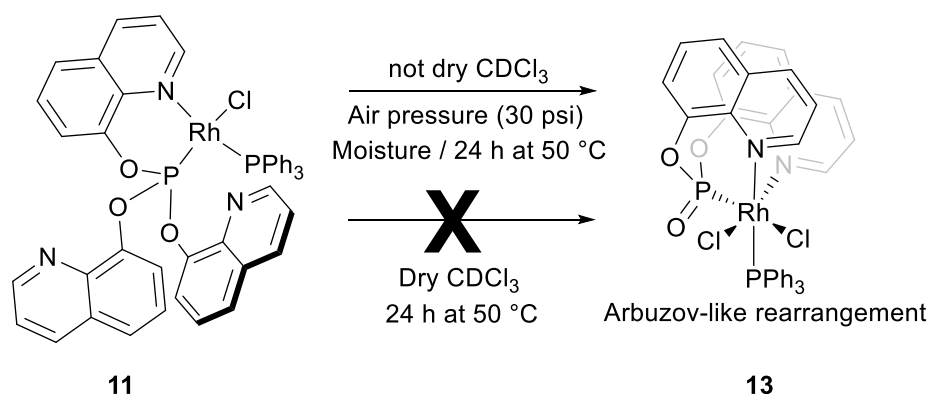


Figure 4.4.  $^{31}\text{P}\{^1\text{H}\}$  NMR (121.5 MHz) reaction monitoring of **11** into **12** at 323 K in  $\text{CDCl}_3$ .

As stated in Chapter I, phosphite can be broken down by hydrolysis or alcoholysis and suffer rearrangements such as the Michaelis-Arbuzov reaction. Nevertheless, once phosphites are coordinated to a transition metal center, they are quite stable and less prone to suffer this kind of transformation. In this sense, an unexpected reactivity was found when **11** was dissolved in  $\text{CDCl}_3$  (not dry, commercially available  $\text{CDCl}_3$  without further purification) charged with 30 psi of air and heated at 50 °C for 24h in a J. Young NMR tube (Scheme 4.3).



Scheme 4.3. Retro-Arbuzov-like dearylation reaction by **11** in not dry/degassed  $\text{CDCl}_3$  solution.

The Michaelis-Arbuzov rearrangement, also known as the Arbuzov rearrangement, Arbuzov reaction, or Arbuzov transformation, is one of the most versatile pathways for the formation of carbon-phosphorus bonds and involves the reaction of an ester of trivalent phosphorus with alkyl halides.<sup>117</sup> There is a variation of the Arbuzov-rearrangement with the same main features but it is called retro-Arbuzov regrouping. This alternative includes the construction of a halide-phosphorus bond instead of an alkyl-phosphorus moiety. Such a retro-Arbuzov reaction is quite rare and it is usually reported solely for the free phosphite (organic reaction) under particular conditions.<sup>118</sup>



A solution of **11** in “wet” CDCl<sub>3</sub> and under aerobic conditions yielded, among others, a new rhodium (III) complex (**13**, Scheme 4.3) following a retro-Arbuzov scheme. The reaction mixture was monitored by <sup>31</sup>P {<sup>1</sup>H} NMR spectroscopy. Under the specified conditions, **11** reacted quite unselectively, as evidenced by the formation of at least 3 phosphorus-rhodium containing species plus free PPh<sub>3</sub> and OPPh<sub>3</sub> (Figure 4.5). The <sup>31</sup>P {<sup>1</sup>H} NMR spectrum shows **13** as the main product as two set of doublet of doublets (dd) resonances at δ 69.3 (<sup>1</sup>J<sub>PRh</sub> = 151.0 Hz, <sup>2</sup>J<sub>PP</sub> = 29.5 Hz) and 55.5 (<sup>1</sup>J<sub>PRh</sub> = 146.0 Hz, <sup>2</sup>J<sub>PP</sub> = 30.1 Hz) ppm. The other phosphorus-rhodium containing compounds formed correspond to the resonances at δ 61.0 (<sup>1</sup>J<sub>PRh</sub> = 130.7 Hz) and 16.2 (<sup>1</sup>J<sub>PRh</sub> = 92.5 Hz) ppm. Unfortunately, these species were not fully identified. Since free PPh<sub>3</sub> and its oxide OPPh<sub>3</sub> were detected, the unidentified compounds are very likely exclusively featuring **1**, or its retro-Arbuzov derivative, as ligand.

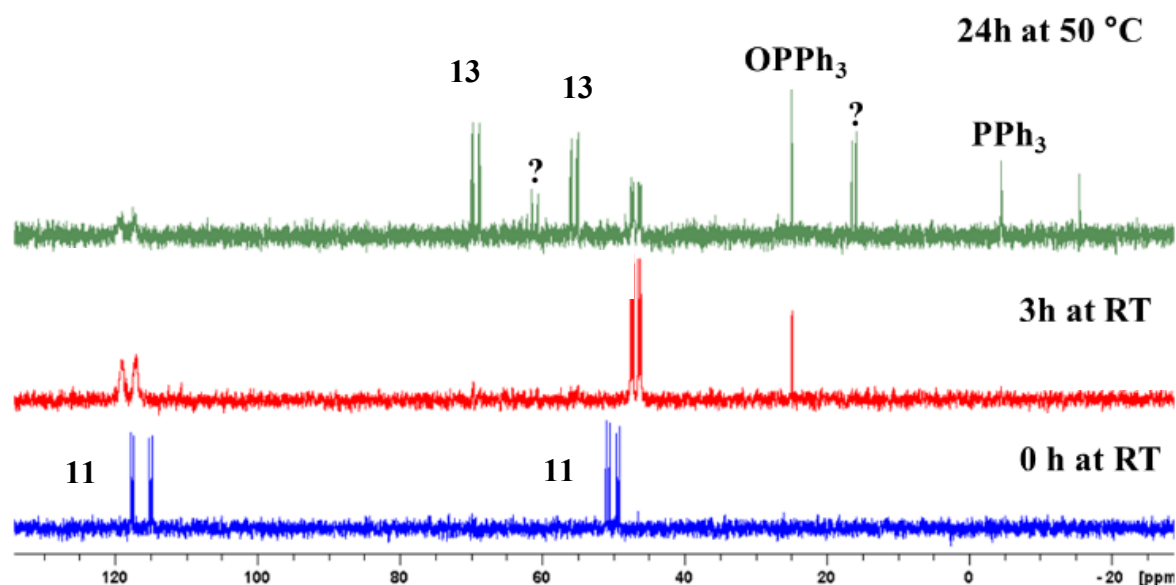


Figure 4.5. <sup>31</sup>P {<sup>1</sup>H} NMR spectrum (121.5 MHz, CDCl<sub>3</sub>) of **11** at 298 K (blue), reaction mixture after 3 h at RT (red) and reaction mixture after 24 h at 50 °C (green).

Although it was a not clean reaction, suitable crystals for X-ray diffraction analysis were obtained from the CDCl<sub>3</sub> solution in the same NMR tube, which confirmed such unusual reactivity for **11** (Figure 4.6). The solid-state structure of **13** reveals that the retro-Arbuzov phosphorus compound binds to the metal center as a tridentate chelate. The OP(OQuin)<sub>2</sub><sup>-</sup> scaffold, a XL<sub>2</sub>-type ligand, coordinates the Rh center in a *fac*-κ<sup>3</sup>(*N,P,N*) mode with its phosphorus atom *cis* to the triphenylphosphine and *cis* to one chloride. The complex exhibits a slightly distorted octahedral geometry, since some angles are away from the ideal value (90°) for an octahedral geometry. Selected bond distances and angles are listed in Table 4.2.

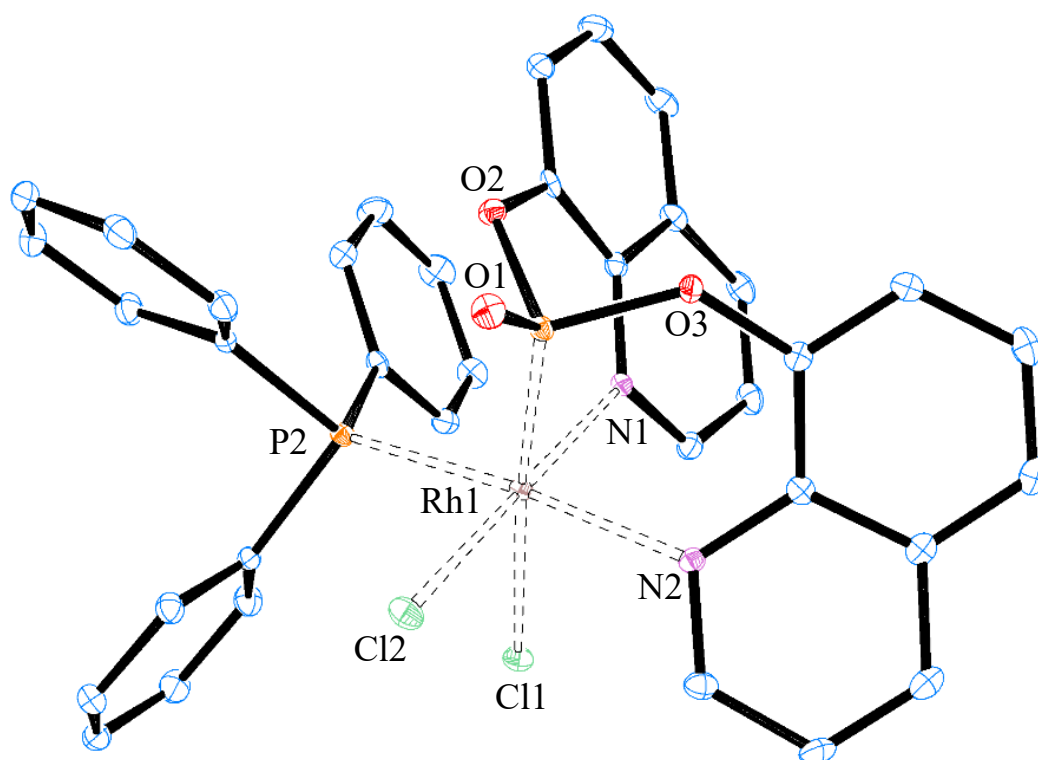


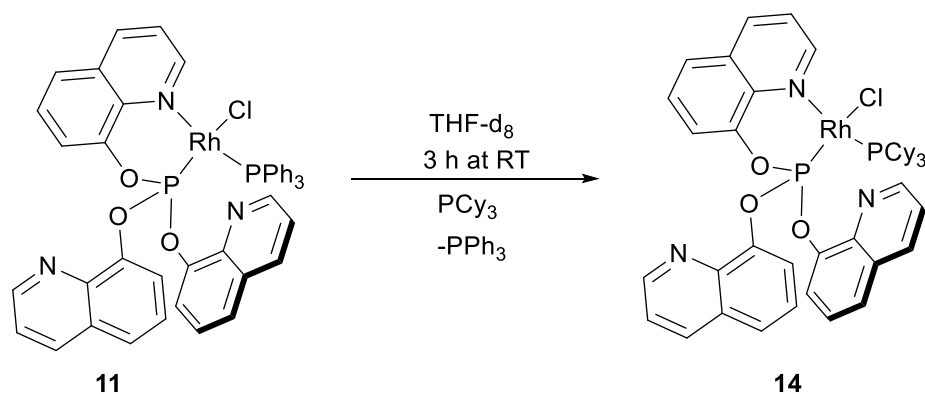
Figure 4.6. ORTEP drawing of the molecular structure of the complex  $[\kappa^3(P,N,N)\{OP(OQuin)_2\}RhCl_2(PPh_3)]$ , **13**. Thermal ellipsoids are drawn at 40% probability level. Hydrogen atoms have been removed for clarity.

The novel compound **13** represents the first *N,P,N*-Rh(III) metal complex ever reported. Some interesting aspects the solid-state structure of **13** will be briefly discussed. The Rh-Cl1 bond is quite long (2.489 Å) likely due the strong bonding between Rh-P1, as expected for a phosphorus anionic species. Likewise, the bond Rh-P2 (PPh<sub>3</sub>, 2.333 Å) is relatively long, which might be due to a strong sigma donation from the quinoline moiety in *trans* position (*trans* influence). Such an elongated Rh-P2 moiety can be a useful reactive position for further applications, *e.g.* ligand substitution (*trans* effect) or catalysis. Also, for catalytic applications, the variable denticity of the ligand  $OP(OQuin)_2^-$  could be important to stabilize reactive intermediates with lower or higher electron count and/or coordination number than **13**.

Table 4.2. Selected geometric parameters (Å, °) for **13**.

Bond distance (Å)		Angles (°)	
Rh—P1	2.186(2)	P1—Rh—N1	84.25 (5)
Rh—P2	2.333(4)	P1—Rh—N2	86.87 (2)
Rh—Cl1 ( <i>trans</i> P1)	2.489(2)	P1—Rh—P2	98.47 (2)
Rh—Cl2 ( <i>trans</i> N1)	2.325(6)	P2—Rh—N1	93.24 (5)
Rh—N1 ( <i>trans</i> Cl2)	2.122(5)	P2—Rh—N2	174.49 (2)
Rh—N2 ( <i>trans</i> P2)	2.145(6)	Cl1—Rh—Cl2	88.41 (2)
P1—O3 ( <i>oxi</i> )	1.474(4)	N1—Rh—N2	88.60 (2)
P1—O2 (Quin N1)	1.631(2)		
P1—O3 (Quin N2)	1.626(6)		

Simple ligand substitution reaction was also examined. The complex **11** reacts with 1.1 equiv. of PCy<sub>3</sub> at room temperature yielding the related species **14** (Scheme 4.4). The reaction mixture was monitored by <sup>31</sup>P{<sup>1</sup>H} NMR and full conversion was achieved after 3 h. The <sup>31</sup>P{<sup>1</sup>H} NMR spectrum exhibits, beside two new sets of doublets of doublets, the presence of free PPh<sub>3</sub> (-5 ppm) and OPPh<sub>3</sub> (23 ppm) as depicted in Figure 4.6.



Scheme 4.4. Ligand exchange reaction at complex **11**.

The <sup>31</sup>P{<sup>1</sup>H} NMR spectrum of **14** shows two doublet of doublets (dd) resonances at  $\delta$  117.8 (<sup>1</sup>J<sub>PRh</sub> = 311.0 Hz, <sup>2</sup>J<sub>PP</sub> = 52.8 Hz, 1) and 55.9 (<sup>1</sup>J<sub>PRh</sub> = 171.1 Hz, <sup>2</sup>J<sub>PP</sub> = 52.8 Hz, PPh<sub>3</sub>) ppm as depicted in Figure 4.6. Such phosphorus chemical shift values are shifted toward upfield (**1**) and downfield (PCy<sub>3</sub>) with regard to the corresponding resonance of the free ligands. Additionally, the chemical shift values and coupling constants of **14** are quite similar to the ones observed for the parent rhodium (I) complex **11**. Again, the spectroscopic evidence strongly suggests a *cis* spatial configuration between both phosphorus ligands in solution.

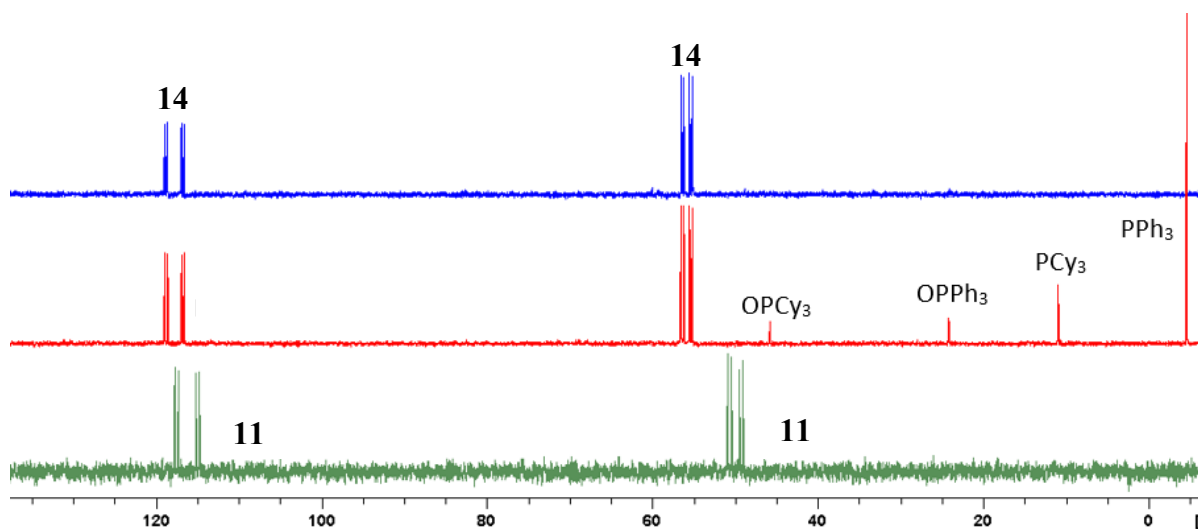


Figure 4.6.  $^{31}\text{P}\{^1\text{H}\}$  NMR spectrum (121.5 MHz,  $\text{THF-}d_8$ ) at 298 K of: **11** (green), reaction mixture **11** +  $\text{PCy}_3$  after 3 h (red) and isolated **14** (blue).

In the aromatic region of the  $^1\text{H}$  NMR spectrum ( $\text{THF-}d_8$ ) four sets of signals that integrate to 6 or 18 protons are found (Figure 4.7), which means that there is a magnetic equivalence between the three quinoline moieties. The resonances represent two separate spin systems. The first of them, an AMX-type system, is assigned to the pyridine scaffold. The signals exhibit a doublet of doublets multiplicity with a chemical shift of  $\delta$  8.83 ( $dd$ ,  $^3J_{\text{HH}} = 4.5$  Hz,  $^4J_{\text{HH}} = 1.7$  Hz), 8.03 ( $dd$ ,  $^3J_{\text{HH}} = 8.3$  Hz,  $^4J_{\text{HH}} = 1.7$  Hz) and 7.15 ( $dd$ ,  $^3J_{\text{HH}} = 8.3$  Hz,  $^4J_{\text{HH}} = 4.5$  Hz) ppm. The largest shift of a signal ( $\delta$  8.83 ppm) corresponds to the H *ortho* to the N atom, which is upfield shifted in comparison with **11**. The second set of resonances,  $\delta$  8.09 ( $d$ ,  $^3J_{\text{HH}} = 7.6$  Hz), 7.45 ( $dd$ ,  $^3J_{\text{HH}} = 8.2$  Hz,  $^4J_{\text{HH}} = 1.5$  Hz) and 7.38 ( $t$ ,  $^3J_{\text{HH}} = 7.9$  Hz) ppm, shows a ABM spin system and is assigned to the phenolate group.

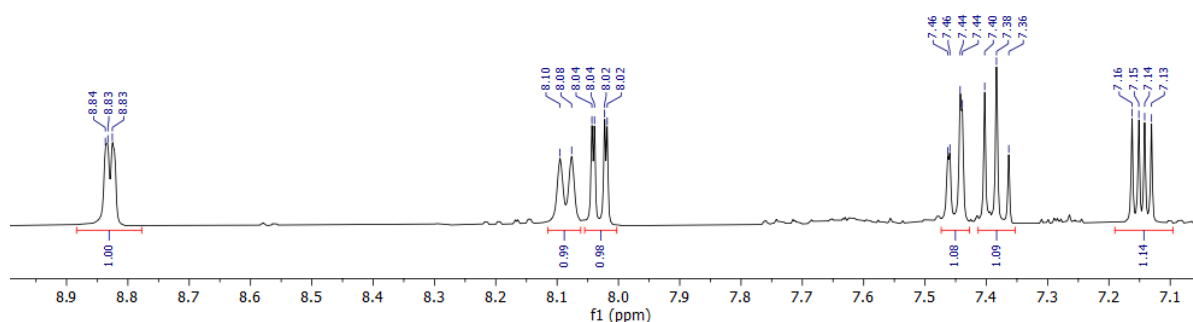


Figure 4.7.  $^1\text{H}$  NMR spectrum (300.1 MHz,  $\text{THF-}d_8$ ) of **14** at 298 K.

The new complex **14** was isolated as red crystals from a saturated THF solution at  $-30^\circ\text{C}$ , and its molecular structure was unambiguously established by single-crystal X-ray diffraction analysis. An ORTEP diagram of such a compound is shown in Figure 4.8, while selected bond lengths and angles are listed in Table 4.3.

The X-ray diffraction analysis of complex **14** reveals the presence of two independent molecules in the unit cell. As demonstrated for **11**, in **14** the ligand **1** binds the metal center as a  $\kappa^2(P,N)$  chelate, forcing a *cis* spatial configuration between both phosphorus ligands. The other two quinoline units are oriented away from the metal center. The complex exhibits a slightly distorted square planar geometry, since the chelate (plane P1/Rh1/N1) is not co-planar with the chlorine and phosphorus atom (plane P2/Rh1/Cl1). The deviation from co-planarity between the planes P1/Rh1/N1 and P2/Rh1/Cl1 is about 10 degrees.

The bond distances Rh-P1 (2.101 Å), Rh-N1 (2.165 Å) and Rh-P2 (2.273 Å) are slightly longer than in **11** (Table 4.3 vs Table 4.1). Meanwhile, the bond Rh-Cl1 (2.383 Å) in **14** is slightly shorter than in **11**. Taking into account that PCy<sub>3</sub> is more basic than PPh<sub>3</sub>, the  $\sigma$ -donation makes the metal center more electron rich, which subsequently elongates the binding to **1**. The most important structural differences between **14** and **11** can be seen in the bond angles. Due to the fact that PCy<sub>3</sub> is bulkier than PPh<sub>3</sub>, the bite angle P1-Rh-N1 (85.3°) is shorter than in **11** and P1-Rh-P2 (99.18°) deviates considerably from 90°.

Table 4.3. Selected geometric parameters (Å, °) for **14**.<sup>a</sup>

<i>Bond distance (Å)</i>		<i>Angles (°)</i>	
Rh—P1	2.101(3)	P1—Rh—P2	99.18 (9)
Rh—P2	2.273(2)	P1—Rh—N1	85.3 (2)
Rh—Cl1	2.383(2)	P1—Rh—Cl	166.21 (9)
Rh—N1	2.165(7)	P2—Rh—Cl	90.18 (8)
$\bar{X}$ P1—O	1.622(7)	N1—Rh—Cl	85.80 (2)

<sup>a</sup> Average of the two independent molecules in the unit cell.

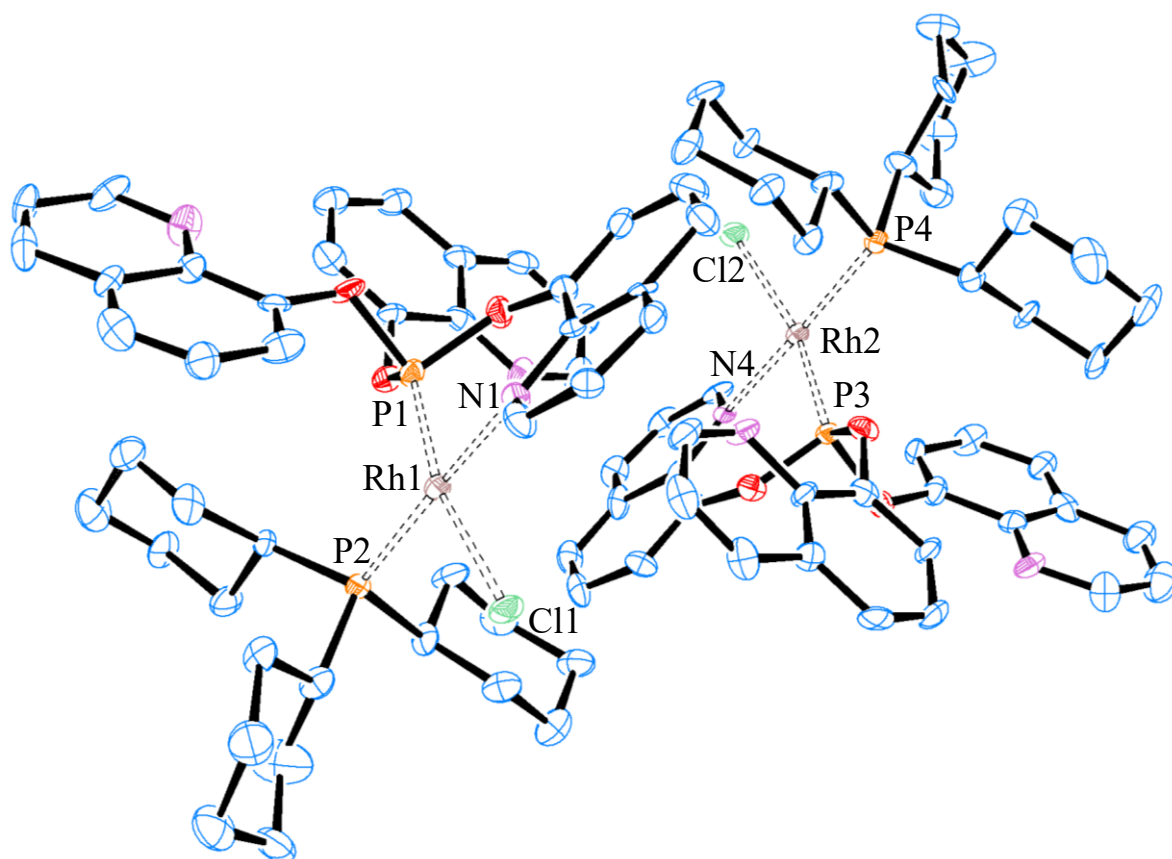
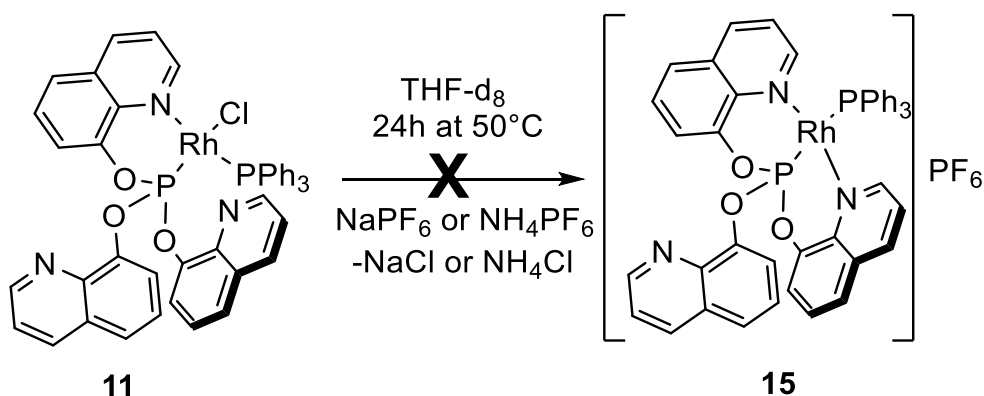


Figure 4.8. ORTEP drawing of the molecular structure of the complex  $[\kappa^2(P,N)\{P(OQuin)_3\}RhCl(PCy_3)]$  (**14**). Thermal ellipsoids are drawn at the 50% probability level. Hydrogen atoms and THF solvate molecules have been removed for clarity. Two independent molecules *per* asymmetric unit were found. The values reported for selected bond distances and angles correspond to the average of both independent molecules.

Finally, chloride abstraction reaction from **11** was carried out to prepare a cationic rhodium derivative (Scheme 4.5). The purpose of such reaction was to study whether one of the uncoordinated quinolines scaffolds would occupy the vacant position left by the chloride ligand.



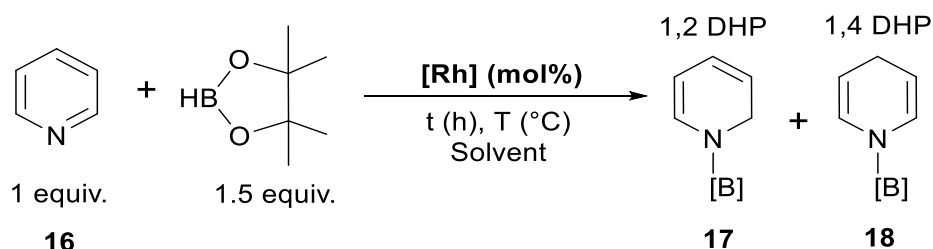
Scheme 4.5. Chloride abstraction reaction from **11**.

Treatment of a solution of the chloride complex **11** with one equivalent of either NaPF<sub>6</sub> or NH<sub>4</sub>PF<sub>6</sub> at room temperature did not lead to the expected cationic complex [ $\kappa^3(N,P,N)$ -P(OQuin)<sub>3</sub>Rh(PPh<sub>3</sub>)]PF<sub>6</sub> (**15**), even when the mixture was left reacting for several hours. Heating the reaction mixture to 50 °C promoted the formation of the retro-Arbuzov product as well as 3 additional phosphorus-containing compounds. It is clear that by heating, the decomposition of **1** prevailed over the removal of the halide.

Once the stability and reactivity of **11** was explored, the research interest was to explore the potential of such a compound as a homogeneous catalyst. Several types of reactions were considered as possible targets to do so and the 1,2-hydroboration of pyridines returned very interesting results.

#### 4.4 Regioselective 1,2-hydroboration of pyridines and quinolines catalyzed by **11**.

Compound **11** was tested as a catalyst precursor for the regioselective hydroboration of pyridine (Py, **16**) with pinacolborane in order to yield 1,2 dihydropyridine (DHP, **17**), as a model reaction (Scheme 4.6). A wide range of reaction parameters, including catalysts, solvents, temperature and the relative ratio of the different reaction components, have been screened to achieve optimal reaction conditions. The reduction of **16** in C<sub>6</sub>H<sub>6</sub> at 80 °C by **11** as (pre)catalyst, produces DHPs in a selective manner (> 99% after 24 h; entry 4, Table 4.4). Under the studied reaction conditions other Rh sources, such as [(COD)RhCl]<sub>2</sub>, [Cp\*RhCl<sub>2</sub>]<sub>2</sub> or [(Ph<sub>3</sub>P)<sub>3</sub>RhCl], returned significant amounts of side products along with some DHPs (entries 1-3, Table 4.4). In particular, unlike the other Rh complexes, **11** seems to be regioselective toward the 1,2-hydroboration of pyridine. In the absence of the catalyst (blank run) no conversion at all was achieved (entry 5), thus confirming the catalytic nature of the transformation.



Scheme 4.6. Hydroboration of pyridine (Py) by a rhodium source yielding dihydropyridines (DHP).

Once **11** was confirmed as the best Rh source among the ones considered here for this transformation, different catalyst loadings were evaluated (Table 4.5). Under the established reaction conditions, the reaction works selectively with a catalyst loading below 1.0 mol% of **11**. Side-products were formed when catalyst loading exceeds 1 mol% but those were not identified

(entries 1-2). The yields drop significantly for catalyst loadings below 0.25 mol%, but the selectivity to the 1,2-product increases (entries 3-5 vs 6-7). This fact could mean that the concentration of the reaction components might play an important role and thus its evaluation was taken into consideration.

Table 4.4. Screening of catalyst in the hydroboration of Py. <sup>a</sup>

Entry	Rh Catalyst	Catalyst loading (mol%)	Conversion (%) <sup>b,c</sup>	DHP Product (%) <sup>c</sup>	Ratio 1,2:1,4	Side products (%) <sup>c</sup>
1	[(COD)RhCl] <sub>2</sub>	0.5 (1 <i>per</i> Rh)	60	15	0:100	45
2	[Cp*RhCl <sub>2</sub> ] <sub>2</sub>	0.5 (1 <i>per</i> Rh)	42	13	16:84	29
3	[(Ph <sub>3</sub> P) <sub>3</sub> RhCl]	1	78	9	0:100	69
4	<b>11</b>	1	55	55	71:29	-
5	-	none	0	-	-	-

[a] Py (11.8 mg, 150  $\mu$ mol, 0.25 M), pinBH (28.8 mg, 225  $\mu$ mol) and [Rh] (0.75  $\mu$ mol, 0.5 mol% /1.50  $\mu$ mol, 1 mol%), were stirred in 0.6 mL C<sub>6</sub>H<sub>6</sub> at 80 °C for 24 h. [b] Conversion determined by <sup>1</sup>H NMR as consumption of Py using hexamethylbenzene (1.35 mg, 8.33  $\mu$ mol) as internal standard after reaction. [c] Average of three individual reactions.

Table 4.5. Screening of catalyst loading in the hydroboration of Py. <sup>a</sup>

Entry	Catalyst loading (mol%)	Conversion (%) <sup>b,c</sup>	DHP Product (%) <sup>c</sup>	Ratio 1,2:1,4	Side products (%) <sup>c</sup>
1	3.0	80	62	52:48	18
2	2.0	74	67	62:38	7
3	1.0	55	55	71:29	-
4	0.75	47	47	74:26	-
5	0.50	44	44	77:23	-
6	0.25	29	29	87:13	-
7 <sup>d</sup>	0.10	17 <sup>d</sup>	17 <sup>d</sup>	87:13	-

[a] Py (11.8 mg, 0.150 mmol, 0.25 M), pinBH (28.8 mg, 0.225 mmol) and **11** (1.50  $\mu$ mol, 1 mol%), were stirred in 0.6 mL C<sub>6</sub>H<sub>6</sub> at 80 °C for 24 h. [b] Conversion determined by <sup>1</sup>H NMR as consumption of Py using hexamethylbenzene (1.35 mg, 8.33  $\mu$ mol) as internal standard after reaction. [c] Average of three individual reactions. [d] Average of two individual reactions.

The effect of pyridine concentration on the reaction selectivity was evaluated (Table 4.6). A catalyst loading of 0.10 mol% of **11** was used. In general, the conversion is better when the



pyridine concentration increases, but either the formation of side products or poor selectivity is observed for [Py] > 2.0 mol/L (entries 6 and 7). Side products were also detected at relatively low substrate concentration (entry 1). The reaction works properly, both effectively and selectively, in the Py concentration range 0.25-1.0 M (entries 2-6).

Table 4.6 Screening of substrate concentration in the hydroboration of Py. <sup>a</sup>

Entry	[Py] (M)	Catalyst loading (mol%)	Conversion (%) <sup>b,c</sup>	DHP Product (%) <sup>c</sup>	Ratio 1,2:1,4	Side products (%) <sup>c</sup>
1	0.063	1.0	34	26	82:18	8
2	0.25	1.0	55 <sup>d</sup>	55 <sup>d</sup>	71:29	-
3	0.25	0.10	17	17	87:13	-
4	0.50	0.10	31	31	87:13	-
5	1.0	0.10	47	47	81:19	-
6	2.0	0.10	57	46	78:22	11
7	4.0	0.10	61	30	65:35	31

[a] Py (11.8 mg, 0.150 mmol), pinBH (28.8 mg, 0.225 mmol) and **11** (see Table), were stirred in 0.6 mL C<sub>6</sub>H<sub>6</sub> at 80 °C for 24 h. [b] Conversion determined by <sup>1</sup>H NMR as consumption of Py using hexamethylbenzene (1.35 mg, 8.33 μmol) as standard. [c] Average of two individual reactions, unless otherwise noted. [d] Average of three individual reactions.

The influence of the relative amount of pinBH with regard to Py on the reaction performance was also examined (Table 4.7). The conversion of Py is better at higher pinBH loadings, but at expenses of the formation of side products (entries 3-7). The hydroboration works properly in a quite limited ratio of [pinBH]/[Py], namely between 1 and 1.5 (entries 1 and 2). The fact that the reaction requires a stoichiometric amount or a slightly excess of pinBH makes it attractive from the perspective of atom-economy.

The effect of selected solvents on the hydroboration of pyridine catalyzed by **11** was also studied (Table 4.8). Under solvent-free conditions Py was fully consumed but the reaction is highly unselective, forming side products rather than actually DHPs (entry 7). Compared with benzene as reaction media, in THF the conversion of Py is higher but the selectivity to the 1,2-regioisomer is lower (entries 2 and 4). Acetonitrile is not a suitable solvent as evidenced by the diminished catalytic activity in comparison with the reference system (entry 6 vs 3). Finally, in toluene both better conversion and higher selectivity to the 1,2-regioisomer was achieved (entry 5 vs 3).

Table 4.7. Screening of pinBH equivalents in the hydroboration of Py. <sup>a</sup>

Entry	pinBH (Eq)	Conversion (%) <sup>b,c</sup>	DHP Product (%) <sup>c</sup>	Ratio 1,2:1,4	Side products (%) <sup>c</sup>
1	1.0	50	50	75:25	-
2	1.5	55 <sup>d</sup>	55 <sup>d</sup>	71:29	-
3	2.0	68	63	68:32	5
4	2.5	71	62	65:35	9
5	3.0	62	48	72:28	14
6	3.5	84	55	66:34	29
7	4.0	83	58	66:34	25

[a] Py (11.8 mg, 0.150 mmol, 0.25 M), pinBH (28.8 mg, 0.225 mmol) and **11** (1.3 mg, 1.50  $\mu$ mol), were stirred in 0.6 mL C<sub>6</sub>H<sub>6</sub> at 80 °C for 24 h. [b] Conversion determined by <sup>1</sup>H NMR as consumption of Py using hexamethylbenzene (1.35 mg, 8.33  $\mu$ mol) as standard. [c] Average of two individual reactions, unless otherwise noted. [d] Average of three individual reactions.

With toluene as solvent, the hydroboration of Py (1.0 M) was performed again in a range of catalyst precursor between 0.5-1.0 mol% with 1.25 and 1.50 equiv. of HBpin at 80 °C for 24 h (entries 1-3 vs 4-6, Table 4.9). Among the first six experiments, five of them returned side products (entries 1-6), which suggests that such concentration of pyridine is detrimental for the selectivity of the reaction. Therefore, the subsequent studies were carried out with a pyridine concentration of 0.75 M (entries 7-8 vs 9-11). By using either 1.25 or 1.50 equiv. of HBpin, no side products were observed and up to 81% conversion with an isomer ratio 1,2:1,4 of 63:37 was achieved (entry 8). Further improvement of the selectivity was attempted by means of the reaction temperature, reaction time and the use of additive(s). The effect of the temperature was tested in a range between 50-80 °C. When the temperature is lowered to 70 °C, both the conversion and the isomer ratio are better (entry 12 vs 8). At 60 or 50 °C, the conversion dropped significantly and the isomer ratio decreased (entry 12 vs 16-17).

Table 4.8 Screening of solvent in the hydroboration of Py. <sup>a</sup>

Entry	Solvent	Catalyst loading (mol%)	Conversion (%) <sup>b,c</sup>	DHP Product (%) <sup>c</sup>	Ratio 1,2:1,4	Side products (%) <sup>c</sup>
1	C <sub>6</sub> H <sub>6</sub>	1.0	55	55	71:29	-
2	THF	1.0	59	59	61:39	-
3	C <sub>6</sub> H <sub>6</sub>	0.25	29 <sup>d</sup>	29 <sup>d</sup>	87:13	-
4	THF	0.25	56	56	58:42	-
5 <sup>e</sup>	Toluene	0.25	36	36	92:8	-
6 <sup>e</sup>	MeCN	0.25	27	27	82:18	-
7 <sup>f</sup>	Neat	0.25	100	-	-	100

[a] Py (11.8 mg, 0.150 mmol, 0.25 M), pinBH (28.8 mg, 0.225 mmol) and **11** (1.5 μmol, 1 mol% / 0.37 μmol, 0.25 mol%), were stirred in 0.6 mL solvent (see Table) at 80 °C for 24 h. [b] Conversion determined by <sup>1</sup>H NMR as consumption of Py using hexamethylbenzene (1.35 mg, 8.33 μmol) as standard. [c] Average of two individual reactions, unless otherwise noted. [d] Average of three individual reactions. [e] 1,3,5-trimethoxybenzene (2.8 mg, 16.67 μmol) as standard. [f] Several side products were formed, and they could not be properly identified by <sup>1</sup>H NMR.

Once the optimal reaction temperature was known, the effect of additive(s) on the hydroboration of Py was evaluated. Suginome *et al*<sup>110</sup> in 2012 noticed that the regioselectivity in this transformation is dependent on the nature of the phosphorus ligand used. Selective 1,4-hydroboration (17:18 = 1:99) was found to be catalyzed by a Rh-PPh<sub>3</sub> catalyst generated *in situ* from [RhCl(COD)]<sub>2</sub> and PPh<sub>3</sub> (P/Rh = 1), although with low yield owing to the formation of unidentified byproducts. In contrast, 1,2- hydroboration selectively took place in high yields, when the reaction was carried out using a rhodium catalyst bearing PCy<sub>3</sub>. In this sense, the addition of 0.75 mol% of PCy<sub>3</sub> to the system was tested (entry 13, Table 4.9). Unfortunately, compared with the respective experiment without additive (entry 8), low conversion and formation of side products were observed. Based on the hypothesis that a presumable cationic complex would be involved on this catalytic transformation, the effect of adding NaPF<sub>6</sub> to the studied system was also verified (entry 14). A very high selectivity to the 1,2-DHP (>95%) was obtained but a low conversion was reached (only 44%).

Table 4.9. Screening of conditions in the hydroboration of Py. <sup>a</sup>

Entry	Eq. pinBH	[Py] (M)	T (°C)	Catalyst loading (mol%)	Conver sion (%) <sup>b,c</sup>	DHP Product (%) <sup>c</sup>	Ratio 1,2:1,4	Side products (%) <sup>c</sup>
1	1.50	1.0	80	1.0	86	67	52:48	19
2	1.50	1.0	80	0.75	82	72	64:36	10
3	1.50	1.0	80	0.50	67	60	71:29	7
4	1.25	1.0	80	1.0	80	71	56:44	9
5	1.25	1.0	80	0.75	80	77	57:43	3
6	1.25	1.0	80	0.50	75	75	63:37	-
7	1.50	0.75	80	1.0	85	85	58:42	-
8	1.50	0.75	80	0.75	81	81	63:37	-
9	1.25	0.75	80	1.0	82	82	54:46	-
10	1.25	0.75	80	0.75	66	66	67:33	-
11	1.25	0.50	80	0.75	52	52	76:24	-
12	1.50	0.75	70	0.75	84	84	70:30	-
13 <sup>d</sup>	1.50	0.75	70	0.75	55	50	85:15	5
14 <sup>e</sup>	1.50	0.75	70	0.75	44	44	95:5	-
15 <sup>f</sup>	1.50	0.75	70	0.75	90	90	60:40	-
16	1.25	0.75	60	0.75	70	70	77:23	-
17	1.25	0.75	50	0.75	66	66	73:27	-
18 <sup>g</sup>	1.50	0.75	70	0.75	76	76	81:19	-
19 <sup>h</sup>	1.50	0.75	70	0.75	68	68	81:19	-
20 <sup>i</sup>	1.50	0.75	70	0.75	55	55	81:19	-

[a] Py (11.8 mg, 0.150 mmol), pinBH (28.8 mg, 0.225 mmol) and **11** (1.5  $\mu$ mol, 1 mol% / 0.75  $\mu$ mol, 0.75 mol%), were stirred in toluene (as much as required for the appropriate Py concentration) at the specified temperature for 24 h. [b] Conversion determined by <sup>1</sup>H NMR as consumption of Py using 1,3,5-trimethoxybenzene (2.8 mg, 16.67  $\mu$ mol) as standard. [c] Average of two individual reactions. [d] 0.75 mol% PCy<sub>3</sub>. [e] 0.75 mol% NaPF<sub>6</sub>. [f] THF 6 mL. [g] 18 h. [h] 12 h. [i] 6 h.

Lastly, in this optimization process, the influence of time over the reaction yield was investigated. By conducting the hydroboration for 18 h was possible to improve the selectivity toward the 1,2 regioisomer (81%), without significantly reducing the yield (76%, entry 18). The attempts to additionally reduce the reaction time (entries 19-20) caused a significant drop in product formation while retaining the same regioisomer ratio.

Under the optimized reaction conditions, 0.75 M Py, 1.5 eq HBpin, 0.75 mol% **11**, 18 h, 70 °C and toluene as solvent, a screening of several pyridines and quinolines was performed to explore the scope and limitations of the catalytic system studied (Table 4.10). Substituted pyridines **16b–i** and quinolines **16j–q** underwent hydroboration using the novel rhodium complex **11** as (pre)catalyst in toluene at 70 °C for 18 h. The reaction of HBpin with 4-tertbutylpyridine (**16b**) and 4-(dimethylamino) pyridine (**16e**), proceeded effectively to give the corresponding 1,2-hydroboration products **17b** and **17e** in moderate yields. The electron deficient 4-trifluoromethylpyridine (**16c**) and the electron rich 4-methoxypyridine (**16d**) were also suitable substrates for the hydroboration protocol described here, leading to the high-yield formation of the corresponding 1,2-dihydropyridines **17c** and **17d**. Remarkably, hydroboration of 3-substituted pyridines such as 3-bromopyridine (**16f**) and 3-picoline (**16g**), gave the 1,2-hydroboration products **17f–g** with high yield (up to >95%) and regioselectivity (>95%). On the contrary, 2-substituted pyridines (**16h–i**) were not reduced under these conditions. The formation of 1,4-DHP compounds was not detected in any of the examples presented above.

For quinolines, the hydroboration proceeded better than with pyridines as substrates. The investigated system tolerates a variety of substrates with both electron-donating and electron-withdrawing substituents and produced 1,2-dihydroquinoline (1,2-DHQ) products with excellent regioselectivities (>95%). Quinolines bearing an electron-donating methyl group at the C3 and C4 position afforded the corresponding 1,2-hydroboration products in excellent yields (**16m–l**, >95%). Likewise, quinolines possessing electron-withdrawing halogen atoms (Cl, and Br) at the C3 or C4 position also proceeded well with the regioselective dearomative 1,2-reduction, affording 1,2-DHQ up to >95% yields (**16n–o**, > 95%). For the quinoline **16p**, substituted at C4 and C7 by Cl, the formation of the corresponding 1,2-DHQ compound is quantitative (**16p**). The reduction of 5,6,7,8-tetrahydroquinoline was also performed quantitatively under these conditions (**16q**). By using 2-trifluoromethylquinoline as a substrate the reduction reaction did not proceed, probably due to steric hindrance.

Table 4.10. Screening of substrates in the hydroboration of pyridines and quinolines.<sup>a-c</sup>

**16b-q** **11** (0.75 mol%) **HBpin** (1.5 equiv) **17b-q**

18 h, 70 °C Toluene

[0.75 M]

### Pyridines

**16b** 47 (33)

**16c** >95 (86)

**16d** >95 (88)

**16e** 25 (14)

**16f** >95 (87)

**16g** 90 (81)

**16h** 0

**16i** 0

### Quinolines<sup>d,e</sup>

**16j** 90 [90:10] (83)

**16k** >95 (90)

**16l** >95 (86)

**16m** >95 (81)

**16n** >95 (90)

**16o** >95 (90)

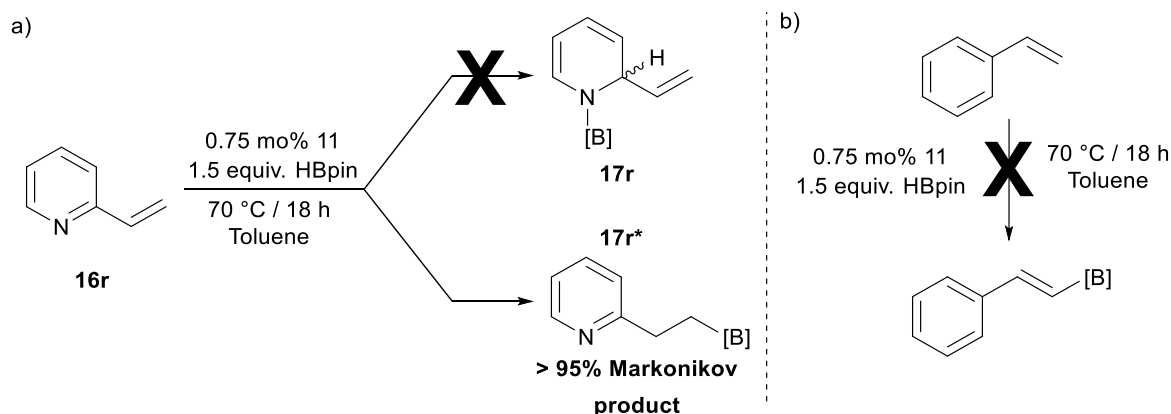
**16p** >95 (90)

**16q** >95 (86)

[a] Py (11.8 mg, 0.150 mmol, 0.25 M), pinBH (28.8 mg, 0.225 mmol) and **11** (0.75  $\mu$ mol, 0.75 mol%), were stirred in 0.6 mL Toluene at 70 °C for 18 h. [b] Conversion determined by <sup>1</sup>H NMR as consumption of the corresponding substrate using 1,3,5-trimethoxybenzene (2.8 mg, 16.67  $\mu$ mol) as standard. [c] Average of two individual reactions. Values in parenthesis (%) correspond to isolated yields. [d] pinBH (24.0 mg, 187  $\mu$ mol, 1.25 equiv.). Values in brackets correspond to the 1,2:1,4 isomeric ratio. [e] 12 h.

Although C2-substituted pyridines are not suitable substrates for its 1,2-hydroboration catalyzed by **11**, the hydroboration of 2-vinylpyridine to get the DHP product **17r** (a, Scheme 4.7) was attempted. Interestingly, HBpin reacted effectively with 2-vinylpyridine (**16r**) to yield the regioselective reduction of the terminal C=C bond instead of the C=N 1,2-hydroboration product **17r** (a, Scheme 4.7). In contrast, the hydroboration of

styrene did not take place under identical reaction conditions (b, Scheme 4.7). This might indicate that the reduction of **16r** possibly occurred by the so called “nitrogen-promoted” hydroboration of alkenes, well exemplified in previous reports from the literature.<sup>119</sup>



Scheme 4.7. Hydroboration of a) 2-vinylpyridine and b) styrene catalyzed by **11**.

#### 4.5 Chapter conclusion

$\text{P}(\text{OQuin})_3$  reacted with two different rhodium (I) sources in order to form **11** in high yield (Scheme 4.1). Compound **11** represents the first example of a heteroleptic rhodium (I) complex where a *P,N*-phosphite and a phosphine ligand are present in the coordination sphere of the metal center. The ligand **1** binds to Rh(I) as a bidentate P–N chelate, as confirmed by X-ray diffraction analysis of the compound  $[\kappa^2P,N\text{-}\{\text{P}(\text{OQuin})_3\}\text{RhCl}(\text{PX}_3)]$  (where X = Ph and Cy, **11** and **14** respectively). For **11**, two different crystalline materials were obtained with different unit cells but with almost identical bond parameters (bond lengths and bond angles).  $[\kappa^2P,N\text{-}\{\text{P}(\text{OQuin})_3\}\text{RhCl}(\text{PPh}_3)]$  was fully characterized in solution by NMR spectroscopy, which suggested the “*cis*” spatial configuration between both phosphorus ligands also in solution. The stability of the new complex **11** toward selected external agents was tested at NMR scale. Through this kind of study, it was possible to chemically transform **11** via ligand dissociation (Scheme 4.2), ligand exchange (Scheme 4.4), and retro-Arbuzov rearrangement (Scheme 4.3) into new Rh complexes. The last reactivity probably represents the first example of a retro-Arbuzov rearrangement for a coordinated phosphite, **13**. Chlorine abstraction (Scheme 5) with  $\text{PF}_6$  inorganic salts was not possible, mainly due to further decomposition of **11** to yield **13** plus other non-identified phosphorus containing compounds. The Rh(I) complex **11** resulted to be a suitable catalyst for the 1,2 regioselective hydroboration of pyridines and quinolines to form 1,2-DHP and 1,2-DHQ, respectively, in high yield. Reaction conditions were optimized for a model reaction (pyridine as model substrate) and the *N*-boryl formation can proceed under mild conditions: 1.5 equiv. of HBpin, 0.75 mol% of **11** as catalyst precursor, 70 °C, 18 h and toluene as reaction media. No base or additive(s) were required, TONs up to 130

were reached and almost 8 molecules of the substrate were converted *per* molecule of catalyst in one hour, which represents the best ever catalytic system reported for this kind of transformation mediated by a late-transition metal. The described protocol tolerates a variety of substrates with both electron-donating and electron-withdrawing substituents and produces 1,2-hydroborated pyridines and quinolines (1,2-DHP and 1,2-DHQ) with high regioselectivities (>95%).

#### 4.6 Experimental section.

##### Synthesis of {(P,N)-(tris(8-quinoliny))phosphite}{tris(phenyl)phosphine}rhodium chloride (I), 11.

###### *From [RhCl(PPh<sub>3</sub>)<sub>3</sub>]:*

To a solution of [RhCl(PPh<sub>3</sub>)<sub>3</sub>] (199.0 mg, 0.215 mmol) in CH<sub>2</sub>Cl<sub>2</sub> (10 mL) was added a solution of P(OQuin)<sub>3</sub> (100.0 mg, 0.215 mmol) in CH<sub>2</sub>Cl<sub>2</sub> (10 mL) at –75 °C, and the mixture was stirred for 2 h. Then, the mixture was left to warm up to room temperature and was stirred overnight. All volatile materials were removed under reduced pressure. The complex was washed twice with dried Et<sub>2</sub>O (20 mL). The solid was dried under vacuum to obtain a pale orange solid (170.0 mg, 91% yield).

###### *From [(COD)RhCl(PPh<sub>3</sub>)]:*

To a solution of [(COD)RhCl(PPh<sub>3</sub>)] (109.0 mg, 0.215 mmol) in CH<sub>2</sub>Cl<sub>2</sub> (10 mL) was added a solution of P(OQuin)<sub>3</sub> (100.0 mg, 0.215 mmol) in CH<sub>2</sub>Cl<sub>2</sub> (10 mL) at –20 °C, and the mixture was stirred for 2 h. Then, the mixture was left to warm up to room temperature and was stirred overnight. All volatile materials were removed under reduced pressure. The complex was washed twice with dried Et<sub>2</sub>O (20 mL). The solid was dried under vacuum to obtain a pale orange solid (150.0 mg, 80% yield).

<sup>1</sup>H NMR (400.1 MHz, THF-d<sub>8</sub>, 25 °C): δ = 9.10 (d, <sup>3</sup>J<sub>HH</sub> = 3.6 Hz, 3H), 8.23 (dd, <sup>3</sup>J<sub>HH</sub> = 8.3 Hz, <sup>3</sup>J<sub>HH</sub> = 1.7 Hz, 3H), 7.85-7.71 (m, 9H), 7.56 (d, <sup>3</sup>J<sub>HH</sub> = 7.8 Hz, 3H), 7.39-7.30 (m, 6H), 7.21-7.05 (m, 9H). <sup>13</sup>C{<sup>1</sup>H} NMR (150.9 MHz, THF-d<sub>8</sub>, 25 °C): δ = 151.7 (s, C2), 147.9 (d, J<sub>PC</sub> = 7.0 Hz, C4), 139.8 (d, J<sub>PC</sub> = 4.5 Hz, C8), 136.8 (s, C9), 136.3 (s, C10), 136.0 (s, PPh<sub>3</sub>), 135.1 (d, <sup>3</sup>J<sub>PC</sub> = 10.9 Hz, PPh<sub>3</sub>) 129.5 (s, C5), 128.4 (d, J<sub>PC</sub> = 2.1 Hz, C6) 126.7 (d, J<sub>PC</sub> = 10.1 Hz, PPh<sub>3</sub>), 122.8 (s, C3), 120.9 (s, PPh<sub>3</sub>), 120.1 (d, J<sub>PC</sub> = 6.4 Hz, C7). <sup>31</sup>P{<sup>1</sup>H} NMR (121.5 MHz, THF-d<sub>8</sub>, 25 °C): δ = 116.1 (dd, <sup>1</sup>J<sub>PRh</sub> = 311 Hz, <sup>2</sup>J<sub>PP</sub> = 53 Hz, P(OQuin)<sub>3</sub>); 49.8 (dd, <sup>1</sup>J<sub>PRh</sub> = 171 Hz, <sup>2</sup>J<sub>PP</sub> = 53 Hz, PPh<sub>3</sub>). LIFDI-MS: m/z calc. for C<sub>27</sub>H<sub>18</sub>N<sub>3</sub>O<sub>3</sub>PRhCl 600.91 [M<sup>+</sup>-PPh<sub>3</sub>]<sup>+</sup>; found 600.91. Anal. Calcd. for C<sub>45</sub>H<sub>33</sub>N<sub>3</sub>O<sub>3</sub>ClP<sub>2</sub>Rh•0.66 C<sub>4</sub>H<sub>8</sub>O•0.33 C<sub>4</sub>H<sub>10</sub>O: C, 62.82; H, 4.48; N, 4.49. Found: C, 62.87; H, 4.38; N, 4.49.



## Reactivity of **11** toward different external agents (at NMR scale).

### *Phosphine (PPh<sub>3</sub>) dissociation in CDCl<sub>3</sub> to yield **12***

Under inert atmosphere, the complex **11** (10.0 mg, 11.5  $\mu$ mol), and CDCl<sub>3</sub> (*ca.* 0.5 mL). were placed in a young NMR tube. The mixture was immediately analyzed by <sup>1</sup>H and <sup>31</sup>P{<sup>1</sup>H} NMR at room temperature (RT). Then, the sample was heated to 50 °C inside the NMR device and spectra were recorded every two hours for six hours. The last NMR spectrum recorded displayed a full conversion of **11** into **12**. <sup>31</sup>P{<sup>1</sup>H} NMR (121.5 MHz, THF-d<sub>8</sub>, 25 °C):  $\delta$  = 90.8 ppm (d, <sup>1</sup>J<sub>PRh</sub> = 162 Hz)

### *Retro-Arbuzov-like dearylation reaction.*

The complex **11** (10.0 mg, 11.5  $\mu$ mol), was placed in a J. Young NMR tube. Then, **11** was dissolved in not dry CDCl<sub>3</sub> (*ca.* 0.5 mL) and the tube was pressurized with air (30 psi), closed and shaken. The sample was heated up to 50 °C in an oil bath for 24 h. After reaching room temperature, the mixture was immediately analyzed by <sup>1</sup>H and <sup>31</sup>P{<sup>1</sup>H} NMR. The <sup>31</sup>P{<sup>1</sup>H} NMR spectrum displayed the formation of **13** along with other side-products. <sup>31</sup>P{<sup>1</sup>H} NMR (121.5 MHz, THF-d<sub>8</sub>, 25 °C):  $\delta$  = 69.3 ppm (dd, <sup>1</sup>J<sub>PRh</sub> = 151 Hz, <sup>2</sup>J<sub>PP</sub> = 30 Hz, P(OQuin)<sub>3</sub>); 55.5 ppm (dd, <sup>1</sup>J<sub>PRh</sub> = 146 Hz, <sup>2</sup>J<sub>PP</sub> = 30 Hz, PPh<sub>3</sub>). Suitable crystals for X-ray diffraction analysis were obtained by slow evaporation of a saturated CDCl<sub>3</sub> solution.

### *PPh<sub>3</sub>/PCy<sub>3</sub> Ligand exchange reaction*

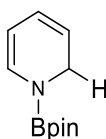
Under inert atmosphere, the complex **11** (10.0 mg, 11.5  $\mu$ mol), PCy<sub>3</sub> (3.3 mg, 11.6  $\mu$ mol), and THF-d<sub>8</sub>(*ca.* 0.5 mL). were placed in a young NMR tube. The mixture was analyzed by <sup>1</sup>H and <sup>31</sup>P{<sup>1</sup>H} NMR after 3 h at RT. Then, all volatile materials were removed under reduced pressure. The new complex was washed twice with dried Et<sub>2</sub>O (20 mL). The product was dried under vacuum to obtain a pale pink solid (170.0 mg, 91% yield). <sup>1</sup>H NMR (400.1 MHz, THF-d<sub>8</sub>, 25 °C):  $\delta$  = 8.83 (d, <sup>3</sup>J<sub>HH</sub> = 4.5 Hz, 3H), 8.03 (dd, <sup>3</sup>J<sub>HH</sub> = 8.3 Hz, <sup>4</sup>J<sub>HH</sub> = 1.7 Hz, 3H), 8.09 (d, <sup>3</sup>J<sub>HH</sub> = 7.6 Hz, 3H), 7.15 (dd, <sup>3</sup>J<sub>HH</sub> = 8.3 Hz, <sup>3</sup>J<sub>HH</sub> = 4.5 Hz, 3H), 7.45 (dd, <sup>3</sup>J<sub>HH</sub> = 8.2 Hz, <sup>4</sup>J<sub>HH</sub> = 1.5 Hz, 3H), 7.38 (t, <sup>3</sup>J<sub>HH</sub> = 7.9 Hz, 3H) 1.66 (m, 21H) 1.26 (m, 9H). <sup>31</sup>P{<sup>1</sup>H} NMR (121.5 MHz, THF-d<sub>8</sub>, 25 °C):  $\delta$  = 117.8 ppm (dd, <sup>1</sup>J<sub>PRh</sub> = 311 Hz, <sup>2</sup>J<sub>PP</sub> = 53 Hz, P(OQuin)<sub>3</sub>); 55.9 ppm (dd, <sup>1</sup>J<sub>PRh</sub> = 171 Hz, <sup>2</sup>J<sub>PP</sub> = 53 Hz, PPh<sub>3</sub>). A suitable sample for X-ray diffraction analysis was obtained as red crystals from a saturated THF solution of **14** at -30 °C.

### General procedure for the 1, 2-regioselective catalytic hydroboration of pyridines.

Pyridine (11.9 mg, 150  $\mu\text{mol}$ ), pinacolborane (28.8 mg, 225  $\mu\text{mol}$ ), **11** (1.0 mg, 1.12  $\mu\text{mol}$ ), and toluene (0.2 mL), were placed in a Schlenk tube. The resulting mixture was stirred for 18 h at 70  $^{\circ}\text{C}$ . Products **17a–g** were purified by flash column chromatography on silica gel and hexane as eluent. For the optimization of the reaction conditions to yield **17a**, hexamethylbenzene (1.4 mg, 83.3  $\mu\text{mol}$ ) was added as standard once the reaction was completed. When toluene or acetonitrile were used as solvent, 1,3,5-trimethoxybenzene instead of hexamethylbenzene was added as standard (2.9 mg, 66.6  $\mu\text{mol}$ ). The mixture was analyzed by  $^1\text{H}$  NMR to determine the conversion of Py and the yields of the products 1,2-DHP and 1,4-DHP. **Note:** N-boryl-1,2-dihydro pyridine/quinoline products **17a–g** are highly air- and moisture-sensitive and decompose rapidly when exposed to the atmosphere.  $^1\text{H}$  NMR data of **17a–g** obtained with this methodology are in accordance with the ones in previous reported procedures.<sup>109-112</sup>

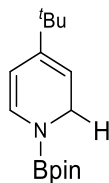
### Spectroscopic data of DHP products

#### *N*-(4,4,5,5-Tetramethyl-1,3,2-dioxaborolan-2-yl)-1,2-dihydropyridine (**17a**).



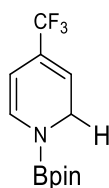
$^1\text{H}$  NMR (400 MHz,  $\text{C}_6\text{D}_6$ ) *major isomer*  $\delta$  6.74 (d,  $J_{\text{HH}} = 7.6$  Hz, 1H), 5.77-5.83 (m, 1H), 5.04-5.14 (m, 2H, overlapped signals), 4.18 (dd,  $J_{\text{HH}} = 4.0, 1.6$  Hz, 2H), 1.00 (s, 12H) ppm. *minor isomer*  $\delta$  6.56 (dt,  $J_{\text{HH}} = 8.4, 1.6$  Hz, 2H), 4.55-4.60 (m, 2H), 2.82 (tt,  $J_{\text{HH}} = 3.2, 1.6$  Hz, 2H), 0.96 (s, 12H) ppm.

#### *N*-(4,4,5,5-Tetramethyl-1,3,2-dioxaborolan-2-yl)-4-tertbutyl-1,2-dihydropyridine (**17b**).

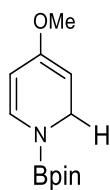


$^1\text{H}$  NMR (400 MHz,  $\text{C}_6\text{D}_6$ )  $\delta$  6.74 (d,  $J_{\text{HH}} = 7.6$  Hz, 1H), 5.77-5.83 (m, 1H), 5.04-5.14 (m, 1H), 4.18 (dd,  $J_{\text{HH}} = 4.0, 1.6$  Hz, 2H), 1.35 (s, 9H), 1.00 (s, 12H) ppm.

#### *N*-(4,4,5,5-tetramethyl-1,3,2-dioxaborolan-2-yl)-4-Trifluoromethyl-1,2-dihydropyridine (**17c**).

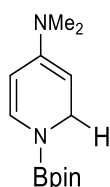


$^1\text{H}$  NMR (400 MHz,  $\text{C}_6\text{D}_6$ )  $\delta$  6.61 (d,  $J_{\text{HH}} = 7.6$  Hz, 1H), 5.22-5.28 (m, 1H), 5.14 (dd,  $J_{\text{HH}} = 7.6, 1.6$  Hz, 1H), 3.86-3.90 (m, 2H), 0.96 (s, 12H) ppm.



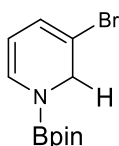
***N*-(4,4,5,5-tetramethyl-1,3,2-dioxaborolan-2-yl)-4-methoxy-1,2-dihydropyridine (17d).**

<sup>1</sup>H NMR (400 MHz, C<sub>6</sub>D<sub>6</sub>) δ = 6.31 (d, *J*<sub>HH</sub> = 7.7 Hz, 1H), 5.66-5.53 (m, 1H), 4.81 (dd, *J*<sub>HH</sub> = 7.7, 1.9 Hz, 1H), 4.02 (s, 3H), 3.42-3.38 (m, 2H), 1.18 (s, 12H) ppm.



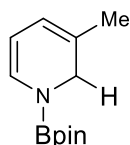
***N*-(4,4,5,5-tetramethyl-1,3,2-dioxaborolan-2-yl)-4-(*N,N*-dimethylamino)-1,2-dihydropyridine (17e).**

<sup>1</sup>H NMR (400 MHz, C<sub>6</sub>D<sub>6</sub>) δ = 6.3 (d, *J*<sub>HH</sub> = 7.7 Hz, 1H), 5.36-5.28 (m, 1H), 4.73 (dd, *J*<sub>HH</sub> = 7.6, 1.7 Hz, 1H), 3.45-3.40 (m, 2H), 2.95 (s, 6H), 1.18 (s, 12H) ppm.



***N*-(4,4,5,5-tetramethyl-1,3,2-dioxaborolan-2-yl)-3-bromo-1,2-dihydropyridine (17f).**

<sup>1</sup>H NMR (400 MHz, C<sub>6</sub>D<sub>6</sub>) δ = 6.30 (d, *J*<sub>HH</sub> = 7.26 Hz, 1H), 5.98 (m, 1H), 4.74 (dd, *J*<sub>HH</sub> = 7.26, 1.4 Hz, 1H), 4.20 (d, *J*<sub>HH</sub> = 1.4 Hz, 2H), 1.19 (s, 12H) ppm.



***N*-(4,4,5,5-Tetramethyl-1,3,2-dioxaborolan-2-yl)-3-methyl-1,2-dihydropyridine (17g).**

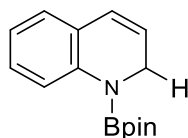
<sup>1</sup>H NMR (400 MHz, C<sub>6</sub>D<sub>6</sub>) δ 6.66 (d, *J*<sub>HH</sub> = 7.2 Hz, 1H), 5.54 (d, *J*<sub>HH</sub> = 5.6 Hz, 1H), 5.08 (dd, *J*<sub>HH</sub> = 7.2, 5.6 Hz, 1H), 4.12 (s, 2H), 1.42 (s, 3H), 1.02 (s, 12H) ppm.

**General procedure for the 1,2 regioselective catalytic hydroboration of quinolines.**

Quinoline (19.4 mg, 150 μmol), pinacolborane (24.0 mg, 187 μmol), **11** (1.0 mg, 0.75 μmol, 0.75 mol%), 1,3,5-trimethoxybenzene (2.9 mg, 66.6 μmol, standard) and toluene (0.2 mL), were placed in a Schlenk tube. The resulting mixture was stirred for 12 h at 70 °C. The mixture was analyzed by <sup>1</sup>H NMR to determine the conversion of the corresponding quinoline and the yields of the 1,2-DHQ products. Products **17j–q** were purified by flash column chromatography on silica gel and hexane as eluent. **Note:** N-boryl-1,2-dihydro pyridine/quinoline products **17j–q** are highly air- and moisture-sensitive and decompose rapidly when exposed to the atmosphere. <sup>1</sup>H NMR data of **17j–q** obtained with this methodology are in accordance with the ones in previous reported procedures.<sup>109-112</sup>

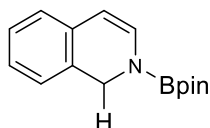
## Spectroscopic data of DHQ products

### *N*-(4,4,5,5-tetramethyl-1,3,2-dioxaborolan-2-yl)-1,2-dihydroquinoline (17j).



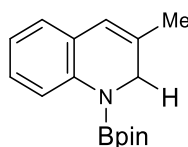
$^1\text{H}$  NMR (400 MHz,  $\text{C}_6\text{D}_6$ ) *major isomer*  $\delta$  7.54 (d,  $J_{\text{HH}} = 8.1$  Hz, 1H), 7.01 – 6.91 (m, 1H), 6.83 – 6.61 (m, 2H), 6.18 (d,  $J_{\text{HH}} = 9.6$  Hz, 1H), 5.60 – 5.53 (m, 1H), 4.02 (dd,  $J_{\text{HH}} = 4.2, 1.8$  Hz, 2H), 1.05 (s, 12H) ppm. *minor isomer* 8.14 (d,  $J_{\text{HH}} = 8.3$  Hz, 1H), 7.13-7.04 (m, 1H), 6.94-6.76 (m, 3H), 4.88-4.75 (m, 1H), 3.31 (d,  $J_{\text{HH}} = 2.4$  Hz, 2H), 1.01 (s, 12H) ppm.

### *N*<sup>2</sup>-(4,4,5,5-tetramethyl-1,3,2-dioxaborolan-2-yl)-1,2-dihydroisoquinoline (17k).



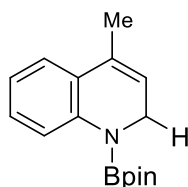
$^1\text{H}$  NMR (400 MHz,  $\text{C}_6\text{D}_6$ )  $\delta$  6.99 (t,  $J_{\text{HH}} = 7.4$  Hz, 1H), 6.88 (td,  $J_{\text{HH}} = 7.4, 0.8$  Hz, 1H), 6.81 (t,  $J_{\text{HH}} = 8.3$  Hz, 2H), 6.72 (d,  $J_{\text{HH}} = 7.4$  Hz, 1H), 5.62 (d,  $J_{\text{HH}} = 7.5$  Hz, 1H), 4.62 (s, 2H), 1.02 (s, 12H) ppm.

### *N*-(4,4,5,5-tetramethyl-1,3,2-dioxaborolan-2-yl)-3-methyl-1,2-dihydroquinoline (17l).

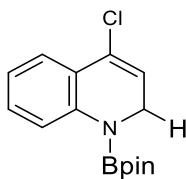


$^1\text{H}$  NMR (400 MHz,  $\text{C}_6\text{D}_6$ )  $\delta$  7.88 (d,  $J_{\text{HH}} = 10$  Hz, 1H), 7.10 (td,  $J_{\text{HH}} = 13.0, 1.5$  Hz, 1H), 6.88 (dd,  $J_{\text{HH}} = 7.5, 2$  Hz, 1H), 6.84 (td,  $J_{\text{HH}} = 7.5, 1.0$  Hz, 1H), 6.01 (s, 1H), 2.07 (s, 2H), 1.49 (s, 3H), 1.05 (s, 12H) ppm.

### *N*-(4,4,5,5-tetramethyl-1,3,2-dioxaborolan-2-yl)-4-methyl-1,2-dihydroquinoline (17m).

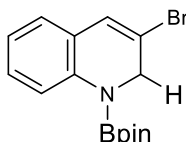


$^1\text{H}$  NMR (400 MHz,  $\text{C}_6\text{D}_6$ )  $\delta$  7.85 (d,  $J_{\text{HH}} = 10$  Hz, 1H), 7.14 (m, 1H), 6.86 (t,  $J_{\text{HH}} = 7.5$  Hz, 1H), 5.46-5.40 (m, 1H), 4.11 (dd,  $J_{\text{HH}} = 4.1, 1.5$  Hz, 2H), 1.80 (s, 3H), 1.05 (s, 12H) ppm.



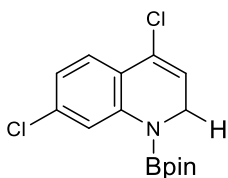
***N*-(4,4,5,5-tetramethyl-1,3,2-dioxaborolan-2-yl)-4-chloro-1,2-dihydroquinoline (17n).**

<sup>1</sup>H NMR (400 MHz, C<sub>6</sub>D<sub>6</sub>) δ 7.85 (d, *J*<sub>HH</sub> = 10 Hz, 1H), 7.14 (m, 2H), 6.86 (t, *J*<sub>HH</sub> = 7.5 Hz, 1H), 5.43-5.37 (m, 1H), 4.13 (d, *J*<sub>HH</sub> = 2.0 Hz, 2H), 1.05 (s, 12H).



***N*-(4,4,5,5-tetramethyl-1,3,2-dioxaborolan-2-yl)-3-bromo-1,2-dihydroquinoline (17o).**

<sup>1</sup>H NMR (400 MHz, C<sub>6</sub>D<sub>6</sub>) δ 7.88 (d, *J*<sub>HH</sub> = 10 Hz, 1H), 7.10 (td, *J*<sub>HH</sub> = 12.1, 1.5 Hz, 1H), δ 6.88 (dd, *J*<sub>HH</sub> = 7.5, 2.3 Hz, 1H), 6.84 (td, *J*<sub>HH</sub> = 7.5, 1.0 Hz, 1H), 6.01 (s, 1H), 2.28 (s, 2H), 1.05 (s, 12H).



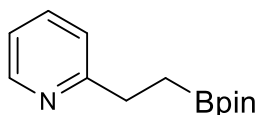
***N*-(4,4,5,5-tetramethyl-1,3,2-dioxaborolan-2-yl)-4,7-dichloro-1,2-dihydroquinoline (17n).**

<sup>1</sup>H NMR (400 MHz, C<sub>6</sub>D<sub>6</sub>) δ 7.85 (d, *J*<sub>HH</sub> = 11 Hz, 1H), 7.14 (s, 1H), 6.86 (d, *J*<sub>HH</sub> = 11 Hz, 1H), 5.35 (m, 1H), 4.13 (d, *J*<sub>HH</sub> = 2.0 Hz, 2H), 1.05 (s, 12H, CH<sub>3</sub>).

**General procedure for regioselective C=C bond hydroboration of 2-vinylpyridine.**

2-Vinylpyridine (15.7 mg, 150 μmol), pinacolborane (28.8 mg, 225 μmol), **11** (1.0 mg, 0.75 μmol, 0.75 mol%), 1,3,5-trimethoxybenzene (2.9 mg, 66.6 μmol, internal standard) and toluene (0.2 mL), were placed in a Schlenk tube. The resulting mixture was stirred for 18 h at 70 °C. The mixture was analyzed by <sup>1</sup>H NMR spectroscopy to determine the conversion of 2-vinylpyridine and the yield of the reduced olefin. Product **17r\*** was purified by flash column chromatography on silica gel and hexane as eluent.

**2-(2-(4,4,5,5-Tetramethyl-1,3,2-dioxaborolan-2-yl)-ethylene)pyridine (17r\*).**



<sup>1</sup>H NMR (400 MHz, C<sub>6</sub>D<sub>6</sub>) δ 8.53 (d, *J*<sub>HH</sub> = 7.6 Hz, 1H), 7.75 (dt, *J* = 4.0, 1.6 Hz, 1H), 7.45 (d, *J*<sub>HH</sub> = 5.6 Hz, 1H), 6.95 (dd, *J*<sub>HH</sub> = 7.6, 5.6 Hz, 1H), 3.58 (t, *J*<sub>HH</sub> = 6.5 Hz, 2H), 2.07-2.01 (m, 2H), 1.00 (s, 12H).

## **Chapter V**

Ru(II)-coordination chemistry of P(OQuin)<sub>3</sub>.

Application in dehydrogenative reactions

## 5.1 Introduction

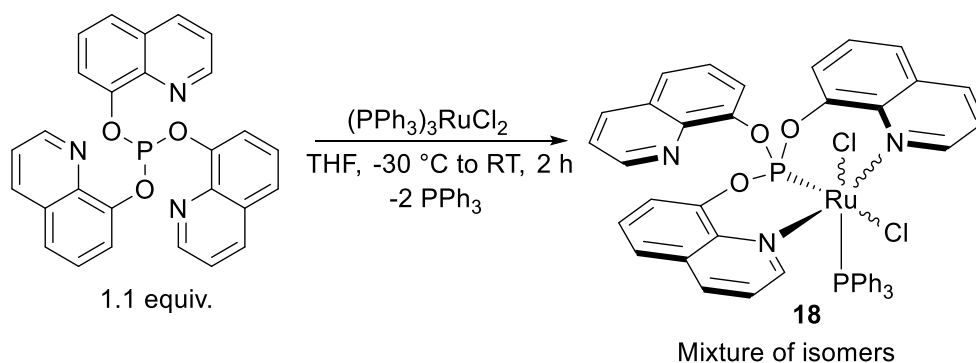
Catalysis is a valuable tool to maximize the efficiency, product selectivity, and sustainability of chemical transformations. The understanding of catalytic performance/activity can be systematically achieved through the utilization of coordination and organometallic compounds as molecularly defined catalysts. One major way to control the reactivity of a metal-containing species is by modifying the structure or the nature of the surrounding ligands. Among the most common donor atoms, C, N and P play a central role.<sup>120</sup> In homogeneous and asymmetric catalysis homotopic or heterotopic polydentate ligands have attracted much attention. Such ligands bearing different donor atoms can induce increased selectivity owing to different electronic and steric properties of the atoms bound to the reactive metal site.<sup>121</sup> Since the late eighties, advances in the field of asymmetric catalysis have been achieved by the use of phosphite ligands with nitrogen-based heterocycles as the fragment that helps to reach a high degree of regiocontrol.<sup>122</sup>

In particular, heterotopic *P,N* ligands, such as **1**, are quite versatile to stabilize metal complexes thanks to the combination of a  $\pi$ -acceptor (P atom) and a  $\sigma$ -donor (N atom). For example, the phosphorus atom might help to stabilize low oxidation state intermediates<sup>21</sup> while the nitrogen donor would make the metal more susceptible to undergo oxidative addition reactions.<sup>22</sup> Such properties are convenient to perform several types of reactions, *e.g.* the dehydrogenative coupling of silanes to yield polysilanes and polysiloxanes. The dehydrogenation of silanes,  $R_2SiH_2$ , to oligo- and polysilicon compounds has been intensively investigated<sup>123</sup> and both  $\sigma$ -bond metathesis according to  $2Si-H \rightarrow Si-Si + H-H$  (metallocene catalysts) or a sequence of oxidative addition/reductive elimination (catalysts with late transition metals) have been reported as plausible mechanistic pathways.<sup>124</sup> However, most of them commonly require the use of additive such as *n*BuLi or similar in a stoichiometric ratio. Therefore, the development of novel polysilicon materials under friendly-environmental and economically feasible methodologies is of great relevance.

Here the synthesis and characterization of a Ru(II) compound bearing the ligand **1** is described. The application of such a complex as a homogeneous catalyst for dehydrogenative reactions, in particular the dehydrocoupling of silanes or dehydrogenation of formic acid, is also discussed. There are no examples of Ru-phosphite complexes as catalyst for this type of reactions.

## 5.2 Synthesis and characterization of the Ru(II) complex

The reaction of **1** with the metal precursor  $[(PPh_3)_3RuCl_2]$  was studied (Scheme 5.1). Ligand **1**, as  $\kappa^3\text{-}N,P,N$ , into the ruthenium center was incorporated by treating  $[(PPh_3)_3RuCl_2]$  in THF with a solution of the ligand **1** in the same solvent at  $-30^\circ\text{C}$ . This reaction resulted in the formation of a mixture of three different isomers according to  $^{31}\text{P}\{^1\text{H}\}$  NMR spectroscopy, with one main product being formed (Figure 5.1). Although the reaction conditions (temperature, order of addition, solvent and/or time) were systematically screened, the isomeric mixture could not be resolved and the reaction always returned the same ratio of isomers as depicted in Figure 5.1.



Scheme 5.1. Synthesis of the ruthenium (II) complex **18**,  $[\kappa^3(N,P,N)\{P(OQuin)_3\}RuCl_2(PPh_3)]$ , the structure of the major isomer is shown.

The  $^{31}\text{P}\{^1\text{H}\}$  NMR spectrum of the reaction mixture shows three pairs of doublets ( $d$ ) resonances at a)  $\delta$  154.1 ppm ( $d$ ,  $^2J_{PP} = 42.0$  Hz, 1) and 35.2 ppm ( $d$ ,  $^2J_{PP} = 42.0$  Hz,  $PPh_3$ ), b)  $\delta$  136.3 ppm ( $d$ ,  $^2J_{PP} = 54.3$  Hz, 1) and 51.6 ppm ( $d$ ,  $^2J_{PP} = 54.3$  Hz,  $PPh_3$ ), and c)  $\delta$  128.1 ppm ( $d$ ,  $^2J_{PP} = 50.2$  Hz, 1) and 42.17 ppm ( $d$ ,  $^2J_{PP} = 50.2$  Hz,  $PPh_3$ ). In addition, a singlet assigned to free  $PPh_3$  is observed at -5.0 ppm. Doublets a) represent the main product of this mixture. In every case, the phosphorus resonance for the coordinated triphenylphosphine ligand is downfield shifted with regard to the corresponding value for the free ligand. Nevertheless, for **1** there is not clear tendency since, with regard to the free ligand, the resonances for sets a) and b) are upfield shifted and those for c) are downfield shifted.



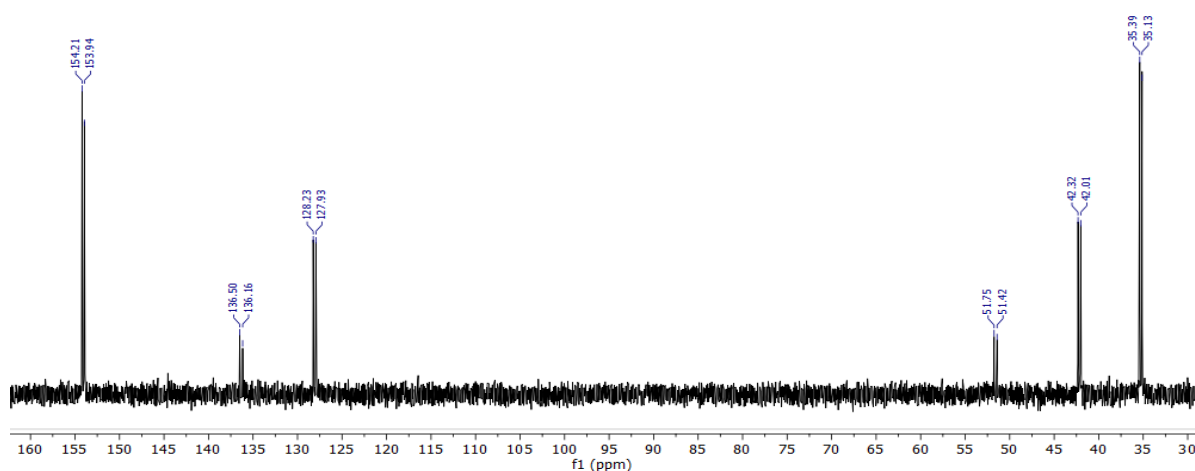


Figure 5.1.  $^{31}\text{P}\{^1\text{H}\}$  NMR spectrum (121.5 MHz) at 298 K of the reaction mixture **1**+  $[(\text{PPh}_3)_3\text{RuCl}_2]$  in THF with a  $\text{C}_6\text{D}_6$  inner capillary as reference.

Ruthenium complexes bearing multidentate ligands, including the so called “pincer ligands”, are some of the most extensively investigated catalysts for organic synthesis and chemical bond activation.<sup>125</sup> For example, the tetradentate tripodal ligands (**H1**-**J1**, Figure 5.2, left) are an important ligand class in coordination chemistry which have received widespread applications in catalysis and material chemistry.<sup>126</sup> However, despite its tetradenticity, these chelates are usually displaying facial (*fac*) geometry upon coordination toward a ruthenium (II) center.<sup>127</sup> The corresponding complexes also experience a dynamic behavior in solution, which results in a mixture of isomer that is difficult to resolve or separate (Figure 5.2, right).<sup>126</sup>

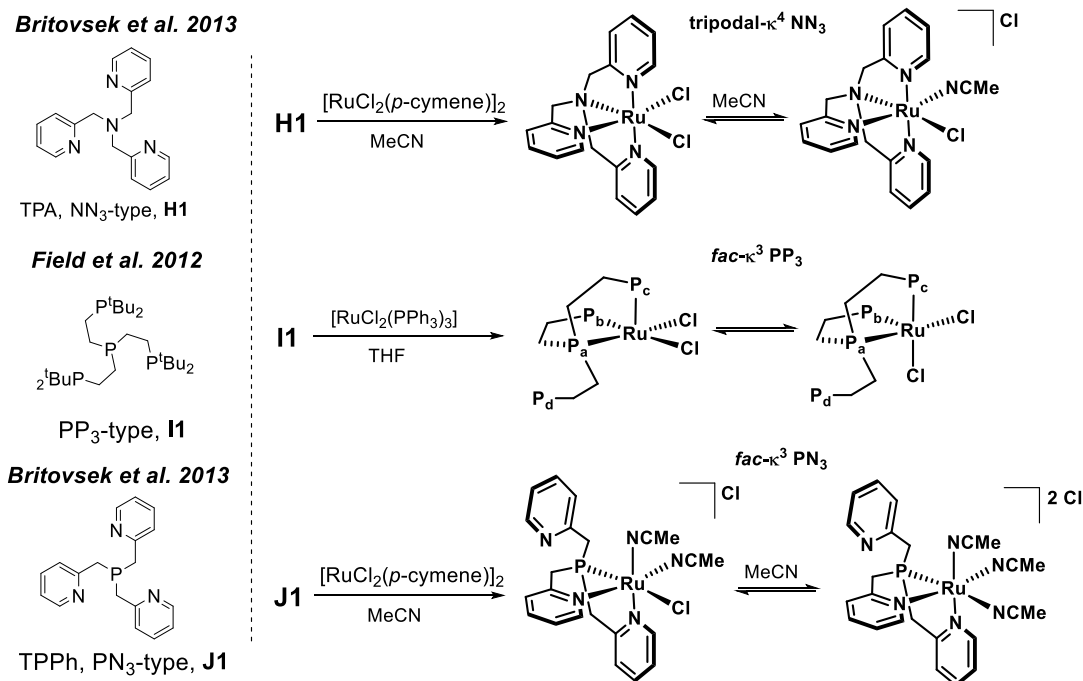
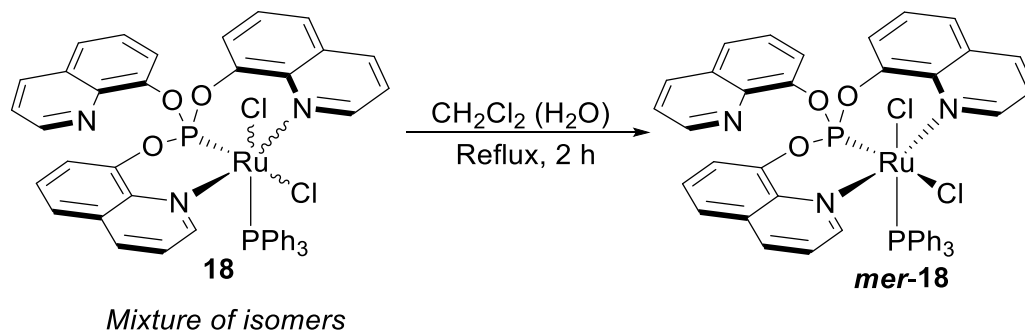


Figure 5.2. Reported tripodal ligands TPA,  $\text{PP}_3$  and TPPh used for coordination chemistry toward Ru (II) metal precursors (left). Dynamic behavior in solution of ruthenium (II) complexes bearing tripodal ligands **H1**-**J1** (right).

Based on this information and after some tests at NMR scale of the reaction mixture, it was possible to find out two aspects of the new ruthenium (II) complexes. First, the compounds are highly stable toward air and moisture, since the NMR tube was opened to air and not changes were observed in its  $^{31}\text{P}\{^1\text{H}\}$  NMR spectrum, even when the sample was warmed up to 50 °C for 2 h. Second, the most remarkable and unexpected behavior of this reaction mixture was observed upon addition of few drops of water into a dry DCM solution of **18**. Surprisingly, under these conditions the isomeric mixture gave rise to the quantitative formation of the main isomer, which was identified as the complex  $[\text{mer-}\kappa^3(\text{N},\text{P},\text{N})\{\text{P}(\text{OQuin})_3\}\text{RuCl}_2(\text{PPh}_3)]$ , (**mer-18**, Scheme 5.2).

Complex **mer-18** is accessible by treating the isomeric mixture with “wet” DCM (directly from a commercially available bottle of DCM) under reflux for 2 h. Upon cooling the solution to room temperature, the coordination compound was obtained after solvent evaporation and two washing steps with diethyl ether. The product is a pale-orange solid quite stable to air/moisture and was isolated in high yield (85%). LIFDI-MS, elemental analysis, X-ray diffraction and NMR spectroscopic data ( $^1\text{H}$ ,  $^{13}\text{C}\{^1\text{H}\}$ , and  $^{31}\text{P}\{^1\text{H}\}$ ) of **mer-18** are in accordance with the proposed formulation. Protons and carbons were assigned using 2D NMR analysis such as COSY, HMQC and HMBC.



Scheme 5.2. Isomers resolution of **18** to yield  $[\text{mer-}\kappa^3(\text{N},\text{P},\text{N})\{\text{P}(\text{OQuin})_3\}\text{RuCl}_2(\text{PPh}_3)]$ , **mer-18**.

The  $^{31}\text{P}\{^1\text{H}\}$  NMR spectrum of **mer-18** shows two sets of doublets ( $d$ ) resonance at  $\delta$  154.1 ppm (**1**) and 35.2 ppm ( $\text{PPh}_3$ ) with the coupling constant  $^2J_{\text{PP}} = 42.5$  Hz (Figure 5.3a). The phosphorus resonance is upfield shifted for **1** and downfield shifted for  $\text{PPh}_3$  with regard to the corresponding value for the free ligands. The chemical shifts and coupling constant ( $^2J_{\text{PP}}$ ) are similar to the ones observed for analogue ruthenium (II) complexes bearing a  $\text{N},\text{P},\text{N}$  and a phosphine ligand at “*fac*” configuration. For example, Braunstein *et al* reported the compound *fac*- $[\text{RuCl}_2(\text{PPh}_3)(\text{N},\text{P},\text{N})]^{128}$  (**K1**, Figure 5.8), for which the  $^{31}\text{P}\{^1\text{H}\}$  NMR (121 MHz,  $\text{CDCl}_3$ ) exhibits two doublets at  $\delta$  52.3 ppm ( $d$ ,  $^2J_{\text{PP}} = 31.2$  Hz,  $\text{N},\text{P},\text{N}$ ) and  $\delta$  46.2 ppm ( $d$ ,  $J_{\text{PP}} = 31.2$  Hz,  $\text{PPh}_3$ ) where  $\text{N},\text{P},\text{N} = \text{bis}(2\text{-oxazolin-2-ylmethyl})\text{phenylphosphine}$ . Also, the  $^{31}\text{P}\{^1\text{H}\}$  NMR

(121 MHz,  $\text{CDCl}_3$ ) spectrum of the complex *fac*-[RuCl<sub>2</sub>(PPh<sub>3</sub>)(*N,P,N*)] (**L1**, Figure 5.8), described by Wagler *et al.*,<sup>129</sup> shows two doublets at  $\delta$  166.4 ppm ( $d$ ,  $^2J_{\text{PP}} = 51.1$  Hz, *N,P,N*) and  $\delta$  41.7 ppm ( $d$ ,  $^2J_{\text{PP}} = 51.1$  Hz, PPh<sub>3</sub>), where *N,P,N* = tris(2-pyridinyl)phosphite.

The  $^1\text{H}$  NMR spectrum of **mer-18** confirms the  $\kappa^3(\text{N,P,N})$  coordination mode of the ligand tris(8-quinolyl)phosphite, as indicated by the presence of two different spin systems for the pyridine scaffold of the quinoline, whose resonances are nicely resolved and quite downfield shifted. These spin systems, both of them AMX-type, were assigned by COSY NMR analysis (Figure 5.4) and the two groups of three sets of signals are a)  $\delta$  11.5, 8.4, 7.9 ppm and b)  $\delta$  10.2, 8.1, 7.3 ppm. The ratio of integral values between a) and b) is 3:6 (Figure 5.3b).

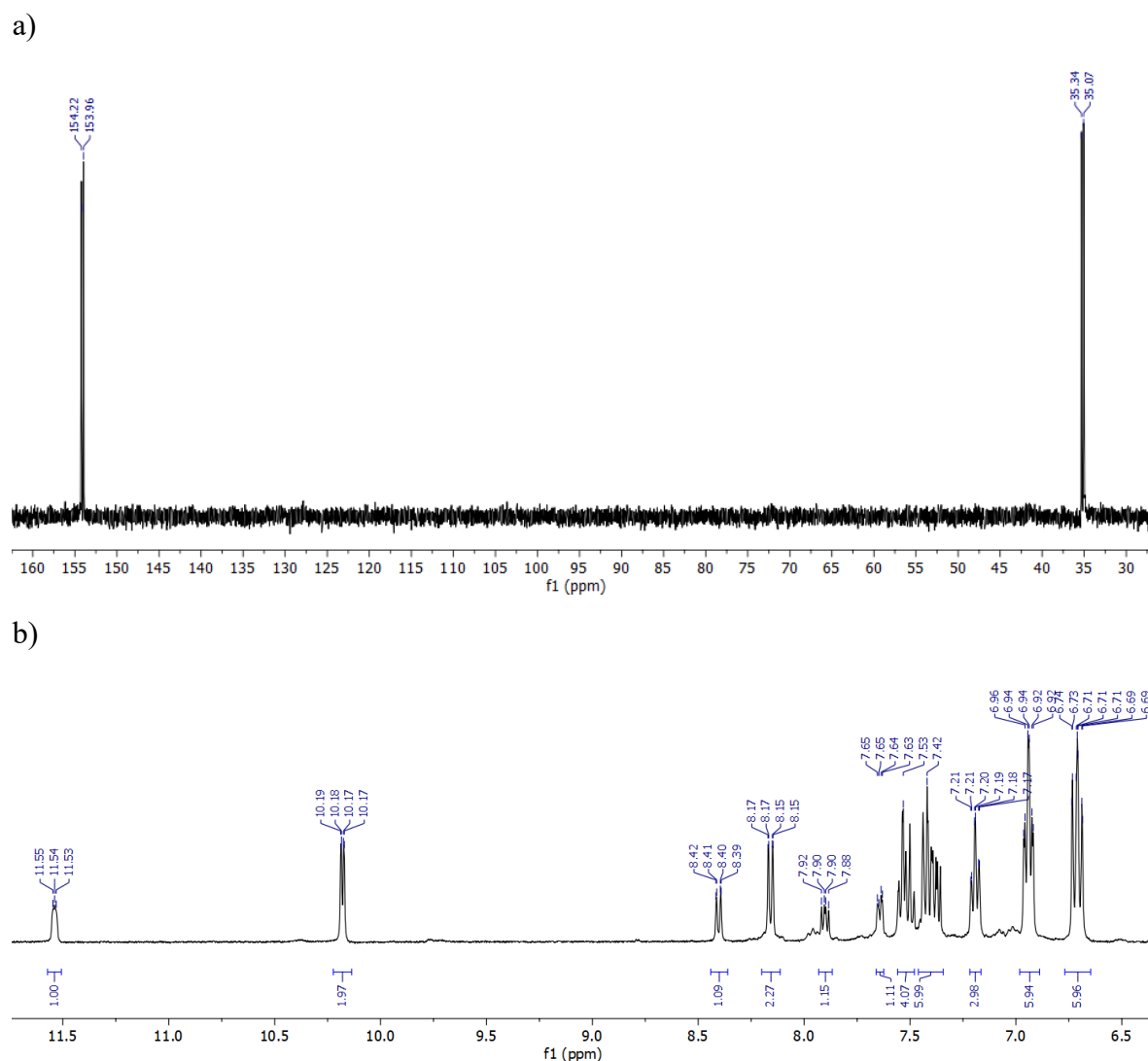


Figure 5.3. a)  $^{31}\text{P}\{^1\text{H}\}$  NMR spectrum (121.5 MHz) and b)  $^1\text{H}$  NMR spectrum (300.1 MHz) at 298 K of **mer-18** in  $\text{CD}_2\text{Cl}_2$ .

The set a) corresponds to the pyridine fragment of the uncoordinated quinoline and the signals exhibit a triplet and doublet of doublet multiplicity, namely  $\delta$  11.54 ( $t$ ,  $^3J_{\text{HH}} = 4.4$  Hz), 8.40 ( $dd$ ,  $^3J_{\text{HH}} = 8.3$  Hz,  $^4J_{\text{HH}} = 1.5$  Hz) and 7.90 ( $dd$ ,  $^3J_{\text{HH}} = 8.2$  Hz,  $^4J_{\text{HH}} = 4.4$  Hz) ppm. The

set b) corresponds to the pyridine moieties of the coordinated quinoline and the signals exhibit a doublet of doublet and multiplet multiplicity, *i.e.*  $\delta$  10.18 (*dd*,  $^3J_{\text{HH}} = 5.4$  Hz,  $^4J_{\text{HH}} = 1.5$  Hz), 8.16 (*dd*,  $^3J_{\text{HH}} = 8.2$  Hz,  $^4J_{\text{HH}} = 1.5$  Hz) and 7.60 (*m*, overlapped signal) ppm. The equivalency between the two coordinated quinolines reveals that there is a symmetry plane into the metal complex molecule.

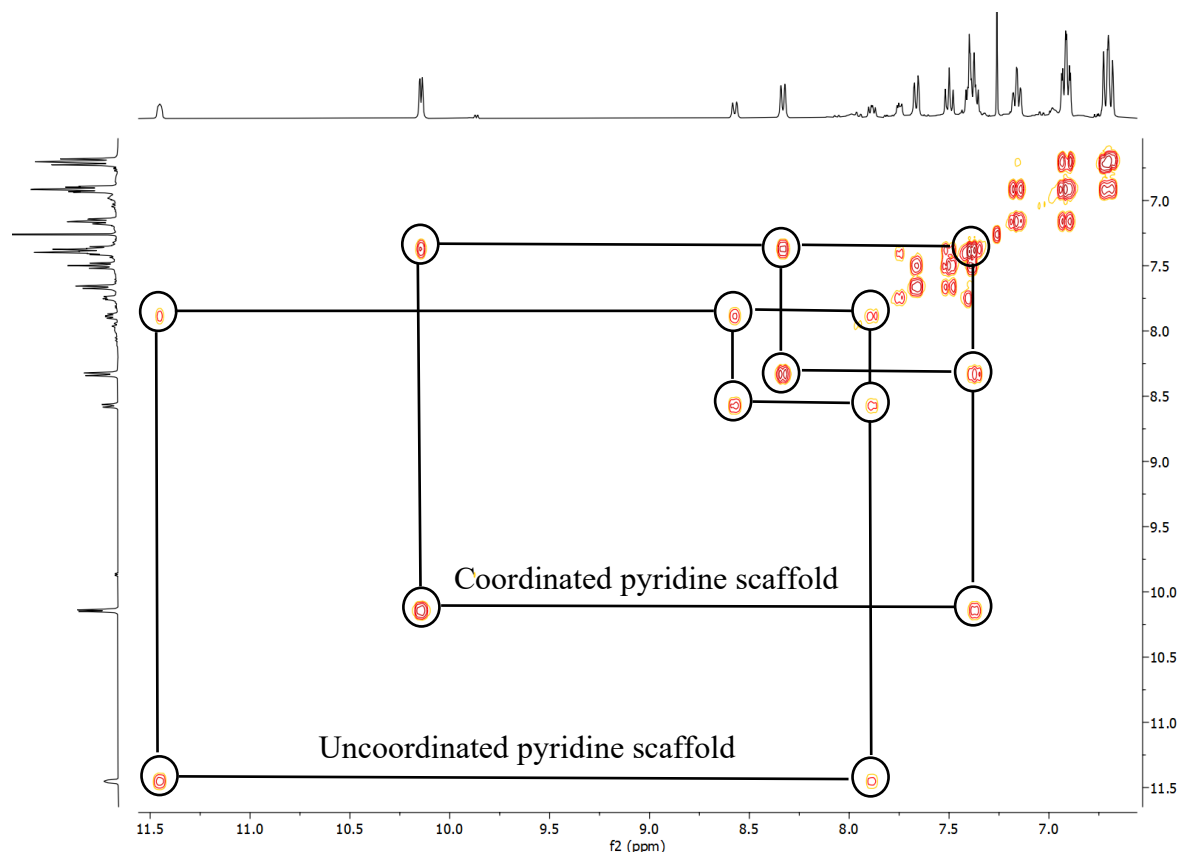
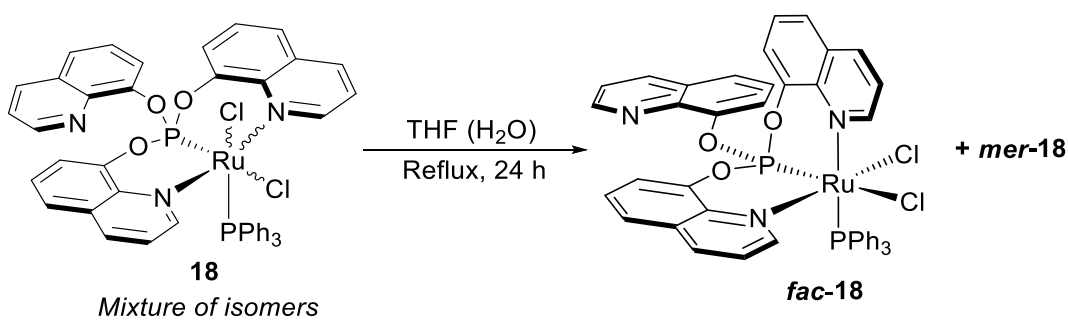


Figure 5.4.  $^1\text{H}$ - $^1\text{H}$  COSY NMR spectrum (300.1 MHz) at 298 K of **mer-18** in  $\text{CDCl}_3$ .

The  $^1\text{H}$  NMR spectra of the  $\kappa^2\text{-}P,N$  systems  $\text{P}(\text{OQuin})_3\text{-M}$  ( $\text{M} = \text{Pd}, \text{Rh}$ ) (Chapters III and IV, respectively) show an equivalency between the three quinoline scaffolds without any distinction of coordinated and uncoordinated fragments. Such behavior is explained in terms of the hemilabile character of the *N*-based heterocycles in **1**. The phenomenon is greatly influenced due to competition between the three quinoline groups with the same coordination probabilities in solution. Unlike the previously discussed  $\kappa^2\text{-}P,N$  systems, the  $^1\text{H}$  NMR spectrum of  $\text{P}(\text{OQuin})_3\text{-Ru}$  shows a clear distinction of coordinated and uncoordinated moieties (Figure 5.2b and 5.3). The signal with the largest shift for the uncoordinated pyridine scaffold ( $\delta = t$ , 11.54 ppm) and for the coordinated pyridine scaffold ( $\delta = d$ , 10.18 ppm) corresponds to the H *meta* and the H *ortho* to N atom, respectively, as confirmed by 2D NMR experiments (COSY, HSQC and HMBC). An NOE effect between the H *ortho* to N atom of the coordinated quinoline and the H *ortho* to  $\text{C}^{\text{quat}}\text{-P}$  of the  $\text{PPh}_3$  was observed by a  $^1\text{H}$ - $^1\text{H}$  NOESY analysis.

The other set of resonances are: multiplets between 7.65-7.35 ppm (9H), as an ABC-type spin system, and multiplets between 7.19-6.62 (15H), as an AMX spin system. Such signals are assigned to the phenolate group of the three quinoline moieties and the phenyl groups of PPh<sub>3</sub> respectively.

In order to promote the selective formation of any of the other isomers present in the mixture **18**, the polarity of the solvent was changed. The complex [*fac*-κ<sup>3</sup>(*N,P,N*){P(OQuin)<sub>3</sub>}RuCl<sub>2</sub>(PPh<sub>3</sub>)], (***fac*-18**, Scheme 5.3), was obtained by treating the isomeric mixture with THF (not dry, directly from a commercially available bottle of THF) under reflux for 24 h. By this mean, the mixture of three different isomers was transformed into a mixture of two of them, where ***fac*-18** is the main product and ***mer*-18** is the minor product (Figure 5.5).



Scheme 5.3. Isomeric resolution of **18** to yield [*fac*-κ<sup>3</sup>(*N,P,N*){P(OQuin)<sub>3</sub>}RuCl<sub>2</sub>(PPh<sub>3</sub>)], ***fac*-18** as main product plus ***mer*-18**.

The <sup>31</sup>P{<sup>1</sup>H} NMR spectrum of the reaction mixture shows two sets of doublets (*d*) resonance at δ 131.9 ppm (**1**) and 43.7 ppm (PPh<sub>3</sub>) with the coupling constant <sup>2</sup>*J*<sub>PP</sub> = 45.3 Hz (Figure 5.5) *plus* the already described ***mer*-18**. The chemical shifts and coupling constant (<sup>2</sup>*J*<sub>PP</sub>) are similar to the ones observed for an analogous ruthenium (II) complex bearing an *N,P,N* phosphite ligand in “*fac*” configuration, reported by Wagler *et al.*, as described above.<sup>129</sup>

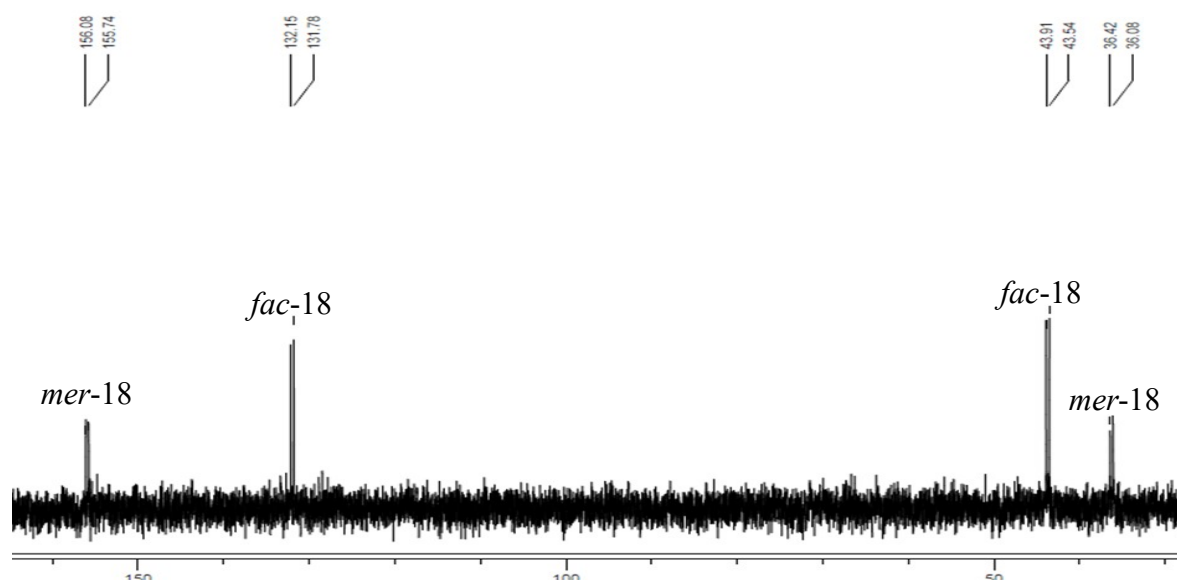


Figure 5.5.  $^{31}\text{P}\{^1\text{H}\}$  NMR spectrum (121.5 MHz) at 298 K of **fac-18** in wet THF with a  $\text{MeCN-d}_3$  inner capillary as reference.

Despite many attempts, it was not possible to achieve the quantitative formation of **fac-18**. Solvents with different polarities, the addition of more water, longer reaction times, and higher or lower temperatures were some of the parameters tested in order to promote the selective and quantitative formation of **fac-18**, without success. So far, the role of the water is not clear. This subject will be studied in detail in a forthcoming extension of this work.

Crystals suitable for X-ray diffraction analysis were obtained from a saturated THF solution of **mer-18** at  $-30\text{ }^\circ\text{C}$  (Figure 5.6). The solid-state structure of **mer-18** reveals that the ligand **1** binds the Ru center as a tridentate chelate through the P atom and two N donors from the heterocycles (N1 and N2 in Figure 5.6). The ligand **1** adopts a  $\kappa^3(\text{N},\text{P},\text{N})$  meridional coordination mode (pincer-like) as shown in the solution  $^1\text{H}$  NMR spectrum. Also, a “cis” spatial configuration for both phosphorus atoms is observed, as expected from the  $^2J_{\text{PP}}$  coupling constants from the  $^{31}\text{P}\{^1\text{H}\}$  NMR. The uncoordinated quinoline unit is oriented away from the metal center. The complex **mer-18** exhibits a considerable distorted octahedral geometry, since the plane defined by P1/Ru1/N1 is not co-planar with the plane N2/Ru1/Cl2. The deviation from co-planarity between those planes is 12.14 degrees. Selected bond distances and angles are listed in Table 5.1. The two aromatic units of both the coordinated quinoline moieties and the free quinoline fragment are slightly twisted, as indicated by the a) C3–C8–C9–N1 / C7–C8–C9–C4, b) C12–C17–C18–N2 / C16–C17–C18–C13 and c) C21–C26–C27–N3 / C25–C26–C27–C22 torsion angles ( $0.26$ ,  $1.19$  and  $1.86^\circ$  respectively, Table 5.1).

Likewise, crystals of **fac-18** were obtained by slow diffusion of diethyl ether into a saturated DMC solution **fac-18** + **mer-18** at room temperature (Figure 5.7). The solid-state structure of **fac-18** reveals that the ligand **1** binds the Ru center as a tridentate chelate through the P atom and two N atoms of the heterocycles (N1 and N2 in Figure 5.7). In this case, ligand **1** displays a  $\kappa^3(N,P,N)$  facial coordination mode, as well as “*cis, cis, cis*” spatial configuration for all of the donor atoms (P, N, Cl). Again, the other quinoline unit is oriented away from the metal center. For **fac-18** the deviation from co-planarity between the planes P1/Ru1/N1 and P2/Ru1/Cl1 is only 3.5 degrees, significantly less than in **mer-18**. Nevertheless, the complex exhibits a distorted octahedral geometry, since there are some angles that are quite away from the ideal 90° value. Selected bond distances and angles are listed in Table 5.1 The two aromatic units of both coordinated quinoline moieties are slightly twisted, as indicated by the a) C3–C8–C9–N1 / C7–C8–C9–C4 and b) C12–C17–C18–N2 / C16–C17–C18–C13 torsion angles (Quin1: 0.46° and Quin2: 0.63° in Table 5.1), also in lesser extent than in **mer-18**. In this case, the two aromatic units of the uncoordinated quinoline moiety are completely co-planar (Quin3 in Table 5.1).

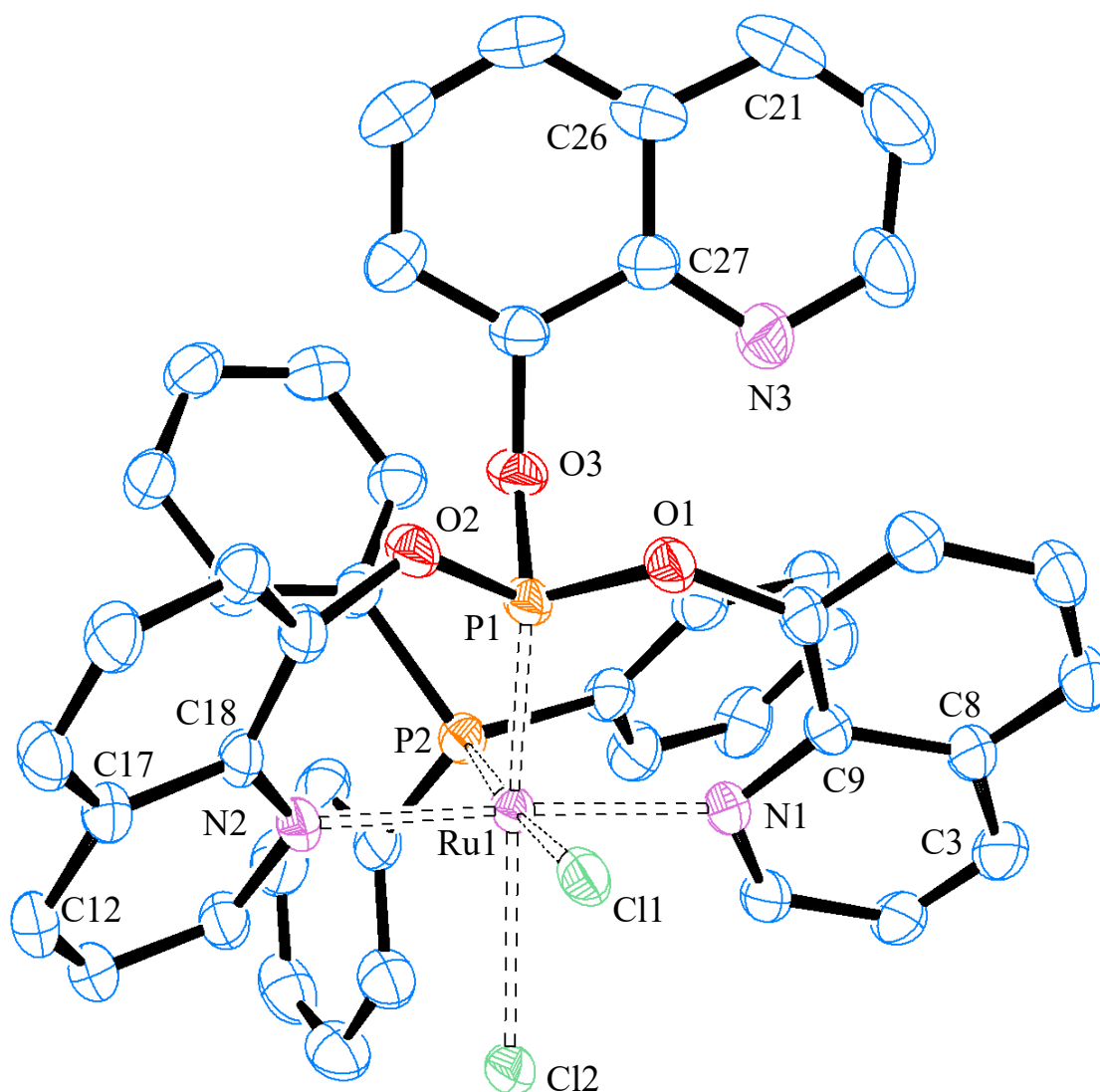


Figure 5.6. ORTEP drawing of the molecular structure of the complex  $[mer-\kappa^3(N,P,N)\{P(OQuin)_3\}RuCl_2(PPh_3)]$ , **mer-18**. Thermal ellipsoids are drawn at 40% probability level. Hydrogen atoms and THF solvate molecule have been removed for clarity.

In **mer-18**, the Ru–P1, Ru–P2, Ru–Cl1 and Ru–Cl2 distances are 2.112(1), 2.348(1), 2.462(1) and 2.524(1) Å, respectively, with an angle between both phosphorus atoms P1–Ru–P2 of 92.9(2)°. Both six-membered rings defined by Ru–N1–C9–C4–O1–P1 and Ru–N2–C18–C13–O2–P1 show a roughly twisted half-chair-shaped conformation. The bite angles P1–Ru–N1 and P1–Ru–N2 are 91.2(1)° and 89.7(1)°, respectively. The P1–O(1–3) bond distances, 1.629(6), 1.598(5), and 1.618(6) Å, are quite shortened with regard to the free ligand but similar to the ones observed when **1** is coordinated to a metal center (Pd or Rh, Chapters III and IV respectively). This is a result of the strong  $\sigma$ -donation from the phosphite to the metal center. The O–P–O angles are around 100°. Concerning **fac-18**, the bond distances around the metal center are almost identical to those of **mer-18** despite of the different coordination mode of **1**. Interestingly, in **fac-18** the highly strained bite angle P1–Rh–N2, which is slightly bigger than



80°, illustrates the strong geometry distortion around the ruthenium atom. The Ru-Cl2 (*trans* to P1) distance is bigger than Ru-Cl1 in both cases (*mer/fac-18*), again as a consequence of the strong  $\sigma$ -donation from the phosphite to the metal center.

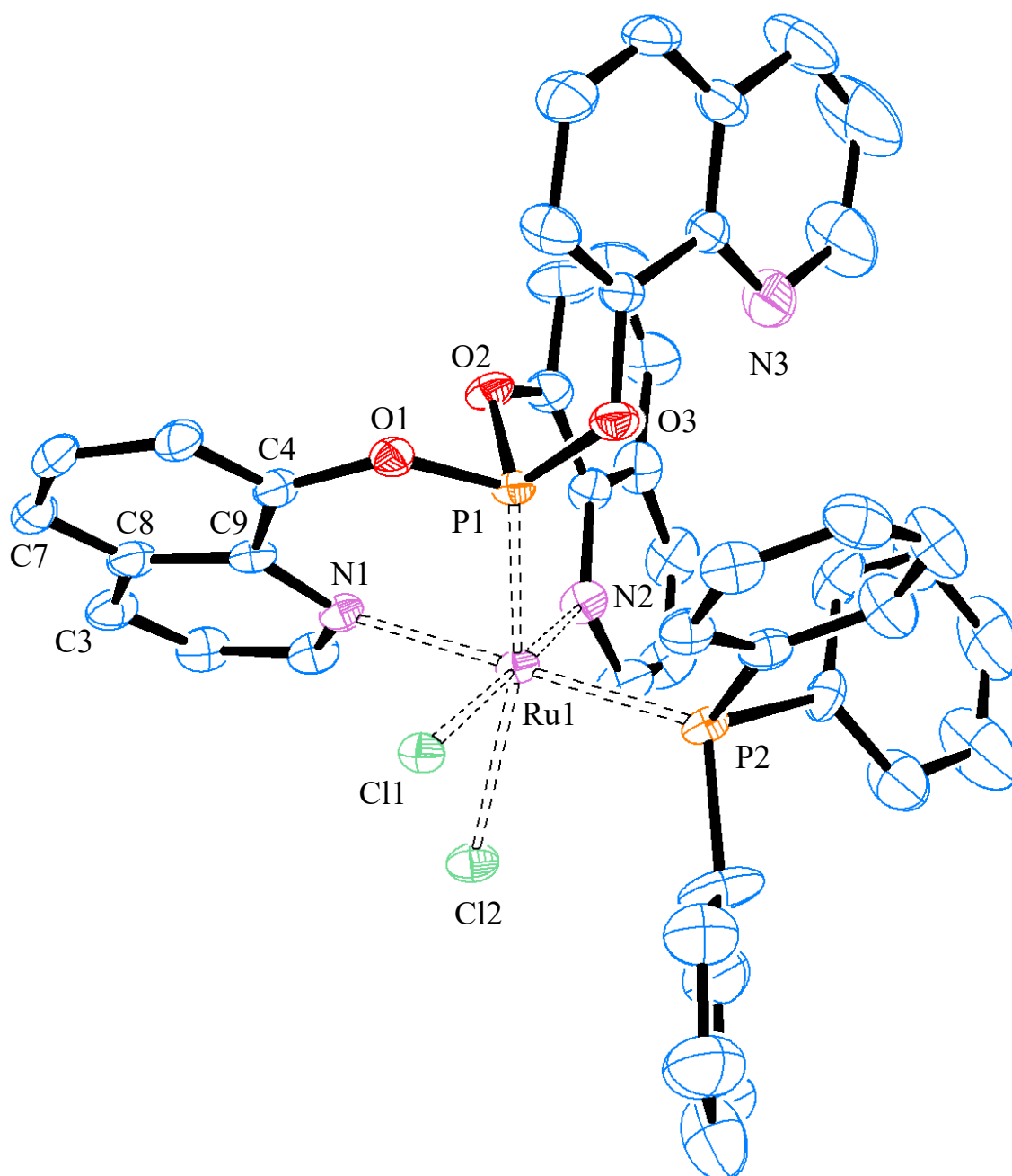


Figure 5.7. ORTEP drawing of the molecular structure of the complex [*fac*- $\kappa^3(N,P,N)\{P(OQuin)_3\}RuCl_2(PPh_3)$ ], *fac-18*. Thermal ellipsoids are drawn at 50% probability level. Hydrogen atoms and DCM/Et<sub>2</sub>O solvate molecules have been removed for clarity.

Some bond parameters observed in *mer-18* and *fac-18* are comparable with the ones described for the related compounds **K1** and **M1** (Figure 5.8 and Table 5.1), reported by Braunstein *et al.*<sup>128</sup> The phosphonite-based complex **M1** has both a Ru-P1 distance and P,N bite angles similar to *mer-18* and *fac-18*. Regarding the chlorine atom *trans* to the P donor in

the chelate, the Ru-Cl distance in *mer*-**18** and *fac*-**18** are longer than in **K1**, due to the fact that **K1** bears a phosphine ligand while both *mer*/*fac*-**18** bear a phosphite ligand.

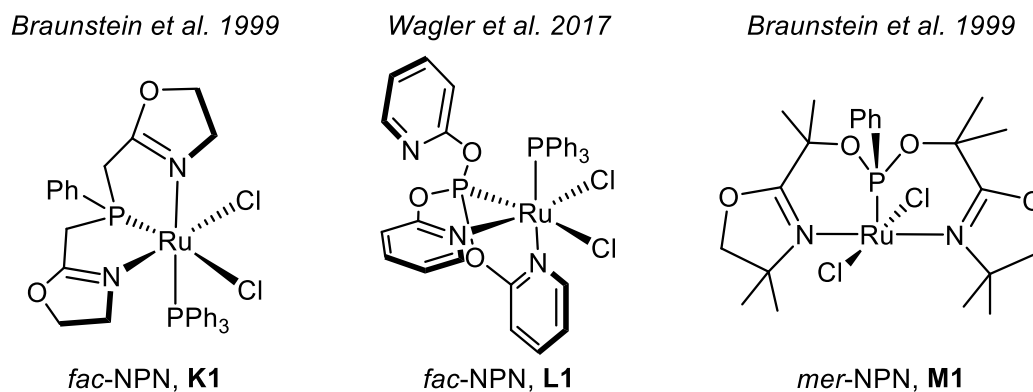
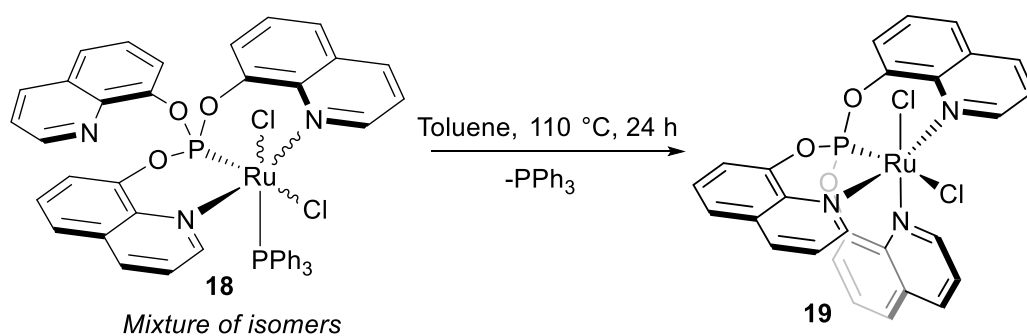


Figure 5.8. Ru(II)-halide complexes bearing *N,P,N* ligands.

Based on the results obtained so far with DCM and THF, toluene was chosen as solvent to study its possible effect on the isomeric resolution of the mixture **18**. In this sense, such a mixture was heated up to 110 °C in toluene at NMR scale. Surprisingly, under these conditions **18** (mixture of isomers) was transformed into a single new ruthenium complex (**19**). This novel compound is the result of PPh<sub>3</sub> dissociation from the starting material, as confirmed by <sup>31</sup>P{<sup>1</sup>H} NMR spectroscopy. This evidence clearly indicates that the three species observed by <sup>31</sup>P{<sup>1</sup>H} NMR for **18** (Figure 5.1) are in fact spatial isomers. The metal complex **19** is highly stable toward air, moisture and high temperatures, even if when refluxed in DMSO (189 °C) for 2 h. The last aspect is very remarkable since one of the major limitations for transition metal complexes as homogeneous catalysts is that most of them decompose at elevated temperatures, which prevents their use in highly endothermic reactions.

The complex [ $\kappa^4P,N_3$ -{P(OQuin)<sub>3</sub>}RuCl<sub>2</sub>], (**19**, Scheme 5.4), is accessible by refluxing **18** in toluene (dry solvent is not required) for 24 h. When the reaction mixture was allowed to reach room temperature, the coordination compound was obtained after solvent evaporation and repetitive washing with diethyl ether in order to remove occluded toluene and free PPh<sub>3</sub> and/or OPPh<sub>3</sub>. The product is a deep-orange solid, which is highly thermally stable, air and moisture stable and was isolated in high yield (90%). LIFDI-MS, elemental analysis and NMR spectroscopic data (<sup>1</sup>H, <sup>13</sup>C{<sup>1</sup>H}, and <sup>31</sup>P{<sup>1</sup>H}) of **19** are in accordance with and support the proposed formulation. Protons and carbons were assigned using 2D NMR analysis such as COSY, HMQC and HMBC.



Scheme 5.4. Synthesis of the ruthenium (II) complex **19**,  $[\kappa^4(P,N_3)\{P(\text{OQuin})_3\}\text{RuCl}_2]$ .

The  $^{31}\text{P}\{^1\text{H}\}$  NMR spectrum shows a singlet (s) resonance at  $\delta$  162.4 ppm (Figure 5.9a). The phosphorus resonance is downfield shifted for **1** with regard to the corresponding value for the free ligand. The  $^1\text{H}$  NMR spectrum confirms the  $\kappa^4(P,N_3)$  coordination mode of the tris(8-quinolyl)phosphite ligand, as indicated by the presence of downfield shifted signals for the pyridine scaffold of the quinoline (Figure 5.8b).

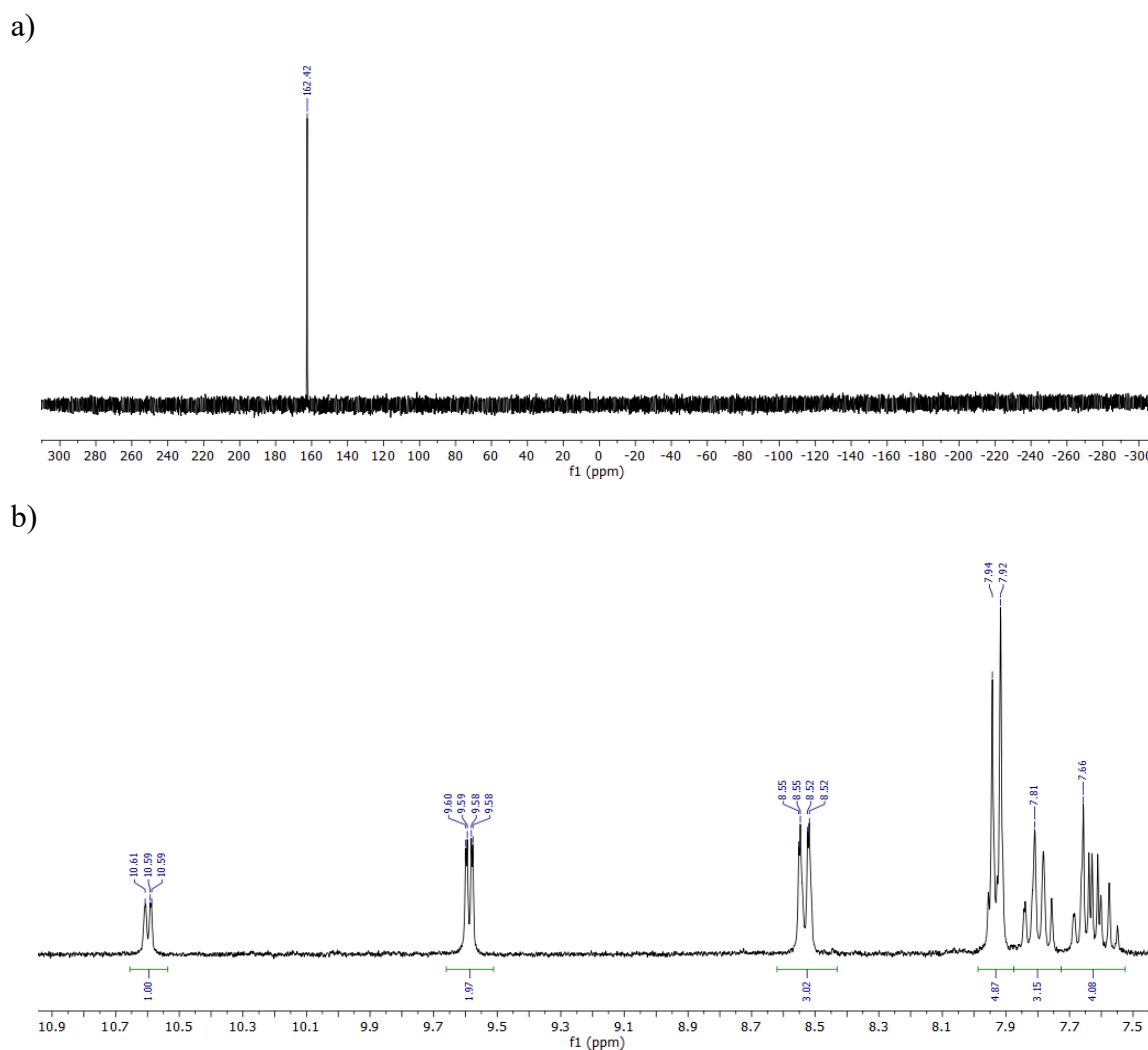


Figure 5.9. a)  $^{31}\text{P}\{^1\text{H}\}$  NMR spectrum (121.5 MHz) and b)  $^1\text{H}$  NMR spectrum (300.1 MHz) at 298 K of **19** in  $\text{CD}_2\text{Cl}_2$ .

The resonances at  $\delta$  10.6 ppm (*d*,  $^3J_{\text{HH}} = 8.5$ , 1H) and  $\delta$  9.6 ppm (*dd*,  $^3J_{\text{HH}} = 5.4$  Hz,  $^4J_{\text{HH}} = 1.5$  Hz, 2H) belong to the *orto* H atoms to the N atom in the pyridine scaffold and their integral values exhibit a 1/2 ratio (Figure 5.8b). The resonance at 8.54 ppm, that integrates to three protons, is an overlapped signal for all three *meta* H atom to the N donor in the pyridine fragment. The signals for the *para* H atoms and the protons from the phenolic rings are very overlapped between 7.99 and 7.55 ppm, accounting for the remaining twelve protons. The equivalency between two quinolines suggests that there is a symmetry plane into the metal complex molecule. Since two quinolines are equivalent and the other one is slightly different, **1** should adopt a scorpion-shape coordination mode. This tetradenticity of **1** is confirmed in the solid stated molecular structure of **19** (Figure 5.10).

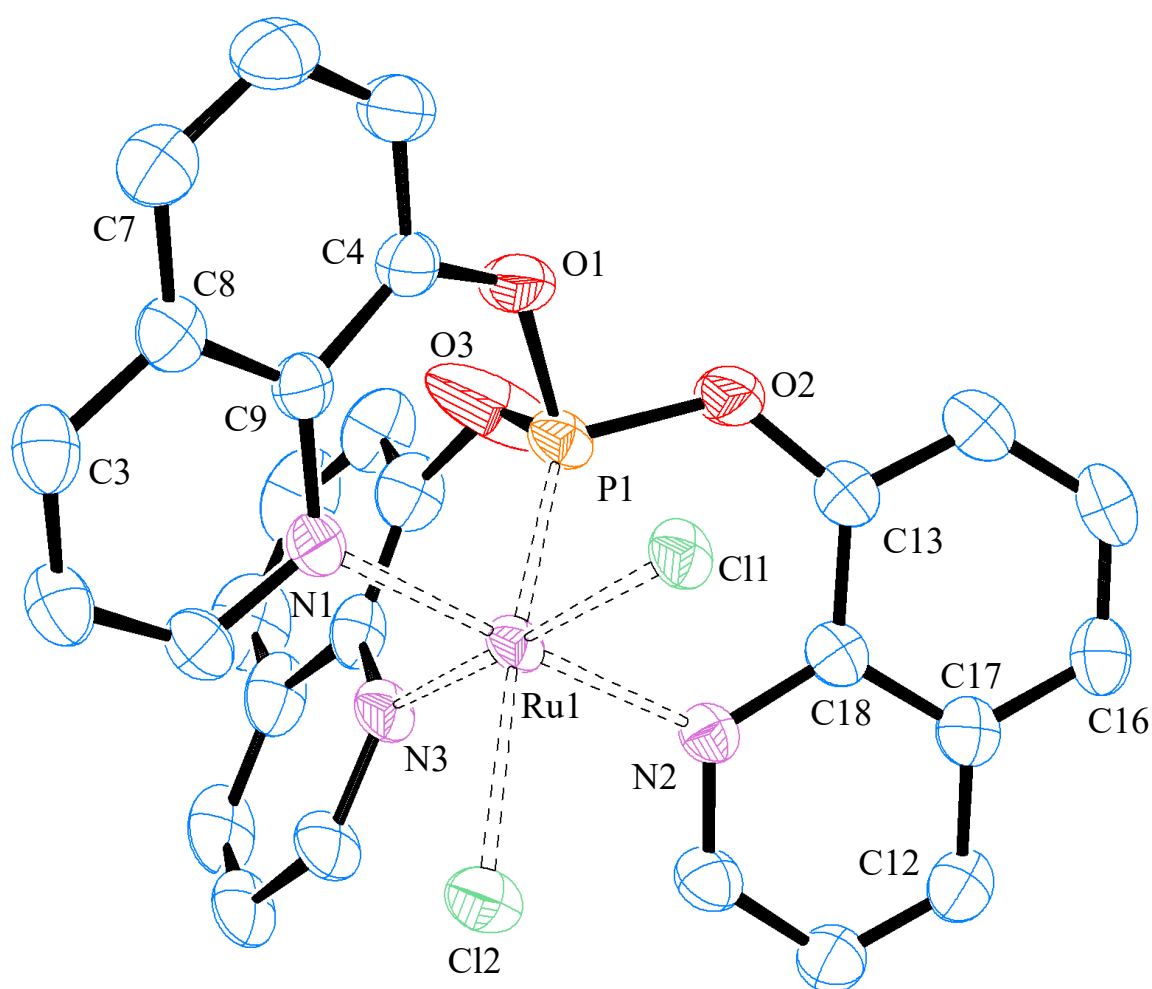


Figure 5.10. ORTEP drawing of the molecular structure of the complex  $[\kappa^4(P,N_3)\{P(OQuin)_3\}RuCl_2]$ , **19**. Thermal ellipsoids are drawn at 40% probability level. Hydrogen atoms and THF/Et<sub>2</sub>O solvate molecules have been removed for clarity.

Crystals suitable for X-ray diffraction analysis were obtained from a saturated THF solution of **19** at  $-30$  °C (Figure 5.10). The solid state structure of **19** reveals that the ligand **1** binds the metal center as a tetradentate chelate through the P atom and the N donors of the

heterocycles (N1, N2 and N3 in Figure 5.10), showing a  $\kappa^4(P,N_3)$  scorpionate-like coordination mode as already observed by solution  $^1\text{H}$  NMR. The complex exhibits a slightly distorted octahedral geometry, since the plane P1/Ru1/N1 is not co-planar with the plane N2/Ru1/Cl2 and such deviation is just about 5 degrees. Nevertheless, the planes P1/Ru1/N3 and Cl1/Ru1/Cl2 are co-planar, forming a symmetry plane for the whole molecule as evidenced previously by the  $^1\text{H}$  NMR spectroscopic data. The two *trans*-coordinated quinoline moieties are slightly twisted, as indicated by the torsion angles ( $0.54^\circ$ ), while the *cis*-coordinated one is completely within the symmetry plane of the complex.

Complex **19** is the first example of a ruthenium complex bearing a tetradentate phosphite ligand in a scorpionate-like coordination mode. In **19**, the Ru–P1, Ru–Cl1 and Ru–Cl2 distances are 2.054(1), 2.400(2), and 2.550(1) Å, respectively, with an angle between both phosphorus atoms P1–Ru–P2 of  $92.9(2)^\circ$ . The two six-membered rings defined by Ru–N1–C9–C4–O1–P1 and Ru–N2–C18–C13–O2–P1 show a roughly twisted half-chair-shaped conformation, while the metallocycle defined by Ru–N3–C27–C22–O3–P1 is near to planarity. Bite angles P1–Ru–N1, P1–Ru–N2 and P1–Ru–N3 are  $89.6(1)^\circ$ ,  $89.6(1)^\circ$  and  $92.3(1)^\circ$ , respectively. Again, the P1–O(1-3) bond distances, 1.591(4), 1.591(4), and 1.578(8) Å, are quite shortened with regard to the free ligand and slightly shorter than in *mer*-**18** and *fac*-**18**. The O–P–O angles are around  $100^\circ$ . The Ru–Cl2 (*trans* to P1) distance is shorter than in *mer*-**18** and *fac*-**18**.

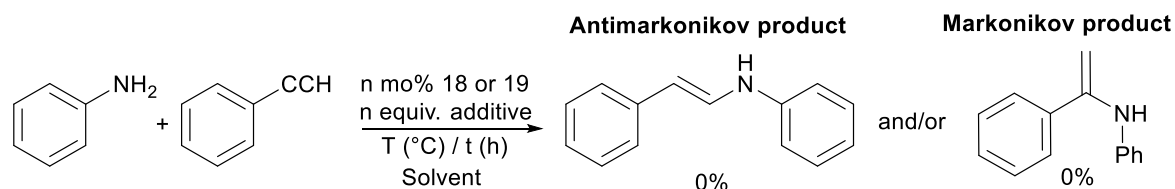
Once the synthesis and characterization of the novel ruthenium complexes had been performed, the potential of such compounds as homogeneous catalysts was explored. Based on previous reports for similar complexes, several types of reactions were considered as possible targets for catalytic applications. For instance, the hydroamination of alkynes was studied but the Ru complexes were inactive for such transformations. Nevertheless, dehydrogenative reactions, such as dehydrogenation of formic acid and dehydrogenative oligomerization of primary and secondary silanes, returned very interesting results, which will be discussed in the following sections.

Table 5.1. Selected geometric parameters (Å, °) for **18**, **18<sup>β</sup>**, **19** and related compounds

	<i>mer</i> - <b>18</b>	<i>fac</i> - <b>18<sup>β</sup></b>	<b>19</b>	<b>K1</b>	<b>M1</b>
<i>Bond distance (Å)</i>					
Ru—P1	2.112(1)	2.119 (1)	2.054 (1)	2.222 (8)	2.088 (6)
Ru—P2	2.348(1)	2.325 (1)	-	2.299 (8)	-
Ru—N1	2.139(3)	2.197 (4)	2.114 (5)	2.085 (2)	2.085 (2)
Ru—N2	2.122(3)	2.141 (4)	2.114 (5)	2.129 (2)	2.093 (2)
Ru—Cl1	<i>trans</i> to P2	<i>trans</i> to N2	<i>trans</i> to N3	<i>trans</i> to N1	2.381 (6)
	2.462(1)	2.473 (4)	2.400 (2)	2.425 (7)	
<i>trans</i> to P1	2.524(1)	2.503 (1)	2.550 (1)	2.468 (7)	2.385 (6)
Ru—Cl2					
<i>Angles (°)</i>					
P1—Ru—N1	91.2 (1)	90.8 (1)	89.6 (1)	-	91.6 (5)
P1—Ru—N2	89.7 (1)	81.2 (1)	89.6 (1)	-	85.7 (5)
P1—Rh—P2	92.9 (2)	98.1 (4)	-	98.6 (3)	-
P1—Ru—Cl1	83.8 (4)	92.1 (4)	86.2 (6)	92.9 (5)	101.5 (2)
P1—Ru—Cl2	165.7 (4)	166.8 (4)	170.7 (6)	164.4 (3)	101.0 (2)
P2—Rh—N1	95.3 (1)	94.9 (3)	-	-	-
Cl1—Rh—Cl2	81.9 (4)	84.7 (4)	84.5 (6)	91.9 (3)	157.3 (2)
$\bar{x}$ O—P—O	99.7 (2)	99.5 (2)	98.4 (3)	-	-
<i>Torsion angles of coordinate quinoline moiety (°)</i>					
Quin1					
C3—C8—C9—N1 / C7—C8—C9—C4	0.26	0.46	0.54	-	-
Quin2					
C12—C17—C18—N2 / C16—C17—C18—C13	1.19	0.63	0.54	-	-
Quin3					
C21—C26—C27—N3 / C25—C26—C27—C22	1.86	0	0	-	-

### 5.3 The hydroamination of alkynes and the new Ru(II) complexes.

The compounds **mer-18** and **19** were tested as catalyst precursors for the hydroamination of alkynes to yield enamines. Aniline and phenyl acetylene were used as model substrates (Scheme 5.5). A wide range of reaction parameters, including catalyst(s), solvent(s), different temperatures, additive(s) (base or inorganic salts), and the relative ratio of the different reaction components, were screened.

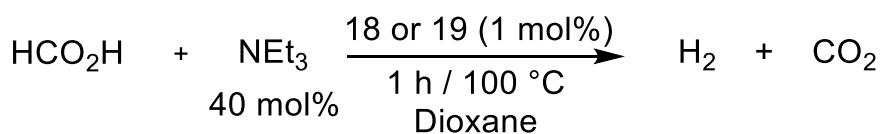


Scheme 5.5. Hydroamination of phenylacetylene with aniline. Complexes **mer-18** and **19** are not active (pre)catalysts for this reaction.

The reaction progress was monitored by  $^1\text{H}$  NMR and GC-MS but unfortunately, despite many attempts, the addition of the NH bond across the C-C triple bond was not achieved. Higher temperatures, higher catalyst loadings or longer reaction times, as well as different substrates were not enough to promote such reactivity. Likewise, compounds **1**, **4** and **11** were also tested as catalysts for this reaction without any success. Under the studied reaction conditions, **mer-18**, **19**, **11**, **4** and **1** itself are not suitable catalyst precursors to promote the hydroamination of alkynes.

### 5.4 Catalytic decomposition of formic acid by the Ru-P(OQuin)<sub>3</sub> complexes.

Hydrogen is an essential reactant in the chemical industry, though its generation from renewable sources and storage in a safe and reversible manner remain challenging. Formic acid ( $\text{HCO}_2\text{H}$ ) is a promising source and storage material in this regard. In the past decade, coordination compounds with pincer ligands became highly attractive catalysts for all kind of (de)hydrogenation reactions.<sup>130</sup> In particular, ruthenium based PNP-pincer complexes allowed for efficient reduction of esters,<sup>131</sup> ketones,<sup>132</sup> nitriles,<sup>133</sup> related hydrogen auto-transfer catalysis,<sup>134</sup> and dehydrogenations<sup>135</sup>. All these processes are enabled by metal-ligand cooperation, where both the metal and the ligand are directly involved in bond activation processes.<sup>136</sup> In this section, well-defined ruthenium-based (**mer-18** and **19**) catalytic systems capable of dehydrogenating  $\text{HCO}_2\text{H}$  to  $\text{CO}_2$  and  $\text{H}_2$  in acidic media are described (Scheme 5.6).



Scheme 5.6. Dehydrogenation of HCO<sub>2</sub>H catalyzed by *mer*-18 or 19.

Several reaction parameters, including catalysts, temperature, use of organic base, and the relative ratio of the different reaction components, were screened. In a simple apparatus (Figure 5.11) containing a 1 M solution of HCO<sub>2</sub>H in dioxane, 40 mol% of NEt<sub>3</sub> and 1 mol% of catalyst *mer*-18 or 19 and equipped with a reflux condenser (with circulating cooling fluid at -20 °C), about 43% yield was achieved after 1 h at 100 °C (Figure 5.12, blue line). The reaction progress was monitored by measuring the displaced volume of produced gas with an inverted water burette. In the absence of the catalyst (blank run) only 8% was achieved (Figure 5.12, grey line) confirming the catalytic nature of the transformation. No conversion was found when the reaction was performed at room temperature or 50 °C. Other solvents, polar (THF, DMF) or non-polar (toluene, benzene) did not improve the catalytic performance. Temperatures above 100 °C are required and this fact represents a disadvantage when it is compared to previous reported systems.<sup>137</sup>

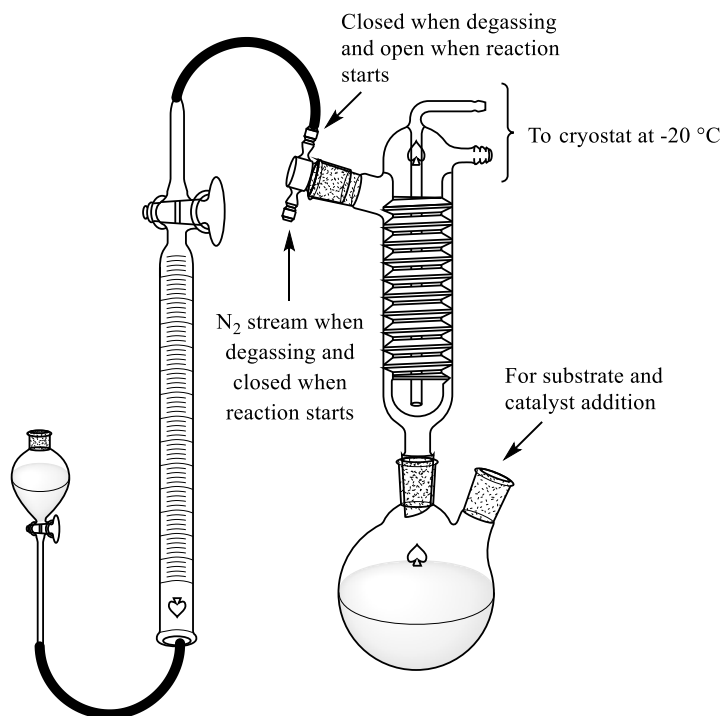


Figure 5.11. Technical set-up for HCO<sub>2</sub>H dehydrogenation in an open system. The production of H<sub>2</sub> can be monitored with a water burette.

Considering that *mer*-18 is transformed into 19 at high temperatures (Scheme 5.4), 19 was used as the catalyst precursor for the rest of the formic acid dehydrogenation experiments. An improvement was achieved when the concentration of formic acid was increased to 2 M in



dioxane, obtaining 63% yield (Figure 5.12, green line). The conversion dropped significantly when the reaction was carried out in the absence of base (Figure 5.12, yellow line). A full conversion of  $\text{HCO}_2\text{H}$  in dioxane at  $100\text{ }^\circ\text{C}$  to produce  $\text{H}_2$  and  $\text{CO}_2$  was achieved after 1 h when the catalyst loading was increased to 2 mol% (Figure 5.12, orange line). The advantage of the catalytic system presented here is based on the robustness of **19**, since it could be reused up to seven times without significantly losing its activity, resulting in a cumulative TON of 350. However, the performance of **19** is still away from the best-known catalyst for formic acid dehydrogenation, which exhibits a TON of 92000 and a TOF of  $9424\text{ h}^{-1}$  using an inexpensive iron-based complex.<sup>138</sup>

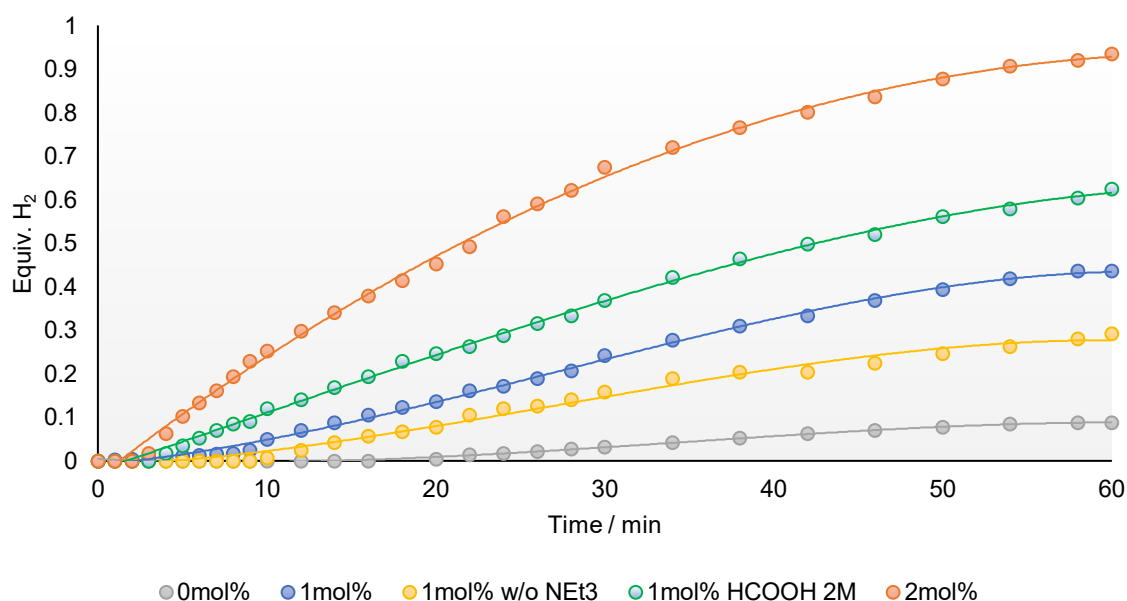
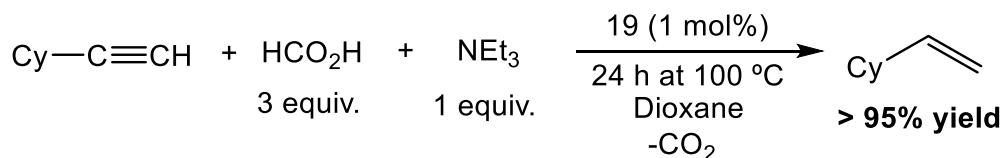


Figure 5.12. Hydrogen formation on time from formic acid decomposition catalyzed by **19**.

Besides the catalytic decomposition of formic acid, the use of it in hydrogen transfer reactions was also investigated, in particular for the reduction of alkynes. The partial hydrogenation of non-activated alkynes to get the corresponding olefins is a challenging and attractive transformation. Therefore, the partial reduction of cyclohexylacetylene was used as model reaction for such a study (Scheme 5.7).



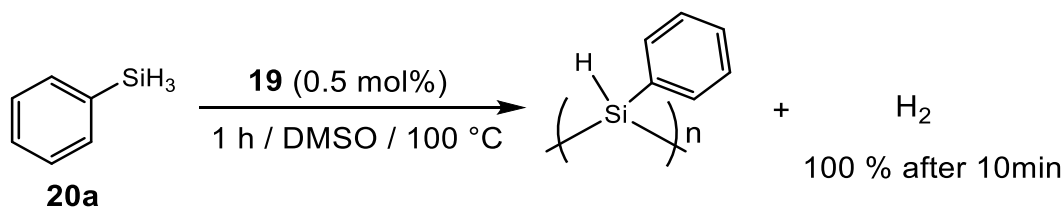
Scheme 5.7. Reduction of cyclohexyl acetylene catalyzed by **19** using  $\text{HCO}_2\text{H}$  as  $\text{H}_2$  source.

Here the reaction conditions tested were those derived from the formic acid dehydrogenation experiments. The reaction mixture was monitored by  $^1\text{H}$  NMR and GC-MS.

The partial reduction of cyclohexyl acetylene to yield the corresponding alkene in dioxane at 100 °C was achieved in a selective manner (>95% after 24 h). In the absence of the catalyst (blank run) no product was detected, confirming the catalytic nature of the transformation. Further extension of this approach should be performed in order to optimize this catalytic application for **19**.

### 5.5 Homo-/Heterodehydrocoupling reaction of silanes catalyzed by **19**.

The pursuit of clean and straightforward alternatives to the Wurtz coupling for the synthesis of polysilanes has focused the attention on dehydrocoupling reactions of silanes catalyzed by transition metals.<sup>139</sup> Among the complexes investigated for their ability to produce these polymers<sup>140</sup> two classes have emerged. One type includes group 4 metallocene derivatives such as Zr,<sup>141</sup> Ti<sup>142</sup> and Hf-metal complexes,<sup>143</sup> which are considered the most active for catalytic dehydrocoupling, since they are capable of producing oligomers and polymers (up to  $M_n = 9920$  and  $M_w = 20400$ , around 200 monomer units) from primary silanes such as PhSiH<sub>3</sub>.<sup>144</sup> These catalysts commonly require the use of additive such as *n*BuLi or similar in a stoichiometric ratio. Catalysts in the second class include many late transition metal complexes based on Ru,<sup>145</sup> Rh,<sup>146</sup> Pt,<sup>147</sup> Ni<sup>148</sup> and Fe<sup>149</sup> bearing phosphine ligands. These are considered relatively inactive for dehydrocoupling, since they do not produce long chains. Actually, up to date, the reaction of primary or secondary silanes with electron-rich metal complexes (Late-TM) appears to give low molecular weight materials (<5 monomer units). Late TM complexes usually catalyze the coupling of secondary silanes to yield dimer, trimer or cyclic oligomers with 4- to 5-membered rings.<sup>150</sup> Their application to the large scale synthesis of these useful oligosilanes has been discouraged by the known activity of such catalysts for a competitive reaction called redistribution of substituents at silicon.<sup>151</sup> In this section, a well-defined ruthenium catalyst (**19**) was tested as a suitable homogeneous catalyst for the dehydrogenative homo-/heterocoupling of silanes to yield polysilanes and polysiloxanes, respectively (Scheme 5.8 / Table 5.2 and 5.3).



Scheme 5.8. Dehydrocoupling of phenylsilane to yield polyphenylsilane catalyzed by **19**.

The catalytic dehydrogenative coupling of silanes was optimized using phenylsilane (**20a**, PhSiH<sub>3</sub>) as a model substrate and compound **19** as catalyst precursor. In a simple apparatus (Figure 5.11) containing a 1 M solution of PhSiH<sub>3</sub> in DMSO and 0.5 mol% of **19**,

about 1 equiv. of H<sub>2</sub> was released after 10 min at 100 °C (Figure 5.13 and entry 1 in Table 5.2). The amount of H<sub>2</sub> was quantified using an inverted burette as show in Figure 5.11., above. Prolonged reaction time result in further dehydrogenation. The generation of a fully dehydrogenated silicon material is suggested by the formation of 1.5 equiv. of H<sub>2</sub> after 1 hour (Figure 5.13). Such full dehydrogenation of primary silanes is the first ever reported for a transition metal-based catalyst (homogeneous or heterogeneous phase). This example presents a new avenue in the production of silicon-based materials and should be further explored in forthcoming research works.

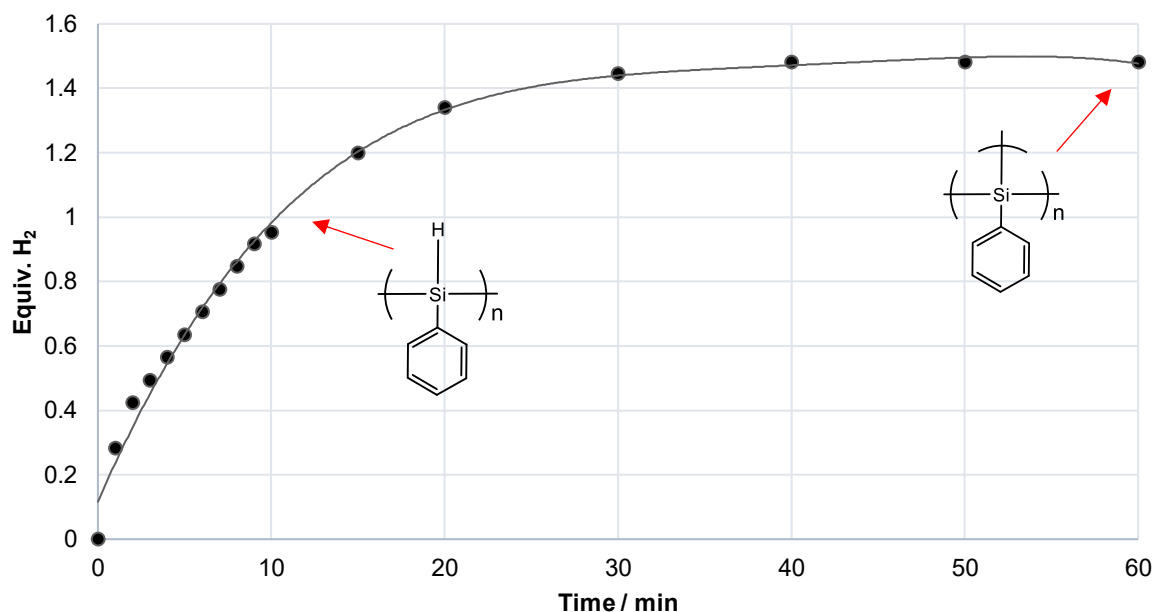


Figure 5.13. Hydrogen formation from dehydrocoupling of phenylsilane catalyzed by **19**.

Although the reaction mixture is a clear solution, without apparent metallic mirror or particles, a poisoning test was performed to investigate the (homogeneous or heterogeneous) nature of the catalytic reaction. When the dehydrocoupling of **20a** was performed in the presence of an excess of Hg (*ca.* 1000 equiv. regard to **19**), no inhibition of the catalytic activity was observed. In the absence of the catalyst (blank run) no hydrogen evolution was observed confirming the catalytic nature of the transformation. No conversion was found when such a reaction was performed at room temperature or 50 °C, thus confirming that temperatures above 100 °C are required. Catalyst loadings of **19** below 0.5 mol% results in a dramatically fall down of the activity (*ca.* <50%). Also, common Ru(II) complexes such as [Cp\*RuCl(COD)], [Cp\*RuCl]<sub>4</sub>, [(*p*-cymene)RuCl]<sub>2</sub> and [(PPh<sub>3</sub>)<sub>3</sub>RuCl<sub>2</sub>] were tested as catalyst (1 mol%) were not effective; hydrogen evolution merely reached 0.2 equiv. H<sub>2</sub> for catalyst [(PPh<sub>3</sub>)<sub>3</sub>RuCl<sub>2</sub>], while [(*p*-cymene)RuCl]<sub>2</sub> produced around 0.1 equiv. H<sub>2</sub>. Ru(II) complexes such as [Cp\*RuCl(COD)] and [Cp\*RuCl]<sub>4</sub>, were inactive catalyst for such transformation.

The turnover numbers (TON) and turnover frequencies (TOF) for the first dehydrogenation step are 200 and 1200 h<sup>-1</sup> respectively. Again, complex **19** could be reused up to 3 times without significantly losing its catalytic activity, reaching a cumulative TON = 600 and producing 900 mmol of H<sub>2</sub> *per* mmol of catalyst. The methodology presented here is one of the most efficient systems based on a late transition metal compounds and avoids the use of additives such as *n*BuLi or similar, commonly required in the metallocene-based catalysis.<sup>148-151</sup> The resulting polymeric material can be easily isolated from the reaction mixture by hexane extraction and solvent evaporation as a colorless oil.

GPC analysis is the appropriate technic to study the molecular weight distribution of the obtained polysilicon materials. Unfortunately, this method was not available in the facilities where the research was conducted. Hence, <sup>1</sup>H, <sup>13</sup>C{<sup>1</sup>H} and <sup>29</sup>Si{<sup>1</sup>H} NMR were used to analyze the reaction mixture as well as the isolated material (Figure 5.14). After 10 min reaction, the <sup>1</sup>H NMR spectrum shows, for both the reaction mixture and the isolated product (Figure 5.14a), signals corresponding to the partially dehydrogenated polymer (PhSiH)<sub>n</sub>. The broad signal between 8-7 ppm corresponds to the aromatic hydrogens and the broad resonance around 5.50 ppm corresponds to the Si-H moiety. This spectrum is in accordance with the one reported for oligomers of PhSiH<sub>3</sub> (>10 monomer units).<sup>150c,152</sup> The <sup>29</sup>Si{<sup>1</sup>H} NMR spectrum (Figure 5.14b) shows a broad signal in a wide range between -70 and -130 ppm, for which the maximum is around -108 ppm. Corey *et al.* reported the <sup>29</sup>Si{<sup>1</sup>H} spectra for oligomers of PhSiH<sub>3</sub> ranging from 4 to 20 monomer units by using deconvolution methods.<sup>153</sup> Linear oligomers with 4 monomer units show a signal at around -59 ppm, while linear oligomers with 20 monomer units resonate around -63 ppm. Apparently, the longer the oligomer's chain length, the lower are the frequencies of the <sup>29</sup>Si{<sup>1</sup>H} resonances. Likewise, the broad resonance is associated to a linear atactic configuration of the formed polyphenylsilane, which means a random distribution of the substituents around the silicon atoms.<sup>160</sup> Accordingly, the NMR spectroscopic data suggests that **19** catalyzes the selective formation of linear oligomers of PhSiH<sub>3</sub> (>20 monomer units). Dimer, trimer, cyclic oligomers or substituent redistribution products were not detected in the reaction mixture. the catalytic properties are remarkable because, to other knowledge, other late transition metal catalysts generally do not produce oligomers with more than 5 monomeric units. GPC analysis should be performed in forthcoming extensions of these results.

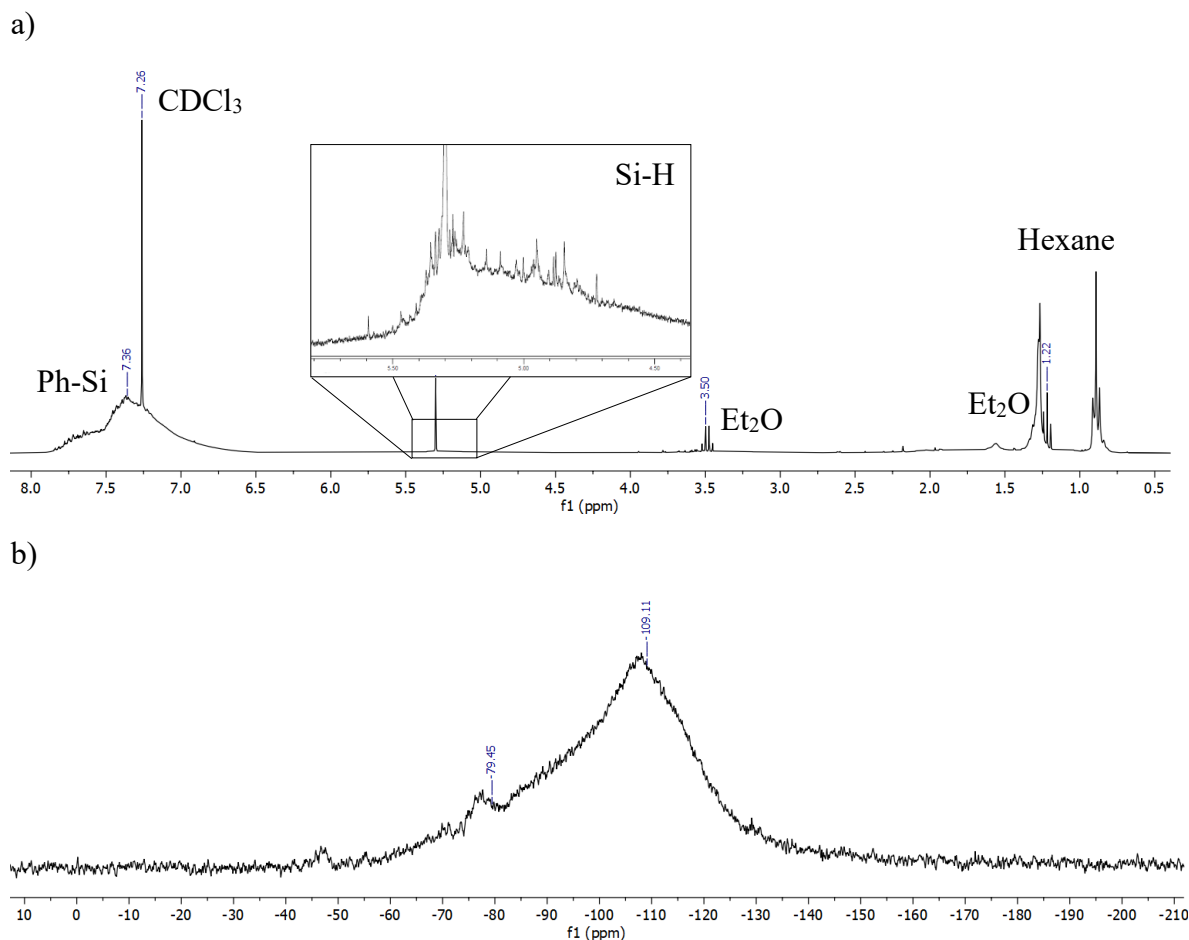
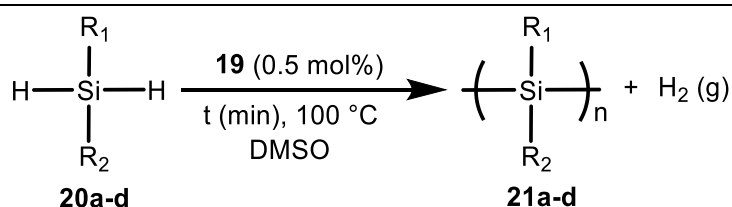


Figure 5.14. a)  $^1\text{H}$  NMR spectrum (300.1 MHz) and b)  $^{29}\text{Si}\{^1\text{H}\}$  NMR spectrum (71.5 MHz) at 298 K of the isolated polymeric material  $(\text{PhSiH})_n$  in  $\text{CDCl}_3$ .

Under the optimized reaction conditions (1 M DMSO solution of hydrosilane, 0.5 mol% of **19** and 100 °C) a screening of selected secondary hydrosilanes was performed to explore the scope and limitations of the catalytic system developed (Table 5.2). Diphenyl- (**20b**, entry 2), methylphenyl- (**20c**, entry 3) and di-*tert*-buthylsilane (**20d**, entry 4) were used as substrates. After 1 h *ca.* 1 equiv.  $\text{H}_2$  was released for both **20b** and **20c**, while for **20d** the reaction required at least 1.5 h. The requirement of longer reaction times for these substrates can be attributed to the steric hindrance around the Si atom and the relative strong Si-H bond. For example, the Si-H bond energy for **20a** is around 377 kJ/mol while for **20c** is 382 kJ/mol.<sup>154</sup> As already described for **20a**, dimers, trimers, cyclic oligomers or substituent redistribution products of hydrosilanes were not detected in the reaction mixtures of **20b-d**.

Table 5.2 Dehydrogenative oligomerization of hydrosilanes catalyzed by **19**.<sup>a</sup>



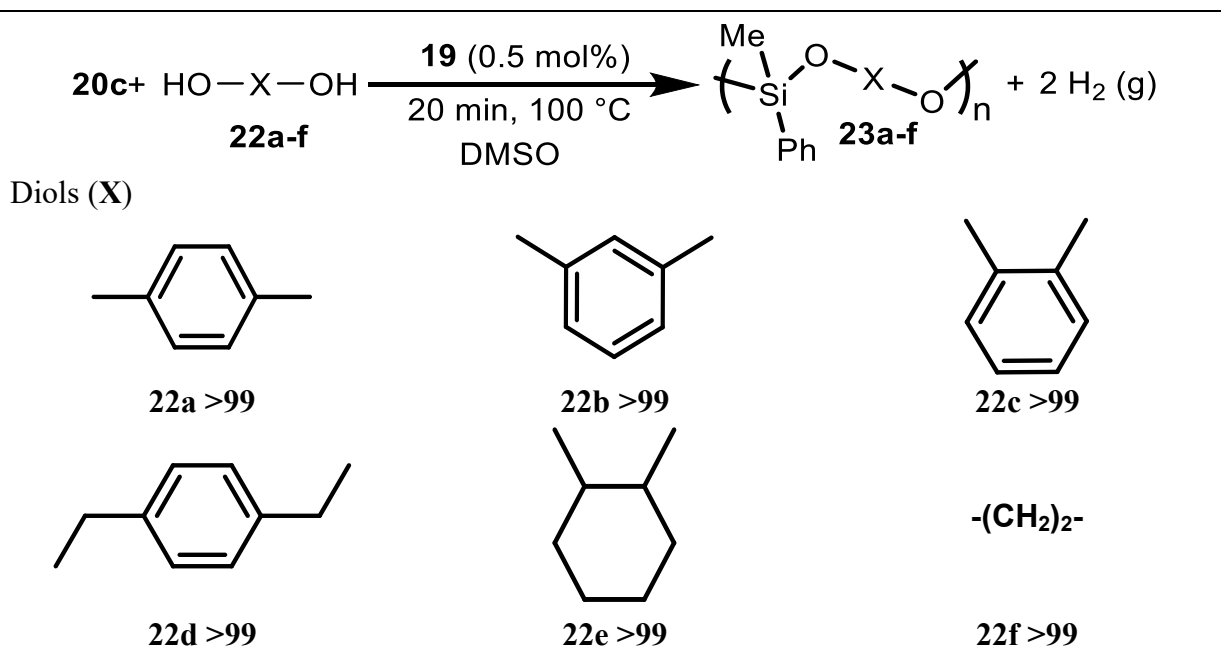
Entry	Substrate	R1	R2	Time (min)	Yield (%) <sup>b,c</sup>
1	<b>20a</b>	H	Ph	10	>99
2	<b>20b</b>	Ph	Ph	60	>99
3	<b>20c</b>	Me	Ph	60	>99
4	<b>20d</b>	tBu	tBu	90	>99

[a] Silane (500  $\mu\text{mol}$ , 1 M) and **19** (2.5  $\mu\text{mol}$ , 0.5 mol%) were stirred in 0.5 mL DMSO at 100  $^\circ\text{C}$  for the specified reaction time (see above). [b] Conversion determined by hydrogen evolution measured in an inverted water burette. [c] Average of three individual reactions.

Regarding another type of polymeric silicon materials of interest, poly(phenylmethyl)siloxanes are important additives for the production of synthetic oil for automotive engines. Its production under attractive and feasible methodologies is of greatest relevance. As consequence, the copolymerization of **20c** with different diols was investigated (Table 5.3). By treating **20c** with 1,4-hydroquinone (**22a**), resorcinol (**22b**) or the sterically hindered catechol (**22c**) in the presence of catalytic amounts of **19** (0.5 mol%) the formation of about 2 equiv.  $\text{H}_2$  after 20 min at 100  $^\circ\text{C}$  was observed. The release of 2 equiv.  $\text{H}_2$  is consistent with the cross-dehydrogenative reactivity. This reaction is faster in comparison with the homo-dehydrocoupling of phenylmethylsilane (**20c**) and it can be attributed to the acidic nature of the protons in the hydroquinones. In the absence of catalyst, no hydrogen evolution was observed. Remarkably, diols such as *p*-phenyldimethanol (**22d**), 1,2-cyclohexanediol (**22e**) and ethylenglicol (**22f**) reacted almost quantitatively within 20 min as shown by the formation of 2 equiv.  $\text{H}_2$  in every case. The corresponding polymeric materials were isolated as nearly colorless oils after extraction with hexane and solvent evaporation. Once again, the starting silane, dimers, trimers, cyclic oligomers or substituent redistribution products of hydrosilanes were not detected in the reaction mixtures.

Table 5.3. Dehydrogenative co-polymerization of hydrosilanes and alcohols catalyzed by **19**.

a-c



[a] Silane (500  $\mu\text{mol}$ , 1 M), diol (500  $\mu\text{mol}$ ) and **19** (2.5  $\mu\text{mol}$ , 0.5 mol%), were stirred in 0.5 mL DMSO at 100  $^\circ\text{C}$  for 20 min. [b] Conversion determined by hydrogen evolution measured in an inverted water burette. [c] Average of three individual reactions.

## 5.6 Chapter conclusion.

In conclusion, the reaction between **1** and  $[(\text{PPh}_3)_3\text{RuCl}_2]$  generates a mixture of diastereomers with the general formula  $[\kappa^3(N,P,N)\{\text{P}(\text{OQuin})_3\}\text{RuCl}_2(\text{PPh}_3)]$  (**18**). This isomer mixture can be easily resolved by refluxing it in not dry dichloromethane yielding *mer*-**18**. Alternatively, the complex *fac*-**18** is the main product when the mixture is refluxed in not dry THF. The solid-state molecular structure for both *mer*-**18** and *fac*-**18** were obtained. The role of water in the isomerization of  $[\kappa^3(N,P,N)\{\text{P}(\text{OQuin})_3\}\text{RuCl}_2(\text{PPh}_3)]$  is not clear yet, but it will be subject of further studies. The compounds *mer/fac*-**18** are stable toward air and moisture, but they further under elimination of  $\text{PPh}_3$  to yield  $[\kappa^4(P,N_3)\{\text{P}(\text{OQuin})_3\}\text{RuCl}_2]$  (**19**), at temperatures above 100  $^\circ\text{C}$ . The new metal complex **19** is very stable at high temperatures, which is desirable for applications. Neither *mer*-**18** nor **19** are suitable catalysts for the hydroamination of alkynes. Also, *mer*-**18** and **19** were tested as catalyst for the catalytic decomposition of formic acid, an important  $\text{H}_2$ -storage material. Full conversion of  $\text{HCO}_2\text{H}$  into  $\text{H}_2$  and  $\text{CO}_2$  was achieved after 1 h in dioxane at 100  $^\circ\text{C}$ , using 2 mol% **19** as catalyst loading. Due to the robustness of **19**, it could be reused up to 7 times without losing its activity and a total TON of 350 was achieved. However, this is still far away from the best-known

reported system for such reaction with a TON of 92000 and a TOF of 9424 h<sup>-1</sup>. Similarly, the reduction of cyclohexyl acetylene using formic acid as H<sub>2</sub>-source and **19** as catalyst was performed. The partial reduction of cyclohexyl acetylene to yield the corresponding alkene in dioxane at 100 °C was achieved in a selective manner (>95%) after 24 h. Further studies should be devoted to this reaction.

Interestingly, **19** is a promising catalyst for the dehydrogenative coupling of primary and secondary silanes as well as its copolymerization with diols. This transformation operates under relatively simple conditions, namely 0.5 mol% **19**, 100 °C and DMSO as solvent. This methodology avoids the use of additives such as <sup>n</sup>BuLi. Also, the fact that the reaction requires a stoichiometric amount of silanes and diols makes it attractive from the perspective of atom-economy. Structural modifications of **19**, such as hydride(s) instead of chloride(s) donors, are envisioned in order to improve/increase its catalytic activity. Additionally, the exploration of the *microscopic reversibility principle* is also proposed. It implies that the Ru(II)-complex **19** should also catalyze the hydrogenolysis of oligo- and polysilanes. In theory, the hydrogenation of Si–Si bonds [ $\Delta H_{\text{diss}}$  (Si–Si) = 73.1–88.0 kcal.mol<sup>-1</sup>] is energetically feasible than the dehydrogenation of silanes [ $\Delta H_{\text{diss}}$  (Si–H) >90 kcal.mol<sup>-1</sup>].<sup>155</sup>

## 5.7 Experimental section.

*Synthesis of {mer-( $\kappa^3$ N,P,N)-(tris(8-quinoliny))phosphite}(tris(phenyl)phosphine)ruthenium dichloride, mer-18.*

Under an argon or nitrogen atmosphere and at –20 °C, a THF solution of P(OQuin)<sub>3</sub> (96.6 mg, 0.21 mmol, 0.042 mM) was added to a THF solution of [(PPh<sub>3</sub>)<sub>3</sub>RuCl<sub>2</sub>] (200.0 mg, 0.21 mmol, 0.021 mM) and the mixture was stirred for 2 h. Then, the mixture was slowly warmed up to room temperature and stirred overnight. All volatile materials were removed under reduced pressure. The isomer mixture of [ $\kappa^3$ (N,P,N){P(OQuin)<sub>3</sub>}RuCl<sub>2</sub>(PPh<sub>3</sub>)] is obtained after washing with dry Et<sub>2</sub>O (3 x 7 mL) in order to remove free PPh<sub>3</sub> and possibly its corresponding oxide. The resulting bright-yellow solid was dried under vacuum (170.0 mg, 91% yield) <sup>31</sup>P{<sup>1</sup>H} NMR (121.5 MHz, THF/C<sub>6</sub>D<sub>6</sub>-inner, 25 °C)  $\delta$  = 154.1 ppm (d, <sup>2</sup>J<sub>PP</sub> = 42.4 Hz, 1) 136.3 ppm (d, <sup>2</sup>J<sub>PP</sub> = 54.3 Hz, 1) 128.1 ppm (d, <sup>2</sup>J<sub>PP</sub> = 50.2 Hz, 1) 51.6 ppm (d, <sup>2</sup>J<sub>PP</sub> = 54.2 Hz, PPh<sub>3</sub>) 42.17 ppm (d, <sup>2</sup>J<sub>PP</sub> = 50.2 Hz, PPh<sub>3</sub>) 35.2 ppm (d, <sup>2</sup>J<sub>PP</sub> = 41.6 Hz, PPh<sub>3</sub>). For the isomeric resolution, the mixture was dissolved in wet CH<sub>2</sub>Cl<sub>2</sub> (20 mL) and refluxed for 2 h. After cooling down to room temperature, 200 mg MgSO<sub>4</sub> were added as dehydrating agent. Filtration and removal of solvent under reduced pressure afforded the *mer*-isomer as a bright-yellow solid (160.0 mg, 85% yield). Suitable crystals for X-ray diffraction were obtained from a saturated THF solution of **18<sup>a</sup>** at –30 °C. <sup>1</sup>H NMR (400.1 MHz, DCM-d<sub>2</sub>, 25 °C):  $\delta$  = 11.54 (t, <sup>3</sup>J<sub>HH</sub> = 4.4 Hz, 1H), 10.18 (dd, <sup>3</sup>J<sub>HH</sub> = 5.4 Hz, <sup>4</sup>J<sub>HH</sub> = 1.5 Hz, 2H), 8.40 (dd, <sup>3</sup>J<sub>HH</sub> = 8.3 Hz, <sup>4</sup>J<sub>HH</sub> = 1.5 Hz, 1H), 8.16 (dd, <sup>3</sup>J<sub>HH</sub> = 8.2 Hz, <sup>4</sup>J<sub>HH</sub> = 1.5 Hz, 2H), 7.90 (dd, <sup>3</sup>J<sub>HH</sub> = 8.2 Hz, <sup>4</sup>J<sub>HH</sub> = 5.4 Hz, 1H),



7.65-7.30 (m, overlapped signal, 11H), 7.19 (t,  $^3J_{\text{HH}} = 6.9$  Hz, 3H), 6.94 (td,  $^3J_{\text{HH}} = 8.2$  Hz,  $^4J_{\text{HH}} = 2.2$  Hz, 6H), 6.71 (t,  $^3J_{\text{HH}} = 9.3$  Hz, 6H).  $^{13}\text{C}\{^1\text{H}\}$  NMR (150.9 MHz, DCM- $d_2$ , 25 °C):  $\delta = 159.7, 157.6, 144.7$  (d,  $J = 4.1$  Hz), 144.6, 144.2, 141.2, 140.5, 133.3, 133.2, 131.3, 130.9, 130.8, 129.9 (d,  $J = 2.1$  Hz), 128.0, 127.7, 127.6, 127.5, 122.9 (d,  $J = 1.8$  Hz), 122.5, 122.3, 122.2, 121.7.  $^{31}\text{P}\{^1\text{H}\}$  NMR (121.5 MHz, DCM- $d_2$ , 25 °C)  $\delta = 154.1$  ppm (d,  $^2J_{\text{PP}} = 42.4$  Hz, 1) 35.2 ppm (d,  $^2J_{\text{PP}} = 41.6$  Hz, PPh<sub>3</sub>) LIFDI-MS:  $m/z$  calc. for  $\text{C}_{27}\text{H}_{18}\text{N}_3\text{O}_3\text{Cl}_2\text{PRu}$  635.40 [ $\text{M}^+-\text{PPh}_3$ ]<sup>+</sup>; found 635.40. Anal. Calcd. for  $\text{C}_{45}\text{H}_{33}\text{N}_3\text{O}_3\text{Cl}_2\text{P}_2\text{Ru} \cdot 1.5 \text{CH}_2\text{Cl}_2 \cdot 0.5 \text{C}_4\text{H}_{10}\text{O}$ : C, 54.66; H, 3.47; N, 3.96. Found: C, 54.84; H, 3.89; N, 4.00. The *fac*-isomer was prepared similarly, but using not dry THF instead of  $\text{CH}_2\text{Cl}_2$ . Suitable crystals for X-ray diffraction of the *fac*-isomer were obtained by slow diffusion of diethyl ether into a saturated DMC solution of *fac*-**18** + *mer*-**18** at room temperature. The  $^{31}\text{P}\{^1\text{H}\}$  NMR for *fac*-**18** was recorded using the crystalline sample for XRD.  $^{31}\text{P}\{^1\text{H}\}$  NMR (121.5 MHz, MeCN- $d_3$ , 25 °C)  $\delta = 131.9$  ppm (d,  $^2J_{\text{PP}} = 45.3$  Hz, 1) 43.7 ppm (d,  $^2J_{\text{PP}} = 45.3$  Hz, PPh<sub>3</sub>).

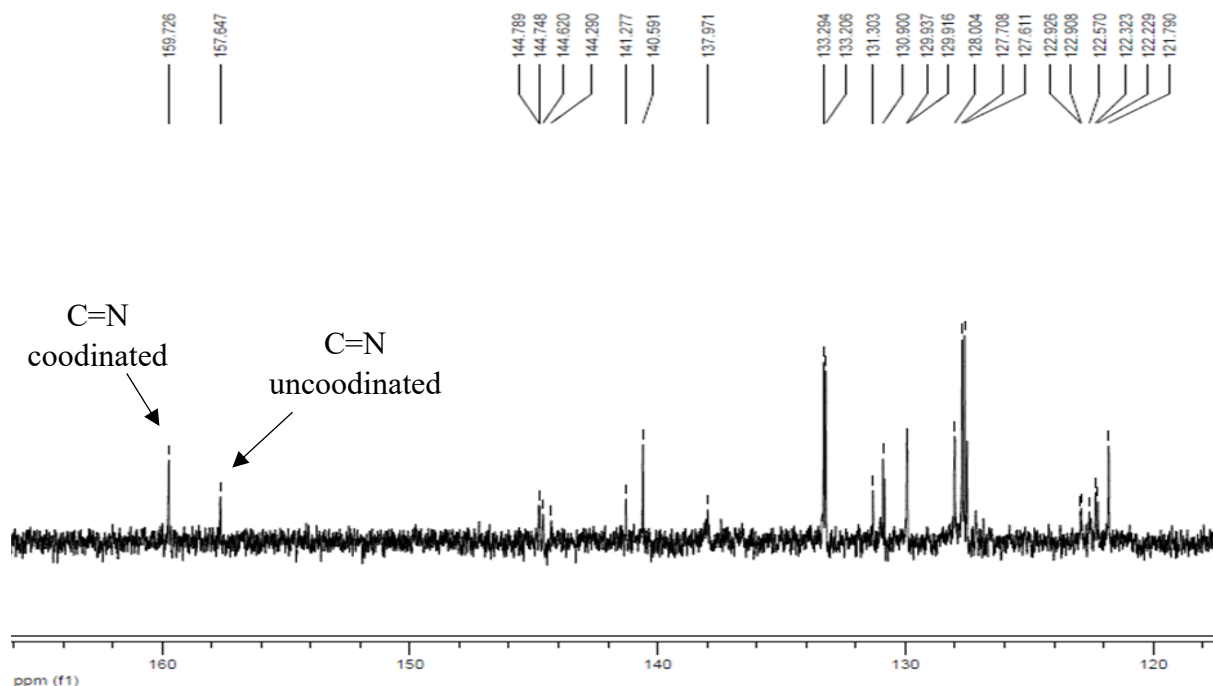


Figure 5.15.  $^{13}\text{C}$  NMR spectrum (150.9 MHz) at 298 K of *mer*-**18** in  $\text{CD}_2\text{Cl}_2$ .

#### *Synthesis of $\{(\kappa^4\text{P}, \text{N}_3)\text{-(tris(8-quinolynyl))phosphite}\}$ ruthenium dichloride, **19**.*

Under atmospheric conditions, the complex  $[\text{mer-}\kappa^3(\text{N}, \text{P}, \text{N})\text{-}\{\text{P}(\text{OQuin})_3\} \text{RuCl}_2(\text{PPh}_3)]$  (200.0 mg, 0.22 mmol) and toluene (*ca.* 20 mL, directly from a commercially available bottle of toluene >99%) were placed in a one-neck round-bottom flask equipped with a reflux condenser. The resulting suspension was refluxed overnight. Then, the mixture was cooled to room temperature and all volatile materials were removed under reduced pressure. The complex **19** was obtained after washing with dry  $\text{Et}_2\text{O}$  (2 x 10 mL) as a bright-orange solid (135.0 mg, 95% yield). Crystals suitable for X-ray diffraction analysis were obtained from a saturated THF

solution of **19** at  $-30\text{ }^{\circ}\text{C}$ .  $^1\text{H}$  NMR (400.1 MHz,  $\text{DCM-d}_2$ ,  $25\text{ }^{\circ}\text{C}$ ):  $\delta = 10.60$  (d,  $^3J_{\text{HH}} = 8.5$ , 1H), 9.59 (dd,  $^3J_{\text{HH}} = 5.4\text{ Hz}$ ,  $^4J_{\text{HH}} = 1.5\text{ Hz}$ , 2H), 8.54 (dd,  $^3J_{\text{HH}} = 8.5\text{ Hz}$ ,  $^4J_{\text{HH}} = 1.7\text{ Hz}$ , 3H), 7.98-7.90 (m, 12H).  $^{13}\text{C}\{^1\text{H}\}$  NMR (150.9 MHz,  $\text{DMSO}/\text{C}_6\text{D}_6$ ,  $25\text{ }^{\circ}\text{C}$ ):  $\delta = 156.6$ , 156.4, 146.9, 146.9, 146.3, 140.6, 140.1, 132.0, 131.8, 129.1, 129.1, 129.0, 129.0 (overlapped into solvent signal) 123.5, 123.4, 122.9, 122.8, 122.3.  $^{31}\text{P}\{^1\text{H}\}$  NMR (121.5 MHz,  $\text{DCM-d}_2$ ,  $25\text{ }^{\circ}\text{C}$ )  $\delta = 154.1$  ppm (s) LIFDI-MS:  $m/z$  calc. for  $\text{C}_{27}\text{H}_{18}\text{N}_3\text{O}_3\text{Cl}_2\text{PRu}$  635.40  $[\text{M}]^+$ ; found 635.40. Anal. Calcd. for  $\text{C}_{27}\text{H}_{18}\text{N}_3\text{O}_3\text{Cl}_2\text{PRu} \cdot 2\text{CHCl}_3 \cdot \text{C}_4\text{H}_8\text{O}$ : C, 41.89; H, 2.94; N, 4.44. Found: C, 42.10; H, 2.43; N, 4.39. Note: the preparation of **19** from isolated *mer*-**18** or the initial isomer mixture is indifferent, both starting materials afford the quantitative formation of **19** following the above-mentioned methodology.

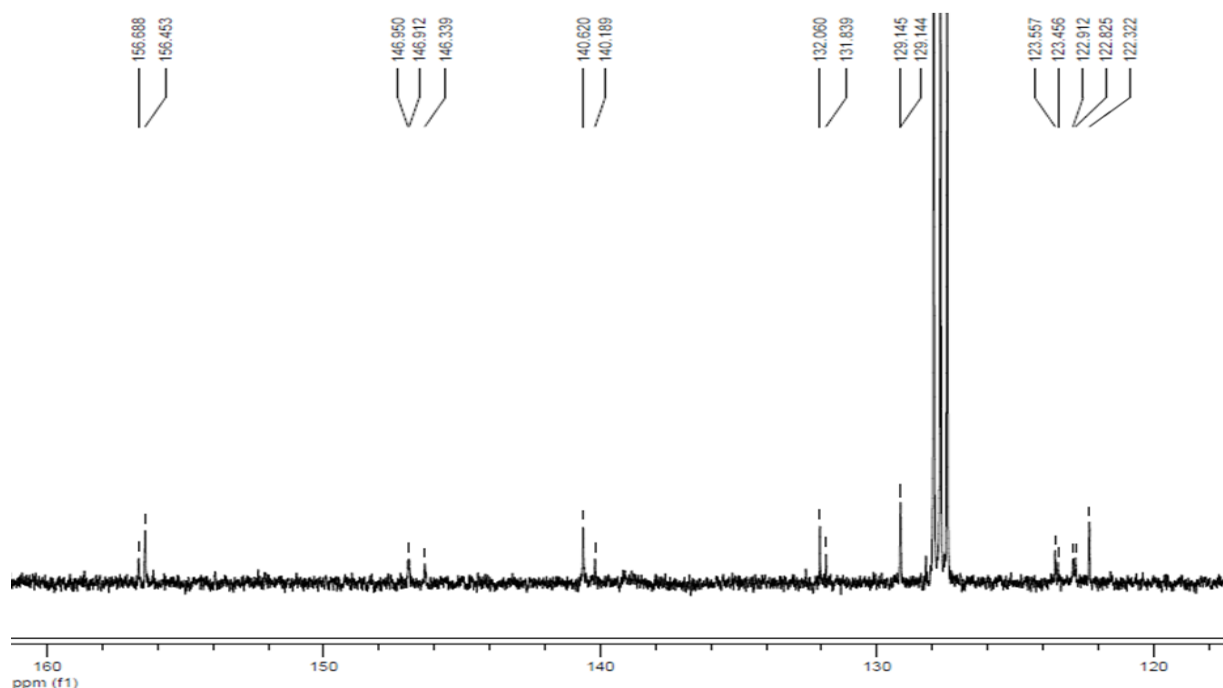


Figure 5.16.  $^{13}\text{C}$  NMR spectrum (150.9 MHz) at 298 K of **19** in  $\text{DMSO}/\text{C}_6\text{D}_6(\text{inner})$ .

#### *General procedure for decomposition of formic acid catalyzed by 19.*

A 5 mL two-neck round-bottom flask was connected to a reflux condenser with nitrogen inlet/outlet and the second neck was septum-capped. The apparatus was purged with nitrogen-vacuum cycles for 20 min. Distilled and degassed  $\text{H}_2\text{CO}_2$  (100.0 mg, 19.6  $\mu\text{L}$ , 0.52 mmol),  $\text{NEt}_3$  (10.5 mg, 14.5  $\mu\text{L}$ , 0.13 mmol) and dry dioxane (*ca.* 0.42 mL) were added. Then complex **19** (6.6 mg, 10.4  $\mu\text{mol}$ , 2 mol%) in  $\text{DMSO}$  (0.1 mL) was added. The reflux condenser was cooled to  $-10\text{ }^{\circ}\text{C}$  and the mixture was stirred vigorously at  $100\text{ }^{\circ}\text{C}$  for 1 h in an open system. Open system refers to the reaction flask connected to a water burette or the reaction flask open to atmosphere (Figure 5.6). The conversion was determined by hydrogen evolution measured in an inverted water burette, achieving 98% conversion to  $\text{CO}_2$  and  $\text{H}_2$  after 1 h. Volume gas collected: 24.9 mL, 0.51 mmol, 98% yield.

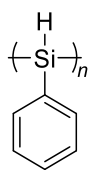
*Partial reduction of cyclohexyl acetylene with formic acid and catalyzed by 19.*

Cyclohexyl actelylene (50.0 mg, 0.46 mmol), formic acid (63.8 mg, 60.4  $\mu$ L, 1.39 mmol), triethylamine (46.7 mg, 64.4  $\mu$ L, 0.46 mmol), compound 19 (2.9 mg, 4.62  $\mu$ mol, 1 mol%), 1,3,5-trimethoxybenzene (8.5 mg, 50.8  $\mu$ mol, 11 mol%, internal standard) and dioxane (1 mL) were placed in a Schlenk tube. The resulting mixture was stirred for 24 h at 100 °C. The crude of reaction was analyzed by  $^1\text{H}$  NMR to determine the conversion of  $\text{CyC}_2\text{H}$  and the yield of the corresponding olefin using the internal standard above mentioned as reference.

*General procedure for oligomerization of hydrosilanes catalyzed by 19.*

A 5 mL two-neck round-bottom flask was connected to a reflux condenser with nitrogen inlet/outlet and the second neck was septum-capped. The apparatus was purged with nitrogen-vacuum cycles for 20 min. Distilled and degassed hydrosilane (1 mmol) and dry DMSO (*ca.* 0.9 mL) were added. Then the (pre)catalyst **19** (4.5 mg, 5.0  $\mu$ mol, 0.5 mol%) in DMSO (0.1 mL) was added. The reflux condenser was cooled to -10 °C and the mixture was vigorously stirred at 100 °C for the specified reaction time (see Table 5.2) in an open system. Open system refers to the reaction flask connected to a water burette or the reaction flask open to atmosphere (Figure 5.6). The conversion was determined by hydrogen evolution measured in an inverted water burette, achieving >99% conversion to oligomer and  $\text{H}_2$  after 10 min for  $\text{PhSiH}_3$ . Volume gas collected: 24.0 mL, 1 mmol, >99% yield. Silicon oligomers can be extracted from the reaction mixture with hexane. Then, all volatile materials were removed under reduced pressure. Silicon oligomers are obtained as a colorless oil.

**Spectroscopic data of  $(\text{PhSiH})_n$  products**



***Polyphenylsilane (21a).***

$^1\text{H}$  NMR (300 MHz,  $\text{C}_6\text{D}_6$ )  $\delta$  8-7 ppm (br, Ph-H), 5.5-4.5 ppm (s, Si-H) (see Figure 5.13a).  $^{13}\text{C}\{^1\text{H}\}$  NMR (90.5 MHz,  $\text{C}_6\text{D}_6$ ): 134, 130, 133, 134.  $^{29}\text{Si}\{^1\text{H}\}$  NMR (71.5 MHz,  $\text{C}_6\text{D}_6$ ):  $\delta$  -70 to -100 ppm (see Figure 5.13b).

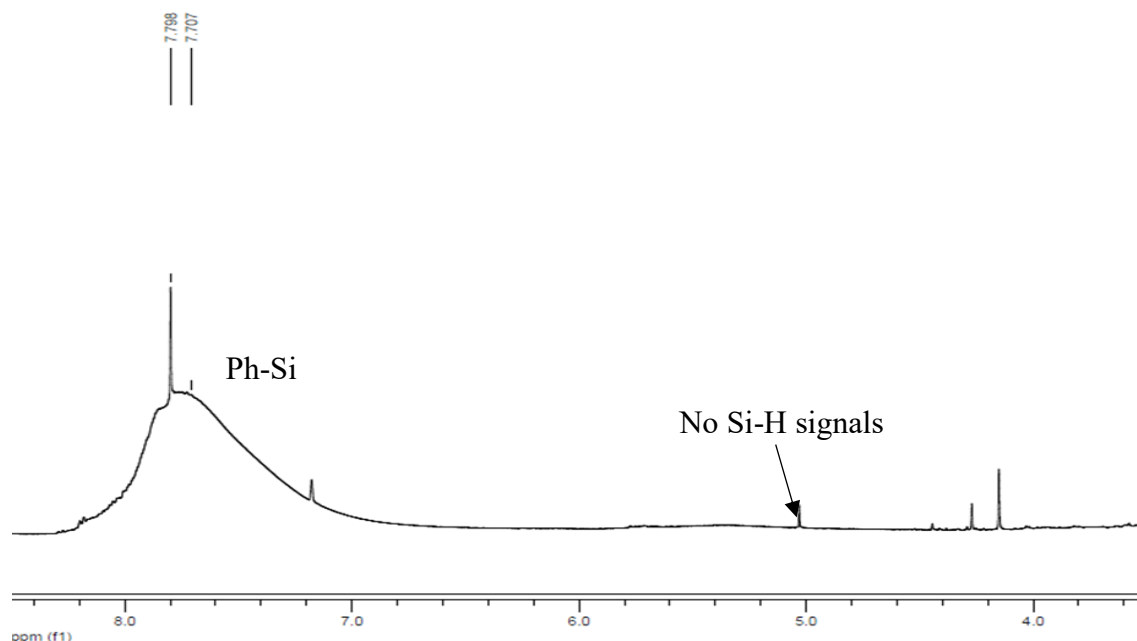


Figure 5.14.  $^1\text{H}$  NMR spectrum (300.1 MHz) at 298 K of isolated polymeric material from  $\text{PhSiH}_3$  (after 60 min reaction) in  $\text{CDCl}_3$ .

*General procedure for co-oligomerization of hydrosilanes and diols catalyzed by **19**.*

A 5 mL two-neck round-bottom flask was connected to a reflux condenser with nitrogen inlet/outlet and the second neck was septum-capped. The apparatus was purged with nitrogen-vacuum cycles for 20 min. Distilled and degassed phenylmethyilsilane (61.1 mg, 68.7  $\mu\text{L}$ , 0.5 mmol), diol (0.5 mmol) and dry DMSO (*ca.* 0.9 mL) were added. Then the complex **19** (2.2 mg, 2.50  $\mu\text{mol}$ , 0.5 mol%) in DMSO (0.1 mL) was added. The reflux condenser was cooled to  $-10\text{ }^\circ\text{C}$  and the mixture was vigorously stirred at  $100\text{ }^\circ\text{C}$  for 20 min while connected to a water burette (Figure 5.6). The conversion was determined by hydrogen evolution measured in an inverted burette, achieving >99% conversion to co-oligomer and  $\text{H}_2$  after 20 min. Volume gas collected: 24.0 mL, 1 mmol, >99% yield. Siloxane oligomers can be extracted from the reaction mixture with hexane. Subsequent solvent evaporation affords a colorless oil.

## SUMMARY AND OUTLOOK

This work describes the development of the novel ligand tris(8-quinoliny)phosphite,  $\text{P}(\text{OQuin})_3$ , (**1**) and its coordination chemistry toward selected second-row transition metal precursors. The ligand **1** binds to palladium (II), rhodium (I) and ruthenium (II), affording several new complexes with very interesting structural features, *e.g.* variable denticity of the ligand. Both **1** and its coordination compounds have been tested as (pre)catalysts for different types of transformations related to “green” chemistry, materials and fine chemical synthesis. The results presented here open a wide variety of research options for future studies.

In Chapter II, a synthetic pathway for the preparation of **1** was developed and optimized. The phosphite **1** was obtained as a white microcrystalline solid in high yield (95%) and can be prepared on a multigram scale (10 g). Phosphite **1** was fully characterized, including single crystal X-ray diffraction analysis. The compound is very sensitive to moisture, but it can be stored at room temperature for months in a glovebox. Phosphite **1** catalyzes the transfer hydrogenation of apolar  $\text{N}=\text{N}$  bonds in azoarenes using ammoniaborane (AB) as reducing agent. A series of symmetrical hydrazines with different functional groups were obtained in high yields. Although it was not possible to identify the catalytically active species, insight into the reaction mechanism was gained through stoichiometric reactions and kinetic experiments. The potential of **1** to promote novel transformations *via* bond activation in small molecules will certainly be an ongoing area of interest in our group. Additional efforts are also being directed to the synthesis of alternative  $\sigma^3\text{-P}$  compounds for the reduction of even less reactive, nonpolar covalent bonds.

Chapter III describes synthesis and characterization of the complex  $[\kappa^2P,N\text{-P}(\text{OQuin})_3\text{PdCl}_2]$  (**4**). This Pd(II) compound is a (pre)catalyst for the solvent-free oxidative coupling of primary amines to yield a series of symmetrical and unsymmetrical imines. Under relatively mild conditions and low catalyst loading,  $\text{O}_2$  in atmospheric air (30 psi, *ca.* 1.72 mmol  $\text{O}_2$ ) was used as the terminal oxidant. TONs up to 230 were reached and almost 60 molecules of the substrate were converted *per* molecule of catalyst in one hour. Kinetic measurements and *in-situ*/variable temperature NMR studies were conducted in order to understand how such reaction proceeds. The NMR spectroscopic data suggests that the dissociation (and oxidation) of the phosphite ligand does not take place under the studied conditions. Likewise, coordination of the amine substrate to the Pd atom occurs through dissociation of the quinoline arm, which indicates that the hemilabile coordination behavior of **1** is key feature, which enables catalytic activity of metal complexes.

Chapter IV describes the preparation and characterization of  $[\kappa^2P,N\text{-}\{\text{P}(\text{OQuin})_3\}\text{RhCl}(\text{PPh}_3)]$  (**11**), as well as the catalytic 1,2-regioselective hydroboration of

pyridines and quinolines. The Rh(I) complex produces 1,2-dihydropyridines and 1,2-dihydroquinolines in high yields, under mild reaction conditions and in the absence of bases or additives. TON/TOF(h<sup>-1</sup>) up to 130/8 were reached, which represents the best late transition metal-based catalytic system reported for this kind of transformation. The developed methodology can tolerate a variety of substrates with both electron-donating and electron-withdrawing substituents.

Finally, in Chapter V, [*mer*-κ<sup>3</sup>(*N,P,N*){P(OQuin)<sub>3</sub>}RuCl<sub>2</sub>(PPh<sub>3</sub>)] (**mer-18**), and [κ<sup>4</sup>(*PN*<sub>3</sub>){P(OQuin)<sub>3</sub>}RuCl<sub>2</sub>] (**19**), were synthesized, characterized and tested as catalyst for challenging transformations. By using 2 mol% of **19** the dehydrogenation of formic acid was achieved after 1 h in dioxane at 100 °C yielding H<sub>2</sub> and CO<sub>2</sub>. The complex **19** could be reused up to 7 times without losing its activity getting a TON of 350. Another catalytic application for **19** is the dehydrogenative oligomerization of primary and secondary silanes as well as its copolymerization with diols. Such reactions proceed under simple conditions: 0.5 mol% [κ<sup>4</sup>(*PN*<sub>3</sub>){P(OQuin)<sub>3</sub>}RuCl<sub>2</sub>], 100 °C and DMSO as solvent. This methodology avoids the use of additives such as *n*BuLi. Remarkably, the coupling partners, diols and silane, can be used in a stoichiometric fashion, so not excess of any of them is required.

Prior to the work presented in this thesis, the coordination chemistry of **1** was unknown and with this work it was possible to study its polydentate and hemilabile character. X-ray diffraction analysis and multinuclear NMR studies confirmed that **1** is able to behave as bi-, tri- and tetradentate ligand. These studies have also revealed, the hemilability of the N donors in **1**, which is a consequence of the competition between the three quinoline groups for coordination to the metal center. In further investigations, the coordination chemistry of **1** toward first-row metal center should be targeted, since these are earth-abundant, relatively cheap, and environmentally benign.

## REFERENCES

- <sup>1</sup> Chorkendorff, I.; Niemantsverdriet, J. W. (2007), «Concepts of modern catalysis and kinetics», Weinheim, Alemania, Wiley-VCH Verlag GmbH & Co. KGaA.
- <sup>2</sup> «Global Catalyst Market: Market Report» (2015), Tercera edición. Acmite Market Intelligence.
- <sup>3</sup> a) Anastas, P.; Warner, J. (1998), «Green chemistry: theory and practice», Nueva York, Estados Unidos, Oxford University Press Inc.; b) Anastas, P.; Kirchhoff, M.; Williamson, T., «Catalysis as a foundational pillar of green chemistry», *Appl. Catal.* **200**, A, 221, 3-13.
- <sup>4</sup> Van Leeuwen, P.W.N.M. (2004), «Homogeneous catalysis: understanding the art», Dordrecht, Holanda. Kluwer Academic Publishers.
- <sup>5</sup> a) Armor, J. N.; «A history of industrial catalysis», *Catal. Today*, **2011**, 163, 3-9, b) Mortreux, A., Petit, F. (1988), «Industrial applications of homogeneous catalysis», Dordrecht, Holanda. Springer Netherlands, c) Cornils, B., Herrmann, W. A., «Concepts in homogeneous catalysis: the industrial view», *Journal of Catalysis*, **2003**, 216, 23-31.
- <sup>6</sup> «All Nobel Prizes in Chemistry. NobelPrize.org. Nobel Media AB 2019». Extracted from: <<https://www.nobelprize.org/prizes/lists/all-nobel-prizes-in-chemistry/>>
- <sup>7</sup> Kamer, P. C. J.; Van Leeuwen, P.W.N.M. (2012), «Phosphorus(III) ligands in homogeneous catalysis: design and synthesis», Chichester, Reino Unido. John Wiley & Sons, Ltd.
- <sup>8</sup> a) Suárez, A., Pizzano, A., Fernández, I., Khiar, N., «Monodentate phosphites with carbohydrate substituents and their application in rhodium catalysed asymmetric hydrosilylation reactions», *Tetrahedron: Asymmetry*, **2001**, 12, 633-643; b) Ilia, G., Iliescu, S., Macarie, L., Popa, A., «Synthesis of Tervalent Phosphorus Esters in Biphasic System Using Potassium Phosphate as Unique Solid Base» *Heteroatom Chemistry*, **2008**, 19, 360-364, c) Grzywa, R., Sokol, A. M., Sienczyk, M., Radziszewicz, M., Kosciolk, B., Carty, M. P., Oleksyszyn, J., «New aromatic monoesters of alpha-aminoalkylphosphonic acids as inhibitors of aminopeptidase N/CD13», *Bioorg. Med. Chem.* **2010**, 18, 2930-2936; d) Amberg, M., Bergsträsser, U., Stapf, G., Hartung, J., «2-chloro-(4R,5R)-bis[(1R,2S,5R)-menth-1-ylloxycarbonyl]-1,3,2-dioxaphospholane: a practical chiral pool-derived reagent for determining enantiomeric purity of alcohols», *J. Org. Chem.*, **2008**, 73, 3907-3910; e) Hernández, J., Ramos, R., Sastre, N., Meza, R., Hommer, H., Salas, M., Gordillo, B.,



---

«Conformational analysis of six-membered ring dioxaphosphinanes. Part 1: Anancomeric thiophosphates», *Tetrahedron*, **2004**, 60, 10927-10941.

<sup>9</sup> a) Mathivet, T.; Monflier, E.; Castanet, Y.; Mortreux, A.; Couturier, J.-L., «Hydroformylation of Higher Olefins by Rhodium/tris-((1H,1H,2H,2H-perfluorodecyl)phenyl)phosphites Complexes in a Fluorocarbon/ Hydrocarbon Biphasic Medium: Effect of Perfluorinated Groups on the Stability of Catalytic System», *Tetrahedron*, **2002**, 58, 3877-3888; b) Pietrusewicz, E.; Sienczyk, M.; Oleksyszyn, J., «Novel diphenyl esters of peptidyl  $\alpha$ -aminoalkylphosphonates as inhibitors of chymotrypsin and subtilisin», *J. Enzyme Inhib. Med. Chem.*, **2009**, 24, 1229-1236; c) Reetz, M. T.; Guo, H.; Ma, J.-A.; Godard, R.; Mynott, R. J., «Helical Triskelion Monophosphites as Ligands in Asymmetric Catalysis», *J. Am. Chem. Soc.*, **2009**, 131, 4136-4142; d) Dabbawala, A. A.; Bajaj, H. C.; Jasra, R. V., «Rhodium complex of monodentate phosphite as a catalyst for olefins hydroformylation», *J. Mol. Cat. A: Chem.*, **2009**, 302, 97-106; e) Park, H.; Kumareswaran, R.; RajanBabu, T. V., «Tunable phosphinite, phosphite and phosphoramidite ligands for the asymmetric hydrovinylolation reactions», *Tetrahedron*, **2005**, 61, 6352-6367.

<sup>10</sup> a) Fernández-Pérez, H.; Etayo, P.; Panossian, A.; Vidal-Ferran, A., «Phosphine–Phosphinite and Phosphine–Phosphite Ligands: Preparation and Applications in Asymmetric Catalysis», *Chem. Rev.*, **2011**, 111, 2119–2176; b) Diéguez, M., Pàmies, O., «Special Issue: Concepts in Asymmetric Catalysis», *Isr. J. Chem.*, **2012**, 52, 572–581; c) Diéguez, M., Andersson, P. G., Pàmies, O. (2012), «Innovative catalysis in organic synthesis: oxidation, hydrogenation, and C–X bond forming reactions», WileyVCH Verlag & Co. KGaA, Weinheim, 1st ed, ch. 7. 9; d) Mata, Y., Pàmies, O., Diéguez, M., «Pyranoside Phosphite-Oxazoline Ligand Library: Highly Efficient Modular P,N Ligands for Palladium-Catalyzed Allylic Substitution Reactions. A Study of the Key Palladium Allyl Intermediates», *Adv. Synth. Catal.*, **2009**, 351, 3217–3234; e) Mazuela, J., Tolstoy, P., Pàmies, O., Andersson, P. G., Diéguez, M., «Phosphite-oxazole/imidazoleligands in asymmetric intermolecular Heck reaction», *Organic & Org. Biomol. Chem.*, **2011**, 9, 941–946; f) Mazuela, M., Pàmies, O., Diéguez, M., «Phosphite-Thiazoline versus Phosphite-Oxazoline for Pd-Catalyzed Allylic Substitution Reactions: A Case for Comparison», *ChemCatChem*, **2013**, 5, 1504–1516; g) Magre, M., Biosca, M., Pàmies, O., Diéguez, M., «Filling the Gaps in the Challenging Asymmetric Hydroboration of 1,1-Disubstituted Alkenes with Simple Phosphite-Based Phosphinooxazoline Iridium Catalysts», *ChemCatChem*, **2015**, 7, 114–120; h) Gavrilov, K. N., Polosukhin, A. I., Bondarev, O. G., Korostylev, A. V., Lyubimov, S. E., Shiryaev, A. A., Starikova, Z. A., Davankov, V. A., «Novel P,N-Bidentate Phosphite Ligands in asymmetric Catalysis», *Mendeleev Commun.*,



**2001**, *11*, 33–35; i) Tsarev, V. N., Konkin, S. I., Shiryaev, A. A., Davankov, V. A., Gavrilov, K. N., «Enantioselective Pd-catalyzed C\*-C, C\*-N, and C\*-S bond formation reactions using first P,P,N,N-tetradentate chiral phosphites», *Tetrahedron: Asymmetry*, **2005**, *16*, 1737–1741; j) Mazuela, J., Pàmies, O., Diéguez, M., «A New Modular Phosphite-Pyridine Ligand Library for Asymmetric Pd-Catalyzed Allylic Substitution Reactions: A Study of the Key Pd- $\pi$ -Allyl Intermediates», *Chem. Eur. J.*, **2013**, *19*, 2416–2432; k) Magre, M., Biosca, M., Norrby, P.-O., Pàmies, O., Diéguez, M., «Theoretical and Experimental Optimization of a New Amino Phosphite Ligand Library for Asymmetric Palladium-Catalyzed Allylic Substitution», *ChemCatChem*, **2015**, *7*, 4091–4107.

<sup>11</sup> a) Pamies, O., Net, G.; Ruiz, A., Claver, C., «A new diphosphane derived from carbohydrates as an effective ligand for asymmetric hydrogenation», *Eur. J. Inorg. Chem.*, **2000**, *2000*, 2011–2016; b) Dieguez, M., Ruiz, A., Claver, C., «Chiral Diphosphites Derived from d-Glucose: New Highly Modular Ligands for the Asymmetric Catalytic Hydrogenation», *J. Org. Chem.*, **2002**, *67*, 3796–3801; c) Dieguez, M., Ruiz, A., Claver, C., «Tunable furanoside diphosphite ligands. A powerful approach in asymmetric catalysis», *Dalton Trans.*, **2003**, *0*, 2957–2963; d) Martorell, A., Claver, C., Fernandez, «The influence of chiral phosphite and phosphonite ligands on the hydrogenation of imines with rhodium and iridium complexes», *Inorg. Chem. Commun.*, **2000**, *3*, 132–135; e) Guiu, E., Muñoz, B., Castillon, S., Claver, C., «Iridium-Catalyzed Enantioselective Hydrogenation of Imines with Xylose Diphosphite and Diphosphinite Ligands», *Adv. Synth. Catal.*, **2003**, *345*, 169–171; f) Gual, A., Axet, M. R., Philippot, K.; Chaudret, B., Denicourt-Nowicki, B. A., Roucoux, A., Castillon, S., Claver, C., «iphosphite Ligands Derived from Carbohydrates as Stabilizers for Ruthenium Nanoparticles: Promising Catalytic Systems in Arene Hydrogenation», *Chem. Commun.*, **2008**, *0*, 2759–2761; g) Axet, M. R., Benet-Buchholz, J., Claver, C., Castillon, S., «New C2-Symmetric Diphosphite Ligands Derived from Carbohydrates: Effect of the Remote Stereocenters on Asymmetric Catalysis», *Adv. Synth. Catal.*, **2007**, *349*, 1983–1988; h) Ionescu, G., Van der Vlugt, J. I., Abbenhuis, H. C. L., Vogt, D., «Synthesis and applications of chiral phosphite ligands derived from incompletely condensed silsesquioxane backbones», *Tetrahedron: Asymmetry*, **2005**, *16*, 3970–3975; i) Lyubimov, S. E., Zhuraviskii, R. P., Rozenberg, V. I., Safronov, A. S., Petrovskii, P. V., Davankov, V. A., «First chiral [2.2]paracyclophane-derived phosphite ligands: synthesis and application in asymmetric reactions», *Russ. Chem. Bull.*, **2008**, *57*, 137–139; j) Zhang, Q., Takacs, J. M., «Click-Connected Ligand Scaffolds: Macrocyclic Chelates for Asymmetric Hydrogenation», *Org. Lett.*, **2008**, *10*, 545–548; k) Kuil, M., Goudriaan, P. E., Kleij, A. W., Tooke, D. M., Spek, A. L., Van Leeuwen, P. W. N. M., Reek, J. N. H., «Rigid bis-zinc(ii)

---

salphen building blocks for the formation of template-assisted bidentate ligands and their application in catalysis», *Dalton Trans.*, **2007**, 0, 2311-2320;; l) Slagt, V. F.; Kaiser, P.; Berkessel, A.; Kuil, M.; Kluwer, A. M.; Van Leeuwen, P. W. N. M.; Reek, J. N. H., «Fine-Tuning Ligands for Catalysis Using Supramolecular Strategies », *Eur. J. Inorg. Chem.*, **2007**, 2007, 4653-4562; m) Sandee, A. J.; Van der Burg, A. M.; Reek, J. N. H., «UREAphos: supramolecular bidentate ligands for asymmetric hydrogenation», *Chem. Commun.*, **2007**, 0, 864-866; n) Meeuwissen, J.; Kuil, M.; van der Burg, A. M.; Sandee, A. J.; Reek, J. N. H., «Application of a Supramolecular-Ligand Library for the Automated Search for Catalysts for the Asymmetric Hydrogenation of Industrially Relevant Substrates», *Chem. Eur. J.*, **2009**, 15, 10272-10279.

<sup>12</sup> Wang, M. F.; Crilley, M. L.; Golding, B. T.; McNally, T.; Robinson, D. H.; Tinker, A., « Synthesis of phosphonates: a modified arbusow procedure», *J. Chem. Soc., Chem. Commun.*, **1991**, 9, 667-668.

<sup>13</sup> Khairullin, V. K.; Sobchuk, T. I., « Preparation and rearrangement of phenylphosphonous mixed esters», *Seriya Khimicheskaya.*, **1965**, 10, 1792-1798

<sup>14</sup> Arbusow, B. A., «Michaelis-arbusow- und perkowreaktionen», *Pure Appl. Chem.*, **1964**, 9, 307-336.

<sup>15</sup> House, J. E.; House, K. A. (**2010**), «Phosphorus, arsenic, antimony, and bismuth. descriptive inorganic chemistry». 2da Edición, capítulo 13, 318.

<sup>16</sup> Van Leeuwen, P.W.N.M.; Kamer, P.C.J.; Claver, C.; Pamies, O.; Dieguez, M., « Phosphite-Containing Ligands for Asymmetric Catalysis», *Chem. Rev.*, **2011**, 111, 2077-2118.

<sup>17</sup> Tolman, C.A., «Steric effects of phosphorus ligands in organometallic chemistry and homogeneous catalysis», *Chem. Rev.*, **1977**, 77, 313-348.

<sup>18</sup> a) Dierskes, P. van Leeuwen, P. W. N. M., «The bite angle makes the difference: a practical ligand parameter for diphosphine ligands», *J. Chem. Soc. Dalton Tras.*, **1999**, 0, 1519-1530. b) Casey, C. P. Whitcker, G. T., «The Natural Bite Angle of Chelating Diphosphines», *Isr. J. Chem.* **1990**, 30. 299-304.

<sup>19</sup> Fernandez-Perez, H.; Etayo, P.; Panossian, A.; Vidal-Ferran, A., «Phosphine–Phosphinite and Phosphine–Phosphite Ligands: Preparation and Applications in Asymmetric Catalysis», *Chem. Rev.*, **2011**, 111, 2119-2176.

- <sup>20</sup> Braunstein, P.; Naud, F., «Hemilability of Hybrid Ligands and the Coordination Chemistry of Oxazoline-Based Systems», *Angew. Chem. Int. Ed.* **2001**, *40*, 680-699.
- <sup>21</sup> Stradiotto, M.; Lundgren, R. J.; Buchwald, S. L.; Milstein, D. (2016), «Ligand design in metal chemistry: reactivity and catalysis», Chichester, Reino Unido. John Wiley & Sons, Ltd.
- <sup>22</sup> Togni, A.; Burckhardt, U.; Gramlich, V.; Pregosin, P. S.; Salzmann, R., « Palladium-Catalyzed Asymmetric Allylic Amination Using Ferrocenyl Pyrazole Ligands: Steric Control of  $\eta^3$ -Allyl Configuration and Site-Selective Nucleophilic Attack», *J. Am. Chem. Soc.*, **1996**, *118*, 1031–1037.
- <sup>23</sup> Carroll, M. P.; Guiry, P. J., «P,N ligands in asymmetric catalysis», *Chem. Soc. Rev.*, **2014**, *43*, 819-833.
- <sup>24</sup> (a) Helmchen, G.; Pfaltz, A. «Phosphinooxazolines A New Class of Versatile, Modular P,N-Ligands for Asymmetric Catalysis», *Acc. Chem. Res.* **2000**, *33*, 336-345. (b) Wiese, B.; Helmchen, G. «Chiral phosphinooxazolines with a bi- or tricyclic oxazoline moiety - applications in Pd-catalyzed allylic alkylations», *Tetrahedron Lett.*, **1998**, *39*, 5727–5730. (c) Dawson, G. J.; Frost, C. G.; Williams, J. M. J.; Coote, S. J., «Asymmetric palladium catalysed allylic substitution using phosphorus containing oxazoline ligands», *Tetrahedron Lett.*, **1993**, *34*, 3149-3150. (d) Vasse, J. L.; Stranne, R.; Zalubovskis, R.; Gayet, C.; Moberg, C. «Influence of Steric Symmetry and Electronic Dissymmetry on the Enantioselectivity in Palladium-Catalyzed Allylic Substitutions», *J. Org. Chem.* **2003**, *68*, 3258-3270
- <sup>25</sup> Guiry, P. J.; Saunders, C. P., «The Development of Bidentate P,N Ligands for Asymmetric Catalysis», *Adv. Synth. Catal.* **2004**, *346*, 497-537.
- <sup>26</sup> For compound A: (a) H. Takaku, Y. Shimada and K. Arai, B, «A Study on Phosphorylation by Means of 8-Quinolyl Phosphates», *Chem. Soc. Jpn.*, **1974**, *47*, 779–780; (b) L. Dumitraşcu, N. Stănciuc, S. Stanciu, G. Răpeanu, «Inactivation kinetics of alkaline phosphatase from different species of milk using quinolyl phosphate as a substrate», *Food Sci. Biotechnol.*, **2014**, *23*, 1773–1778; (c) Sain, D., Kumari, C., Kumar, A., Nayek, H. P., Dey, S., «Lead ion induced chemodosimeter approach of a tripodal hydroxyl-quinoline based phospho-ester through P–O bond cleavage», *Dalton Trans.*, **2016**, *45*, 9187-9192. For compound B: (d) El-Shahat, M. F., Monshi, M. A. S., El-Sawi, E., Mostafa, M. Z., «8-quinoliny-ethylphosphate i) 8-quinoliny mono-ethyl ortho-phosphate and its complexes with some transition metals », *J. Chem. Soc. Pakistan*, **1982**, *4*, 227–233; e) Nakamura, M., Okamoto, Y., Takamuku, S., « Photochemical reactions of tri-1-naphthyl and tris(8-quinolyl) phosphates», *Phosphorus Sulfur Silicon Relat.*

*Elem.*, **1995**, 106, 137–144. For compound C: (f) Iwata, K., Kanno, M., Wada, S. (Toyo Ink Mfg. Co., Ltd.), JP 2011079950, **2011**. For compound D: (g) El-Sawi, E., El-Shahat, M. F., Moti, F. A., El-Messary, S., «Mercuration of 8-hydroxyquinoline phosphates», *J. Chem. Soc. Pakistan*, **1984**, 6, 77–82; (h) Browne, K. A., Bruice, T. C., «Chemistry of phosphodiesterases, DNA, and models. 2. The hydrolysis of bis(8-hydroxyquinoline) phosphate in the absence and presence of metal ions», *J. Am. Chem. Soc.*, **1992**, 114, 4951–4958. For compound E: (i) Lamande, L., Munoz, A., «Stabilisation de cations oxophosphenium par liaisons datives P←N», *Tetrahedron Lett.*, **1991**, 32, 75–78. For compound F: (j) Nifant'ev, E. E., Tuseev, A. P., Val'dman, D. I., Morozov, P. A., Val'dman, A. I., «», *Zh. Prikl. Khim.* **1979**, (S.-Peterburg, Russ. Fed.), 52, 1343–1346. For compound G: (k) Koenig, M., El Khatib, F., Munoz, A., Wolf, R., «Stabilisation d'ozonides du phosphore», *Tetrahedron Lett.*, **1982**, 23, 421–424; (l) El Khatib, F., Caminade, A. M., Koenig, M., «Ozonides du phosphore stabilite et stereochemie», *Phosphorus Sulfur*, **1984**, 20, 55–66. For compound H: (m) Arena, C. G., Calabrò, G., Franciò, G., Faraone, F., «New phosphoramidite and phosphito-N chiral ligands based on 8-substituted quinolines and (S)-binaphthol; applications in the Cu-catalyzed enantioselective conjugate addition of diethylzinc to 2-cyclohexen-1-one», *Tetrahedron-Asymmetry*, **2000**, 11, 2387–2392; (n) Delapierre, G., Brunel, J. M., Constantieux, T., Buono, G., «Design of a new class of chiral quinoline–phosphine ligands. Synthesis and application in asymmetric catalysis», *Tetrahedron-Asymmetry*, **2001**, 12, 1345–1352; (o) Drommi, D., Faraone, F., Franciò, G., «Asymmetric Induction and Configurational Stability at the Metal Center in Half-Sandwich ( $\eta^6$ -*p*-Cymene)ruthenium(II) and ( $\eta^5$ -Pentamethylcyclopentadienyl)rhodium(III) Complexes Containing Chiral Phosphito-N and Phosphonito-N Ligands», *Organometallics*, **2002**, 21, 761–764. For compound I: (p) Benito-Garagorri, Lackner-Warton, D., W., Standfest-Hauser, C. M., Mereiter, K., Kirchner, K., «Synthesis and characterization of iron and ruthenium complexes bearing P–N ligands based on 8-hydroxyquinoline», *Inorg. Chim. Acta*, **2010**, 363, 3674–3679. For compound J: (q) Franciò, G., Drommi, D., Faraone, C., Tiripicchio, A., «Synthesis of Phosphonito,N and Phosphito,N ligands based on quinolines and (R)-binaphthol or substituted biphenol and of their rhodium(I), palladium(II) and platinum(II) complexes», *Inorg. Chim. Acta*, **2002**, 338, 59–68. For compound K: (r) Said, M. A., Pülm, M., Herbst-Irmer, R., Kumara Swamy, K. C., «Bi- and tricyclic penta- and hexacoordinated phosphoranes with varying ring sizes: Synthesis, structures, and reactivity», *J. Am. Chem. Soc.*, **1996**, 118, 9841–9849. For compound L: (s) Crociani, B., Antonaroli, S., Burattini, M., Benetollo, F., Scrivanti, A., Bertoldini, M., «Palladium complexes of 8-(di-*tert*-butylphosphinoxy) quinoline», *J. Organomet. Chem.*, **2008**, 693, 3932–3938. For compounds M–O: (t) Cook, E., Masuda, J. D.,

---

Xia, A., Can., «Synthesis, characterization, and application of palladium complexes containing 8-quinolyl phosphinite ligands», *J. Chem.*, **2010**, 88, 93–103.

<sup>27</sup> Akemark, B.; Krakenberger, B.; Hansson, S.; Vitagliano, A., «Ligand effects and nucleophilic addition to ( $\eta^3$ -allyl) palladium complexes. A carbon-13 NMR study», *Organometallics*, **1987**, 6, 620-628.

<sup>28</sup> a) Francio, G.; Scopelliti, R.; Arena, C. G.; Bruno, G.; Drommi, D.; Faraone, F., «IrPd, IrHg, IrCu, and IrTl Binuclear Complexes Bridged by the Short-Bite Ligand 2-(Diphenylphosphino)pyridine. Catalytic Effect in the Hydroformylation of Styrene Due to the Monodentate P-Bonded 2-(Diphenylphosphino)pyridine Ligands of trans-[Ir(CO)(Ph<sub>2</sub>PPy)<sub>2</sub>Cl]», *Organometallics*, **1998**, 17, 338-347; b) Alonso, M. A.; Casares, J. A.; Espinet, P.; Soulantica, K., «Rhodium Complexes with the Chelating and Binucleating Ligands P(CH<sub>2</sub>CH<sub>2</sub>Py)<sub>n</sub>Ph<sub>3-n</sub> (Py = 2-Pyridyl; n = 1, 2): Structures and Fluxional Behavior», *Inorg. Chem.*, **2000**, 39, 705-711.

<sup>29</sup> Gavrilov, K. N.; Polosukhin, A. I., «Chiral P, N-bidentate ligands in coordination chemistry and organic catalysis involving rhodium and palladium», *Russian Chemical Reviews*, **2000**, 69, 661-682.

<sup>30</sup> Garagorri, D. B.; Lackner-Warton, W.; Standfest-Hauser, C. M.; Mereiter, K.; Kirchner, K., «Synthesis and characterization of iron and ruthenium complexes bearing P–N ligands based on 8-hydroxyquinoline», *Inorganica Chimica Acta*, **2010**, 363, 3674–3679.

<sup>31</sup> Drommi, D.; Faraone, F.; Francio, G., «Asymmetric Induction and Configurational Stability at the Metal Center in Half-Sandwich ( $\eta^6$ -*p*-Cymene)ruthenium(II) and ( $\eta^5$ -Pentamethylcyclopentadienyl)rhodium(III) Complexes Containing Chiral Phosphito-N and Phosphonito-N Ligands», *Organometallics*, **2002**, 21, 761-764.

<sup>32</sup> Francio, G.; Scopelliti, R.; Arena, C. G.; Bruno, G.; Drommi, D.; Faraone, F., «IrPd, IrHg, IrCu, and IrTl Binuclear Complexes Bridged by the Short-Bite Ligand 2-(Diphenylphosphino)pyridine. Catalytic Effect in the Hydroformylation of Styrene Due to the Monodentate P-Bonded 2-(diphenylphosphino)pyridine Ligands of trans-[Ir(CO)(Ph<sub>2</sub>PPy)<sub>2</sub>Cl]», *Organometallics*, **1998**, 17, 338-347.

<sup>33</sup> Klausmeyer, K.K.; Feazell, R.P.; Reibenspies, J.H., «Two-, Three-, and Four-Coordinate Ag(I) Coordination Polymers Formed by the Novel Phosphinite PPh<sub>2</sub>(3-OCH<sub>2</sub>C<sub>5</sub>H<sub>4</sub>N)», *Inorg. Chem.*, **2004**, 43, 1130-1136.

- <sup>34</sup> Delapierre, G.; Brunel, J.M.; Constantieux, T.; Buono, G., «Design of a new class of chiral quinoline–phosphine ligands. Synthesis and application in asymmetric catalysis», *Tetrahedron: Asymmetr.*, **2001**, 12, 1345-1352.
- <sup>35</sup> (a) Bandoli, G.; Dolmella, A.; Crociani, L.; Antonaroli, S.; Crociani, B., «Structural studies on iminophosphine ligands and their palladium complexes», *Transition Met. Chem.*, **2000**, 25, 17-25. (b) Sprinz, J.; Kiefer, M.; Helmchem, G.; Reggelin, M.; Huttner, G.; Walter, O.; Zsolnai, L., «Catalysis of allylic substitutions by Pd complexes of oxazolines containing an additional P, S, or Se Center. X-ray crystal structures and solution structures of chiral  $\pi$ -allyl palladium complexes of phosphinoaryloxazolines», *Tetrahedron Lett.*, **1994**, 35, 1523-1526. (c) Baltzer, N.; Macko, L.; Schaffner, S.; Zehnder, M., «Synthesis, and Solution and Solid-State Structures of  $(\eta^3\text{-Allyl})\{(4S)\text{-}4\text{-benzyl-}2\text{-}[2'\text{-(diphenylphosphino)phenyl]}\text{-}4,5\text{ dihydrooxazole P,N}\}$  palladium(II) Hexafluorophosphates. Comparison with Dichloro $\{(4S)\text{-}2\text{-}[2'\text{-(diphenylphosphino)phenyl]}\text{-}4,5\text{-dihydro-}4\text{-phenyloxazole-P,N}\}$ zinc(II)», *Helv. Chim. Acta*, **1996**, 79, 803-812. (d) Schaffner, S.; Macko, L.; Neuburger, M.; Zehnder, M., «Variants of Solid-State and Solution Structures of  $(\eta^3\text{-Allyl})\text{-}\{2\text{-}[2'\text{-(diphenylphosphino)phenyl]}\text{-}4,5\text{-dihydrooxazole-P,N}\}$ palladium(II) hexafluorophosphates and tetraphenylborates», *Helv. Chim. Acta*, **1997**, 80, 463-471.
- <sup>36</sup> Braunstein, P.; Zhang, J.; Welter, R., «Monohapto-allyl Pd(ii) complexes with bidentate hybrid P,N ligands», *Dalton Trans.*, **2003**, 507-509.
- <sup>37</sup> Börner, A. (2008), «Phosphorus ligands in asymmetric catalysis», Wiley- VCH, Weinheim,.
- <sup>38</sup> Dieguez, M.; Pamies, O.; Claver, C., «Recent advances in Rh-catalyzed asymmetric hydroformylation using phosphite ligands», *Tetrahedron:Asymmetry*, **2004**, 15, 2113-2122.
- <sup>39</sup> Alexakis, A.; Bäckvall, J. E.; Krause, N.; Pamies, O.; Dieguez, M., «Enantioselective copper-catalyzed conjugate addition and allylic substitution reactions», *Chem. Rev.*, **2008**, 108, 2796-2823.
- <sup>40</sup> (a) Noyori, R. (1994), «Asymmetric catalysis in organic synthesis», Wiley: New York. (b) Ojima, I. (2010), «Catalytic asymmetric synthesis», Wiley: Hoboken, NJ. (c) Jacobsen, E. N.; Pfaltz, A.; Yamamoto, H. (1999), «Comprehensive asymmetric catalysis», Springer: Berlin. (d) Blaser, H. U.; Schmidt, E., «In asymmetric catalysis on industrial scale», Wiley: New York, (2004).



<sup>41</sup> (a) Hilgraf, R.; Pfaltz, A., «Chiral Bis(N-sulfonylamino)phosphine- and TADDOL-Phosphite-Oxazoline Ligands: Synthesis and Application in Asymmetric Catalysis», *Adv. Synth. Catal.*, **2005**, 347, 61-77. (b) Dieguez, M.; Mazuela, J.; Pamies, O.; Verendel, J. J.; Andersson, P. G., «Biaryl phosphite-oxazolines from hydroxyl aminoacid derivatives: highly efficient modular ligands for Ir-catalyzed hydrogenation of alkenes», *Chem. Commun.*, **2008**, 3888-3890. (c) Mazuela, J.; Verendel, J. J.; Coll, M.; Sch  fner, B.; B  rner, A.; Andersson, P. G.; Pamies, O.; Dieguez, M., «Iridium Phosphite– Oxazoline Catalysts for the Highly Enantioselective Hydrogenation of Terminal Alkenes», *J. Am. Chem. Soc.*, **2009**, 131, 12344-12353. (d) Dieguez, M.; Mazuela, J.; Pamies, O.; Verendel, J. J.; Andersson, P. G., «Chiral Pyranoside Phosphite– Oxazolines: A New Class of Ligand for Asymmetric Catalytic Hydrogenation of Alkenes», *J. Am. Chem. Soc.*, **2008**, 130, 7208-7209. (e) Mazuela, J.; Paptchikhine, A.; Pamies, O.; Andersson, P. G.; Dieguez, M., «Adaptative Biaryl Phosphite– Oxazole and Phosphite–Thiazole Ligands for Asymmetric Ir-Catalyzed Hydrogenation of Alkenes», *Chem.—Eur. J.*, **2010**, 16, 4567-4576. (f) Gavrilov, K. N.; Marksimova, M. G.; Zheglov, S. V.; Bondarev, O. G.; Benetski, E. B.; Lyubimov, S. E.; Petrovskii, P. V.; Kabro, A. A.; Hey-Hawkins, E.; Moiseev, S. K.; Kalinin, V. N.; Davankov, V. A. Eur., «Ferrocenyliminophosphites as Easy-to-Modify Ligands for Asymmetric Catalysis», *J. Org. Chem.*, **2007**, 4940-4947. (g) Goulioukina, N. S.; Bondarenko, G. N.; Bogdanov, A. V.; Gavrilov, K. N.; Beletskaya, I. P., «Asymmetric Hydrogenation of  $\alpha$ -Keto Phosphonates with Chiral Palladium Catalysts», *Eur. J. Org. Chem.* **2009**, 510-515. (h) Pamies, O.; Andersson, P. G.; Dieguez, M., «Extending the Substrate Scope of Bicyclic P-Oxazoline/Thiazole Ligands for Ir-Catalyzed Hydrogenation of Unfunctionalized Olefins by Introducing a Biaryl Phosphoroamidite Group» *Chem. Eur. J.* **2015**, 21, 3455-3464.

<sup>42</sup> (a) Hilgraf, R.; Pfaltz, A., «Chiral Bis(N-sulfonylamino)phosphine- and TADDOL-Phosphite-Oxazoline Ligands: Synthesis and Application in Asymmetric Catalysis», *Adv. Synth. Catal.*, **2005**, 347, 61-77. (b) Pamies, O.; Dieguez, M.; Claver, C., «New Phosphite– Oxazoline Ligands for Efficient Pd-Catalyzed Substitution Reactions», *J. Am. Chem. Soc.*, **2005**, 127, 3646-3647. (c) Mata, Y.; Dieguez, M.; Pamies, O.; Claver, C., «New Carbohydrate-Based Phosphite-Oxazoline Ligands as Highly Versatile Ligands for Palladium-Catalyzed Allylic Substitution Reactions», *Adv. Synth. Catal.*, **2005**, 347, 1943-1947. (d) Pretot, R.; Pfaltz, A., «New ligands for regio- and enantiocontrol in Pd-catalyzed allylic alkylations», *Angew. Chem., Int. Ed.*, **1998**, 37, 323-325. (e) Gavrilov, K. N.; Tsarev, V. N.; Zheglov, S. V.; Lyubimov, S. E.; Shyryaev, A. A.; Petrovskii, P. V.; Davankov, V. A., «P,N-Bidentate aryl phosphite ligands based on chiral 2-imino-, 2-oxazolinyl and 2-oxazolidinyl phenols and their

catalytic activity», *Medeleev Commun.*, **2004**, 260-263. (f) Gladiali, S.; Loriga, G.; Medici, S.; Taras, R., «Binaphthalene-templated N, S-and N, P-heterobidentate ligands with an achiral oxazoline pendant: Synthesis and assessment in asymmetric catalysis», *J. Mol. Catal., A: Chem.*, **2003**, 196, 27-38. (g) Mata, Y.; Pamies, O.; Dieguez, M., «Pyranoside Phosphite-Oxazoline Ligand Library: Highly Efficient Modular P,N Ligands for Palladium-Catalyzed Allylic Substitution Reactions. A Study of the Key Palladium Allyl Intermediates», *Adv. Synth. Catal.*, **2009**, 351, 3217-3234.

<sup>43</sup> (a) Chen, Y.-L.; Fröhlich, R.; Hoppe, D., «Copper-catalyzed asymmetric addition of Et<sub>2</sub>Zn to 2-cyclohexen-1-one and 2-carbamoyloxy-2-cyclohexen-1-one with phosphoramidite, phosphite, and bidentate phosphite-oxazoline ligands», *Tetrahedron: Asymmetry*, **2009**, 20, 1144-1149. (b) Knobel, A. K.; Escher, I. H.; Pfaltz, A., «Enantioselective Copper-Catalyzed 1,4-Addition of Organozinc Reagents to Enones Using Chiral Oxazoline-Phosphite Ligands», *Synlett*, **1997**, 1429-1431. (c) Escher, I. H.; Pfaltz, A., «New chiral oxazoline-phosphite ligands for the enantioselective copper-catalyzed 1, 4-addition of organozinc reagents to enones», *Tetrahedron*, **2000**, 56, 2879-2888. (d) Mata, Y.; Dieguez, M.; Pamies, O.; Biswas, K.; Woodward, S., «Sugar-phosphite-oxazoline and phosphite-phosphoroamidite ligand libraries for Cu-catalyzed asymmetric 1, 4-addition reactions», *Tetrahedron: Asymmetry*, **2007**, 18, 1613-1617.

<sup>44</sup> (a) Hu, Y.; Liang, X.; Wang, J.; Zheng, Z.; Hu, X., «Highly enantioselective 1, 4-conjugate addition of diethylzinc to acyclic enones with chiral phosphite-pyridine ligands derived from H8-NOBIN», *Tetrahedron: Asymmetry*, **2003**, 13, 3907-3915. (b) Wan, H.; Hu, Y.; Liang, Y.; Gao, S.; Wang, J.; Zheng, Z.; Hu, X., «Highly Enantioselective Conjugate Addition of Diethylzinc to Acyclic Enones with Fine-Tunable Phosphite-Pyridine Ligands», *J. Org. Chem.*, **2003**, 68, 8277-8280. (c) Liang, Y.; Gao, S.; Wan, H.; Hu, Y.; Chan, H.; Zheng, Z.; Hu, Y., «Development of new chiral P,N ligands and their applications in enantioselective 1,4-conjugate additions of diethylzinc to chalcones», *Tetrahedron: Asymmetry*, **2003**, 13, 3211-3217. (d) Luo, X.; Hu, Y.; Hu, X., «Diastereomeric phosphite-pyridine ligands for enantioselective 1, 4-conjugate additions», *Tetrahedron: Asymmetry*, **2005**, 16, 1227-1231. (e) Xie, Y.; Huang, H.; Mo, W.; Fan, X.; Shen, Z.; Shen, Z.; Sun, N.; Hu, B.; Hu, X., «Design and synthesis of new chiral pyridine-phosphite ligands for the copper-catalyzed enantioselective conjugate addition of diethylzinc to acyclic enones», *Tetrahedron: Asymmetry*, **2009**, 20, 1425-1432.



<sup>45</sup> Dieguez, M.; Ruiz, A.; Claver, C., «New chiral amino-phosphite and phosphite-phosphoroamidite ligands for the copper-catalyzed asymmetric 1, 4-addition of diethylzinc to cyclohexenone», *Tetrahedron: Asymmetry*, **2001**, 12, 2861-2866.

<sup>46</sup> (a) Weng, Z.; Teo, S.; Hor, T.S.A., «Metal unsaturation and ligand hemilability in Suzuki coupling», *Acc. Chem. Res.*, **2007**, 676-684. (b) Bedford, R.B.; Cazin, C.S.J.; Holder, D., «The development of palladium catalysts for CC and C-heteroatom bond forming reactions of aryl chloride substrates», *Coord. Chem. Rev.*, **2004**, 248, 2283-2321. (c) Chen, M.-T.; Huang, C.-A.; Chen, C.-T., «Synthesis, Characterization, and Catalytic Applications of Palladacyclic Complexes Bearing C,N,S-Donor Ligands», *Eur. J. Inorg. Chem.*, **2008**, 3142-3149; (d) Kingston, J.V.; Verkade, J.G., «Synthesis and Characterization of R<sub>2</sub>PNP(iBuNCH<sub>2</sub>CH<sub>2</sub>)<sub>3</sub>N: A New Bulky Electron-Rich Phosphine for Efficient Pd-Assisted Suzuki–Miyaura Cross-Coupling Reactions», *J. Org. Chem.*, **2007**, 72, 2816-2822; (e) Schneider, S.K.; Roembke, P.; Julius, G.R.; Raubenheimer, H.G.; Herrmann, W.A., «Pyridin-, Quinolin- and Acridinylidene Palladium Carbene Complexes as Highly Efficient C–C Coupling Catalysts», *Adv. Synth. Catal.*, **2006**, 348, 1862-1873; (f) O'Brien, C.J.; Kantchev, E.A.B.; Valente, C.; Hadei, N.; Chass, G.A.; Lough, A.; Hopkinson, A.C.; Organ, M.G., «Easily Prepared Air- and Moisture-Stable Pd–NHC (NHC=N-Heterocyclic Carbene) Complexes: A Reliable, User-Friendly, Highly Active Palladium Precatalyst for the Suzuki–Miyaura Reaction», *Chem. Eur. J.*, **2006**, 12, 4743-4748; (g) Rosa, G.R.; Rosa, C.H.; Rominger, F.; Dupont, J.; Monteiro, A.L., «A mixed NCP pincer palladacycle as catalyst precursor for the coupling of aryl halides with aryl boronic acids», *Inorg. Chim. Acta*, **2006**, 359, 1947-1954. (h) Song, C.; Ma, Y.; Chai, Q.; Ma, C.; Jang, W.; Andrus, M.B., «Palladium catalyzed Suzuki–Miyaura coupling with aryl chlorides using a bulky phenanthryl N-heterocyclic carbene ligand», *Tetrahedron*, **2005**, 61, 7438-7446.

<sup>47</sup> Arena, C. G.; Calabro, G.; Francio, G.; Faraone, F., «New phosphoramidite and phosphito-N chiral ligands based on 8-substituted quinolines and (S)-binaphthol; applications in the Cu-catalyzed enantioselective conjugate addition of diethylzinc to 2-cyclohexen-1-one», *Tetrahedron: Asymmetry*, **2000**, 11, 2387-2392.

<sup>48</sup> a) Andersson, P. G.; Munslow, I. J. (2008), «Modern reduction methods», Wiley-VCH Verlag GmbH & Co. KGaA, Weinheim; b) De Vries, J. G. (2007), «The handbook of homogeneous hydrogenation», Wiley-VCH, Weinheim; c) Cervený, L. (1986), «Catalytic hydrogenation», Elsevier Science, the Netherlands, p. 27.

<sup>49</sup> Wang, D., Astruc, D., «The golden age of transfer hydrogenation», *Chem. Rev.*, **2015**, 115, 6621-6686.

<sup>50</sup> For selected examples on transition-metal catalyzed TH reactions, see: a) Landaeta, V. R., Salazar-La Rosa, A. D., Rodríguez-Lugo, R. E., «Transfer hydrogenation of ketones catalyzed by iridium-bulky phosphine complexes», *Inorg. Chim. Acta*, **2018**, 470, 303-311; b) Bayón Castañón, E., Kaposi, M., Reich, R. M., Kühn, F. E., «Water-soluble transition metal complexes of ruthenium(ii), osmium(ii), rhodium(iii) and iridium(iii) with chelating N-heterocyclic carbene ligands in hydrogenation and transfer hydrogenation catalysis», *Dalton Trans.*, **2018**, 47, 2318-2329; c) Maity, A., Sil, A., Patra, S. K., «Ruthenium (II) Complexes of 4'-(Aryl)-2, 2': 6', 2''-terpyridyl Ligands as Simple Catalysts for the Transfer Hydrogenation of Ketones», *Eur. J. Inorg. Chem.*, **2018**, 2018, 4063-4073; d) Rahaman, S. M. W., Daran, J.-C., Manoury, E., Poli, R., «The cyclooctadiene ligand in [IrCl(COD)]<sub>2</sub> is hydrogenated under transfer hydrogenation conditions: A study in the presence of PPh<sub>3</sub> and a strong base in isopropanol», *J. Organomet. Chem.*, **2017**, 829, 14-21; e) Gichumbi, J. M., Omondi, B., Friedrich, H. B., «Half-Sandwich Osmium (II) Complexes with Bidentate N, N-Chelating Ligands and Their Use in the Transfer Hydrogenation of Ketones», *Eur. J. Inorg. Chem.*, **2017**, 2017, 915-924; f) Farrell, K., Melle, P., Gossage, R. A., Müller-Bunz, H., Albrecht, M., «Transfer hydrogenation with abnormal dicarbene rhodium (III) complexes containing ancillary and modular poly-pyridine ligands», *Dalton Trans.*, **2016**, 45, 4570-4579; g) Mejía, E., Aardoom, R., Togni, A., «Asymmetric transfer hydrogenation of ketones catalyzed by rhenium complexes with chiral ferrocenylphosphane ligands», *Eur. J. Inorg. Chem.*, **2012**, 2012, 5021-5032; and references cited therein.

<sup>51</sup> a) Ferraro, A., Bernardi, L., Fochia, M., «Organocatalytic Enantioselective Transfer Hydrogenation of  $\beta$ -Amino Nitroolefins», *Adv. Synth. Catal.*, **2016**, 358, 1561-1565; b) Herrera, R. P. (2016), «Topics in current chemistry: organocatalytic transfer hydrogenation and hydrosilylation reactions», Springer International Publishing, 374, p. 29; c) Zhu, C., Saito, K., Yamanaka, M., Akiyama, T., «Benzothiazoline: versatile hydrogen donor for organocatalytic transfer hydrogenation», *Acc. Chem. Res.*, **2015**, 48, 388-398; d) Zhaobin, W., Fujin, A., Zheng, W., Wanxiang, Z., Guangyu, Z., Zhenyang, L., Jianwei, S., «Organocatalytic asymmetric synthesis of 1, 1-diarylethanes by transfer hydrogenation», *J. Am. Chem. Soc.*, **2015**, 137, 383-389; e) Bertelsen, S., K. Jorgensen, A., «Organocatalysis—after the gold rush», *Chem. Soc. Rev.*, **2009**, 38, 2178-2189; f) List, B., «Introduction: organocatalysis», *Chem. Rev.*, **2007**, 107, 5413-5415; g) Gaunt, M. J., Johansson, C. C. C., «Recent developments in the use of catalytic asymmetric ammonium enolates in chemical synthesis», *Chem. Rev.*, **2007**, 107, 5596-5605.

<sup>52</sup> a) Stephens, F. H., Pons, V., Baker, R. T., «Ammonia–borane: the hydrogen source par excellence?», *Dalton Trans.*, **2007**, 2613-2626; b) Grant, D. J., Dixon, D. A., «Thermodynamic Properties of Molecular Borane Phosphines, Alane Amines, and Phosphine Alanes and the  $[\text{BH}_4^-][\text{PH}_4^+]$ ,  $[\text{AlH}_4^-][\text{NH}_4^+]$ , and  $[\text{AlH}_4^-][\text{PH}_4^+]$  Salts for Chemical Hydrogen Storage Systems from ab Initio Electronic Structure Theory», *J. Phys. Chem. A*, **2005**, 109, 10138-10147; c) Dixon, D. A., Gutowski, M., «Thermodynamic Properties of Molecular Borane Amines and the  $[\text{BH}_4^-][\text{NH}_4^+]$  Salt for Chemical Hydrogen Storage Systems from ab Initio Electronic Structure Theory», *J. Phys. Chem. A*, **2005**, 109, 5129-5135.

<sup>53</sup> For selected examples on transition-metal mediated activation of AB, see: a) Takahashi, H., Watanabe, T., Tobita, H., «Bifunctional Iron-Amino Complexes: Highly Efficient Catalysts for Dehydrogenation of Ammonia-Borane», *Chem. Lett.*, **2018**, 47, 296-299; b) Esteruelas, M. A., Nolis, P., Oliván, M., Oñate, E., Vallribera, A., Vélez, A., «Ammonia borane dehydrogenation promoted by a pincer-square-planar rhodium (I) monohydride: A stepwise hydrogen transfer from the substrate to the catalyst», *Inorg. Chem.*, **2016**, 55, 7176-7181; c) Zhang, X., Kam, L., Williams, T. J., «Dehydrogenation of ammonia borane through the third equivalent of hydrogen», *Dalton Trans.*, **2016**, 45, 7672-7677; d) Rossin, A., Rossi, A., Peruzzini, M., Zanobini, F., «Chemical Hydrogen Storage: Ammonia Borane Dehydrogenation Catalyzed by NP3 Ruthenium Hydrides ( $\text{NP}_3=\text{N}(\text{CH}_2\text{CH}_2\text{PPh}_2)_3$ )», *ChemPlusChem*, **2014**, 79, 1316-1325; e) Baker, R. T., Gordon, J. C., Hamilton, C. W., Henson, N. J., Lin, P.-H., Maguire, S., Murugesu, M., Scott, B. L., Smythe, N. C., «Iron complex-catalyzed ammonia–borane dehydrogenation. A potential route toward B–N-containing polymer motifs using earth-abundant metal catalysts», *J. Am. Chem. Soc.*, **2012**, 134, 5598-5609; f) Staubitz, A., Robertson, A. P. M., Manners, I., «Ammonia-borane and related compounds as dihydrogen sources», *Chem. Rev.*, **2010**, 110, 4079-4124; g) Kim, S.-K., Han, W.-S., Kim, T.-J., Kim, T.-Y., Nam, S. W., Mitoraj, M., Pieko, Ł., Michalak, A., Hwang, S.-J., Kang, S. O., «Palladium catalysts for dehydrogenation of ammonia borane with preferential B–H activation», *J. Am. Chem. Soc.*, **2010**, 132, 9954-9955; h) Käß, M., Friedrich, A., Drees, M., Schneider, S., «Ruthenium complexes with cooperative PNP ligands: bifunctional catalysts for the dehydrogenation of ammonia–borane», *Angew. Chem. Int. Ed.* **2009**, 48, 907; «Rutheniumkomplexe mit kooperativen PNP-Liganden: Bifunktionale katalysatoren für die Dehydrierung von Amminboran», *Angew. Chem.* **2009**, 121, 922-924; i) Blaquiere, N., Diallo-Garcia, S., Gorelsky, S. I., Black, D. A., Fagnou, K., «Ruthenium-catalyzed dehydrogenation of ammonia boranes», *J. Am. Chem. Soc.*, **2008**, 130, 14034-14035; j) Keaton, R. J., Blacquiere, J. M., Baker, R. T., «Base metal catalyzed dehydrogenation of ammonia–borane

for chemical hydrogen storage» *J. Am. Chem. Soc.*, **2007**, 129, 1844-1845; k) Chandra, M., Xu, Q., «A high-performance hydrogen generation system: Transition metal-catalyzed dissociation and hydrolysis of ammonia-borane», *J. Power Sources*, **2006**, 156, 190-194; l) Denny, M. C., Pons, V., Hebden, T. J., Heineley, D. M., Goldberg, K. I., «Efficient catalysis of ammonia borane dehydrogenation», *J. Am. Chem. Soc.*, **2006**, 128, 12048-12049.

<sup>54</sup> Rossin, A., Peruzzini, M., «Ammonia-borane and amine-borane dehydrogenation mediated by complex metal hydrides», *Chem. Rev.*, **2016**, 116, 8848-8872.

<sup>55</sup> a) Zhou, Q., Zhang, L., Meng, W., Feng, X., Yang, J., Du, H., «Borane-catalyzed transfer hydrogenations of pyridines with ammonia borane», *Org. Lett.*, **2016**, 18, 5189-5191; b) Summerscales, O. T., Gordon, J. C., «Regeneration of ammonia borane from spent fuel materials», *Dalton Trans.*, **2013**, 42, 10075-10084; c) Sutton, A. D., Burrell, A. K., Dixon, D. A., Garner, E. B. III, Gordon, J. C., Nakagawa, T., Ott, K. C., Robinson, Vasiliu, J. P., M., «Regeneration of ammonia borane spent fuel by direct reaction with hydrazine and liquid ammonia», *Science*, **2011**, 331, 1426-1429; d) Smythe, N. C., Gordon, J. C., «Ammonia borane as a hydrogen carrier: dehydrogenation and regeneration», *Eur. J. Inorg. Chem.*, **2010**, 2010, 509-521; e) Davis, B. L., Dixon, D. A., Garner, E. B., Gordon, J. C., Matus, M. H., Scott, B., Stephens, F. H., «Efficient regeneration of partially spent ammonia borane fuel», *Angew. Chem.* **2009**, Int. Ed., 48, 6812-6816; f) Hausdorf, S., Baitalow, F., Wolf, G., Mertens, F. O. R. L., «A procedure for the regeneration of ammonia borane from BNH-waste products», *Int. J. Hydrogen Energy*, **2008**, 33, 608-614; g) Staubitz, A., Besora, M., Harvey, J. N., Manners, I., «Computational Analysis of Amine-Borane Adducts as Potential Hydrogen Storage Materials with Reversible Hydrogen Uptake», *Inorg. Chem.*, **2008**, 47, 5910-5918.

<sup>56</sup> Boom, D. H. A., Jupp, A. R., Slootweg, J. C., «Dehydrogenation of AmineBoranes using p-block Compounds», *Chem. Eur. J.*, **2019**, 25, 9133-9152,.

<sup>57</sup> Wang, F., Planas, O., Cornella, J., «Bi (I)-catalyzed transfer-hydrogenation with ammonia-borane», *J. Am. Chem. Soc.*, **2019**, 141, 4235-4240.

<sup>58</sup> a) Zeng, G., Maeda, S., Taketsugu, T., Sakaki S., «Catalytic Hydrogenation of Carbon Dioxide with Ammonia-Borane by Pincer-Type Phosphorus Compounds: Theoretical Prediction», *J. Am. Chem. Soc.*, **2016**, 138, 13481-13484; b) Zeng, G., Maeda, S., Taketsugu, T., Sakaki S., «Catalytic Transfer Hydrogenation by a Trivalent Phosphorus Compound: Phosphorus-Ligand Cooperation Pathway or P<sup>III</sup>/P<sup>V</sup> Redox Pathway?», *Angew. Chem. Int. Ed.* **2014**, 53, 4633-4637.

- 
- <sup>59</sup> a) Zhao, W., McCarthy, S. M., Lai, T. Y., Yennawar, H. P., Radosevich, A. T., «Reversible Intermolecular E–H Oxidative Addition to a Geometrically Deformed and Structurally Dynamic Phosphorous Triamide», *J. Am. Chem. Soc.*, **2014**, 136, 17634-17644; b) McCarthy, S. M., Lin, Y.-C., Devarajan, D., Chang, J. W., Yennawar, H. P., Rioux, R. M., Ess, D. H., Radosevich, A. T., «Intermolecular N–H Oxidative Addition of Ammonia, Alkylamines, and Arylamines to a Planar  $\sigma^3$ -Phosphorus Compound via an Entropy-Controlled Electrophilic Mechanism», *J. Am. Chem. Soc.*, **2014**, 136, 4640-4650; c) Dunn, N. L., Ha, M., Radosevich, A. T., «Main Group Redox Catalysis: Reversible  $P^{III}/P^V$  Redox Cycling at a Phosphorus Platform», *J. Am. Chem. Soc.*, **2012**, 134, 11330-11333.
- <sup>60</sup> Chong, C.-C., Hirao, H., Kinjo, R., «A Concerted Transfer Hydrogenolysis: 1,3,2-Diazaphosphenolene-Catalyzed Hydrogenation of N=N Bond with Ammonia–Borane», *Angew. Chem. Int. Ed.*, **2014**, 53, 3342-3346.
- <sup>61</sup> Chong, C.-C., Hirao, H., Kinjo, R., «Metal-Free  $\sigma$ -Bond Metathesis in 1,3,2-Diazaphosphenolene-Catalyzed Hydroboration of Carbonyl Compounds», *Angew. Chem. Int. Ed.* **2015**, 54, 190-194.
- <sup>62</sup> Gudat, D., «A very peculiar family of N-heterocyclic phosphines: unusual structures and the unique reactivity of 1, 3, 2-diazaphosphenolenes», *Dalton Trans.*, **2016**, 45, 5896-5907.
- <sup>63</sup> Adams, M. R., Tien, C.-H., Huchenski, B. S. N., Ferguson, M. J., Speed, A. W. H., «Diazaphosphenolene precatalysts for imine and conjugate reductions», *Angew. Chem. Int. Ed.*, **2017**, 56, 6268-6271.
- <sup>64</sup> Lin, Y.-C., Hatzakis, E., McCarthy, S. M., Reichl, K. D., Lai, T.-Y., Yennawar, H. P., Radosevich, A. T., «P–N Cooperative Borane Activation and Catalytic Hydroboration by a Distorted Phosphorous Triamide Platform», *J. Am. Chem. Soc.*, **2017**, 139, 6008-6016.
- <sup>65</sup> a) Rao, B., Chong, C. C., Kinjo, R., «Metal-Free Regio- and Chemoselective hydroboration of pyridines catalyzed by 1, 3, 2-diazaphosphenium triflate», *J. Am. Chem. Soc.*, **2018**, 140, 652-656; b) Chong, C. C., Rao, B., Kinjo, R., «Metal-Free Catalytic Reduction of  $\alpha$ ,  $\beta$ -Unsaturated Esters by 1, 3, 2-Diazaphosphenolene and Subsequent C–C Coupling with Nitriles», *ACS Catal.*, **2017**, 7, 5814-5819.
- <sup>66</sup> a) Hynes, T., Welsh, E. N., McDonald, R., Ferguson, M. J., Speed, A. W. H., «Pyridine Hydroboration with a Diazaphosphenolene Precatalyst», *Organometallics*, **2018**, 37, 841-844; b) Tien, C.-H., Adams, M. R., Ferguson, M. J., Johnson, E. R., Speed, A. W. H., «Hydroboration

---

Catalyzed by 1, 2, 4, 3-Triazaphospholenes», *Org. Lett.*, **2017**, 19, 5565-5568; c) Adams, M. R., Tien, C.-H., McDonald, R., A. Speed, W. H., «Asymmetric Imine Hydroboration Catalyzed by Chiral Diazaphospholenes», *Angew. Chem. Int. Ed.*, **2017**, 56, 16660-16663.

<sup>67</sup> Reed, J. H., Donets, P. A., Miaskiewicz, S., Cramer, N., «A 1, 3, 2-Diazaphospholene-Catalyzed Reductive Claisen Rearrangement», *Angew. Chem. Int. Ed.*, **2019**, 58, 8893–8897.

<sup>68</sup> Kirsten, L., Steyl, G., Roodt, A., *Acta Crystallogr., Sect. E: Struct. Rep. Online*, 63, o2828–o2830, **2007**.

<sup>69</sup> Kownacki, I., Marciniak, B., Steinberger, H., Kubicki, M., Hoffmann, M., Ziarko, A., Szubert, K., Majchrzak, M., Rubinsztajn, S., «Effect of triorganophosphites on platinum catalyzed curing of silicon rubber», *Appl. Catal., A*, **2009**, 362, 106–114.

<sup>70</sup> Sherrill, C. D., «Energy component analysis of  $\pi$  interactions», *Acc. Chem. Res.*, **2013**, 46, 1020–1028.

<sup>71</sup> Staubitz, A., Robertson, A. P. M., Manners, I., «Ammonia-borane and related compounds as dihydrogen sources», *Chem. Rev.*, **2010**, 110, 4079-4124.

<sup>72</sup> Kim, S., Kang, H. J., Yang, S., «Selective reduction of aldehydes with 8-oxyquinoline dihydroboronite in the presence of boron trifluoride etherate», *Tetrahedron Lett.*, **1984**, 25, 2985-2986.

<sup>73</sup> Brandsma, L., Gusarova, N. K., Gusarov, A. V., Verkruijsse, H. D., Trofimov, B. A., «Efficient One-Pot Procedures for the Preparation of Secondary Phosphines», *Synth. Commun.*, **1994**, 24, 3219-3223.

<sup>74</sup> Bures, J., «A simple graphical method to determine the order in catalyst», *Angew. Chem. Int. Ed.*, **2016**, 55, 2028–2031.

<sup>75</sup> Yang, X., Zhao, L., Fox, T., Wang, Z.-X., Berke, H., «Transfer Hydrogenation of Imines with Ammonia-Borane: A Concerted Double-Hydrogen-Transfer Reaction», *Angew. Chem. Int. Ed.*, **2010**, 49, 2058-2062; Yang, X., Zhao, L., Fox, T., Wang, Z., Berke, H., «Transferhydrierungen von Iminen mit Borazan: eine konzertierte doppelte Wasserstoff-Übertragungsreaktion?», *Angew. Chem.*, **2010**, 122, 2102-2106.



- <sup>76</sup> Bhattacharya, P.; Krause, J. A.; Guan, H., «Mechanistic studies of ammonia borane dehydrogenation catalyzed by iron pincer complexes», *J. Am. Chem. Soc.*, **2014**, *136*, 11153–11161.
- <sup>77</sup> Xu, W.; Fan, H.; Wuc, G.; Chen, P., «Comparative study on reducing aromatic aldehydes by using ammonia borane and lithium amidoborane as reducing reagents», *New J. Chem.*, **2012**, *36*, 1496–1501.
- <sup>78</sup> (a) Adams, J. P.; Robertson, G., «Imines, enamines and related functional groups», *Contemp. Org. Synth.*, **1997**, *4*, 183–195. (b) Severin, R.; Doye, S., «», *Chem. Soc. Rev.*, *36*, 1407–1420, **2007**. (c) Pelletier, G.; Bechara, W. S.; Charette, A. B., «The catalytic hydroamination of alkynes», *J. Am. Chem. Soc.*, **2010**, *132*, 12817–12819. (d) Yim, J. C.-H.; Schafer, L. L., «Efficient Anti-Markovnikov-Selective Catalysts for Intermolecular Alkyne Hydroamination: Recent Advances and Synthetic Applications», *Eur. J. Org. Chem.*, **2014**, *2014*, 6825–6840. (e) Yadav, D. K. T.; Bhanage, B. M., «Base-mediated synthesis of imines and amines from N-phenylureas and alcohols», *Synlett*, **2014**, *25*, 1611–1615. (f) Choi, J.-H.; Precht, M. H. G., «Tuneable hydrogenation of nitriles into imines or amines with a ruthenium pincer complex under mild conditions», *ChemCatChem*, **2015**, *7*, 1023–1028. (g) Azizi, N.; Edrisi, M., «Deep eutectic solvent catalyzed eco-friendly synthesis of imines and hydrobenzamides», *Monatsh. Chem.*, **2015**, *146*, 1695–1698. (h) Border, E. C.; Blair, V. L.; Andrews, P. C., «An Efficient Microwave Method for the Synthesis of Imines», *Aust. J. Chem.*, **2015**, *68*, 844–848. (i) Giles, R. G.; Heaney, H.; Plater, M. J., «Reactions of nitrilium salts with indole and pyrrole and their derivatives in the synthesis of imines, ketones and secondary amines», *Tetrahedron*, **2015**, *71*, 7367–7385. (j) Yadav, D. K. T.; Bhanage, B. M., «Base-catalyzed synthesis of amides and imines via C–C and C [double bond, length as m-dash] C bond cleavage», *RSC Adv.*, **2015**, *5*, 12387–12391.
- <sup>79</sup> (a) Largeron, M., «Protocols for the catalytic oxidation of primary amines to imines», *Eur. J. Org. Chem.*, **2013**, *2013*, 5225–5235. (b) Qin, W.; Long, S.; Panunzio, M.; Biondi, S., «Schiff bases: a short survey on an evergreen chemistry tool», *Molecules*, **2013**, *18*, 12264–12289.
- <sup>80</sup> Chen, B.; Wang, L.; Gao, S., «Recent advances in aerobic oxidation of alcohols and amines to imines», *ACS Catal.*, **2015**, *5*, 5851–5876.
- <sup>81</sup> For oxidative cross-coupling of amines and alcohols to yield imines see: (a) Zheng, J.; Li, J.; Wei, H.; Yu, J.; Su, H.; Wang, X., «The investigation of gold/zirconia as a photocatalyst for

the direct synthesis of imines from alcohols and aniline», *Mat. Sci. Semicon. Proc.*, **2015**, 32, 131–136. (b) Tamura, M.; Tomishige, K., «Redox Properties of CeO<sub>2</sub> at Low Temperature: The Direct Synthesis of Imines from Alcohol and Amine», *Angew. Chem., Int. Ed.*, **2015**, 54, 864–867. (c) Chen, B.; Shang, S.; Wang, L.; Zhang, Y.; Gao, S., «Mesoporous carbon derived from vitamin B 12: a high-performance bifunctional catalyst for imine formation», *Chem. Commun.*, **2016**, 52, 481–484. For dehydrogenative (with liberation of H<sub>2</sub>) coupling of amines and alcohols to form imines see: (d) Gnanaprakasam, B.; Zhang, J.; Milstein, D., «Direct Synthesis of Imines from Alcohols and Amines with Liberation of H<sub>2</sub>», *Angew. Chem. Int. Ed. Engl.*, **2010**, 49, 1468–1471. (e) Zeng, G.; Li, S., «Insights into Dehydrogenative Coupling of Alcohols and Amines Catalyzed by a (PNN)–Ru (II) Hydride Complex: Unusual Metal–Ligand Cooperation», *Inorg. Chem.*, **2011**, 50, 10572–10580. (f) Maggi, A.; Madsen, R., «Dehydrogenative synthesis of imines from alcohols and amines catalyzed by a ruthenium N-heterocyclic carbene complex», *Organometallics*, **2012**, 31, 451–455. (g) Srimani, D.; Ben-David, Y.; Milstein, D., «Direct Synthesis of Pyrroles by Dehydrogenative Coupling of β-Aminoalcohols with Secondary Alcohols Catalyzed by Ruthenium Pincer Complexes», *Angew. Chem., Int. Ed.*, **2013**, 52, 4012–4015. (h) Saha, B.; Wahidur Rahaman, S. M.; Daw, P.; Sengupta, G.; Bera, J. K., «Metal–ligand cooperation on a diruthenium platform: selective imine formation through acceptorless dehydrogenative coupling of alcohols with amines», *Chem. Eur. J.*, **2014**, 20, 6542–6551. (i) Hasanayn, F.; Harb, H., «A metathesis model for the dehydrogenative coupling of amines with alcohols and esters into carboxamides by Milstein's [Ru (PNN)(CO)(H)] catalysts», *Inorg. Chem.*, **2014**, 53, 8334–8349. (j) Ruch, S.; Irrgang, T.; Kempe, R., «New Iridium Catalysts for the Selective Alkylation of Amines by Alcohols under Mild Conditions and for the Synthesis of Quinolines by Acceptor-less Dehydrogenative Condensation», *Chem. Eur. J.*, **2014**, 20, 13279–13285. (k) Trincado, M.; Banerjee, D.; Grützmacher, H., «Molecular catalysts for hydrogen production from alcohols», *Energy Environ. Sci.*, **2014**, 7, 2464–2503. (l) Bain, J.; Cho, P.; Voutchkova-Kostal, A., «Recyclable hydrotalcite catalysts for alcohol imination via acceptorless dehydrogenation», *Green Chem.*, **2015**, 17, 2271–2280. (m) Mukherjee, A.; Nerush, A.; Leitus, G.; Shimon, L. J. W.; Ben-David, Y.; Espinosa-Jalapa, N. Á.; Milstein, D., «Manganese-Catalyzed Environmentally Benign Dehydrogenative Coupling of Alcohols and Amines to Form Aldimines and H<sub>2</sub>: A Catalytic and Mechanistic Study», *J. Am. Chem. Soc.*, **2016**, 138, 4298–4301. Also the coupling of nitriles with amines toward imine is possible: (n) Srimani, D.; Feller, M.; Ben-David, Y.; Milstein, D., «Catalytic coupling of nitriles with amines to selectively form imines under mild hydrogen pressure», *Chem. Commun.*, **2012**, 48, 11853–11855.



- <sup>82</sup> (a) Yadav, D. K. T.; Bhanage, B. M., «Rhodium-catalyzed synthesis of quinolines and imines under mild conditions», *RSC Adv.*, **2015**, 5, 51570–51575. (b) Marui, K.; Nomoto, A.; Akashi, H.; Ogawa, A., «Green oxidation of amines to imines based on the development of novel catalytic systems using molecular oxygen or hydrogen peroxide», *Synthesis*, **2016**, 48, 31–42.
- <sup>83</sup> (a) Biswas, S.; Dutta, B.; Mullick, K.; Kuo, C.-H.; Poyraz, A. S.; Suib, S. L., «Aerobic oxidation of amines to imines by cesium-promoted mesoporous manganese oxide», *ACS Catal.*, **2015**, 5, 4394–4403. (b) Kumar, R.; Gleissner, E. H.; Tiu, E. G. V.; Yamakoshi, Y., «C70 as a Photocatalyst for Oxidation of Secondary Benzylamines to Imines», *Org. Lett.*, **2016**, 18, 184–187. (c) Sudarsanam, P.; Malleshm, B.; Rangaswamy, A.; Rao, B. G.; Bhargava, S. K.; Reddy, B. M., «Promising nanostructured gold/metal oxide catalysts for oxidative coupling of benzylamines under eco-friendly conditions», *J. Mol. Catal. A: Chem.*, **2016**, 412, 47–55.
- <sup>84</sup> Rao, B. G.; Sudarsanam, P.; Rangaswamy, A.; Reddy, B. M., «Highly Efficient CeO<sub>2</sub>–MoO<sub>3</sub>/SiO<sub>2</sub> Catalyst for Solvent-Free Oxidative Coupling of Benzylamines into N-Benzylbenzaldimines with O<sub>2</sub> as the Oxidant», *Catal. Lett.*, **2015**, 145, 1436–1445.
- <sup>85</sup> (a) Lv, X.; Zhou, Y.; Zhang, A.; Zhou, L.; Zeng, Q., «A straightforward green synthesis of N-(tert-butylsulfinyl)imines», *Toxicol. Environ. Chem.*, **2015**, 98, 1155–1162. (b) Chen, B.; Wang, L.; Dai, W.; Shang, S.; Lv, Y.; Gao, S., «Metal-free and solvent-free oxidative coupling of amines to imines with mesoporous carbon from macrocyclic compounds», *ACS Catal.*, **2015**, 5, 2788–2794.
- <sup>86</sup> Bu, J.; Fang, J.; Leow, W. R.; Zheng, K.; Chen, X., «Single-crystalline rutile TiO<sub>2</sub> nano-flower hierarchical structures for enhanced photocatalytic selective oxidation from amine to imine», *RSC Adv.*, **2015**, 5, 103895–103900.
- <sup>87</sup> (a) Qin, Y.; Zhang, L.; Lv, J.; Luo, S.; Cheng, J.-P., «Bioinspired Organocatalytic Aerobic C–H Oxidation of Amines with an ortho-Quinone Catalyst», *Org. Lett.*, **2015**, 17, 1469–1472. Chemoselective preparation of cross-coupled imines through the synergistic combination of copper (II) acetate and o-iminoquinone under ambient conditions: (b) Largeron, M.; Fleury, M.-B., «A Metalloenzyme-Like Catalytic System for the Chemoselective Oxidative Cross-Coupling of Primary Amines to Imines under Ambient Conditions», *Chem. Eur. J.*, **2015**, 21, 3815–3820.
- <sup>88</sup> The combination Cu (I)/TEMPO (TEMPO: 2,2,6,6-tetramethylpiperdiny-N-oxyl) is an active and highly effective catalyst for the aerobic oxidation of amines to imines in open air at room temperature under neat conditions: Huang, B.; Tian, H.; Lin, S.; Xie, M.; Yu, X.; Xu, Q.,

---

«Cu (I)/TEMPO-catalyzed aerobic oxidative synthesis of imines directly from primary and secondary amines under ambient and neat conditions», *Tetrahedron Lett.*, **2013**, 54, 2861–2864.

<sup>89</sup> The complex [VO(Hhpic)<sub>2</sub>] (H<sub>2</sub>hpic: 3-hydroxypicolinic acid) is an active catalyst for the self-coupling of benzylamines via atmospheric oxidation at 120 °C: Kodama, S.; Yoshida, J.; Nomoto, A.; Ueta, Y.; Yano, S.; Ueshima, M.; Ogawa, A., «Direct conversion of benzylamines to imines via atmospheric oxidation in the presence of VO (Hhpic) 2 catalyst», *Tetrahedron Lett.*, **2010**, 51, 2450–2452.

<sup>90</sup> Wang, L.; Chen, B.; Ren, L.; Zhang, H.; Lü, Y.; Gao, S., «Vanadium catalyzed direct synthesis of imines from amines or alcohols and amines by an aerobic oxidative reaction under mild conditions», *Chin. J. Catal.*, **2015**, 36, 19–23.

<sup>91</sup> Stahl and Wendlandt reported the aerobic oxidation of secondary amines that employs ZnI<sub>2</sub> and 1,10-phenanthroline-5,6-dione as a bifunctional *o*-quinone catalyst: Wendlandt, A. E.; Stahl, S. S., «Bioinspired aerobic oxidation of secondary amines and nitrogen heterocycles with a bifunctional quinone catalyst», *J. Am. Chem. Soc.*, **2014**, 136, 506–512.

<sup>92</sup> The oxidative coupling of benzylamines to imines by molecular oxygen in the presence of very low catalyst loadings of Co (II)  $\beta$ -tetrakis-(trifluoromethyl)-meso-tetraphenylporphyrin: Zhao, S.; Liu, C.; Guo, Y.; Xiao, J.-C.; Chen, Q.-Y. «Oxidative Coupling of Benzylamines to Imines by Molecular Oxygen Catalyzed by Cobalt(II)  $\beta$ -Tetrakis(trifluoromethyl)-meso-tetraphenylporphyrin», *J. Org. Chem.*, **2014**, 79, 8926–8931.

<sup>93</sup> The Fe(NO<sub>3</sub>)<sub>3</sub>/TEMPO system can readily catalyze the aerobic oxidative reactions of primary and secondary amines, by using air as the oxidant, for the preparation of imines: Zhang, E.; Tian, H.; Xu, S.; Yu, X.; Xu, Q., «Iron-catalyzed direct synthesis of imines from amines or alcohols and amines via aerobic oxidative reactions under air», *Org. Lett.*, **2013**, 15, 2704–2707.

<sup>94</sup> The aerobic oxidative preparation of imines from alcohols and amines by using several silver (I) NHC complexes as catalysts: Han, L.; Xing, P.; Jiang, B., «Selective aerobic oxidation of alcohols to aldehydes, carboxylic acids, and imines catalyzed by a Ag-NHC complex», *Org. Lett.*, **2014**, 16, 3428–3431.

<sup>95</sup> A palladium (II)–porphyrin complex is an efficient catalyst for photoinduced oxidative C-H functionalization by using oxygen as terminal oxidant. When this methodology was applied to

secondary amines to obtain imines, the system proceeds with very high yields (> 90%) in short reaction time (1.5 h) and with low catalyst loading (0.005 mol%): To, W.-P.; Liu, Y.; Lau, T.-C.; Che, C.-M., «A Robust Palladium (II)–Porphyrin Complex as Catalyst for Visible Light Induced Oxidative C-H Functionalization», *Chem. Eur. J.*, **2013**, 19, 5654–5664.

<sup>96</sup> Complexes with photoactivity have also been explored for imine formation from secondary amines: Chow, P. K.; Ma, C.; To, W.-P.; Tong, G. S. M.; Lai, S.-L.; Kui, S. C. F.; Kwok, W.-M.; Che, C.-M., «Strongly Phosphorescent Palladium(II) Complexes of Tetradentate Ligands with Mixed Oxygen, Carbon, and Nitrogen Donor Atoms: Photophysics, Photochemistry, and Applications», *Angew. Chem., Int. Ed.*, **2013**, 52, 11775–11779.

<sup>97</sup> Complexes with photoactivity have also been explored for imine formation from secondary amines: To, W.-P.; Tong, G. S.-M.; Lu, W.; Ma, C.; Liu, J.; Chow, A. L.-F.; Che, C.-M., «Luminescent Organogold (III) Complexes with Long-Lived Triplet Excited States for Light-Induced Oxidative C-H Bond Functionalization and Hydrogen Production», *Angew. Chem., Int. Ed.*, **2012**, 51, 2654–2657.

<sup>98</sup> The photo-induced self-coupling of benzylamines to imines by Ir(I) complexes: (a) Rueping, M.; Vila, C.; Szadkowska, A.; Koenigs, R. M.; Fronert, J., «Photoredox catalysis as an efficient tool for the aerobic oxidation of amines and alcohols: Bioinspired demethylations and condensations», *ACS Catal.*, **2012**, 2, 2810–2815. (b) Jin, J.; Shin, H.-W.; Park, J. H.; Park, J. H.; Kim, E.; Ahn, T. K.; Ryu, D. H.; Son, S. U., «Iridium complexes containing bis (imidazoline thione) and bis (imidazoline selone) ligands for visible-light-induced oxidative coupling of benzylamines to imines», *Organometallics*, **2013**, 32, 3954–3959.

<sup>99</sup> (a) Glorius, F., «Asymmetric hydrogenation of aromatic compounds», *Org. Biomol. Chem.*, **2005**, 3, 4171–4175. (b) Zhou, Y.-G., «Asymmetric hydrogenation of heteroaromatic compounds», *Acc. Chem. Res.*, **2007**, 40, 1357–1366. (c) Comins, D. L.; O'Connor, S.; Alawar, R. S. (2008), «In comprehensive heterocyclic chemistry III», Katritzky, A. R., Ramsden, C. A., Scriven, E. F. V., Taylor, R. J. K., Eds.; *Elsevier Science*; Vol 7, p 41. (d) Ahamed, M.; Todd, M. H., «Catalytic Asymmetric Additions of Carbon-Centered Nucleophiles to Nitrogen-Containing Aromatic Heterocycles», *Eur. J. Org. Chem.*, **2010**, 5935–5942. (e) Roche, S. P.; Porco, J. A. Jr., «Dearomatization strategies in the synthesis of complex natural products», *Angew. Chem., Int. Ed.*, **2011**, 50, 4068–4093.

<sup>100</sup> For reviews on dihydropyridines, see: (a) Eisner, U.; Kuthan, «Chemistry of dihydropyridines», *J. Chem. Rev.*, **1972**, 72, 1–42. (b) Stout, D. M.; Meyers, A. I., «Recent

advances in the chemistry of dihydropyridines», *Chem. Rev.*, **1982**, 82, 223-243. (c) Sliwa, W., «», *Heterocycles*, **1986**, 24, 181. (d) Lavilla, R., «Recent developments in the chemistry of dihydropyridines», *J. Chem. Soc., Perkin Trans.* **2002**, 1, 1141-1156. (e) Edraki, N.; Mehdipour, A. R.; Khoshneviszadeh, M.; Miri, R., «Dihydropyridines: evaluation of their current and future pharmacological applications», *Drug Discovery Today*, **2009**, 14, 1058-1066.

<sup>101</sup> For examples of 1,2-dihydropyridines utilized in synthesis of natural products and biologically active compounds, see: (a) Wender, P. A.; Schaus, J. M.; White, A. W., «General methodology for *cis*-hydroisoquinoline synthesis: synthesis of reserpine», *J. Am. Chem. Soc.*, **1980**, 102, 6157-6159. (b) Marazano, C.; Goff, M.-T. L.; Fourrey, J.-L.; Das, B. C., «An unequivocal synthesis of 1-benzyl-3-ethyl-1,6-dihydropyridine and its use for a biogenetically modelled synthesis of (±)-catharanthine », *J. Chem. Soc., Chem. Commun.*, **1981**, 389-391. (c) Raucher, S.; Bray, B. L., «Total synthesis of (+/-)-catharanthine», *J. Org. Chem.*, **1985**, 50, 3236-3237. (d) Sundberg, R. J.; Cherney, R. J., «Synthesis of analogs of Iboga alkaloids. Investigation of electrophilic, palladium-catalyzed and radical cyclizations for preparation of 5, 6-homoiboga derivatives», *J. Org. Chem.*, **1990**, 55, 6028-6037. (e) Polniaszek, R. P.; Dillard, L. W., «Stereospecific total syntheses of decahydroquinoline alkaloids (.+.-)-195A and (.+.-)-2-epi-195A», *J. Org. Chem.*, **1992**, 57, 4103-4110. (f) Comins, D. L.; Brooks, C. A.; Alawar, R. S.; Goehring, R. R., «IMDA/Retro-Mannich Approach to *cis*-Perhydroquinoline Lycopodium Alkaloids: Asymmetric Synthesis of (+)-Luciduline», *Org. Lett.*, **1999**, 1, 229-232. (g) Zhao, G.; Deo, U. C.; Ganem, B., «Selective fowler reductions: asymmetric total syntheses of isofagomine and other 1-azasugars from methyl nicotinate», *Org. Lett.*, **2001**, 3, 201-203. (h) Satoh, N.; Akiba, T.; Yokoshima, S.; Fukuyama, T., «A practical synthesis of (-)-Oseltamivir», *Angew. Chem., Int. Ed.*, **2007**, 46, 5734-5736. (i) Barbe, G.; Charette, A. B., «Total synthesis of (+)-lepadin B: Stereoselective synthesis of nonracemic polysubstituted hydroquinolines using an RC-ROM Process», *J. Am. Chem. Soc.*, **2008**, 130, 13873-13875.

<sup>102</sup> Fowler, F. W., «Synthesis of 1, 2-and 1, 4-dihydropyridines», *J. Org. Chem.*, **1972**, 37, 1321-1323.

<sup>103</sup> The direct conversion of unactivated pyridine to dihydropyridine derivatives requires strong nucleophiles such as organolithiums or use of alkali metals. For examples, see: (a) Evans, J. C. W.; Allen, C. F. H., «2-Phenylpyridine», *Org. Synth.*, **1938**, 18, 70. (b) Sulzbach, R. A., «Darstellung und Eigenschaften von 1, 4-bis (trimethylsilyl)-1, 4-dihydropyridin», *J. Organomet. Chem.*, **1970**, 24, 307-314.

<sup>104</sup> Successful catalytic partial hydrogenation is limited to the pyridines bearing a carbonyl functional group at the C3 position, which gives isolable carbonyl-conjugated 1,2-dihydropyridines and 1,4,5,6-tetrahydropyridines. For examples, see: (a) Freifelder, M., «Hydrogenation in the Pyridine Series. I. Catalytic Reduction of the Isomeric Acetylpyridines», *J. Org. Chem.*, **1964**, 29, 2895-2898. (b) Quan, P. M.; Quin, L. D., «1, 4, 5, 6-Tetrahydropyridines from Catalytic Reduction of Nicotinoyl Derivatives and Their Ring Opening with Hydrazine», *J. Org. Chem.*, **1966**, 31, 2487-2490. (c) Eisner, U., «Synthesis of 1, 2-dihydropyridines», *J. Chem. Soc. D, Chem. Commun.*, **1969**, 1348-1349.

<sup>105</sup> For examples of catalytic hydrogenation of pyridines to form piperidine derivatives, see: (a) Hamilton, T. S.; Adams, R., «Reduction of pyridine hydrochloride and pyridonium salts by means of hydrogen and platinum-oxide platinum black. Xviii», *J. Am. Chem. Soc.*, **1928**, 50, 2260-2263. (b) Adkins, H.; Kuick, L. F.; Farlow, M.; Wojcik, B., «Hydrogenation of derivatives of pyridine», *J. Am. Chem. Soc.*, **1934**, 56, 2425-2428. (c) Freifelder, M.; Stone, G. R., «Reductions with Ruthenium. II. Its Use in the Hydrogenation of Pyridines», *J. Org. Chem.*, **1961**, 26, 3805-3808. For a recent example of asymmetric hydrogenation, see: (d) Glorius, F.; Spielkamp, N.; Holle, S.; Goddard, R.; Lehmann, C. W., «Efficient asymmetric hydrogenation of pyridines», *Angew. Chem., Int. Ed.*, **2004**, 43, 2850-2852. See also ref 105a and 105b.

<sup>106</sup> For heterogeneous catalyst conditions, see: Cook, N. C.; Lyons, J. E., «Dihydropyridines from silylation of pyridines», *J. Am. Chem. Soc.*, **1966**, 88, 3396-3403.

<sup>107</sup> For homogeneous catalyst conditions, see: (a) Hao, L.; Harrod, J. F.; Lebus, A.-M.; Mu, Y.; Shu, R.; Samuel, E.; Woo, H.-G., «Homogeneous catalytic hydrosilylation of pyridines», *Angew. Chem., Int. Ed.*, **1998**, 37, 3126-3129. (b) Harrod, J. F.; Shu, R.; Woo, H. G.; Samuel, E., «Titanocene (III) catalyzed homogeneous hydrosilation-hydrogenation of pyridines», *Can. J. Chem.*, **2001**, 79, 1075-1085. (c) Gutsulyak, D. V.; van der Est, A.; Nikonov, G. I., «Facile catalytic hydrosilylation of pyridines», *Angew. Chem., Int. Ed.*, **2011**, 50, 1384-1387. For a commentary, see: (d) Osakada, K., «1, 4-Hydrosilylation of Pyridine by Ruthenium Catalyst: A New Reaction and Mechanism», *Angew. Chem., Int. Ed.*, **2011**, 50, 3845-3846.

<sup>108</sup> Oshima, K.; Ohmura, T.; Sugimoto, M.; Oshima, K.; Ohmura, T.; Sugimoto, M., «Palladium-Catalyzed Regioselective Silaboration of Pyridines Leading to the Synthesis of Silylated Dihydropyridines», *J. Am. Chem. Soc.*, **2011**, 133, 7324-7327.

- 
- <sup>109</sup> Dudnik, A. S.; Weidner, V. L.; Motta, A.; Delferro, M.; Marks, T., «Atom-efficient regioselective 1, 2-dearomatization of functionalized pyridines by an earth-abundant organolanthanide catalyst», *J. Nat. Chem.*, **2014**, 6, 1100.
- <sup>110</sup> Oshima, K.; Ohmura, T.; Suginome, M., «Regioselective synthesis of 1, 2-dihydropyridines by rhodium-catalyzed hydroboration of pyridines», *J. Am. Chem. Soc.*, **2012**, 134, 3699-3702.
- <sup>111</sup> For reviews on transition-metal-catalyzed hydroboration, see: (a) Burgess, K.; Ohlmeyer, M., «Transition-metal promoted hydroborations of alkenes, emerging methodology for organic transformations», *J. Chem. Rev.*, **1991**, 91, 1179-1191. (b) Beletskaya, I.; Pelter, A., «Hydroborations catalysed by transition metal complexes», *Tetrahedron*, **1997**, 53, 4957-5026. (c) Crudden, C. M.; Edwards, D., «Catalytic Asymmetric Hydroboration: Recent Advances and Applications in Carbon–Carbon Bond-Forming Reactions», *Eur. J. Org. Chem.*, **2003**, 4695-4712. (d) Carroll, A.-M.; O’Sullivan, T. P.; Guiry, P., «The Development of Enantioselective Rhodium-Catalysed Hydroboration of Olefins», *J. Adv. Synth. Catal.*, **2005**, 347, 609-631. (e) Brown, J. M. (2005), «In modern rhodium-catalyzed organic reactions», Evans, P. A., Ed.; Wiley-VCH: Weinheim; p 33.
- <sup>112</sup> Arrowsmith, M.; Hill, M. S.; Hadlington, T.; Kociok-Köhne, G.; Weetman, C., «Magnesium-catalyzed hydroboration of pyridines», *Organometallics*, **2011**, 30, 5556-5559.
- <sup>113</sup> Sakai, N.; Mano, S.; Nozaki, K.; Takaya, H., «Highly enantioselective hydroformylation of olefins catalyzed by new phosphine phosphite-rhodium (I) complexes», *J. Am. Chem. Soc.*, **1993**, 115, 7033-7034.
- <sup>114</sup> Rubio, M.; Vargas, S.; Suarez, A.; Olivarez, E.; Pizzano, A., «Tuning of the Structures of Chiral Phosphane-Phosphites: Application to the Highly Enantioselective Synthesis of  $\alpha$ -Acyloxy Phosphonates by Catalytic Hydrogenation», *Chem. Eur. J.*, **2007**, 13, 1821–1833.
- <sup>115</sup> Choinopoulos, I.; Papageorgiou, I.; Coco, S.; Simandiras, E.; Koinis S., «Modification of Wilkinson's catalyst with triphenyl phosphite: Synthesis, structure, <sup>31</sup>P NMR and DFT study of *trans*-[RhCl (P (OPh) <sub>3</sub>)(PPh<sub>3</sub>)<sub>2</sub>]», *Polyhedron*, **2012**, 45, 255–261.
- <sup>116</sup> Burling, S.; Field, L. D.; Messerle, B. A.; Vuongb, K. Q.; Turner, P., «Rhodium (I) and iridium (I) complexes with bidentate N, N and P, N ligands as catalysts for the hydrothiolation of alkynes», *Dalton Trans.*, **2003**, 4181-4191.



- 
- <sup>117</sup> a) Bhattacharya, A. K.; Thyagarman; G., «Michaelis-arbuzov rearrangement», *Chem. Rev.*, **1981**, 81, 415-430. b) Brill, T. E.; Landon, S., «Arbuzov-like dealkylation reactions of transition-metal-phosphite complexes», *J. Chem. Rev.*, **1984**, 84, 577-585.
- <sup>118</sup> Alfonsov, V.A., Trusenev, A.G., Gainullin, R.M., «Reaction of dialkyldithiotrimethylsilylphosphites with acyl halides», *Russ. Chem. Bull.*, **1992**, 41, 799–803.
- <sup>119</sup> Pang, M.; Wu, C.; Zhuang, X.; Zhang, F.; Su, M.; Tong, Q.; Tung, C.; Wang, W., «Addition of a B–H Bond across an Amido–Cobalt Bond: CoII–H-Catalyzed Hydroboration of Olefins», *Organometallics*, **2018**, 37, 1462–1467.
- <sup>120</sup> (a) Collman, J. P., Hegedus, L. S., Norton, J. R., Finke, R. G., **(1987)**, «Principles and applications of organotransition metal chemistry», University Science Book, CA; Yamamoto, A., **(1986)**, «Organotransition metal chemistry», Wiley, New York, (b) A. Togni and L. M. Venanzi, «Nitrogen donors in organometallic chemistry and homogeneous catalysis», *Angew. Chem., Int. Ed. Engl.*, **1994**, 33, 497-526; (c) Mayer, H. A., Kaska, W. C., «Stereochemical control of transition metal complexes by polyphosphine ligands», *Chem. Rev.*, **1994**, 94, 1239-1272.
- <sup>121</sup> Williams, J. M. J., «The ups and downs of allylpalladium complexes in catalysis», *Synlett*, **1996**, 705-710.
- <sup>122</sup> Brunner, H., Obermann, U. Wimmer, P., «Asymmetric catalysis. 44. Enantioselective monophenylation of diols with cupric acetate/pyridinyloxazoline catalysts», *Organometallics*, **1989**, 8, 821-826; Bolm, C., «Bis (4, 5-dihydrooxazolyl) derivatives in asymmetric catalysis», *Angew. Chem., Int. Ed. Engl.*, **1991**, 30, 542-543; Pfaltz, A., «Design of chiral ligands for asymmetric catalysis: from C<sub>2</sub>-symmetric semicorrins and bisoxazolines to non-symmetric phosphinooxazolines», *Acta Chem. Scand.*, **1996**, 50, 189-194.
- <sup>123</sup> a) Feigl A., Bockholt A., Weis J., Rieger B., **(2011)**, «In modern synthetic and application aspects of polysilanes: an underestimated class of materials? Silicon polymers», (Ed.: M. A. Muzafarov) Springer Berlin Heidelberg: Berlin, pp. 1 - 31. b) Corey, J. Y., «Dehydrocoupling of hydrosilanes to polysilanes and silicon oligomers: A 30 year overview», *Adv. Organomet. Chem.*, **2004**, 51, 1 - 52.

<sup>124</sup> a) Lipke, M. C., Liberman-Martin, A. L., Tilley, T. D., «Electrophilic activation of silicon–hydrogen bonds in catalytic hydrosilations», *Angew. Chem. Int. Ed.*, **2017**, 56, 2260 - 2294. b) Nikonov G. I., «Recent Advances in Nonclassical Interligand Si... H Interactions», *Adv. Organomet. Chem.* **2005**, 53, 217-310. c) Lachaize S., Sabo-Etienne S., « $\sigma$ -Silane Ruthenium Complexes: The Crucial Role of Secondary Interactions», *Eur. J. Inorg. Chem.*, **2006**, 2115 - 2127. d) Corey J. Y., «Reactions of hydrosilanes with transition metal complexes and characterization of the products», *Chem. Rev.*, **2011**, 111, 863-1071. e) Corey J. Y., «Reactions of hydrosilanes with transition metal complexes», *Chem. Rev.* **2016**, 116, 11291 - 11435.

<sup>125</sup> Relevant literature about Ru-complexes bearing multidentate ligands:(a) Gunanathan, C.; Milstein, D., «Bond Activation and Catalysis by Ruthenium Pincer Complexes», *Chem. Rev.* **2014**, 114, 12024-12087.; b) Zhang, J.; Leitus, G.; Ben-David, Y.; Milstein, D. «Facile Conversion of Alcohols into Esters and Dihydrogen Catalyzed by New Ruthenium Complexes», *J. Am. Chem. Soc.* **2005**, 127, 10840-10841. c) Gnanaprakasam, B.; Zhang, J.; Milstein, D. «Direct Synthesis of Imines from Alcohols and Amines with Liberation of H<sub>2</sub>», *Angew. Chem., Int. Ed.* **2010**, 49, 1468-1471. d) Gunanathan, C.; Milstein, D. «Selective Synthesis of Primary Amines Directly from Alcohols and Ammonia», *Angew. Chem., Int. Ed.* **2008**, 47, 8661-8664. e) Salem, H.; Shimon, L. J. W.; Diskin-Posner, Y.; Leitus, G.; Ben-David, Y.; Milstein, D. «Formation of Stable *trans*-Dihydride Ruthenium(II) and 16-Electron Ruthenium(0) Complexes Based on Phosphinite PONOP Pincer Ligands. Reactivity toward Water and Electrophiles», *Organometallics* **2009**, 28, 4791-4806. f) Gargir, M.; Ben-David, Y.; Leitus, G.; Diskin-Posner, Y.; Shimon, L. J. W.; Milstein, D. «PNS-Type Ruthenium Pincer Complexes», *Organometallics* **2012**, 31, 6207-6214. g) Balaraman, E.; Gnanaprakasam, B.; Shimon, L. J. W.; Milstein, D. «Direct Hydrogenation of Amides to Alcohols and Amines under Mild Conditions», *J. Am. Chem. Soc.* **2010**, 132, 16756-16758. h) Barrios-Francisco, R.; Balaraman, E.; Diskin-Posner, Y.; Leitus, G.; Shimon, L. J. W.; Milstein, D. «PNN Ruthenium Pincer Complexes Based on Phosphinated 2,2'-Dipyridinemethane and 2,2'-Oxobispyridine. Metal–Ligand Cooperation in Cyclometalation and Catalysis», *Organometallics* **2013**, 32, 2973-2982.

<sup>126</sup> a) Blackman, A. G. «Tripodal Tetraamine Ligands Containing Three Pyridine Units: The other Polypyridyl Ligands» *Eur. J. Inorg. Chem.* **2008**, 2633-2647. b) Blackman, A. G. «The coordination chemistry of tripodal tetraamine ligands», *Polyhedron* **2005**, 24, 1-39.



<sup>127</sup> Relevant literature about tetradentate ligands: a) Gilbert-Wilson, R.; Field, L. D.; Bhadbhade, M. M. . «New Superhindered Polydentate Polyphosphine Ligands  $P(CH_2CH_2PtBu_2)_3$ ,  $PhP(CH_2CH_2PtBu_2)_2$ ,  $P(CH_2CH_2CH_2PtBu_2)_3$ , and their Ruthenium(II) Chloride Complexes», *Inorg. Chem.* **2012**, 51, 3239-3246. b) Bjernemose, J.; Hazell, A.; McKenzie, C. J.; Mahon, M. F.; Preuss-Nielsen, L.; Raithby, P. R.; Simonsen, O.; Toftlund, H.; Wolny, J.A., «Synthesis and characterization of ruthenium (II) complexes with polypicolylamine ligands», *Polyhedron* **2003**, 22, 875-885. c) Bhadbhade, M. M.; Field, L. D.; Gilbert-Wilson, R.; Guest, R. W.; Jensen, P. «Ruthenium Hydride Complexes of the Hindered Phosphine Ligand Tris (3-diisopropylphosphinopropyl) phosphine», *Inorg. Chem.* **2011**, 50, 6220-6228. d) Whiteoak, C. J.; Nobbs, J. D.; Kiryushchenkov, E.; Pagano, S.; White, A. J. P.; Britovsek, G. J. P., «Tri(pyridylmethyl)phosphine: the elusive congener of TPA shows surprisingly different coordination behavior», *Inorg. Chem.* **2013**, 52, 7000-7009. (e) Gericke, R.; Wagler, J. «Ruthenium complexes of diphenylphosphino derivatives of carboxylic amides: Synthesis and characterization of bidentate P,N- and P,O-chelate ligands and their reactivity towards  $[RuCl_2(PPh_3)_3]$ », *Polyhedron* **2016**, 120, 134-141.

<sup>128</sup> Braunstein, P.; Fryzuk, M. D.; Naud, F.; Rettig, S. J.; «Catalytic transfer hydrogenation of ketones by the use of ruthenium complexes incorporating the new tridentate ligand, bis (2-oxazolin-2-ylmethyl) phenylphosphine», *J. Chem. Soc., Dalton Trans.*, **1999**, 589–594.

<sup>129</sup> a) Gericke, R.; Wagler, J., «Ruthenium complexes of diphenylphosphino derivatives of carboxylic amides: Synthesis and characterization of bidentate P, N-and P, O-chelate ligands and their reactivity towards  $[RuCl_2(PPh_3)_3]$ », *Polyhedron*, **2016**, 120, 134-141. b) Gericke, R.; Wagler, J., « Ruthenium complexes of phosphino derivatives of carboxylic amides: Synthesis and characterization of tridentate P,E<sub>2</sub> and tetradentate P,E<sub>3</sub> (E = N,O) ligands and their reactivity towards  $[RuCl_2(PPh_3)_3]$ », *Polyhedron*, **2017**, 125, 57-67.

<sup>130</sup> a) Nielsen, M., Alberico, E., Baumann, W., Drexler, H.-J., Junge, H., Gladiali, S., Beller, M., «Low-temperature aqueous-phase methanol dehydrogenation to hydrogen and carbon dioxide», *Nature*, **2013**, 495, 85–89; b) Zeng, R., Feller, M., Ben-David, Y., Milstein, D., «Hydrogenation and hydrosilylation of nitrous oxide homogeneously catalyzed by a metal complex», *J. Am. Chem. Soc.*, **2017**, 139, 5720–5723; c) Mellmann, D., Spronholz, P., Junge, H., Beller, M., «Formic acid as a hydrogen storage material–development of homogeneous catalysts for selective hydrogen release», *Chem. Soc. Rev.*, **2016**, 45, 3954–3988; d) Kothandaraman, J., Goeppert, A., Czaun, M.G. Olah, A., Prakash, G. K. S., «Conversion of CO<sub>2</sub> from Air into Methanol Using a Polyamine and a Homogeneous Ruthenium Catalyst», *J.*

*Am. Chem. Soc.*, **2016**, 138, 778–781; e) Rodriguez-Lugo, R. E., Trincado, M., Vogt, M., Tewes, F., Santiso-Quinones, G., Grützmacher, H., «A homogeneous transition metal complex for clean hydrogen production from methanol–water mixtures», *Nat. Chem.*, **2013**, 5, 342–347; f) vandenBosch, B., Chen, H.-C., vander, V-lugt, J. I., Brouwer, A. M., Reek, J. N. H., «A Noble-Metal-Free System for Photodriven Catalytic Proton Reduction», *ChemSusChem*, **2013**, 6, 790–793; g) Oldenhof, S., De Bruin, B., Lutz, M., Siegler, M. A., Patureau, F. W., vanderVlugt, J. I., Reek, J. N. H., «Base-Free Production of H<sub>2</sub> by Dehydrogenation of Formic Acid Using An Iridium–bisMETAMORPhos Complex», *Chem. Eur. J.*, **2013**, 19, 11507–11511; h) Bertini, F., Glatz, M., Gorgas, N., Stöger, B., Peruzzini, M., Veiros, L. F., Kirchner, K., Gonsalvi, L., «Carbon dioxide hydrogenation catalysed by well-defined Mn (I) PNP pincer hydride complexes», *Chem. Sci.*, **2017**, 8, 5024–5029; 9; j) Hu, P., Diskin-Posner, Y., Ben-David, Y., Milstein, D., «Reusable homogeneous catalytic system for hydrogen production from methanol and water», *ACS Catal.*, **2014**, 4, 2649–2652; k) Maenaka, Y., Suenobu, T., Fukuzumi, S., «Catalytic interconversion between hydrogen and formic acid at ambient temperature and pressure», *Energy Environ.Sci.*, **2012**, 5, 7360–7367; l) Himeda, Y., «Highly efficient hydrogen evolution by decomposition of formic acid using an iridium catalyst with 4, 4'-dihydroxy-2, 2'-bipyridine», *Green Chem.*, **2009**, 11, 2018–2022.

<sup>131</sup> a) Kuriyama, W., Matsumoto, T., Ogata, O., Ino, Y., Aoki, K., Tanaka, S., Ishida, K., Kobayashi, T., Sayo, N., Saito, T., «Catalytic hydrogenation of esters. Development of an efficient catalyst and processes for synthesising (R)-1, 2-propanediol and 2-(1-menthoxy) ethanol», *Org. Process Res. Dev.*, **2012**, 16, 166–171; b) Ogata, O., Nakayama, Y., Nara, H., Fujiwhara, M., Kayaki, Y., «Atmospheric Hydrogenation of Esters Catalyzed by PNP-Ruthenium Complexes with an N-Heterocyclic Carbene Ligand», *Org. Lett.*, **2016**, 18, 3894–389.

<sup>132</sup> a) Sandoval C. A., Ohkuma T., Muñiz K., Noyori R., «Mechanism of asymmetric hydrogenation of ketones catalyzed by BINAP/1, 2-diamine– ruthenium (II) complexes», *J. Am. Chem. Soc.*, **2003**, 125, 13490–13503; b) Noyori, R., Ohkuma, T., «Asymmetric catalysis by architectural and functional molecular engineering: practical chemo- and stereoselective hydrogenation of ketones», *Angew. Chem. Int. Ed.*, **2001**, 40, 40–73; «Asymmetrische Katalyse mit hinsichtlich Struktur und Funktion gezielt entworfenen Molekülen: die chemo- und stereoselektive Hydrierung von Ketonen», *Angew. Chem.*, **2001**, 113, 40–75.

<sup>133</sup> a) Neumann, J., Bornschein, C., Jiao, H., Junge, K., Beller, M., «Hydrogenation of aliphatic and aromatic nitriles using a defined ruthenium PNP pincer catalyst», *Eur. J. Org. Chem.*, **2015**, 5944–5948; b) Reguillo, R., Grellier, M., Vautravers, N., Vendier, L., Sabo-Etienne, S., «Ruthenium-catalyzed hydrogenation of nitriles: insights into the mechanism», *J. Am. Chem. Soc.*, **2010**, 132, 7854–7855.

<sup>134</sup> a) Marichev, K. O., Takacs, J. M., «Ruthenium-catalyzed amination of secondary alcohols using borrowing hydrogen methodology», *ACS Catal.*, **2016**, 6, 2205–2210; b) Pena-Lopez, N., Neumann, H., Beller, M., «Ruthenium pincer-catalyzed synthesis of substituted  $\gamma$ -butyrolactones using hydrogen autotransfer methodology», *Chem. Commun.*, **2015**, 51, 13082–13085; c) Kessler, J. A., Iluc, V. M., «Ag(I) and Tl(I) Precursors as Transfer Agents of a Pyrrole-Based Pincer Ligand to Late Transition Metals», *Inorg. Chem.*, **2014**, 53, 12360–12371.

<sup>135</sup> a) Pinggen, D., Choi, J.-H., Allen, H., Murray, G., Ganji, P., vanLeeuwen, P. W. N. M., Prechtl, M. H. G., Vogt, D., «Amide versus amine ligand paradigm in the direct amination of alcohols with Ru-PNP complexes», *Catal. Sci. Technol.*, **2018**, 8, 3969–3976; b) Zhang L., Nguyen D. H., Raffa G., Trivelli X., Capet F., Desset S., Paul S., Dumeignil F., Gauvin R. M., «Catalytic conversion of alcohols into carboxylic acid salts in water: scope, recycling, and mechanistic insights», *ChemSusChem.*, **2016**, 9, 1413–1423; c) Celenligil-Cetin R., Watson L. A., Guo C., Foxman B. M., Ozerov O. V., «Decarbonylation of acetone and carbonate at a pincer-ligated Ru center», *Organometallics*, **2005**, 24, 186–189; d) Pan Y., Pan C.-L., Zhang Y., Li H., Min S., Guo X., Zheng B., Chen H., Anders A., Lai Z., Zheng J., Huang K.-W., «Selective Hydrogen Generation from Formic Acid with Well-Defined Complexes of Ruthenium and Phosphorus–Nitrogen PN3-Pincer Ligand», *Chem. Asian J.*, **2016**, 11, 1357–1360.

<sup>136</sup> a) Khusnutdinova, J. K., Milstein, D., «Metal–ligand cooperation», *Angew. Chem. Int. Ed.*, **2015**, 54, 12236–12273; «Metall-Ligand-Kooperation», *Angew. Chem.*, **2015**, 127, 12406–12445; b) Dub, P. A., Gordon, J. C., «Metal–ligand bifunctional catalysis: the “accepted” mechanism, the issue of concertedness, and the function of the ligand in catalytic cycles involving hydrogen atoms», *ACS Catal.*, **2017**, 7, 6635–6655.

<sup>137</sup> Agapova, A., Alberico, E., Kammer, A., Junge, H., Beller, M., «Catalytic Dehydrogenation of Formic Acid with Ruthenium-PNP-Pincer Complexes: Comparing N-Methylated and NH-Ligands», *ChemCatChem*, **2019**, 11, 1910–1914.

<sup>138</sup> Boddien, A., Mellmann, D., Gärtner, F., Jackstell, R., Junge, H., Dyson, P. J., Laurenczy, G., Ludwig, R., Beller, M., «Efficient dehydrogenation of formic acid using an iron catalyst», *Science*, **2011**, 333, 1733-1736.

<sup>139</sup> (a) Tilley, T. D., «Mechanistic aspects of transition-metal catalyzed dehydrogenative silane coupling reactions», *Comments Inorg. Chem.*, **1990**, 10, 37-51. (b) Corey, J. Y., «Catalytic dehydrocoupling of organosilanes», *Adv. Silicon Chem.*, **1991**, 1, 327. (c) Gauvin, F.; Harrod, J. F.; Woo, H. G., «Catalytic Dehydrocoupling: A General Strategy for the Formation of Element–Element Bonds», *Adv. Organomet. Chem.*, **1998**, 42, 363. (d) Reichl, J. A.; Berry, D. H., «Recent Progress in Transition Metal-Catalyzed Reactions of Silicon, Germanium, and Tin», *Adv. Organomet. Chem.*, **1999**, 43, 197.

<sup>140</sup> Polysilanes are of interest for their unusual electronic and optical properties, arising from extensive electron delocalization along the all-silicon backbone: (a) West, R. J., « $\alpha,\omega$ -Oligosilyl Dianions and Their Application in the Synthesis of Homo- and Heterocyclosilanes», *Organomet. Chem.*, **1986**, 300, 327. (b) Miller, R. D.; «Polysilane high polymers», *Michl, J. Chem. Rev.*, **1989**, 89, 1359. (c) Hamada, T. J., «Effects of main chain conformation on third-order non-linear optical susceptibilities of polysilanes Theoretical study on their second hyperpolarizabilities and bulk susceptibilities», *Chem. Soc., Faraday Trans.*, **1998**, 94, 509-517.

<sup>141</sup> Zr-based catalyst for dehydrogenative coupling of silanes: Imori, T.; Tilley, T. D., «The influence of catalyst structure on the dehydropolymerization of phenylsilane», *Polyhedron*, **1994**, 13, 2231. (b) Dioumaev, V. K.; Harrod, J. F., «A systematic analysis of the structure-reactivity trends for some 'cation-like' early transition metal catalysts for dehydropolymerization of silanes», *J. Organometal. Chem.*, **1996**, 521, 133-143. (c) Dioumaev, V. K.; Rahimian, K.; Gauvin, F.; Harrod, J. F., «Stereostructures of linear and cyclic polyphenylsilanes produced by dehydrocoupling in the presence of group 4 metallocene catalysts», *Organometallics*, **1999**, 18, 2249-2255.

<sup>142</sup> Ti-based catalyst for dehydrogenative coupling of silanes: (a) Wang, Q.; Corey, J. Y., «Dehydrocoupling reactions of hydrosilanes with group 4 metallocenes  $\text{Cp}_2\text{MY}_2$  ( $\text{M} = \text{Ti, Zr, Hf}$ ;  $\text{Y} = \text{F, OPh, NMe}_2$ )», *Can. J. Chem.*, **2000**, 78, 1434-1440. (b) Corey J. Y., Zhu X. H., «Condensation of primary silanes in the presence of  $\text{Cp}_2\text{MCl}_2/\text{nBuLi}$  ( $\text{M} = \text{Ti, Zr, Hf}$ )», *J. Organomet. Chem.*, **1992**, 439, 1-17.

<sup>143</sup> Hf-based catalyst for dehydrogenative coupling of silanes: (a) Tilley, T. D.; Woo, H.-G., «Catalytic dehydrogenative polymerization of silanes to polysilanes by zirconocene and hafnocene catalysts. a new polymerization mechanism», in «Inorganic and Organometallic Oligomers and Polymers», (H. F. Harrod, R. M. Laine, Eds.), Kluwer Academic Publishers, Netherlands, 1991, p. 3. (b) Shaltout, R. M.; Corey, J. Y., «Catalytic Dehydrocoupling of Hydrosilanes with Trimethylsilyl Substituted Hafnocene and Ansa-Hafnocene Complexes», *Main Group Chem.*, **1995**, 1, 115-126. (c) Dioumaev, V.K., Harrod J.F., «A systematic analysis of the structure-reactivity trends for some 'cation-like'early transition metal catalysts for dehydropolymerization of silanes», *J. Organomet. Chem.*, **1996**, 521, 133-143.

<sup>144</sup> (a) Imori, T., Tilley, T.D., «The influence of catalyst structure on the dehydropolymerization of phenylsilane », *Polyhedron*, **1994**, 13, 2231; (b) Dioumaev V.K., Harrod J.F., «A systematic analysis of the structure-reactivity trends for some 'cation-like'early transition metal catalysts for dehydropolymerization of silanes», *J. Organomet. Chem.*, 1996, 521, 133-143. (c) Tilley, T.D., «Mechanistic aspects of transition-metal catalyzed dehydrogenative silane coupling reactions», *Comments Inorg. Chem.*, **1990**, 10, 37-51; (d) Corey, J.Y., «Catalytic dehydrocoupling of organosilanes», *Adv. Silicon Chem.*, **1991**, 1, 327; (e) Gauvin, F., Harrod, J.F., Woo, H.G., «Catalytic Dehydrocoupling: A General Strategy for the Formation of Element–Element Bonds », *Adv. Organomet. Chem.*, **1998**, 42, 363; (f) Reichl, J.A., Berry, D.H., «Recent progress in transition metal-catalyzed reactions of silicon, germanium, and tin», *Adv. Organomet. Chem.*, **1999**, 43, 197-265. (g) Corey, J. Y., «Dehydrocoupling of hydrosilanes to polysilanes and silicon oligomers: A 30 year overview», *Adv. Organomet. Chem.* **2004**, 51, 1-52.

<sup>145</sup> Ru-based catalysts for dehydrogenative coupling of silanes: (a) Sakakura, T.; Kumberger, O.; Tan, R. P.; Aruther, M.-P.; Tanaka, M., «Ruthenium complex-catalysed selective redistribution reaction of aryltrihydrosilanes and desilanative polymerization of bis (trihydrosilyl) benzenes», *J. Chem. Soc., Chem. Commun.*, **1995**, 193-194. (b) Yokoyama, K.; Taniguchi, K.; Kiso, Y. *Jap. Pat. App.*, 88/251,577. *Chem. Abstr.* **1990**, 112, 8036t. (c) Yagihashi, Y.; Takatsuna, K.; Okumura, Y. *Jap. Pat. Appl.*, 89/3,907. *Chem. Abstr.* **1991**, 114, 7467p.

<sup>146</sup> Rh-based catalysts for dehydrogenative coupling of silanes: (a) Brown-Wensley, K. A., «Formation of Si-Si bonds from Si-H bonds in the presence of hydrosilation catalysts», *Organometallics*, **1987**, 6, 1590-1591. (b) Chang, L. S.; Corey, J. Y., «Dehydrogenative coupling of diarylsilanes», *Organometallics*, **1989**, 8, 1885-1893. (c) Co-rey, J. Y.; Chang, L.

S.; Corey, E. R., «Dehydrogenative coupling of heterocyclic dihydrosilanes», *Organometallics*, **1987**, 6, 1595-1596. (d) Rosenberg, L.; Davis, C. W.; Yao, J., «Catalytic dehydrogenative coupling of secondary silanes using Wilkinson's catalyst», *J. Am. Chem. Soc.*, **2001**, 123, 5120-5121. (e) Rosenberg, L.; Kobus, D. N., «Dehydrogenative coupling of primary alkyl silanes using Wilkinson's catalyst», *J. Organomet. Chem.*, **2003**, 685, 107-112. (e) Aizenberg, M.; Ott, J.; Elsevier, C. J.; Milstein, D., «Rh (I) and Rh (III) silyl PMe<sub>3</sub> complexes. Syntheses, reactions and <sup>103</sup>Rh NMR spectroscopy», *J. Organomet. Chem.*, **1998**, 551, 81-92. (f) Berris, C.; Diefenbach, S. P. U. S. Patent 5,003,100; *Chem. Abstr.*, **1992**, 115, 115263y. (g) Fryzuk, M. D.; Rosenberg, L.; Rettig, S., «Reactions of silanes with the binuclear hydride  $[(\text{Me}_2\text{CH})_2\text{PCH}_2\text{CH}_2\text{P}(\text{CHMe}_2)_2\text{Rh}]_2(\mu\text{-H})_2$ . Catalytic deuterium exchange on diphenylsilane and X-ray structure of  $[(\text{Me}_2\text{CH})_2\text{PCH}_2\text{CH}_2\text{P}(\text{CHMe}_2)_2]\text{Rh}]_2(\mu\text{-H})(\mu\text{-}\eta^2\text{-HSiPh}_2)$ », *J. Organometallics*, **1991**, 10, 2537-2539. (h) Fryzuk, M. D.; Rosenberg, L.; Rettig, S., «Reaction of primary silanes with dinuclear rhodium hydride complexes: silane coupling reactions», *J. Inorg. Chim. Acta*, **1994**, 222, 345-364. (i) Berris C, Diefenbach S.P., U.S. 5003100; CAN 115, 115263, **1992**.

<sup>147</sup> Pt-based catalysts for dehydrogenative coupling of silanes: (a) Tanaka, M.; Bannu, P. S. C., *Jpn. Kokai Tokkyo Koho JP 10 67, 859. Chem. Abstr.*, **1998**, 128, 244538f. (b) Chauhan, B. P. S.; Shimizu, T.; Tanaka, «New vistas in dehydrocoupling polymerization of hydrosilanes: Platinum complex-catalyzed dehydrocoupling of cyclic and acyclic secondary silanes», *M. Chem. Lett.*, **1997**, 785-786. (c) Itazaki, M.; Nishihara, Y.; Osakada, K., «Platinum complex-catalyzed hydrosilylation and isomerization of methylenecyclopropane derivatives. Effect of structures of the substrate and catalyst», *J. Org. Chem.*, **2002**, 67, 6889-6895. (d) Tanaka, M.; Bannu, P., JP 10 67859 CAN 128, 244528, **1998**.

<sup>148</sup> Ni-based catalysts for dehydrogenative coupling of silanes: (a) Boudjouk, P.; Rajkumar, A. B.; Parker, W. L., «Nickel catalysed coupling of phenylhydrosilanes», *J. Chem. Soc. Chem. Commun.*, **1991**, 245. (b) Groux, L. F.; Zargarian, D., «Structure and Reactivity of the Cationic Nickel Compound  $[(\eta^3\text{:}\eta^1\text{-Ind}(\text{CH}_2)_2\text{NMe}_2)\text{Ni}(\text{PPh}_3)]^+[\text{BPh}_4]^-$ », *Organometallics*, **2001**, 20, 3811-3817. (c) Fontaine, F.-G.; Kadkhodazadeh, T.; Zargarian, D., «Nickel indenyl complexes as precatalysts for dehydropolymerization of phenylsilane», *Chem. Commun.*, **1998**, 1253-1254. (d) Fontaine, F.-G.; Zargarian, D., «Dehydrogenative Oligomerization of PhSiH<sub>3</sub> Catalyzed by (1-Me-Indenyl)Ni(PR<sub>3</sub>)(Me)», *Organometallics*, **2002**, 21, 401-408.

<sup>149</sup> Fe-based catalyst for dehydrogenative coupling of silanes: (a) Park, M. J.; Lee, S. L.; Park, M. K.; Han, B. H., «Redistribution of (Aryl, Benzyl, Octyl) silane and Dehydrogenative



Coupling of Methylphenylsilane Using an Activated Metal Catalysts Prepared by the Reduction of Transition Metal Chlorides with Lithium Metal Powder», *Bull. Korean Chem. Soc.*, **2000**, 21, 336-338. (b) Semenov, V. V.; Cherepennikova, N. F.; Makarenko, N. P., «Reaction of tris (trimethylsilyl) silane with pentacarbonyliron», *Russ. J. Gen. Chem.*, **1999**, 69, 910-912; *Chem. Abstr.*, **1999**, 737783. (c) Schubert, U.; Knorr, M., «Transition-metal silyl complexes. 29. Formation of dihydride complexes from hydrido (silyl) tetracarbonyliron derivatives», *Inorg. Chem.*, **1989**, 28, 1765-1766. (d) Parish, R. V.; Riley, B. F. J., «Studies in Mössbauer spectroscopy. Part 12. Characterization of complexes containing iron–silicon bonds», *J. Chem. Soc. Dalton Trans.*, **1979**, 482.

<sup>150</sup> See, for example (a) Fryzuk, M.D., Rosenberg, L., Rettig, S.J., «Reaction of primary silanes with dinuclear rhodium hydride complexes: silane coupling reactions », *Inorg. Chim. Acta*, **1994**, 222, 345, and references therein. There are very few examples of late metal activities for the production of longer silicon chains (DP]/6). These include (b) Chauhan, B.P.S., Shimizu, T., Tanaka, M., «New vistas in dehydrocoupling polymerization of hydrosilanes: Platinum complex-catalyzed dehydrocoupling of cyclic and acyclic secondary silanes », *Chem. Lett.*, **1997**, 785; (c) Fontaine, F.-G., Kadkhodazadeh, T., Zargarian, D., «Nickel indenyl complexes as precatalysts for dehydropolymerization of phenylsilane», *Chem. Commun.*, **1998**, 1253-1254.

<sup>151</sup> Curtis, M.D., Epstein, P.S., «Redistribution Reactions on Silicon Catalyzed by Transition Metal Complexes», *Adv. Organomet. Chem.*, **1981**, 19, 213-255.

<sup>152</sup> Rosenberg, L.; Kobus, D. N., «Dehydrogenative coupling of primary alkyl silanes using Wilkinson's catalyst», *J. Organometal. Chem.*, **2003**, 685, 107-112.

<sup>153</sup> Grimmond, B. J.; Corey, J. Y., «Catalytic Dehydropolymerization of PhSiH<sub>3</sub> to Polyphenylsilane with Substituted Group IV Metallocenes», *Organometallics*, **1999**, 18, 2223-2229.

<sup>154</sup> Bo-Hye, K., Hee-Gweon, H., «Frontiers in organometallic chemistry». Nova science publishers, New York, 2006, 243.

<sup>155</sup> Luo, Y. R., (2003), «Handbook of bond dissociation energies in organic compounds», CRC Press, Boca Raton, 380.

**Agreement on the Joint Supervision of a Doctoral Thesis  
between  
Universität Regensburg  
and  
Universidad Simón Bolívar**

In view of the following

In Germany:

Considering the existing German laws and regulations, in particular the existing regulations of the University of Regensburg (hereafter: UR) for the award of the academic degree of a Doctor of Natural Sciences (Dr. rer. nat), PO Dr. rer. nat., §§ 19 – 23.

In Venezuela:

Considering the regulations to award jointly the academic degree of Doctor from Universidad Simón Bolívar (hereafter: USB), dated November 28, 2018; relative to the principles, procedures, and conditions for the joint award of the academic degree of Doctor between USB and other foreign institutions

Considering the General Regulations for Graduate Studies at Universidad Simón Bolívar, dated October 9, 2013,

Universität Regensburg, located in Universitätsstr. 31, 93053 Regensburg, Germany, represented by its President, Prof. Dr. Udo Hebel;

and Universidad Simón Bolívar, located in Valle de Sartenejas, Carretera Nacional de Baruta – Hoyo de La Puerta, Municipio Baruta, Edo. Miranda, Venezuela, represented by its Rector, Prof. Dr. Enrique Planchart, and duly authorized by USB's Directive Council on its march 11, 2020 meeting,

In furtherance of the common aim of both Universities of promoting international cooperation

**Convenio para la Supervisión Conjunta  
de una Tesis Doctoral  
entre  
Universität Regensburg  
y  
la Universidad Simón Bolívar**

En virtud de lo siguiente:

En Alemania:

Considerando las leyes y regulaciones alemanas existentes, en particular las regulaciones existentes de la Universität Regensburg (de aquí en adelante UR) para el otorgamiento del grado académico de Doctor en Ciencias Naturales (Dr. re. nat.), PO Dr. rer. nat., §§ 19 – 23.

En Venezuela:

Considerando las regulaciones para el otorgamiento conjunto del grado académico de Doctor de la Universidad Simón Bolívar (de aquí en adelante USB), de fecha 28 de noviembre de 2018, relacionadas con los principios, procedimientos y condiciones para el otorgamiento conjunto del grado de doctor entre la USB y otras instituciones externas,

Considerando el Reglamento General de los Estudios de Postgrado de la Universidad Simón Bolívar, de fecha 9 de octubre de 2013,

La Universität Regensburg, ubicada en Universitätsstr. 31, 93053 Regensburg, Alemania, representada por su Presidente, Prof. Dr. Udo Hebel;

y la Universidad Simón Bolívar, ubicada en el Valle de Sartenejas, Carretera Nacional Baruta-Hoyo de La Puerta, Municipio Baruta, Edo. Miranda, Venezuela, representada por su Rector, Prof. Dr. Enrique Planchart, debidamente autorizado por el Consejo Directivo en su sesión del 11 de marzo de 2020,

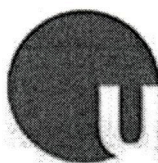
Para fomentar el objetivo común de ambas universidades de promover la cooperación

*Handwritten signatures and initials:*  
Raffa...  
N. Lag...  
SP...  
P...





UNIVERSIDAD SIMÓN BOLÍVAR



Universität  
Regensburg

and mobility of researchers, the parties give their consent to the preparation of a doctoral thesis under joint supervision and agree on a common framework to the joint supervision and award of the doctoral degree under their common responsibility,

The undersigned Universities agree to the preparation of a doctoral thesis, whose completion and defense will take place under the joint responsibility of both institutions in accordance with the following conditions:

1. This agreement applies to:

**Mr. MIGUEL ANGEL CHACÓN TERÁN,**  
(the "Candidate")

2. The research topic is: SYNTHESIS OF POTENTIALLY POLYDENTATE BULKY PHOSPHITE LIGAND(S) AND ITS (THEIR) TRANSITION METAL COORDINATION COMPOUNDS, AND USE OF THE COMPOUNDS OBTAINED IN HOMOGENEOUS CATALYSIS.
3. The thesis will be directed by: Prof. Robert Wolf, PhD at Institut für Anorganische Chemie of the Fakultät für Chemie und Pharmazie, Universität Regensburg, and Prof. Rafael Rodríguez, PhD, Centro de Química, Instituto Venezolano de Investigaciones Científicas, who have assumed the task of jointly advising the Candidate on all aspects of his thesis work.
4. The Candidate must be admitted for doctoral studies at both Universities by the respective Graduate Studies Committees. The Candidate will enroll at each of the Universities for the duration of the respective stay. Enrolment at the home or the host institution can require payment of student service or other fees.
5. The Candidate must be covered by sufficient health/medical insurance, public or private, while at Universidad Simón Bolívar, and at Universität Regensburg. The Candidate is responsible for purchasing the insurance policy.

internacional y la movilidad de los investigadores, las partes dan su consentimiento para la preparación de una tesis doctoral bajo supervisión conjunta y acuerdan un marco común para dicha supervisión conjunta y el otorgamiento del título de doctorado bajo su responsabilidad conjunta,

Las Universidades firmantes acuerdan la realización de una tesis doctoral, cuya elaboración y defensa tendrá lugar bajo la responsabilidad conjunta de ambas instituciones de acuerdo con las siguientes condiciones:

1. Este convenio se aplica a:

**Sr. MIGUEL ANGEL CHACÓN TERÁN,**  
(el "Candidato")

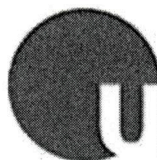
2. El tema de la investigación es: SÍNTESIS DE LIGANDO(S) FOSFITO VOLUMINOSO(S) POTENCIALMENTE POLIDENTADO(S) Y SU(S) COMPUESTOS DE COORDINACIÓN DE METALES DE TRANSICIÓN, Y EL USO DE LOS COMPUESTOS OBTENIDOS EN CATÁLISIS HOMOGÉNEA
3. La tesis será dirigida por: Prof. Robert Wolf, PhD en el Instituto de Química Inorgánica de la Facultad de Química y Farmacia, Universität Regensburg, y el Prof. Rafael Rodríguez, PhD, Centro de Química, Instituto Venezolano de Investigaciones Científicas, quienes han asumido la tarea de conjuntamente guiar al Candidato en todos los aspectos de su trabajo de tesis.
4. El candidato debe ser admitido para estudios de doctorado en ambas Universidades por los respectivos comités de admisión. El candidato se inscribirá en cada Universidad por el período de la permanencia respectiva. La inscripción en la Universidad de origen o la Universidad anfitriona puede requerir el pago de matrícula, servicios estudiantiles, u otros costos.
5. El Candidato debe contar con un seguro médico público o privado de cobertura suficiente, mientras esté en la Universität Regensburg, o en la Universidad Simón Bolívar. El Candidato es responsable de adquirir la póliza de seguro.

*Refuge*  
*h. Wuy*  
*CP*  
*f*  
*pol*





UNIVERSIDAD SIMÓN BOLÍVAR



Universität  
Regensburg

The Candidate will reside, in both countries, in a personal living place. The Candidate has to bear all the related costs, including but not limited to housing, food and transportation, unless such costs are covered by scholarship or any kind of funding. For the research stay at Universität Regensburg the Candidate will receive funding through the international PhD Program *iPUR* at the UR. The scholarship consists of a travel grant (fixed amount 1.850€) and a monthly allowance of 1.000€ (fixed amount) for the duration of up to three months, which may be repeated. The Candidate will also receive funding through the Deutscher Akademischer Austauschdienst (DAAD, German Academic Exchange Service) to cover the second period of research at UR. The scholarship consists of a travel grant (fixed amount 1.850€) and a monthly allowance of 1.000€ (fixed amount) for the duration of up to nine months.

6. The estimated duration for research on the thesis is set provisionally at three years beginning April 2017. This period can be extended, as may be necessary, in accordance with the existing regulations governing the award of doctoral degrees of both institutions.

Work for the preparation of the thesis will be carried out at both institutions. The period of stay at each of the institutions should be at least 30% of the total time spent in the thesis work.

The minimum period of stay to obtain the double degree within the agreement on the Joint Supervision of a Doctoral Thesis within the frame of the *iPUR* – PhD Program at UR is 6 months.

For USB, the minimum requirement to obtain the double degree within this agreement is to successfully approve 50% of the credit units of the Doctoral in Chemistry Program at USB, considering that at USB doctoral students are required to

En ambas localidades, el candidato estará residenciado en una vivienda personal. El candidato debe cubrir todos los gastos relacionados, incluyendo, sin estar limitado a, vivienda, alimentación y transporte, a menos que dichos gastos estén cubiertos por una beca u otro tipo de fondos. Durante su estancia de investigación en la Universität Regensburg el candidato recibirá fondos a través del Programa Internacional de PhD *iPUR* de la UR. Esta beca consiste en un monto fijo para viajes (1.850 €) y un subsidio mensual fijo de 1.000 € para una duración de hasta tres meses, el cual se puede repetir. El Candidato adicionalmente recibirá financiamiento a través del Servicio Alemán de Intercambio Académico (DAAD) para cubrir el segundo período de investigación en la UR. Esta beca consiste en un monto fijo para viajes (1.850 €) y un subsidio mensual fijo de 1.000 € para una duración de hasta nueve meses.

6. La duración estimada de la investigación de esta tesis se establece provisionalmente en tres años, comenzando en abril 2017. Este período puede ser extendido según fuera necesario, en concordancia con los reglamentos existentes que regulan el otorgamiento de grados de doctor en ambas instituciones.

El trabajo para la elaboración de la tesis se llevará a cabo en ambas instituciones. El período de permanencia en cada institución debe corresponder por lo menos al 30% del tiempo total invertido en el trabajo de tesis.

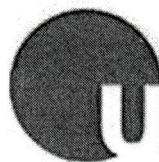
El período mínimo de permanencia en la UR para obtener el grado conjunto en el marco del presente Convenio para la Supervisión Conjunta de una Tesis Doctoral y dentro del marco del programa de PhD *iPUR* de la UR es de 6 meses.

Para la USB, el requerimiento mínimo para obtener el grado conjunto dentro del marco de este convenio es inscribir y aprobar en la USB satisfactoriamente el 50% de las unidades crédito

*Ref. 100*  
*2.1.10*  
*ED*  
*[Signature]*  
*[Signature]*



UNIVERSIDAD SIMÓN BOLÍVAR



Universität  
Regensburg

enroll and pass 46 credit units of specialized coursework, 6 credit units corresponding to seminars related to the thesis, 12 credit units in research topics which may be related or not to the thesis, and 24 credit units in thesis work. Furthermore, the candidate must have attended three academic periods of departmental seminars at USB's Chemistry Department, and successfully presented the knowledge exam, the thesis proposal, and the second language proficiency test.

**Proposed schedule:**

**April –November 2017 at UR**

- Training and research

**December 2017-June 2018 at USB**

- Specialized and methodological coursework
- Second language proficiency test

**July 2018 – December 2018 at UR**

- Research work

**January – March 2019 at USB**

- Doctoral knowledge exam
- Thesis proposal presentation

**April-June 2019 at UR**

- Research work

**July 2019 – March 2020 at USB**

- Methodological coursework
- Thesis preparation

7. The thesis will be written in English according to the formal guidelines of the USB and has to be submitted at the lead institution, the USB. The thesis will be assessed by the two supervisors, before it will be forwarded to the examination committee. The examination committee will decide whether the thesis will be accepted or rejected. Only if the committee accepts the thesis, the oral examination will take place After the oral

del Programa de Doctorado en Química, considerando que los estudiantes de doctorado deben inscribir y aprobar 46 unidades crédito en asignaturas especializadas, 6 unidades crédito en asignaturas metodológicas, 12 unidades crédito en tópicos de investigación que pueden estar relacionados con la tesis, y 24 unidades crédito de tesis doctoral. Adicionalmente, el Candidato debe haber atendido el seminario del Departamento de Química durante tres trimestres, así como presentado y aprobado el examen de conocimiento, la defensa del anteproyecto de tesis y el examen de competencia instrumental en un segundo idioma.

**Cronograma propuesto:**

**Abril –noviembre 2017 en la UR**

- Entrenamiento e investigación

**Diciembre 2017-junio 2018 en la USB**

- Asignaturas especializadas y metodológicas
- Examen de suficiencia de segundo idioma

**Julio 2018 – diciembre 2018 en la UR**

- Investigación

**Enero – marzo 2019 en la USB**

- Examen de conocimiento doctoral
- Propuesta de tesis doctoral

**Abril-Junio 2019 en la UR**

- Investigación

**Julio 2019 – marzo 2020 en la USB**

- Asignaturas metodológicas
- Tesis doctoral

7. El manuscrito de la tesis será redactado en inglés de acuerdo con el formato de la USB y ha de ser presentado en la institución principal, la USB. La redacción del manuscrito será evaluada por los dos supervisores, antes de ser enviada al comité evaluador. El comité evaluador decidirá si la tesis será aceptada o rechazada. Únicamente cuando el comité acepte la tesis, la defensa oral podrá realizarse. Luego de la defensa oral, la tesis debe ser calificada de acuerdo con la siguiente tabla:

Raffa  
G. W.  
P.  
P.



defense, the thesis must be graded according to the following table:

Universität Regensburg	Universidad Simón Bolívar
Summa cum laude (grade 0)	Aprobada con Mención Sobresaliente
Magna cum laude (grade 1)	Aprobada
Cum Laude (grade 2)	
Rite (grade 3)	
Insufficienter (grade 4)	Reprobada o Rechazada

8. The defense of the thesis and any other final examinations, will take place only once, at Universidad Simón Bolívar, Caracas, Venezuela. In exceptional circumstances, members of the examination committee can join the defense by video-conferencing. A majority of examiners must always be present in the examination room.
9. The result of the defense of the thesis and examinations will be recognized by both institutions.
10. Travel costs for members of the examination committee, shall be assumed by their own institutions.
11. The members of the examination committee shall be determined by written agreement of the two institutions. The committee shall be composed equally of academic teachers/scholars of both institutions, who shall be authorized to act as examiners. The committee will consist of at least five members; two of them will be the thesis supervisors, insofar as this does not conflict with applicable regulations at either institution.
- At least two external examiners, not associated with either of the institutions, in agreement with the regulations approved by the Directive Council from Universidad Simón Bolívar, shall serve on the examination committee.

8. La defensa de la tesis y cualquier otro examen final, se llevará a cabo solo una vez, en la Universidad Simón Bolívar, Caracas, Venezuela. En circunstancias excepcionales, algunos miembros del comité examinador pueden unirse a la defensa mediante una videoconferencia. La mayoría de los examinadores siempre deben estar presentes físicamente en la sala del examen.
9. El resultado de la defensa de la tesis y los exámenes será reconocido por ambas instituciones.
10. Los gastos de viaje de los miembros del comité examinador serán asumidos por sus propias instituciones.
11. Los miembros del comité examinador se determinarán mediante acuerdo escrito entre las dos instituciones. El comité estará compuesto igualitariamente por personal académico de ambas instituciones, quienes estarán autorizados a actuar como examinadores. El comité estará compuesto por al menos cinco miembros; dos de los cuáles serán los supervisores de tesis, en la medida en que esto no entre en conflicto con los reglamentos aplicables en ninguna de las instituciones.
- Al menos dos examinadores externos, no asociados con ninguna de las instituciones, de acuerdo con los reglamentos aprobados por el Consejo

*Handwritten signatures and initials:*  
 Raff...  
 M. G...  
 C. P...  
 R...  
 P...  
 P...

12. The two institutions will recognize the result of the jointly supervised doctoral procedure and the validity of the doctoral degree awarded.

After the successful completion of the procedure, and on the basis of the report of the doctoral thesis committee, the two Universities will separately award the Candidate with the doctoral degree and issue their respective doctoral diploma. The diploma issued by Universidad Simón Bolívar should indicate that the academic degree was awarded jointly with the Universität Regensburg, within the framework of the specific agreement subscribed by both parties. The elaboration of the diploma will be carried out according to the corresponding institutional guidelines.

13. At USB, there will be single grades for the coursework and the thesis. For the final grade at UR, the oral defense at USB will be assessed and given a grade according to the table set out in clause 7. After successful completion of the oral defense and the publication, the partner institutions will issue the appropriate certificate bearing an annotation that both certificates constitute a combined doctoral certificate. The UR awards the degree of Doctor of Natural Sciences (Dr. rer. nat.). USB awards the degree of Doctor en Química.

The equivalency of grades is fixed as follows (see also article 7):

Universität Regensburg	Universidad Simón Bolívar
Summa cum laude (grade 0)	Aprobada con Mención Sobresaliente
Magna cum laude (grade 1)	Aprobada
Cum Laude (grade 2)	
Rite (grade 3)	

Directivo de la Universidad Simón Bolívar, deberán formar parte del comité examinador.

12. Ambas instituciones reconocerán el resultado del proceso de evaluación del doctorado supervisado conjuntamente y la validez del título de doctorado otorgado.

Luego de completar exitosamente todos los requisitos, y sobre la base del informe del comité de tesis doctoral, ambas universidades otorgarán al candidato por separado el título de Doctor y emitirán su respectivo Diploma de Doctorado. El diploma emitido por la Universidad Simón Bolívar, debería indicar que el título académico ha sido otorgado conjuntamente con la Universität Regensburg en el marco del convenio específico suscrito por ambas partes y su elaboración se realizará atendiendo los lineamientos institucionales correspondientes.

13. En la USB se otorgarán calificaciones individuales para las asignaturas y para la tesis. Para la calificación final en la UR, la defensa oral en la USB será evaluada y calificada de acuerdo con la cláusula 7. Después de completar con éxito la defensa oral y la publicación de la tesis, las instituciones asociadas emitirán el certificado correspondiente con la acotación de que ambos certificados constituyen un certificado doctoral combinado. La UR otorga el grado de Doctor en Ciencias Naturales (Dr. rer. nat.), la USB otorga el grado de Doctor en Química.

La equivalencia entre las calificaciones se establece como sigue (véase también el artículo 7):



Insufficienter (grade 4)	Reprobada o Rechazada
<p>14. The conditions of title and document publication, of thesis document registration, and reproduction, as well as the results of any research conducted by the Candidate, are subject to the rules of the Universität Regensburg and to the rules of Universidad Simón Bolívar in the subject.</p> <p>For the purpose of this agreement, the parties will have equal rights in the results of the research conducted by the Candidate (50%-50%), unless each parties' contribution can be separated into different and individual contributions. In this case, each result will belong to the author that made that contribution. Universities undertake to safeguard the confidentiality of the thesis until they have requested the corresponding intellectual property rights.</p> <p>The Candidate agrees to respect the regulations in force in both countries in respect to intellectual property and copyright.</p> <p>15. The thesis will be written in English. The abstract will be written in English. The oral defense of the thesis and examinations will be held in English. The thesis will include an extended abstract of the work, between 4- and 5-pages length, written in Spanish, as well as copies of the final evaluation document and of this agreement of joint supervision, in order to comply with USB's regulations, and considering that Spanish is the official language at USB.</p> <p>16. This agreement will enter into full force and effect from the date of the last signature stated below. This agreement is issued in three identical copies.</p>	<p>14. Las condiciones para la publicación de títulos y documentos, de registro y reproducción de documentos de tesis, así como los resultados de cualquier investigación realizada por el Candidato, están sujetos a las reglas de la Universität Regensburg y a las reglas de la Universidad Simón Bolívar sobre el tema.</p> <p>A los fines de este convenio, las partes tendrán los mismos derechos sobre los resultados de la investigación realizada por el Candidato (50% -50%), a menos que la contribución de cada parte se pueda separar en contribuciones diferentes e individuales. En este caso, cada resultado pertenecerá al autor que hizo esa contribución. Las universidades se comprometen a salvaguardar la confidencialidad de la tesis hasta que hayan solicitado los derechos de propiedad intelectual correspondientes.</p> <p>El Candidato se compromete a respetar los reglamentos vigentes en ambos países con respecto a la propiedad intelectual y los derechos de autor.</p> <p>15. La tesis se redactará en inglés. El resumen será escrito en inglés. La defensa oral de la tesis y los exámenes se realizarán en inglés. La tesis incluirá un resumen extendido del trabajo, entre 4 y 5 páginas, escrito en español, así como copia del acta de evaluación y de este convenio de supervisión conjunta, a fin de cumplir con los reglamentos de la USB y considerando que el español es el idioma oficial de la USB.</p> <p>16. Este convenio entrará en vigencia a partir de la fecha de la última firma indicada a continuación. Este Convenio se emite en tres copias idénticas.</p>

Regensburg, Germany; Date: 8.7.20

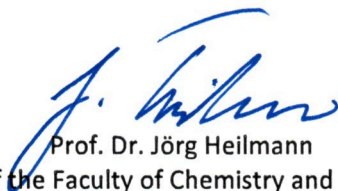
Valle de Sartenejas, Venezuela; Fecha:



Prof. Dr. Udo Hebel  
President  
Universität Regensburg



Prof. Dr. Enrique Blanchart  
Rector  
Universidad Simón Bolívar



Prof. Dr. Jörg Heilmann  
Dean of the Faculty of Chemistry and Pharmacy



Prof. Aura Cova  
Decana de Estudios de Postgrado



Prof. Robert Wolf  
Thesis Supervisor, UR



Prof. Rafael Rodríguez  
Tutor, USB



Miguel Ángel Chacón Terán  
The Candidate / El Candidato

# MIGUEL ÁNGEL CHACÓN TERÁN

Venezuelan, 29 years-old  
Phone: (+48) 508 359 216  
[mchacon233@gmail.com](mailto:mchacon233@gmail.com) / [17-90794@usb.ve](mailto:17-90794@usb.ve)

ul. Żwirki i Wigury 101, CNBCh-UW  
02-089 Warszawa

**Spanish:** Native; **English:** Good; **German:** Basics

## EDUCATION

---

- Ph.D.** Universität Regensburg, (International double dissertation program) *Regensburg, DE*  
PhD on Natural Science (Dr. rer. Nat.)  
Graduated, Nov 2020  
Research Advisor: Dr. Robert Wolf ([robert.wolf@ur.de](mailto:robert.wolf@ur.de))
- Ph.D.** Simon Bolivar University *Caracas, VE*  
PhD in Chemistry  
Graduated, Nov 2020  
Research Advisor: Dr. Rafael Rodriguez ([rrlugo19@gmail.com](mailto:rrlugo19@gmail.com))  
Dr. Vanessa Landaeta ([vlandaeta@usb.ve](mailto:vlandaeta@usb.ve))
- Lic.** The University of Zulia *Maracaibo, VE*  
Licentiate on Education Chemistry  
Graduated, Oct 2012  
Research Advisor: Dr. Edgar Ocando ([eocando@ivic.gob.ve](mailto:eocando@ivic.gob.ve))

## RESEARCH EXPERIENCE

---

Eight years of experience in the field of inorganic/molecular/coordination chemistry and catalysis, particularly in the synthesis of functionalized phosphorus and boron compounds and their corresponding metal complexes. Skills in homogeneous catalysis and kinetic studies of catalytic processes. Experience with MBraun workstations for inert atmosphere manipulation, dual lines using high vacuum / argon, standard Schlenk techniques and spectroscopic analysis (NMR, FT-IR, GC-MS, others).

**Postdoctoral researcher** *Warsaw, PL*  
*Unorthodox concept in olefin metathesis, MAESTRO 11.*  
Centrum Nauk Biologiczno-Chemicznych Uniwersytetu Warszawskiego  
Advisor: Prof. Dr. Karol Grela and Dr. Anna Kajetanowicz.  
Nov 2020 – Oct 2021

**Dissertation project.** *Caracas/Regensburg, VE/DE*  
*Tris(8-Quinolyl)Phosphite: Synthesis, Coordination Chemistry and Catalytic Applications*  
Simon Bolivar University / Universität Regensburg  
Advisor: Prof. Dr. Robert Wolf, Dr. Rafael Rodriguez and Prof. Dr. Vanessa Landaeta.  
Apr 2016 – Jul 2020

**International research stay.** *Regensburg, DE*  
*Development of novel Rh(I) and Ru(II) systems for environmentally friendly catalytic reactions*  
Universität Regensburg  
Advisor: Prof. Dr. Robert Wolf and Dr. Rafael Rodriguez.  
Jun 2018 – Apr 2019

**International research stay.** *Regensburg, DE*  
*Organocatalytic transformation promoted by P(OQuin)<sub>3</sub> and alternative H<sub>2</sub> sources*  
Universität Regensburg  
Advisor: Prof. Dr. Robert Wolf and Dr. Rafael Rodriguez.  
Feb 2017 – Dec 2017



**Internship as graduate student.**Regensburg, **DE***Synthesis of alkene metalates complexes ( $Fe^{-2}$ ,  $Fe^{-1}$ ,  $Co^{-1}$ )*

Universität Regensburg

Advisor: Prof. Dr. Robert Wolf and Dr. Rafael Rodriguez.

Jul 2016 – Sep 2016

**Research Assistant/Lab Technician.**Caracas, **VE***Synthesis of functionalized phosphines and its coordination chemistry toward Rh(I) and Ir (I) precursors*

Venezuelan Institute for Scientific Research (IVIC)

Advisor: Dr. Edgar Ocando

Feb 2013 – Mar 2016

**Licentiate research project**Caracas, **VE***Synthesis of diallylphosphines and its coordination chemistry toward Rh(I) precursors.*

Venezuelan Institute for Scientific Research (IVIC)

Advisor: Dr. Edgar Ocando

Jan 2012 – Dec 2012

**PUBLICATIONS**

---

**Journal Publications**

**Chacon-Teran, M.**; Rodríguez-Lugo, R.; Wolf, R.; Landaeta, V., “Transfer hydrogenation of azocompounds with ammonia-borane using a simple acyclic phosphite precatalyst” *Eur. J. Inorg. Chem.* **2019**, 39/40, 4336–4344. (Full paper, selected by *EurJIC* editors as an outstanding contribution from Latin-American)

Rodríguez-Lugo, R.; **Chacon-Teran, M.**; De Leon, S.; Vogt, M.; Landaeta, V., “Synthesis, Characterization and Pd (II)-Coordination Chemistry of the Ligand Tris(quinolin-8-yl)phosphite. Application in Catalytic Aerobic Oxidation of Amines” *Dalton Trans.*, **2018**, 47, 2061-2072. (Full paper)

**Journal Papers prior to Submission**

**Chacon-Teran, M.**; Rodríguez-Lugo, R.; Wolf, R.; Landaeta, V., “1,2-Regioselective hydroboration of pyridines and quinolines catalyzed by a novel Rh(I) complex bearing  $P(OQuin)_3$ ”. **2020**. (Full paper)

**Chacon-Teran, M.**; Rodríguez-Lugo, R.; Wolf, R.; Landaeta, V., “Synthesis of Ru(II)-halide complexes bearing a hindered tetradentate phosphite. An efficient catalyst to yield polysilicon compounds”. **2020**. (Full paper)

**TEACHING EXPERIENCE**

---

Simon Bolivar University, Caracas, VE

Jan **2018** up to date

Instructor Professor, Department of Chemistry

- Taught Laboratory of General Chemistry II, an undergraduate course averaging 15 students per trimester, covering the following topics: Qualitative analysis, electrochemistry 101 and methods for separating mixtures.
- Developed quizzes, exams, and homework

**FELLOWSHIPS AND AWARDS**

---

DAAD Research grant

Regensburg, **DE**

Universität Regensburg

Jun 2018 – Apr 2019

Full Fellowship (Fellowship sponsored by IUPAC to attend to Summer School)

Venice, **IT**

2018 IUPAC Postgraduate Summer School on Green Chemistry

Jul 2018

**Poster Prize / Inorganic subject area**

4th RSC twitter poster conference 2018  
Mar 2018

Cambridge, UK

**iPur Research Grant (DAAD-IPID4all)**

Universität Regensburg  
May 2017 – Jul 2017

Regensburg, DE

**ACG-Europacat 2017's bursary**

Applied Catalysis Group / Royal Society of Chemistry  
Feb 2017

Cambridge, UK

**Travel Grants for PhD Students and Post-doctoral Researchers**

Dalton Division / Royal Society of Chemistry  
Jul 2016

Cambridge, UK

**iPur Research Grant (DAAD-IPID4all)**

Universität Regensburg  
Jul 2016 – Sep 2016

Regensburg, DE

**Student bursary Award ICOMC 2016**

27th International Conference on Organometallic Conference  
Jul 2016

Melbourne, AU

**Full Fellowship (Fellowship sponsored by ACS to attend to Summer School)**

2016 ACS Summer School on Green Chemistry & Sustainable Energy  
Jun 2016

Golden, US

---

**CONGRESS AND SCIENTIFIC EVENTS**

---

**Poster Presentation, Chacon-Teran, M.** Rodríguez-Lugo, R.; Wolf, R. Landaeta, V. “Metal-free transfer hydrogenation of azobenzene with  $H_3N-BH_3$  as an alternative  $H_2$  source using  $P(OQuin)_3$  as precatalyst” 4th RSC twitter poster conference 2018. Mar **2018**. (**Poster Prize / Inorganic subject area**)

**Poster Presentation, Chacon-Teran, M.** Rodríguez-Lugo, R.; Wolf, R. Landaeta, V. “Metal-free transfer hydrogenation of azobenzene with  $H_3N-BH_3$  as an alternative  $H_2$  source using  $P(OQuin)_3$  as precatalyst” 13th European Congress on Catalysis (EuropaCat 2017). Florence, IT. Aug **2017**.

**Poster Presentation, Chacon-Teran, M.** Rodríguez-Lugo, Landaeta, V. “Free-Solvent oxidative coupling of primary amines to yield imines by palladium(II) and platinum(II)-P,N-phosphite complex” 27th International Conference on Organometallic Chemistry (ICOMC 2016). Melbourne, AU. Jul **2016**. (**Outstanding research**)

**Poster Presentation, Chacon-Teran, M.** Rodríguez-Lugo, R.; Wolf, R. Landaeta, V. “Oxidative coupling of primary amines to yield imines by a palladium(II)-P,N-phosphite complex under green chemistry conditions.” ACS Summer School on Green Chemistry & Sustainable Energy. Golden, US. Jun **2016**.

**Poster Presentation, Chacon M.,** Silva N., Sanchez L., Santiago Coll D., Garcia J.M., Ocando E. “Synthesis of Vaska's type complex  $trans-RHCl(CO)[tBu-P(CH_2CH=CH_2)_2]$  from  $[RH(acac)(CO)_2]$ .” Latin American Symposium on Coordination and Organometallic Chemistry (SILQCOM 2013). Huatulco, MX. Oct **2013**.

---

**REFERENCES**

---

**Dr. Rafael Rodriguez Lugo**

Venezuelan Institute for Scientific Research  
Associated researcher

Email: [rafael-Emilio.Rodriguez-Lugo@chemie.uni-regensburg.de](mailto:rafael-Emilio.Rodriguez-Lugo@chemie.uni-regensburg.de) / [rrlugo19@gmail.com](mailto:rrlugo19@gmail.com)

**Prof. Dr. Robert Wolf**

Universität Regensburg  
Associated professor

Email: [robert.wolf@ur.de](mailto:robert.wolf@ur.de)

Web: <https://www.uni-regensburg.de/chemistry-pharmacy/inorganic-chemistry-wolf/index.html>

**Prof. Dr. Vanessa Landaeta**

Simón Bolívar University

Associated professor

Email: [vlandaeta@usb.ve](mailto:vlandaeta@usb.ve) / [vlandaeta@gmail.com](mailto:vlandaeta@gmail.com)